

# Identification and characterization of novel ligands for purinergic P2X receptors

## **Dissertation**

zur

Erlangung des Doktorgrads (Dr. rer. nat.)

der

Mathematisch-naturwissenschaftlichen Fakultät

der

Rheinischen Friedrich-Wilhelms-Universität Bonn

vorgelegt von

**Claudia Spanier**

aus

Saarburg

Bonn 2016



Angefertigt mit Genehmigung der Mathematisch-naturwissenschaftlichen Fakultät der  
Rheinischen Friedrich-Wilhelms-Universität Bonn.

1. Gutachter: Prof. Dr. Christa E. Müller
2. Gutachter: PD Dr. Anke C. Schiedel

Tag der Promotion: 30.03.2016

Erscheinungsjahr: 2016



Die vorliegende Arbeit wurde in der Zeit von November 2010 bis November 2015 am Pharmazeutischen Institut der Rheinischen Friedrich-Wilhelms-Universität Bonn unter der Leitung von Prof. Dr. Christa E. Müller durchgeführt.



**Für meine Eltern**





---

## Table of Contents

<b>1</b>	<b>GENERAL INTRODUCTION .....</b>	<b>1</b>
<b>1.1</b>	<b>The ionotropic receptor family .....</b>	<b>1</b>
<b>1.2</b>	<b>Purinergic receptors.....</b>	<b>6</b>
1.2.1	P0, P1 and P2 receptors.....	6
1.2.2	P2X receptors .....	7
1.2.3	P2X receptor topology.....	7
1.2.4	P2X receptors – standard agonists.....	12
1.2.5	P2X receptors – standard antagonists.....	13
1.2.6	The P2X1 receptor subtype .....	14
1.2.6.1	P2X1 receptor antagonists .....	15
1.2.6.2	P2X1 receptor allosteric modulators.....	17
1.2.7	The P2X2 receptor subtype .....	17
1.2.7.1	P2X2 receptor antagonists .....	18
1.2.7.2	P2X2 receptor allosteric modulators.....	19
1.2.8	The P2X3 receptor subtype .....	20
1.2.8.1	P2X3 receptor antagonists .....	22
1.2.8.2	P2X3 receptor allosteric modulators.....	24
1.2.9	The P2X4 receptor subtype .....	24
1.2.9.1	P2X4 receptor antagonists .....	25
1.2.9.2	P2X4 receptor allosteric modulators.....	26
1.2.10	The P2X5 receptor subtype .....	28
1.2.11	The P2X6 receptor subtype .....	29
1.2.12	The P2X7 receptor subtype .....	30
1.2.12.1	P2X7 receptor antagonists .....	31
1.2.12.2	P2X7 receptor allosteric modulators.....	33
<b>1.3</b>	<b>Objective.....</b>	<b>35</b>
<b>2</b>	<b>MATERIAL AND METHODS .....</b>	<b>36</b>
<b>2.1</b>	<b>Material .....</b>	<b>36</b>
2.1.1	Chemicals.....	36

2.1.2	Consumable supplies .....	37
2.1.3	Devices .....	37
2.1.4	Compounds and compound libraries.....	39
2.1.5	Solutions and reagents.....	39
2.1.6	Pipetting schemes .....	41
2.1.6.1	ATP solutions used for determination of inhibitory potency .....	41
2.1.6.2	ATP solutions used for determination of enhancing potency .....	42
2.1.6.3	Standard dilution scheme of ATP (50 mM stock solution) .....	42
2.1.6.4	Standard dilution scheme of P2X receptor agonists (1 mM stock solution) .....	43
2.1.6.5	Dilutions of standard antagonists for the determination of Z'-factor .....	43
2.1.6.6	Standard dilution scheme for test compounds (10 mM stock solution) .....	44
2.1.6.7	Standard dilution scheme for test compounds (1 mM stock solution) .....	44
2.1.6.8	Standard dilution scheme for test compounds (0.1 mM stock solution) .....	45
<b>2.2</b>	<b>Methods.....</b>	<b>45</b>
2.2.1	Cell culture .....	45
2.2.2	Measurement of calcium influx in transfected 1321N1 astrocytoma cells .....	46
2.2.2.1	Experimental setup .....	47
2.2.2.2	Data analysis .....	51
2.2.3	Measurement of compound toxicity and cell viability .....	54
2.2.3.1	Experimental setup .....	54
2.2.3.2	Data analysis .....	56
<b>3</b>	<b>CHARACTERIZATION OF THE S15V MUTANT OF RAT P2X3 RECEPTOR. 57</b>	
<b>3.1</b>	<b>Introduction .....</b>	<b>57</b>
<b>3.2</b>	<b>Z'-factor for determination of assay quality .....</b>	<b>59</b>
<b>3.3</b>	<b>Potency of standard agonists and antagonists .....</b>	<b>60</b>
3.3.1	Standard agonists.....	60
3.3.2	Standard antagonists .....	62
<b>3.4</b>	<b>Potency of amino- and desaminoanthraquinone derivatives .....</b>	<b>63</b>
3.4.1	Inhibitory potency.....	64
3.4.1.1	Scaffold C, D and E of aminoanthraquinones .....	64
3.4.1.2	Scaffold A and B of aminoanthraquinones .....	68

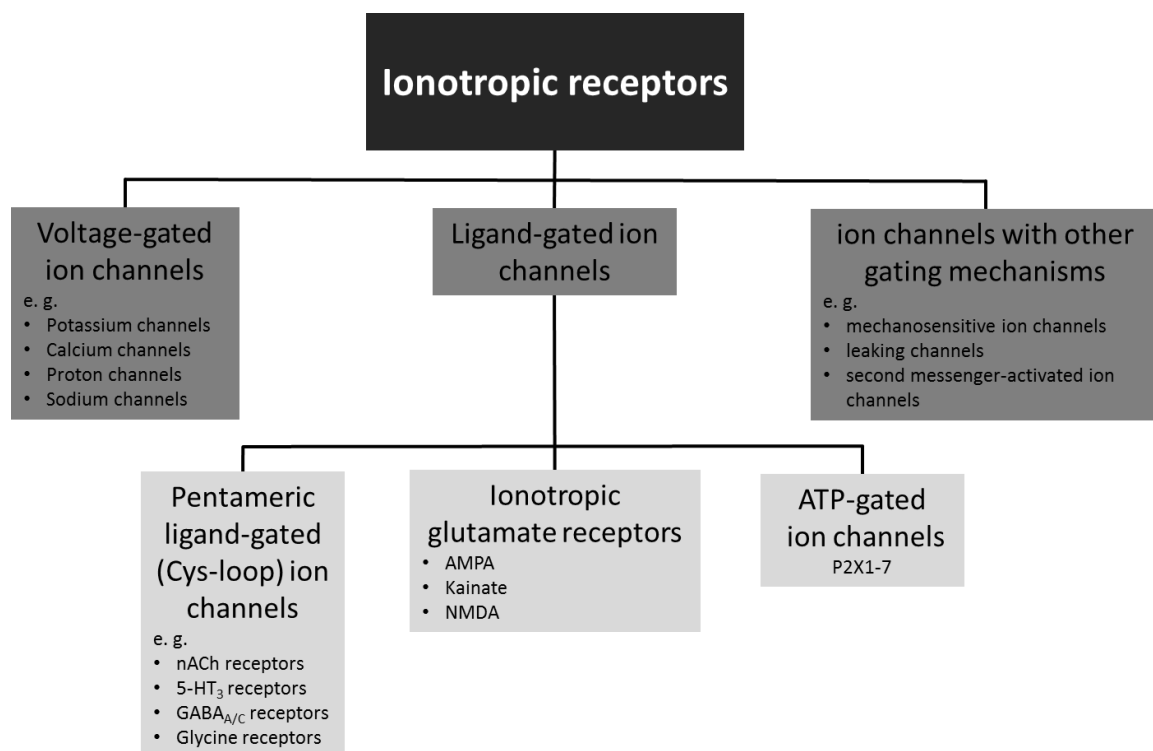
3.4.1.3	Determination of inhibition mechanism .....	71
3.4.1.4	Desaminoanthraquinone derivatives .....	73
3.4.2	Enhancement of ATP potency .....	74
3.4.2.1	Anthraquinone derivatives .....	75
3.4.2.2	Further investigations of enhancement effect of anthraquinone derivatives .....	79
3.4.2.3	Desaminoanthraquinone derivatives .....	85
3.4.3	Cytotoxicity .....	87
3.4.4	Selectivity towards other P2X receptor subtypes .....	88
<b>3.5</b>	<b>Discussion.....</b>	<b>90</b>
<b>4</b>	<b>INHIBITORY POTENCY OF POLYOXOMETALATES AT P2X RECEPTORS ..</b>	<b>93</b>
<b>4.1</b>	<b>Introduction .....</b>	<b>93</b>
<b>4.2</b>	<b>Z'-factor for determination of assay quality .....</b>	<b>98</b>
<b>4.3</b>	<b>Inhibitory potency of polyoxotungstates, vanadates and rhenium clusters at P2X receptors .....</b>	<b>99</b>
4.3.1	Polyoxotungstates .....	99
4.3.2	PEGylated polyoxotungstates.....	104
4.3.3	PEGylated POMs at P2X7.....	106
4.3.4	Rhenium cluster compounds.....	108
4.3.5	Vanadium-based polyoxometalates.....	110
4.3.6	Determination of inhibition mechanism of selected polyoxometalates.....	111
4.3.7	Cytotoxicity of polyoxometalates.....	116
<b>4.4</b>	<b>Discussion.....</b>	<b>118</b>
<b>5</b>	<b>INTERACTION OF APPROVED DRUGS WITH P2X RECEPTORS.....</b>	<b>121</b>
<b>5.1</b>	<b>Introduction .....</b>	<b>121</b>
<b>5.2</b>	<b>Determination of Z'-factor.....</b>	<b>125</b>
<b>5.3</b>	<b>Inhibitory potency of approved drugs at P2X receptors .....</b>	<b>125</b>
5.3.1	Screening .....	125
5.3.1.1	Steroids.....	127
5.3.1.2	Tricyclic antidepressants and phenothiazines.....	132
5.3.1.3	Imidazole-containing antifungal drugs.....	134

5.3.1.4	Butyrophenones.....	136
5.3.1.5	Thyroid hormones and related drugs .....	138
5.3.1.6	Bisphosphonates.....	139
5.3.1.7	Various screening hits without structural relation .....	140
5.3.2	Structure-activity-relationships of bisacodyl and niclosamide derivatives .....	149
5.3.2.1	Bisacodyl derivatives.....	150
5.3.2.2	Niclosamide derivatives .....	152
5.3.2.3	Selectivity of niclosamide derivatives .....	159
5.3.3	Determination of inhibition mechanism at P2X3 and P2X7 receptors.....	160
<b>5.4</b>	<b>Enhancement of maximal ATP effect .....</b>	<b>164</b>
5.4.1	ATP concentrations used for receptor stimulation.....	164
5.4.2	Enhancing hits at the rat P2X3 receptor .....	165
5.4.3	Enhancing hits at the human P2X7 receptor .....	169
<b>5.5</b>	<b>Discussion.....</b>	<b>176</b>
<b>6</b>	<b>SUMMARY.....</b>	<b>182</b>
<b>7</b>	<b>CONCLUSION AND OUTLOOK.....</b>	<b>193</b>
<b>8</b>	<b>REFERENCE LIST .....</b>	<b>194</b>
	<b>ABBREVIATIONS.....</b>	<b>223</b>
	<b>DANKSAGUNG .....</b>	<b>227</b>
	<b>PUBLICATION LIST.....</b>	<b>229</b>

# 1 General Introduction

## 1.1 The ionotropic receptor family

Ionotropic receptors play a substantial role in signal transmission in nerves, muscles and synapses. These membrane-located excitable elements are proteins capable of forming a pore through which ions can flow across either plasma membranes or membranes of intracellularly located organelles. The ion flow follows the concentration gradient, and can reach a very fast flow rate (e. g. 10 million ions/s at the acetylcholine receptor).<sup>1</sup> Ionotropic channels can be subdivided into different classes based on their regulatory mechanisms. The two most prominent subfamilies are voltage-gated ion channels, which are regulated by changes in voltage, and ligand-gated ion channels, which are controlled by chemical transmitters (see Figure 1.1).



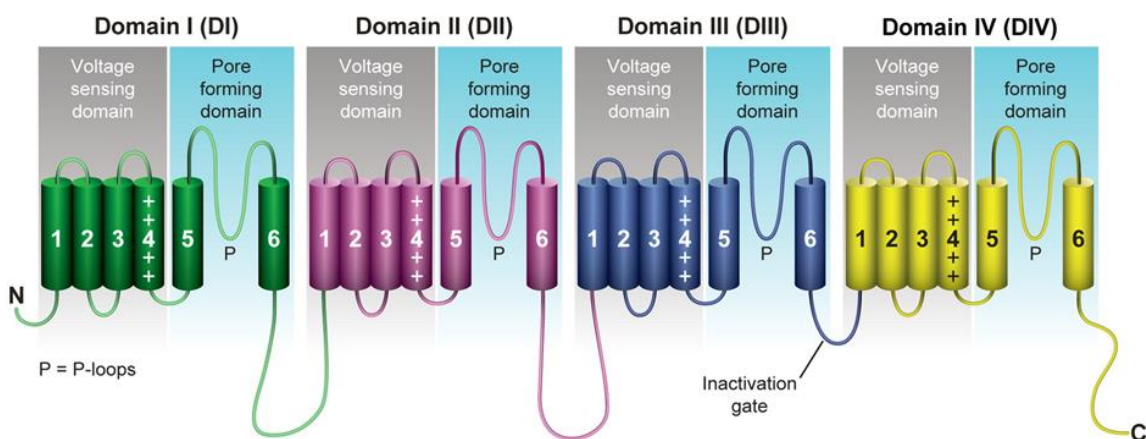
**Figure 1.1:** Overview of the different subclasses of ionotropic receptors and their subtypes.<sup>2-6</sup>

Other ion channels are opened for example after mechanic stimuli, by second messengers, changes in temperature or by light. Mechanotransduction is the conversion of mechanical forces into biochemical signals. It plays a very important role in the sensation of touch, hearing and

pain. Very prominent examples are the Piezo channels Piezo1 and Piezo2, which were identified in 2010 in mouse as ion channels which open in response to pressure via a piezo-electrically driven glass probe.<sup>7</sup> The classification of mechanically activated ion channels is difficult, because a lot of different cellular structures are involved in the process of mechanotransduction, and the representative structures often do not only respond to mechanical forces but also to other stimuli. Furthermore, predictable models of probable candidates like the Piezo channels indicate them to be very large proteins with 30 to 40 transmembrane domains. This topology lacks similarity to known ion channels, which are generally much smaller, as will be discussed in more detail further on.<sup>2</sup>

Leaking ion channel is a term used for voltage-independent ion channels which allow ion trespass across membranes at normal resting potential. An example for this type of ion channel is the sodium leaking channel NALCN, which was discovered 1999 in rodents.<sup>8</sup> It is reported to have high structural similarity to voltage-gated sodium and calcium channels, but is not susceptible to depolarization signals. Additionally, the channel activity is regulated by second messenger activity such as acetylcholine via muscarinic acetylcholine receptors.<sup>9</sup> Therefore, the NALCN is an example for the capability of being activated by different stimuli.

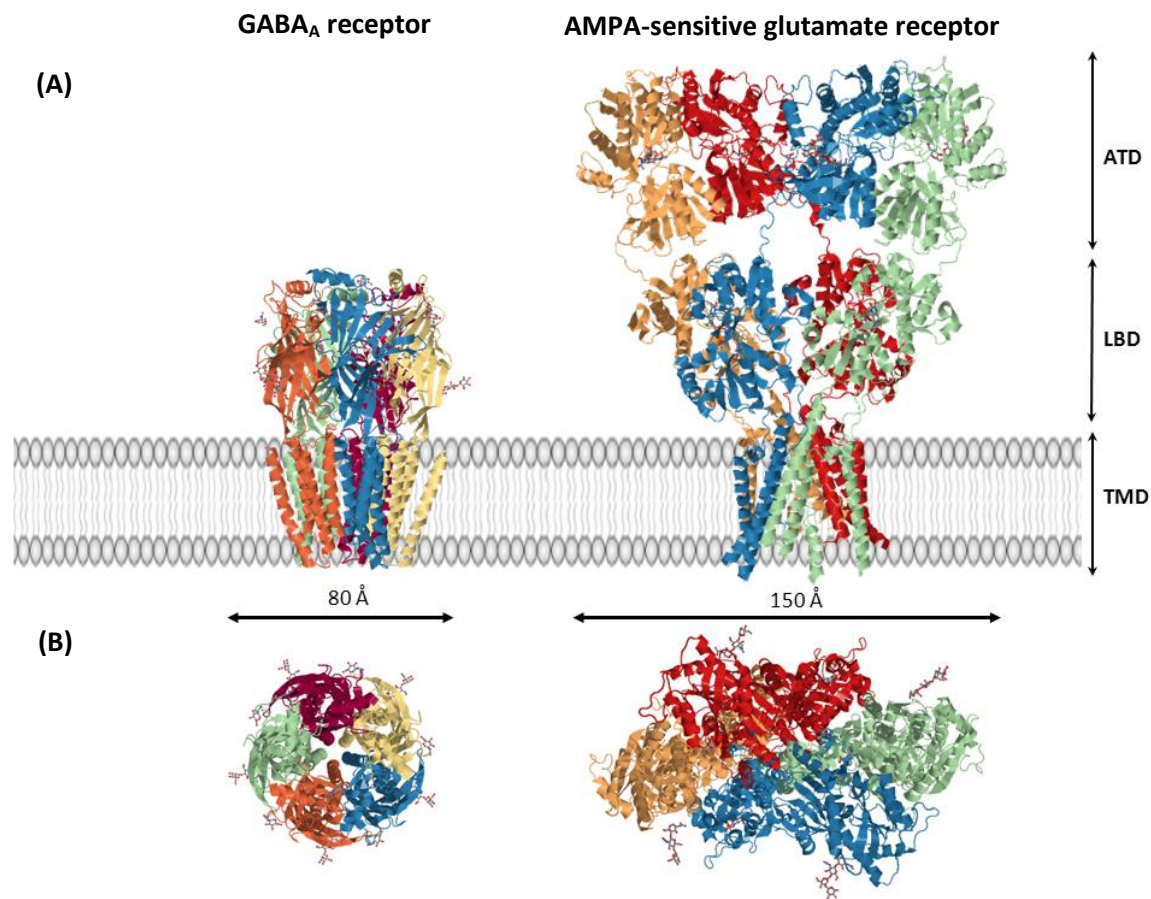
The two most prominent ones of those subfamilies are voltage-gated (VGICs) and ligand-gated ion channels (LGICs). VGICs are switched from closed to open state by changes in membrane potential. The first successfully cloned and sequenced VGICs were the voltage-gated Na<sup>+</sup> channel (VGNC) from electroplax of *Electrophorus electricus*,<sup>10</sup> the voltage-gated Ca<sup>2+</sup> channel (VGCC) from rabbit skeletal muscle<sup>11</sup> and the voltage-gated K<sup>+</sup> channel (VGKC) from *Drosophila*.<sup>12</sup> Primary sequence analysis revealed VGNCs and VGCCs to be built by a single peptide ( $\alpha$ -subunit) comprised of four homologous domains linked by three extra- and intracellular loops (see Figure 1.2).



**Figure 1.2:** Topology of the human sodium channel  $\alpha$ -subunits.<sup>13</sup>

The gating mechanism and general structure were confirmed by crystallization of the voltage-gated sodium channel from *Arcobacter butzleri* (NavAb) in its closed state.<sup>14</sup> Each of the four domains contains six transmembrane helical segments (TM) named S1 to S6, and can be subdivided into two parts, the voltage-sensing domain (VSD), reaching from S1 to S4, and the pore-forming domain, containing S5, S6 and its large amphiphilic extracellular loop (P-loop). The pore-forming domain is responsible for the selective permeability of ions through the cell membrane, while the VSD is involved in the regulation of channel opening upon membrane depolarization. All four domains are arranged in a pseudo-tetrameric fashion with the four pore-forming domains building the ion passing pore. The most important feature in the VSD is S4, containing positively charged arginine and lysine residues roughly in every third position. It is suggested that in the case of membrane depolarization, those positively charged residues of the S4 domain are displaced towards the extracellular surface. This initiates a conformational change which is transferred to the pore-forming domains, resulting in the opening of the channel pore. This process is reversed upon membrane repolarization. The missing current sensitivity of leaking channels despite high structural similarity is attributed to a reduced number of positively charged amino acids in the S4 domain. During the depolarization state, the channel enters a state of inactivation. No matter how high the electrical stimulus, the channel is not capable of opening during this refractory period, due to the inactivation gate of the channel folding inside the pore. When normal membrane potential is restored and the sensory domain reaches its resting position, the channel's opening capability is restored.<sup>13, 15</sup>

Ligand-gated ion channels represent the second largest subfamily of ionotropic receptors. In contrast to voltage-gated ion channels, the opening of the channel pore is not linked to a change of the membrane potential but to the interaction of specific ligands, in most cases neurotransmitters, with their respective orthosteric site in the receptor protein. The binding of the ligand induces a conformational change leading to the opening of the pore. The resulting ion flow in VGIC is driven by the electrochemical gradient. Many LGIC can be found in the central nervous system, where they manage fast transmission between single cells. LGIC can roughly be divided into three different subclasses, the pentameric or Cys-loop ion channels, the tetrameric ionotropic glutamate receptors and the trimeric purinergic P2X receptors. The pentameric ion channels are the largest group of the three, including very prominent agents such as the nicotinic acetylcholine receptor (nACh), the 5-hydroxytryptamine receptor subtype 3 (5-HT<sub>3</sub>) and the  $\gamma$ -aminobutyric acid receptor subtype A (GABA<sub>A</sub>, see Figure 1.1).



**Figure 1.3:** Crystal structures of the human GABA<sub>A</sub>-beta3 homopentameric receptor (PDB code 4COF) bound to the agonist benzamidine at 2.97 Å resolution and the AMPA-sensitive homomeric rat glutamate A2 receptor (PDB code 3KG2) in complex with the competitive antagonist ZK200775 at 3.6 Å resolution viewed (A) parallel to the membrane and (B) from a perpendicular point of view. Structures are presented as cartoon diagram with each single subunit colored differently.<sup>16-18</sup>

The more common term Cys-loop ion channels is based on the presence of a large loop formed by disulfide-bridged cysteine residues in the extracellular domain. The crystal structure of the human GABA<sub>A</sub> receptor is presented as an example in Figure 1.3. A functional receptor protein is built of five identical or different subunits arranged perpendicular to the membrane. The N-terminus of one single subunit is located extracellularly and contains around 200 amino acids. It is followed by three transmembrane domains named M1 to M3, and an extracellular loop bearing high divergence in size and amino acid sequence, mainly folded as β-sandwich sheets. The C-terminus is located extracellularly, and is preceded by a fourth transmembrane helix (M4). The ion channel pore is built by an inner ring of the second transmembrane domains M2 of each subunit. It is surrounded by an outer ring of 15 α-helices, the M1, M3 and M4 segments of all five subtypes, which separate the inner ring from the membrane. The amino acids of the M2 domain are highly homologous, remitting in an arrangement of each identical residue in form of



concentric rings. They are involved in the ion selectivity filter among other things. The center of the pore contains a ring of leucine and is maximally constricted due to hydrophobic interactions between neighboring helices, hindering ions from passing through. The binding of agonist induces a tilting movement of the upper sections of the M2 domains to the outward that results in a separation of the helices at midpoint, and opens the channel pore. The number of agonist binding sites varies between 2 to 5 depending on the receptor and its stoichiometry. They are localized in the extracellular loop, usually at the interface between adjacent extracellular domains of two subunits. The number of occupied binding pockets necessary for full channel opening depends on subtype and heterogeneity, e. g. the heteromeric muscle nACh receptor needs occupation of its both agonist binding sites for full efficacy.<sup>4, 19</sup>

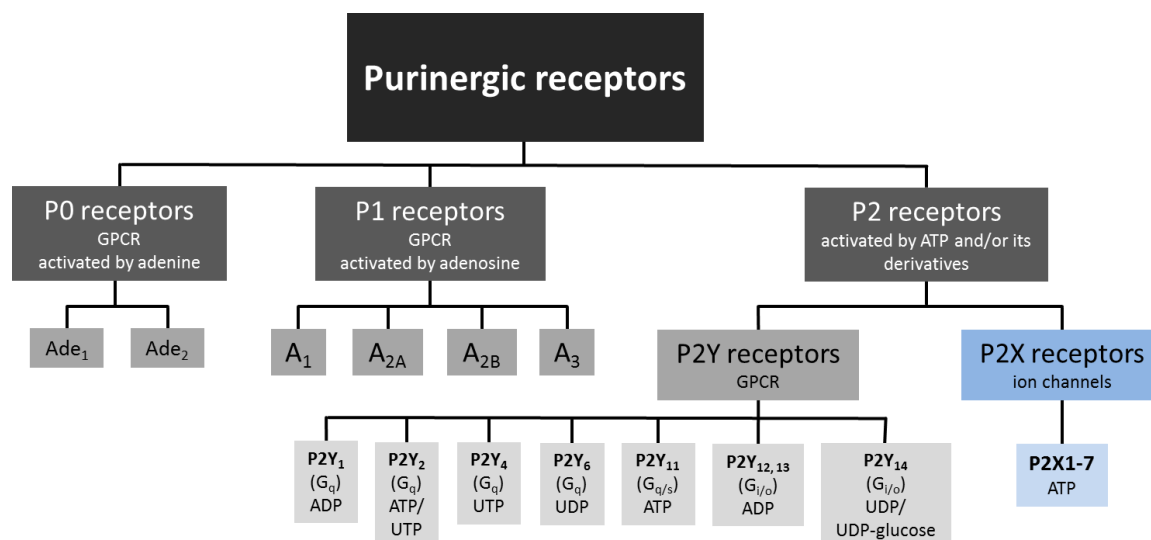
The second subclass of ligand-gated ion channels is the group of ionotropic glutamate receptors. Glutamate is the most important excitatory neurotransmitter in the central nervous system. The respective ion channel receptors can be further subdivided into three classes:  $\alpha$ -amino-3-hydroxy-5-methyl-4-isoxazolepropionic acid (AMPA), mainly permeable for sodium or calcium ions, depending on the stoichiometry, kainic acid (KA) and N-methyl-D-aspartate (NMDA), permeable for calcium.<sup>20</sup> The crystal structure of the rat AMPA glutamate receptor is presented in Figure 1.3. The structure of all three subclasses is quite similar, despite their kinetic and pharmacological differences. The most detailed information results from the X-ray crystal structure of the rodent AMPA receptor.<sup>17</sup> All subtypes assemble as tetrameric proteins of various stoichiometry. Only AMPA and selective kainate subtypes are forming homomers. The large extracellular amino terminal domain (ATD) includes the N-terminus and is followed by a ligand-binding domain (LBD). The LBD contains the binding sites for agonists and antagonists and a transmembrane domain (TMD). The latter forms the actual ion channel. The AMPA receptor is much larger than the pentameric Cys-loop or the P2X receptors (see Figure 1.3). The tetrameric structure is kept together by the strong interactions in the TMD compartment, interactions between the front and back LBD subunits and interactions between the left and right ATD compartments. The channel opening is initiated by the binding of the agonist, in this case glutamate, to the LBD, which induces a conformational change. The TMD is built of three complete and one half  $\alpha$ -helices of each subunit. The second transmembrane domain M2 of each subunit does not cross the membrane completely but folds back to the intracellular side of the receptor, thus forming the ion channel gate. Like many excitatory channels, glutamate receptors are prone to desensitization in the continuous presence of agonist to protect neurons from excessive excitation.<sup>5</sup>

ATP-gated ion channels, the P2X receptors, represent the third group of ligand-gated ion channels. Since the whole subfamily of P2X receptors is the main focus of this project, all subtypes are introduced comprehensively in the following chapter.

## 1.2 Purinergic receptors

### 1.2.1 P0, P1 and P2 receptors

The story of purinergic signaling started in 1929, when Karl Lohman first isolated and identified pyrophosphoric acid and adenosine phosphates in fasciated muscle tissue.<sup>21</sup> For a long time, ATP was considered to only be the main form of energy transfer inside living organisms, despite early hints of intracellular signal transduction processes induced by extracellular exposure to purine nucleotides.<sup>22</sup> In 1972, Geoffrey Burnstock published evidence of ATP also acting as a cotransmitter in almost all nerves of the central and peripheral nervous system.<sup>23</sup> ATP-mediated transmission was termed as “purinergic signaling”, and the first two classes of purine activated receptors, P1 and P2, were identified.<sup>24</sup> The classification was based on the different activities of purine derivatives ATP, ADP, AMP, adenosine and methylxanthines like caffeine on the respective receptor subtypes and effects on second messenger systems, especially the adenylate cyclase.<sup>25</sup>



**Figure 1.4:** Classification of purinergic receptors and their endogenous agonists.

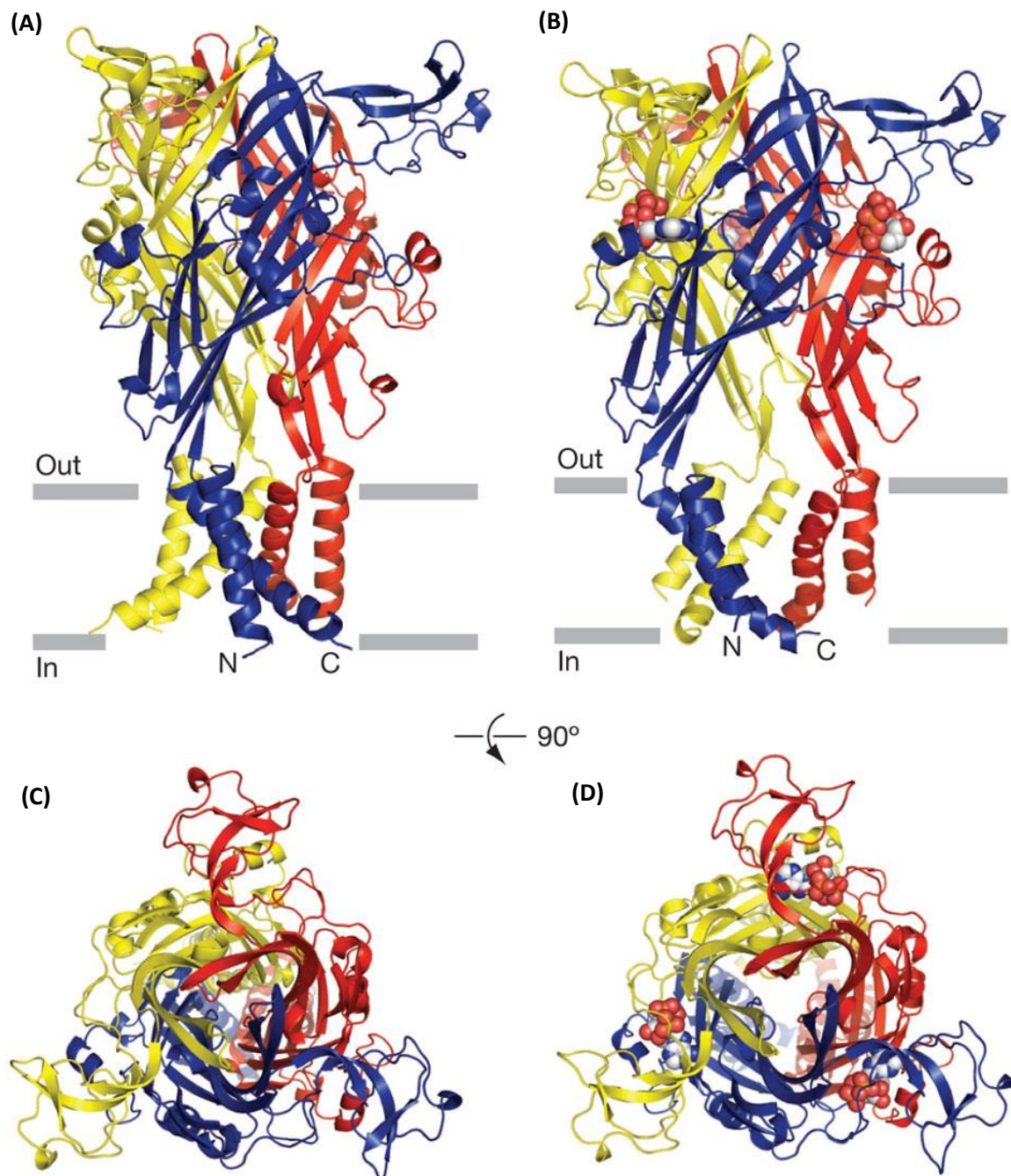
Figure 1.4 illustrates all known purinergic receptor subtypes. P0 represent the youngest class of purinergic receptors with the recently discovered Ade<sub>1</sub> and Ade<sub>2</sub> receptors, both G-protein-coupled and activated by the purine base adenine.<sup>26</sup> P1 receptors are G-protein-coupled receptors and comprise four subtypes A<sub>1</sub>, A<sub>2A</sub>, A<sub>2B</sub> and A<sub>3</sub>, all activated by adenosine. The P2 class is further subdivided in ion channel P2X receptors, all activated by ATP,<sup>27, 28</sup> and GPCR P2Y receptors activated by ATP, ADP, UTP, UDP or UDP-glucose. Eight P2Y subtypes (P2Y<sub>1</sub>, P2Y<sub>2</sub>, P2Y<sub>4</sub>, P2Y<sub>6</sub> and P2Y<sub>11-14</sub>) are known, distinguishable (i) by the G-protein coupled to the receptor and therefore the effect on the associated second messenger system and (ii) the respective endogenous agonist.<sup>25, 29, 30</sup>

### 1.2.2 P2X receptors

P2X receptors are the only non-GPCR subclass in the purinergic receptor family. They are expressed ubiquitously in the whole body, but particularly in the central nervous system and in microglia cells, vas deferens, bladder, smooth muscle cells and pain sensing neurons.<sup>31-35</sup> P2X receptors have been a central focus of research for a long time. Very particular interest lies in their occurrence in fast conducting excitatory neurons and their influence on the immune system and coagulation.<sup>36, 37</sup>

### 1.2.3 P2X receptor topology

The ATP-gated P2X receptors are the third main LGIC subfamily next to the pentameric Cys-loop channels and the tetrameric ionotropic glutamate receptors.<sup>6</sup> Seven different subtypes have been identified. Their size lies between 384 (P2X4) and 595 (P2X7) amino acids.<sup>38</sup> The tertiary structure of one subunit is composed of two hydrophobic transmembrane domains, positioning both N- and C-terminus intracellularly, and a large extracellular domain, containing ten highly conserved cysteine residues forming five disulfide bonds, 14 glycine residues, two to six potential glycosylation sites and the ATP binding sites. The binding of the agonist causes a conformational change that opens the ion pore and enables the flow of Ca<sup>2+</sup>, Na<sup>+</sup> and K<sup>+</sup> across the membrane.<sup>39</sup> All P2X receptor subtypes except P2X7 enter a desensitized state upon prolonged exposure to the physiological agonist ATP, meaning that the receptor is temporarily unable to open despite the binding of the agonist. The kinetics of desensitization depends on the P2X receptor subtype. While P2X1 and P2X3 desensitize very rapidly, the process is noticeably slower for the remaining subtypes.<sup>35, 40, 41</sup>

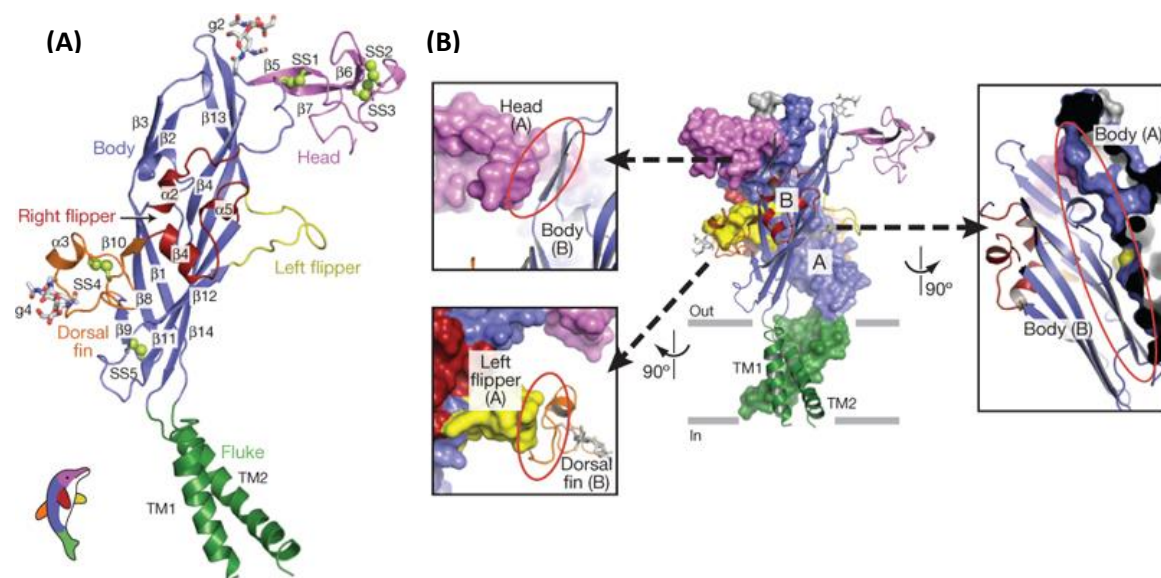


**Figure 1.5:** Crystal structure of the homomeric truncated zebrafish P2X4 receptor in (A, C) its closed and (B, D) its open state while bound to ATP, viewed (A, B) parallel to the membrane and (C, D) from the extracellular site. Each single subunit is highlighted in a different color (blue, yellow, red).<sup>42</sup>

Most information about the molecular architecture of P2X receptor stems from the crystal structure of the zebrafish P2X4 receptor (zfP2X4) in its closed and its open state.<sup>42, 43</sup> Both confirmed the previously proposed trimeric assembly.<sup>44, 45</sup> Homomeric receptors contain three subunits of the same type, receptor heteromers contain two different subunits in various

stoichiometry.<sup>46</sup> The crystal structure allows the detailed molecular analysis of the three-dimensional shape of one subunit itself and the fully assembled functional receptor.

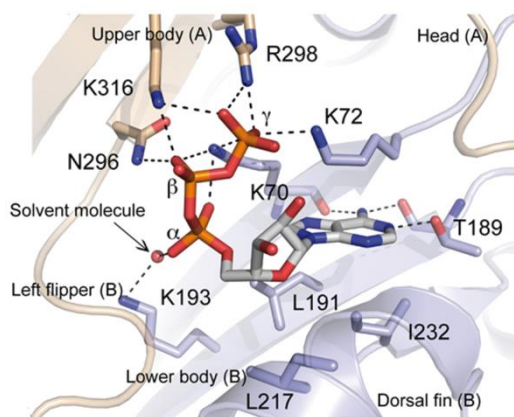
Kawate et al. crystallized the truncated homomeric zfP2X4 receptor in 2009 at a 3.1 Å resolution in its closed resting state with no bound antagonist.<sup>43</sup> The receptor is shaped like a chalice with a large hydrophilic and glycosylated extracellular domain about 70 Å above and the transmembrane domains spanning roughly 28 Å through the membrane (see Figure 1.5). The transmembrane ion channel pore is composed of six  $\alpha$ -helices. Each subunit contributes two  $\alpha$ -helices, both in antiparallel orientation towards each other and angled in an approximately 45° angle from the membrane axis. The three TM2 helices are oriented inwards, building the pore restriction in the closed resting state of the receptor, surrounded by the TM1 helices in a peripheral ring. The shape of one single subunit of one receptor is compared to a dolphin (see Figure 1.6), with transmembrane domains posing as the flukes and the extracellular region as the upper body domain. The core domain of the upper body contains two  $\beta$ -sheets, tightly knit together by strong interactions and therefore determining the high rigidity of the upper region. The body domain is augmented by the head domain, the dorsal fin and right and left flipper. The head domain contains three  $\beta$  strands and one  $\alpha$ -helix. All three are mainly involved in the subunit-subunit-interface, along with the body domain.



**Figure 1.6:** (A) Fold of one single and (B) intersubunit contacts of two zebrafish P2X4 subunits named A and B. The shape is compared to a dolphin.  $\alpha$ -Helices (TM1 and 2,  $\alpha$ 2-5),  $\beta$ -sheets ( $\beta$ 1-14), disulfide bonds (SS1-5) and glycosylation sites (g2 and g4) are indicated.<sup>43</sup>

Several mutagenesis studies, e. g. cysteine scanning mutagenesis, identified amino acid residues crucial for channel opening.<sup>47-52</sup> Polar, aromatic and positively and negatively charged residues in the proposed ATP binding pocket and its immediate vicinity were exchanged. It was assumed that  $Mg^{2+}$  forms a complex with ATP, leading to the postulation that negatively charged amino acids like aspartate or glutamate could also contribute to ATP recognition by P2X receptors.<sup>53</sup> This could not be confirmed, making ATP in its fully negatively charged state the primary ionic form to activate P2X receptors.<sup>54, 55</sup>

The ATP-binding sites were predicted to be located in the extracellular domain, about 45 Å from the ion channel domain, between two subunit interfaces. Every functional receptor contains three binding sites.<sup>47, 49-51, 56, 57</sup> It was assumed that highly conserved positively charged amino acids following the pattern of a so-called Walker motif [GxxxxGKT] are involved in ATP recognition.<sup>47</sup> This motif was previously identified in several other ATP-binding proteins.<sup>58</sup> Hattori et al. confirmed the postulated location by the successful crystallization of the zFP2X4 receptor in its open state bound to ATP at 2.8 Å resolution, but identified a binding motif completely different from the Walker motif.<sup>42, 55</sup>

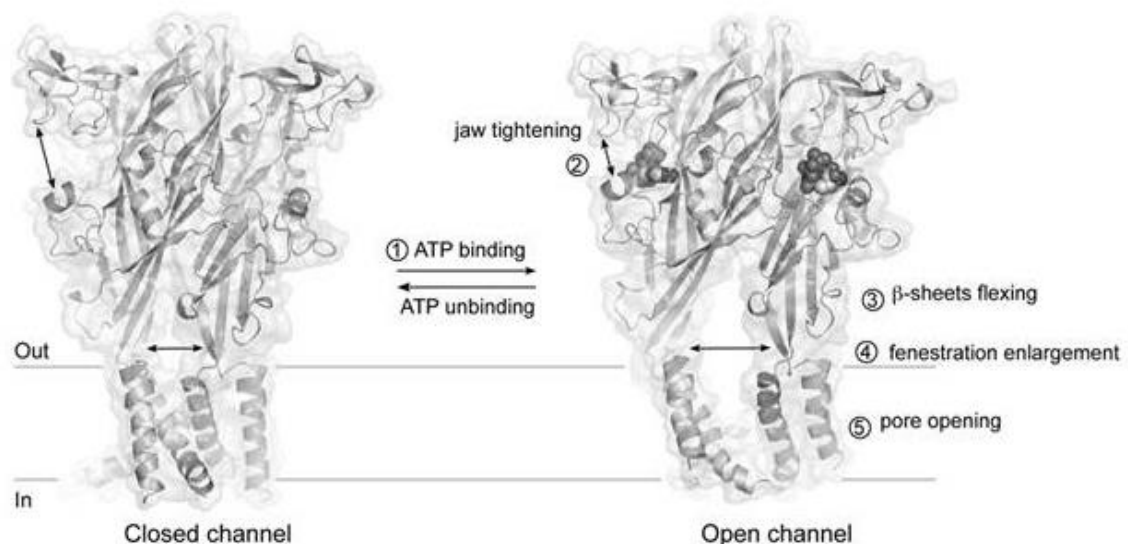


**Figure 1.7:** Close-up view of the ATP-binding site with bound ATP. The glycerol (solvent) molecule involved in the recognition of the  $\alpha$ -phosphate by K193 is shown as a red sphere. Hydrogen bonding is indicated by black dashed lines.<sup>55</sup>

The pocket consists of the head domain, upper body chain and left flipper of one subunit and the lower body and the dorsal fin of the second domain, respectively. Figure 1.7 illustrates the exact binding conformation of ATP and the strictly conserved amino acids participating in ATP recognition. ATP adopts a U-shape, with the  $\beta$ - and  $\gamma$ -phosphate residues orientated towards the adenine ring. The base is buried head first into the binding pocket and the phosphate chain is oriented towards the outer surface. This conformation allows the intensive interaction of the negatively charged

phosphate groups with positively charged amino acid residues lining the binding pocket. The most important residue in ATP recognition is Lys70 (K70) of the lower body of the second subunit. It resides in the center of the triphosphate U-shape and interacts with all three phosphates by the formation of salt bridges and intensive hydrogen bonding. The  $\beta$ -phosphate residue additionally interacts with Asn296 (N296) and Lys316 (K316) of the upper body domain of the first subunit. The latter also participates in interactions with the  $\gamma$ -phosphate, together

with Lys72 (K72) of the second subunit and Arg298 (R298) of the first subunit. Both lysine residues K70 and K72 were identified as the highly conserved crucial binding motif in ATP recognition prior to the crystal structure, and confirmed in other P2X receptors in humans and rodents.<sup>48, 59-61</sup> The  $\alpha$ -phosphate was found to interact with Lys193 of the lower body domain of the second chain via a bridging molecule (glycerol in the crystal structure), that is suggested to be replaced by several water molecules under physiological conditions. The adenine base buried deep into the pocket is recognized by Thr189 (T189) and Lys70 (K70) of the lower body domain of the second subunit by the formation of hydrogen bonds with the side chains and the main carbonyl structures, respectively. Leu191 (L191) of the lower body domain and Ile232 (I232) of the dorsal fin of the second subunit additionally fix the adenine ring by hydrophobic interactions. The lack of activity of ADP and AMP at P2X receptors is explained by the insufficient interaction due to the shortened phosphate side chain, therefore weakening the bonding to the receptor.

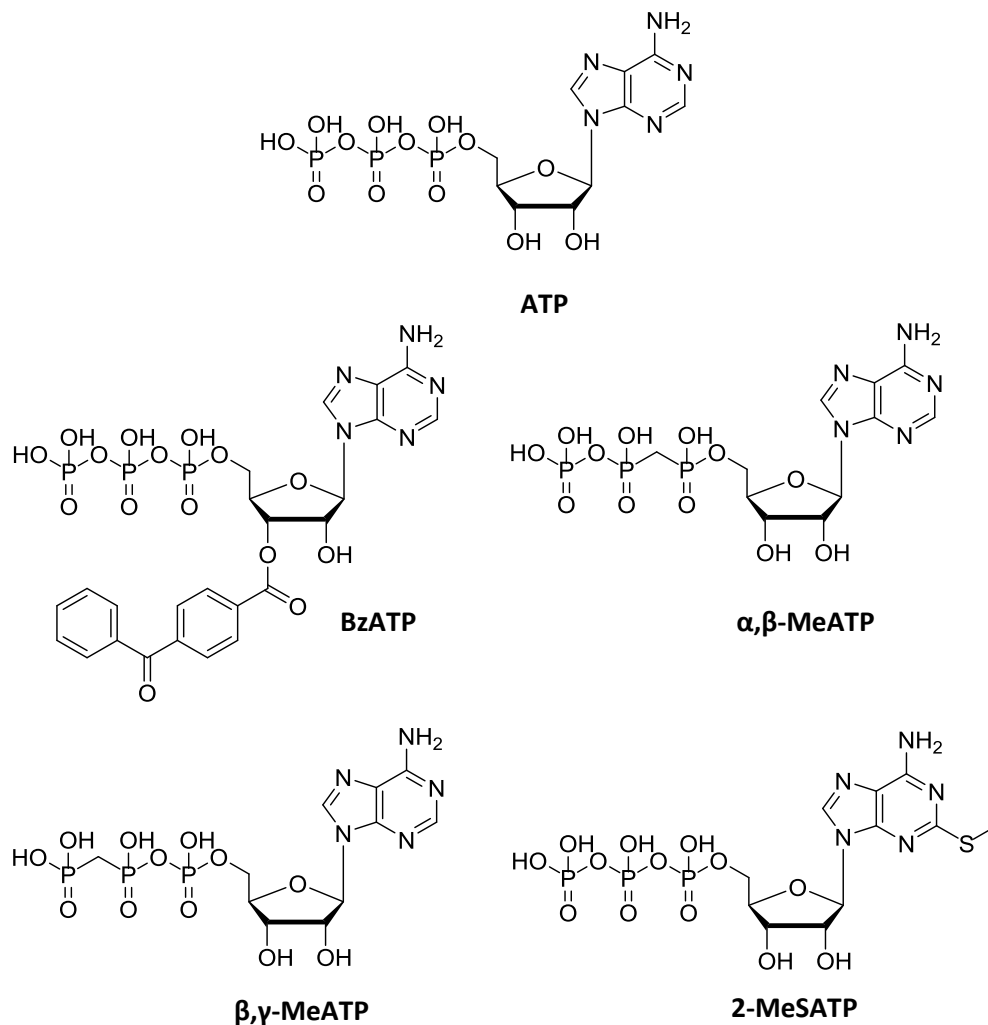


**Figure 1.8:** Reasonable mechanism of ATP-gated activation of the zebrafish P2X4 receptor. Sequential steps 1 to 5 are indicated.<sup>55</sup>

The ATP binding induces an upper movement of the dorsal fin closer to the head domain and an outward movement of the left flipper. Due to the shape, it is often referred to as jaw tightening. Since both are coupled to the lower body domain, the movement is transferred and the whole lower body domain is flexed in an outward direction due to the rigidity of the contained  $\beta$ -sheets. The connected TM domains are moved as well, widening the fenestrations and thus opening the ion channel pore (see Figure 1.8) allowing ions like  $\text{Na}^+$ ,  $\text{K}^+$  and  $\text{Ca}^{2+}$  to pass through.

### 1.2.4 P2X receptors – standard agonists

Several derivatives of the physiological agonist ATP are also potent agonists at P2X receptors. The structures can be seen in Figure 1.9. EC<sub>50</sub> values for all functional homomeric P2X receptor subtypes are summarized in Table 1.1.



**Figure 1.9:** Structures of standard P2X receptor agonists.

A very prominent feature is the relatively weak potency of the physiological agonist ATP at the homomeric P2X<sub>7</sub> receptor, especially in comparison to the much higher activity of the ATP analog BzATP. The lacking activity of the methylene-swapped derivatives α,β- and β,γ-meATP at several subtypes indicate the importance of the phosphate side chain in agonist binding and recognition.



**Table 1.1:** EC<sub>50</sub> and IC<sub>50</sub> concentrations of standard agonists and antagonists at homomeric P2X receptors. Data are presented as mean ± SEM.<sup>28, 40, 62-70</sup>

	EC <sub>50</sub> [μM]					
	P2X1	P2X2	P2X3	P2X4	P2X5	P2X7
ATP	0.1-0.7	2-8	1.2-4.1	1-10	0.5-4	2000-4000
BzATP	0.7-24	6-30	0.04-0.08	3	1-6	10
α,β-meATP	0.1-1	> 100	1-2	4-300	1-12	> 300
β,γ-meATP	2	> 300	> 300	> 300	10	> 300
2-meSATP	0.1-1	1	0.3	10-100	0.5	200

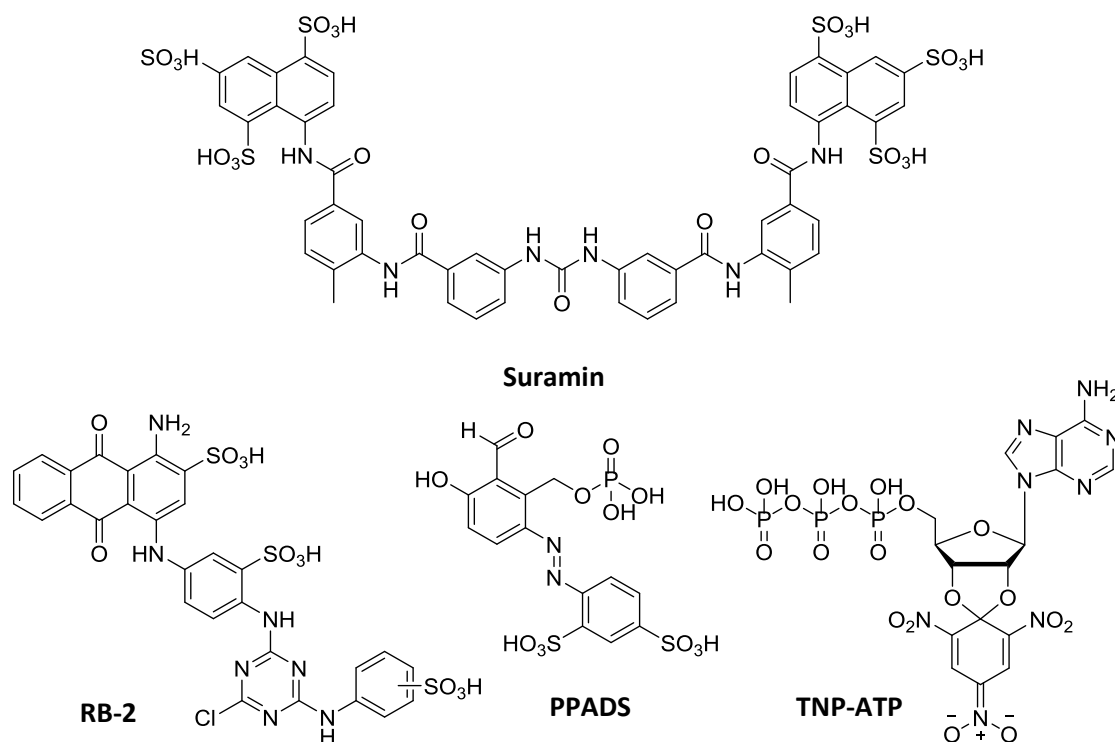
	IC <sub>50</sub> [μM] or EC <sub>50</sub> Enhancement [μM]*, respectively					
Suramin	1-2	10	3	> 300	2-3	> 300
RB-2	9-36	0.5	1.4 <sup>a, b</sup>	3 <sup>a</sup>	18.3	4.3
TNP-ATP	0.006	2	0.001	1-15	0.6-0.7	> 30 μM
PPADS	1	1-3	1.5	> 300	0.2-0.6	10-45

<sup>a</sup>: EC<sub>50</sub>Enhancement of positive allosteric modulation at the respective receptor

<sup>b</sup>: Enhancement only by the *ortho*-isomer (Cibacron Blue 3GA)

### 1.2.5 P2X receptors – standard antagonists

Early on, several weak, non-selective, nucleotide and non-nucleotide antagonists of P2X receptors were discovered. Anthraquinone- and ATP-derived structures are presented in Figure 1.10 and Table 1.1.



**Figure 1.10:** Structures of standard P2X receptor antagonists.

Those compounds are not selective for any of the P2X receptors and show weak to potent inhibitory activity. The large polysulfonated suramin is capable of inhibiting not only P2X and P2Y receptors, but also G-proteins and various proteases including the HIV reverse transcriptase.<sup>71, 72</sup> Suramin, PPADS and RB-2 represent lead structures for the development of further potent P2X receptor inhibitors, which is discussed in more detail in chapter 3.1.

### 1.2.6 The P2X1 receptor subtype

The P2X1 receptor is particularly expressed in smooth muscle and blood cells. It plays a major role in the control of urinary tract and bladder function, of vasoconstriction, platelet aggregation and regulation of vas deferens.<sup>36, 73-78</sup> The receptor was first cloned from rodent vas deferens and expressed in *Xenopus* oocytes in 1994, and was identified to be 399 amino acids long.<sup>79</sup>

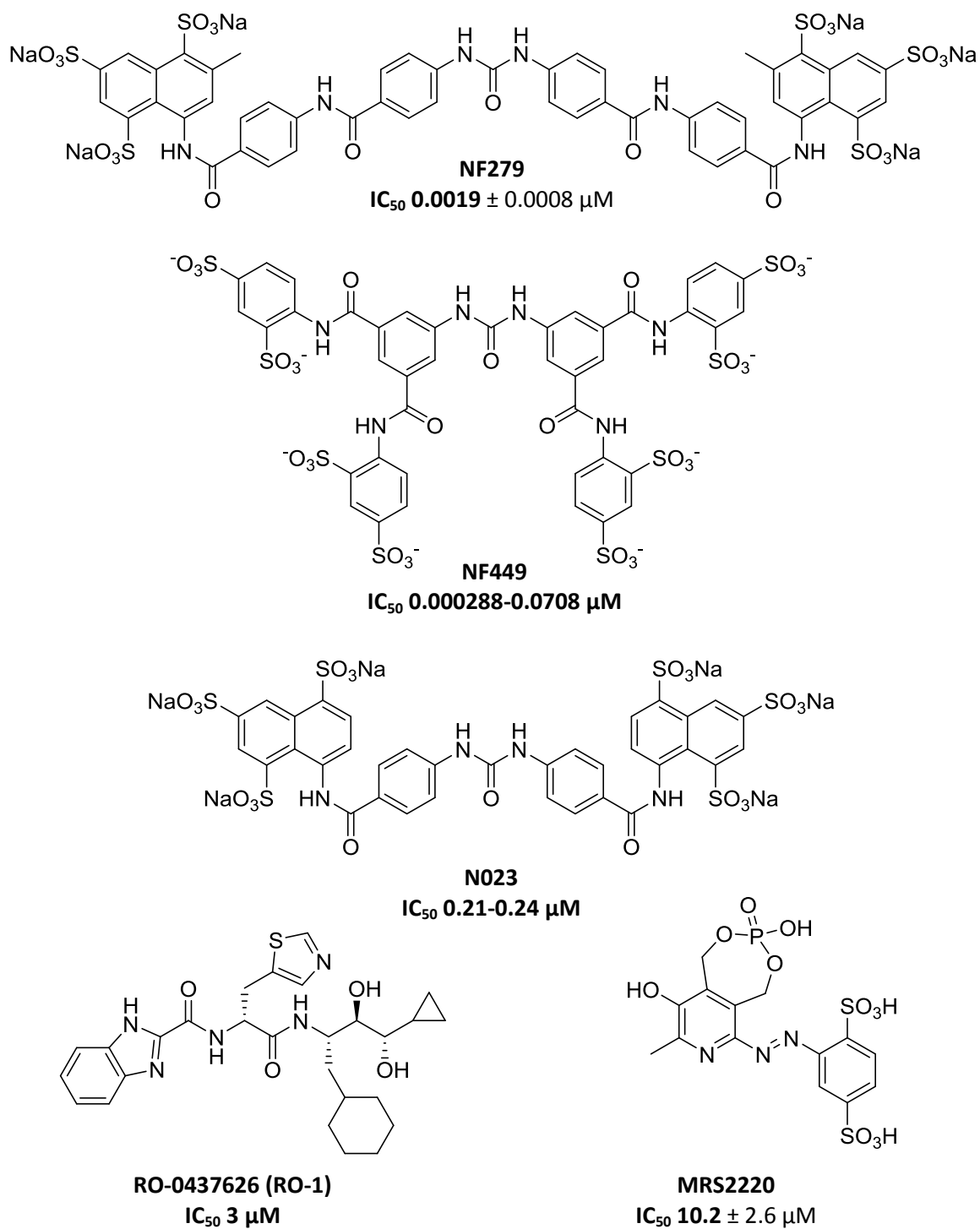
The physiological agonist at the P2X1 receptor is ATP. Its activity at the homomeric receptor is comparable to the synthetic ATP analog  $\alpha,\beta$ -meATP (see Table 1.1). Upon agonist stimulation, the channel opens only for milliseconds. Simultaneously, a rapid desensitization of the receptor is observed, when agonist stimulation occurs longer than a few hundred milliseconds and the applied agonist concentration is higher than 1  $\mu$ M.<sup>38</sup> This process can be reversed, but resensitization takes much longer. Upon repeated agonist application in less than 10-minute intervals, the responsive currents are getting progressively smaller, and receptor internalization can be detected.<sup>28, 79, 80</sup> These features influence the functional effects of ATP. In the human leukemia cell line HL60, P2X1 receptor expression could be observed, but measurable currents were only observed after pretreatment with apyrase. This phenomenon was ascribed to high extracellular ATP concentrations, caused by constant release by adjacent cells and leading to continuous desensitization of the P2X1 receptor. Apyrase cleaves the extracellular ATP, leading to resensitization.<sup>81</sup> Similar effects can be observed concerning receptor internalization. The receptor reappears in the extracellular membrane when the extracellular ATP concentration is diminished.<sup>80</sup> The desensitization can be reversed by introducing parts of the slow desensitizing P2X2 receptor into the structure of the P2X1 subunit, yielding receptor chimeras. This was detected using mutagenesis experiments to exchange the extracellular loop, one or both transmembrane domains as well as N- and C-terminus, respectively. Four variant amino acids located immediately before TM1, 20RMNL23, were identified to play a particular role in desensitization. When swapped to the respective P2X2 receptor sequence, desensitization slowed significantly.<sup>82</sup> The exchange of the N-domain to the respective P2X2 receptor part diminished receptor desensitization from  $90 \pm 1\%$  to  $2 \pm 0.3\%$  during 10 second application of

ATP 100  $\mu$ M. The respective C-domain exchange rendered a non-functional channel.<sup>83</sup> Site-directed mutagenesis and molecular modeling experiments at the P2X1 receptor formed a large part in structural elucidation of P2X receptor assembling and function, which could be proven by the two successful crystal structures (see chapter 1.2.2).<sup>47, 52, 60, 84</sup>

The rapid desensitization occurs milliseconds after exposure to agonist and aggravates experimental characterization of the P2X1 receptor. In order to stabilize the receptor and enable functional experiments like measurement of calcium influx without influencing binding properties of the receptor, the whole first transmembrane domain including the N-terminal region of the human P2X1 receptor was exchanged to the respective part of the P2X2 receptor by PD Dr. Anke Schiedel in our lab. The mutant was then retrovirally transfected in 1321N1 astrocytoma cells by Dr. Aliaa Abdelrahman, rendering a cell line stably expressing the human P2X1-2 chimera. In previous experiments, only the transmembrane parts or the respective termini were replaced, not the complete domain with the attached terminus.<sup>82, 83</sup> We replaced the complete first transmembrane domain including the N-terminus (i) to stabilize the P2X1 receptor to the level of the P2X2 receptor and (ii) to not influence the gating and ATP binding mechanism and guarantee a fully functional receptor, since the gating TM2 remained unchanged. This stable receptor mutant transfected in 1321N1 astrocytoma cells was used in all experiments discussed in this dissertation. When results at the P2X1 receptor are discussed, the P2X1-2 receptor is meant.

### **1.2.6.1 P2X1 receptor antagonists**

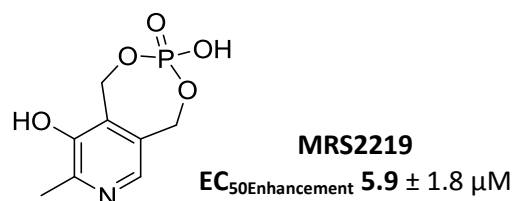
Several potent P2X1 receptor antagonists could be identified. Figure 1.11 shows the structures of 8,8'-[carbonyl-bis(imino-4,1-phenylenecarbonylimino-4,1-phenylene-carbonyl-imino)]bis-1,3,5-naphthalene trisulfonic acid (NF279), 8,8'-[carbonyl-bis(imino-3,1-phenylenecarbonylimino)]bis-1,3,5-naphthalene trisulfonic acid (NF023) and 4,4',4'',4'''-[carbonylbis-(imino-5,1,3-benzenetriyl-bis(carbonylimino))]tetrakis-1,3-benzene disulfonic acid (NF449), all truncated suramin derivatives with nanomolar inhibitory potency at the P2X1 receptor.<sup>85</sup> Other P2X1 receptor antagonists are PPADS derived MRS2220 and the benzimidazole-2-carboxamide derivative RO-0437626 (RO-1). Suramin-derived compounds are described to be competitive antagonists. PPADs-derived structures are described as acting non-surmountable with very slow receptor resensitization.<sup>86</sup> RO-0437626 was the first P2X1 receptor antagonist proven to be selective towards P2X2, P2X3 and the heteromeric P2X2/3 receptor, but showed a relatively weak potency.<sup>87</sup>



**Figure 1.11:** Structures and inhibitory potency of suramin-derived P2X1 antagonists NF279, NF449 and NF023, PPADS-derived MRS2220 and RO-0437626, also known as RO-1.<sup>86-91</sup>

### 1.2.6.2 P2X1 receptor allosteric modulators

One allosteric modulator of the P2X1 receptor has been identified until now. During the development of the PPADS-derived antagonists, one compound was found to potentiate ATP-induced currents at the P2X1 receptor with an  $EC_{50\text{Enhancement}}$  concentration of  $5.9 \pm 1.8 \mu\text{M}$ . The effect was selective towards the P2X2, P2X3 and P2X4 receptor.<sup>86</sup> The structure of the compound, MRS2219, is presented in Figure 1.12.



**Figure 1.12:** Structure and enhancing potency of PPADS-derived P2X1 positive allosteric modulator MRS2219.<sup>86</sup>

### 1.2.7 The P2X2 receptor subtype

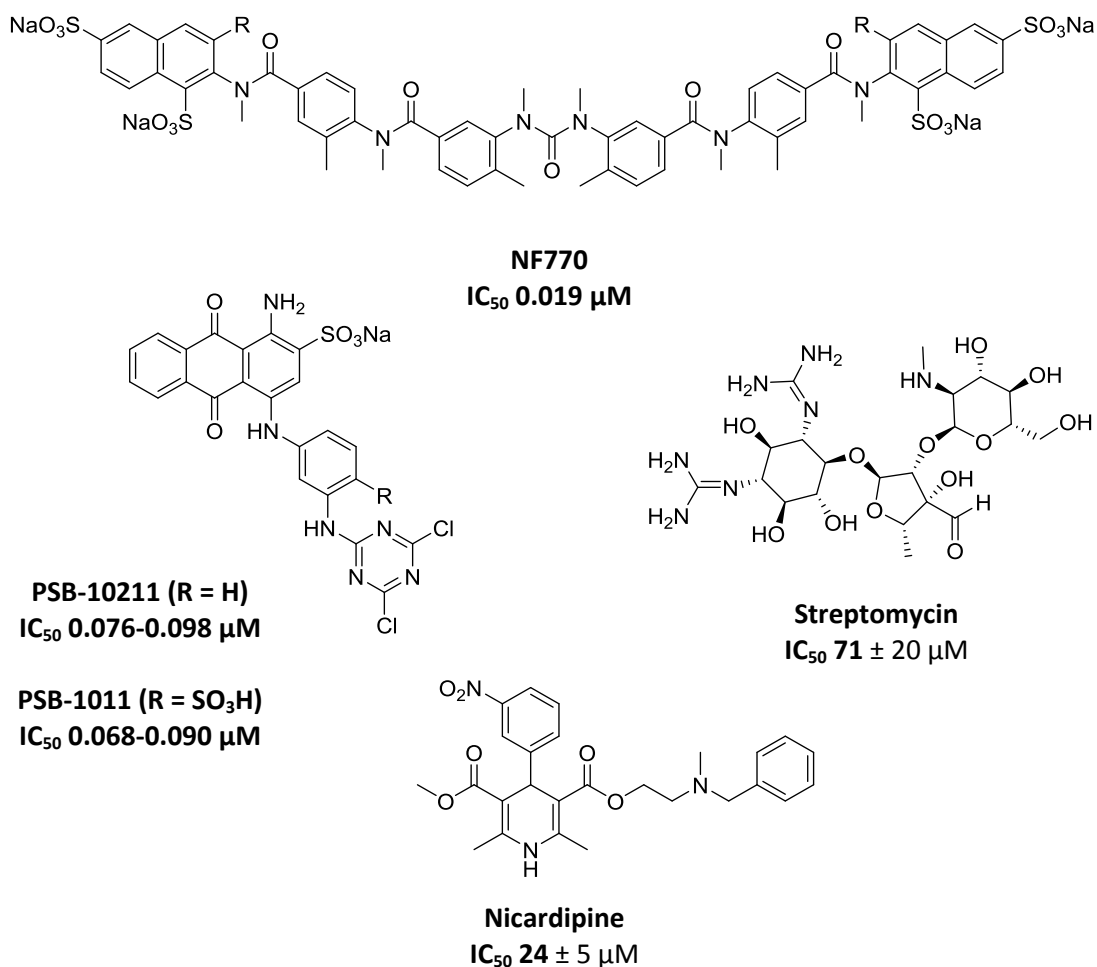
The human P2X2 receptor was cloned from pituitary and pancreas, and is 471 amino acids long.<sup>92</sup> It is expressed ubiquitously in the body, especially in the peripheral and the central nervous system, smooth muscle cells, pancreas and sensory nerves.<sup>93-95</sup> Receptor homomers as well as heteromeric assemblies can be found, mostly in combination with P2X3 or P2X6 subunits in various stoichiometry. The heteromeric P2X2/3 receptor contains one P2X2 and two P2X3 subunits, while the respective P2X6 heteromer is formed by two P2X2 and one P2X6 subunit.<sup>96</sup> Mutagenesis studies on the P2X2 receptor contributed to clarification of P2X receptor topology. Examples are the identification of an important salt bridge between Glu63 (E63) and Arg274 (R274) at the subunit interface in direct vicinity of the ATP binding site. This salt bridge is possibly involved in transferring the conformational change upon agonist binding to the ion pore. Another example is the identification of amino acids Thr336 (T336) and Thr339 (T339) as being a vital part of the closed channel gate.<sup>97, 98</sup>

The activity of the P2X2 receptor can be modulated allosterically by low concentrations of transition metals zinc and copper. Copper is capable of enhancing ATP-gated currents of the rat P2X2 receptor more than 25-fold at 10  $\mu\text{M}$  concentration. Site-directed mutagenesis studies revealed that the bivalent cations are not recognized by cysteine, but by histidine residues in the extracellular loop, namely His120, His192, His213 and His245. They are proposed to be part of a common allosteric metal binding site. There is evidence that copper and other metals like nickel

and mercury potentiate the receptor.<sup>99</sup> These findings are in contrast to the human P2X2 and the P2X1 receptor, where zinc shows concentration-dependent receptor inhibition. At P2X3, zinc also shows weak potentiation of ATP-induced current.<sup>100, 101</sup> The P2X2 receptor shows desensitization, but much slower than the P2X1 receptor. It is therefore considered as stable and non-desensitizing, and is accessible to functional experiments, e. g. measurement of calcium influx.<sup>38</sup>

### **1.2.7.1 P2X2 receptor antagonists**

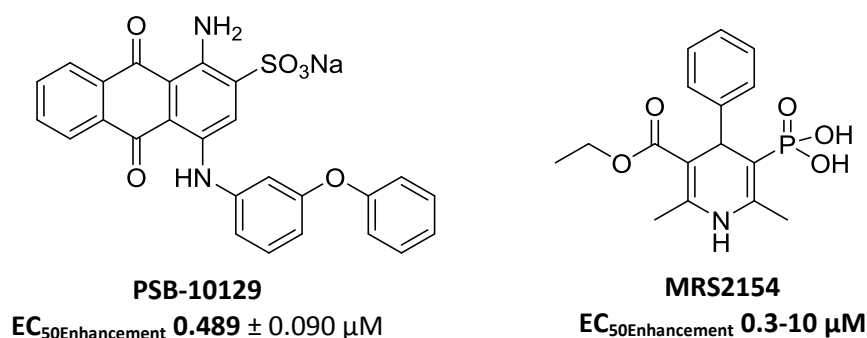
Several non-selective antagonists of the P2X2 receptor homomer are known, including the already discussed compounds suramin, PPADS and TNP-ATP. Suramin and RB-2 were used as templates for the development of new and selective P2X2 receptor antagonists. Suramin-analog 7,7'-(carbonylbis(imino-3,1-phenylene-carbonylimino-3,1-(4-methyl-phenylene)carbonylimino))bis-(1-methoxy-naphthalene)-3,6-disulfonic acid (NF770) is described to be more potent and selective towards the P2X2 receptor in rodents, and is described to inhibit the receptor in a competitive way.<sup>102</sup> RB-2 derivatives PSB-1011 and PSB-10211 were presented in 2011 as the first potent and selective competitive rodent P2X2 receptor antagonists.<sup>103</sup> Nicardipine, a dihydropyridine calcium channel blocker, was identified as an antagonist at the rat P2X2 receptor with almost ninefold preference in comparison to the P2X4 receptor.<sup>104</sup> Streptomycin and related aminoglycoside antibiotics are further approved drugs identified as weak P2X2 receptor antagonists. Further analysis identified them as noncompetitive antagonists, which block the open channel and stabilize the receptor in an open non-conductive way.<sup>105</sup>



**Figure 1.13:** Structures and inhibitory potency of P2X2 receptor antagonists NF770, PSB-10211, PSB-1011, streptomycin and nicardipine.<sup>102-105</sup>

### 1.2.7.2 P2X2 receptor allosteric modulators

Nicardipine derivative MRS2154 and anthraquinone compound sodium 1-amino-4-(3-phenoxyphenylamino)-9,10-dioxo-9,10-dihydroanthracene-2-sulfonate (PSB-10129) were identified as potent positive allosteric modulator (PAMs). They enhanced the ATP-induced currents of the P2X2 receptor when used in high nanomolar to low micromolar concentrations, demonstrating that inhibiting and enhancing effects lie close together structurally and cannot generally be applied to a whole library of similar compounds.<sup>103, 104</sup> The structure and potency can be seen in Figure 1.14.



**Figure 1.14:** Structures of RB-2- and nicardipine-derived positive allosteric P2X<sub>2</sub> modulators PSB-10129 and MRS2154.<sup>103, 104</sup>

### 1.2.8 The P2X<sub>3</sub> receptor subtype

The cDNA of the P2X<sub>3</sub> receptor was first cloned from dorsal root ganglion sensory neurons of the rat in 1995, and is 397 amino acids long.<sup>68</sup> It is expressed on primary sensory neurons and other cells in the CNS as well as the bladder, and closely associated with genesis and transmission of neuropathic pain, which could be confirmed in a knock out mouse model.<sup>75, 106, 107</sup> The receptor can be found on pre- and postsynaptic membranes of various ganglia of the somatosensory signal pathway, where ATP is released from neurons together with fast conducting glutamate and other neurotransmitters involved in forwarding of pain signals. The homomeric P2X<sub>3</sub> receptor is a non-selective cation conducting channel with high permeability for calcium ions.<sup>108</sup> It is further characterized by high ion permeability in its open state and fast desensitization followed by a long regeneration period, which is observed after exposure to the physiological agonist ATP.<sup>68</sup> Sokolova et al. promoted two types of desensitization observed in rodent sensory neurons. The first one was a fast process occurring after 50 msec by 10 μM ATP, and the second one a slow process after 35 sec by 0.01 μM ATP, which inhibited the receptors without previous activation. The latter was termed high affinity desensitization (HAD). The effect is attributed to the high affinity of ATP at the P2X<sub>3</sub> receptor.<sup>109</sup> The recovery from desensitization is agonist-specific and takes seconds to minutes. Furthermore, it is dependent on the temperature (the higher the temperature, the faster the recovery) and the extracellular ion concentration (acceleration by increased calcium and decreased magnesium concentrations).<sup>110</sup> Naproxen, a non-steroidal anti-inflammatory drug, is capable of accelerating the desensitization process of recombinant P2X<sub>3</sub> receptors. This is considered to be a possible explanation for its effectiveness against migraines.<sup>111</sup> The recovery time depends on the agonist. Resensitization occurs very fast when the receptor is stimulated with β,γ-meATP, but is unusually slow when 2-meSATP is used.<sup>109</sup>



The discovery that the functional properties of recombinant P2X3 receptors, e. g. the different responses to agonist  $\alpha,\beta$ -me-ATP, do not properly correlate with P2X receptors tested in dorsal root ganglions is explained by the formation of heteromeric assemblies of two different subtypes.<sup>108</sup> These receptor heteromers have a different pharmacological properties and do not desensitize. P2X2/3 receptors were the first identified and the best characterized P2X heteromer. The stoichiometry was initially found to be fixed of one P2X2 and two P2X3 subunits.<sup>49, 112</sup> Recently, evidence has been presented that this ratio is not exclusive and that the stoichiometry also depends on the expression level of both receptor subunits.<sup>113</sup> The assembly of heteromeric receptors appears not to be controlled by the extracellular loop, but by the transmembrane domain, in particular TM2 and the intracellular region located directly before it.<sup>114</sup> The structural differences subsequently also influence agonist and antagonist pharmacology. Potent ligands like agonist [ $\gamma$ -<sup>32</sup>P]8-Azido-ATP or antagonists Ip<sub>5</sub>I and RO-85 are active at the homomeric, but not the heteromeric receptor.<sup>46, 115-117</sup>

Desensitization of the homomeric P2X3 receptor hinders functional experiments like patch-clamp or measurement of calcium influx. Heteromeric assembly allows no experimental estimation of the P2X3 properties of new potential ligands, since the heteromeric P2X2/3 receptor shows a complete different pharmacology. Several studies were conducted to create stable receptor mutants with no change of receptor pharmacology. Neelands et al. exchanged the N-terminal region and the associated transmembrane domain to the respective part of the P2X2 receptor. Patch-clamp experiments demonstrated that agonists ATP and  $\alpha,\beta$ -meATP activate the receptor to the same extent, but the kinetic of desensitization of the P2X2-3 receptor chimera is much slower than for the homomeric receptor.<sup>62</sup> The long recovery time was attributed to the high affinity of both agonists, which bind effectively to the receptor in concentrations below those required for successful receptor activation. The return to normal excitability is delayed by the slow dissociation of the agonist.<sup>69</sup>

The N-terminal region seems to be responsible for the fast desensitization kinetics of the P2X3 receptor. The comparison of the primary receptor of the N-terminus of rat P2X2 and P2X3 receptors showed that 20 out of 47 amino acids of both subunits are identical. By site-directed mutagenesis of single and longer parts of different amino acids, it was discovered that the exchange of three amino acids located directly before the transmembrane domain against the respective P2X2 equivalent is sufficient to slow the desensitization process significantly. Further experiments revealed that changing the serine in position 15 of the native rat P2X3 receptor to valine or other hydrophobic amino acids like isoleucine or phenylalanine is enough to significantly reduce receptor desensitization to the level of the P2X2 receptor. Agonist and

antagonist affinity was proposed to not be affected by the site-directed mutagenesis.<sup>118</sup> Dr. Ralf Hausmann kindly provided the non-desensitizing valine mutant S15V of the rat P2X3 receptor stably transfected in 1321N1 astrocytoma cells. This cell line was used in all experiments discussed in this dissertation. When results at the P2X3 receptor are mentioned, the S15VrP2X3 receptor mutant is meant.

The stabilizing effect of the same mutation could also be seen for the human P2X3 receptor, but since the attempt to stably transfect the construct into 1321N1 astrocytoma cells failed repeatedly, it was not available for testing.

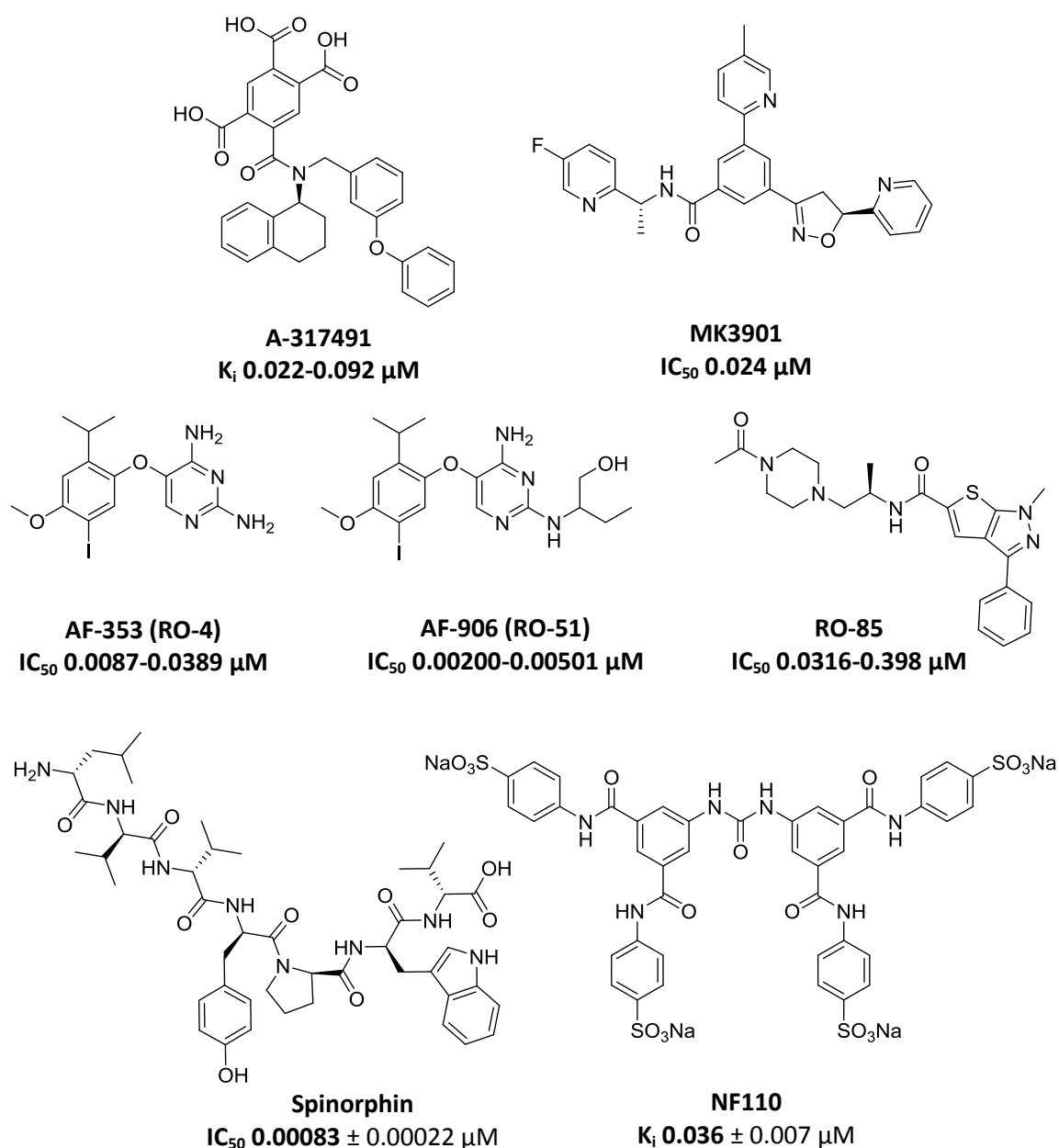
### **1.2.8.1 P2X3 receptor antagonists**

Several selective antagonists of the P2X3 receptor have already been described. The first small potent drug-like competitive P2X3 receptor antagonist discovered was A-317491 with  $K_i$  concentrations in the low nanomolar range at human and rat P2X3 and P2X2/3 receptors, respectively. It is highly selective over other P2 or neurotransmitter receptors ( $IC_{50} > 10 \mu M$ ).<sup>119</sup> The (S)-enantiomer was potent, the (R)-configured derivative called A-317344 was completely inactive. Another potent and selective P2X3 antagonist is AF-353, also called RO-4, a small drug-like and highly selective non-competitive P2X3 and P2X2/3 receptor antagonist. The compound is structurally related to the antibacterial drug trimethoprim, which itself does not have any inhibitory potency at the P2X3 receptor.<sup>120</sup>  $IC_{50}$  values were determined for human and rat P2X3 and human P2X2/3 receptors. It was deemed the better *in vivo* tool over A-317491 due to improved bioavailability and higher plasma-free fraction.<sup>121</sup> The structure was further optimized by introduction of features with increased polarity, leading to the potent antagonist AF-906 (RO-51). AF-906 shows inhibitory potency in the low nanomolar range at both human P2X3 and P2X2/3 receptors.<sup>122</sup> AF-219, an aryloxy-pyrimidinediamine,<sup>122</sup> has been described as a potent allosteric P2X3 receptor antagonist and was recently evaluated in clinical phase II studies for treatment of chronic cough, osteoarthritic joint pain and asthma. Until now, the structure of the compound is undisclosed.<sup>123</sup>

Another very potent antagonist is thienopyrazole derivative RO-85. The compound is slightly more potent at the rat than the human P2X3 receptor, but selective not only toward the other P2X receptor subtypes but also towards heteromeric P2X2/3 receptors. The high metabolic stability and good bioavailability make it a valid candidate for clinical testing.<sup>117</sup> Another potent P2X3 antagonist is MK-3901, which was successfully tested in a chronic inflammatory and neuropathic pain experimental model and is also reported to have good bioavailability.<sup>124</sup> The

suramin-derived compound NF110 was shown to inhibit P2X3 with low nanomolar potency and was found to be less potent at P2X1, P2X2, P2X4 and P2X7, despite the high structural similarity to P2X1 receptor antagonist NF449.<sup>125</sup>

Spinorphin is a very effective non-competitive antagonist of human P2X3 receptor with subnanomolar affinity and was selective towards mouse P2X1 and human P2X7 receptor.<sup>126</sup> All mentioned antagonists and respective  $IC_{50}$  and  $K_i$  values are shown in Figure 1.15.



**Figure 1.15:** Structures and inhibitory potency of P2X3 antagonists A-317491, MK-3901, AF-353 (RO-4), AF-906 (RO-51), RO-85 and spinorphin.<sup>117, 119, 121, 122, 124-126</sup>

### 1.2.8.2 P2X3 receptor allosteric modulators

Cibacron Blue 3GA, the purified *ortho*-isomer of RB-2 (see Figure 1.10), was identified as a PAM of human and rat P2X3 receptor by Alexander *et al.* in 1999.<sup>127</sup> It enhanced the ATP-induced calcium influx and transmembrane currents three- to seven times higher than the normal level with low micromolar potency ( $EC_{50\text{Enhancement}} = 1.4 \pm 0.5 \mu\text{M}$ ). The enhancing effect is not dependent on the agonist, since it is also observed when the receptor is stimulated with the ATP analogs BzATP, 2-meSATP or  $\alpha,\beta$ -me-ATP.

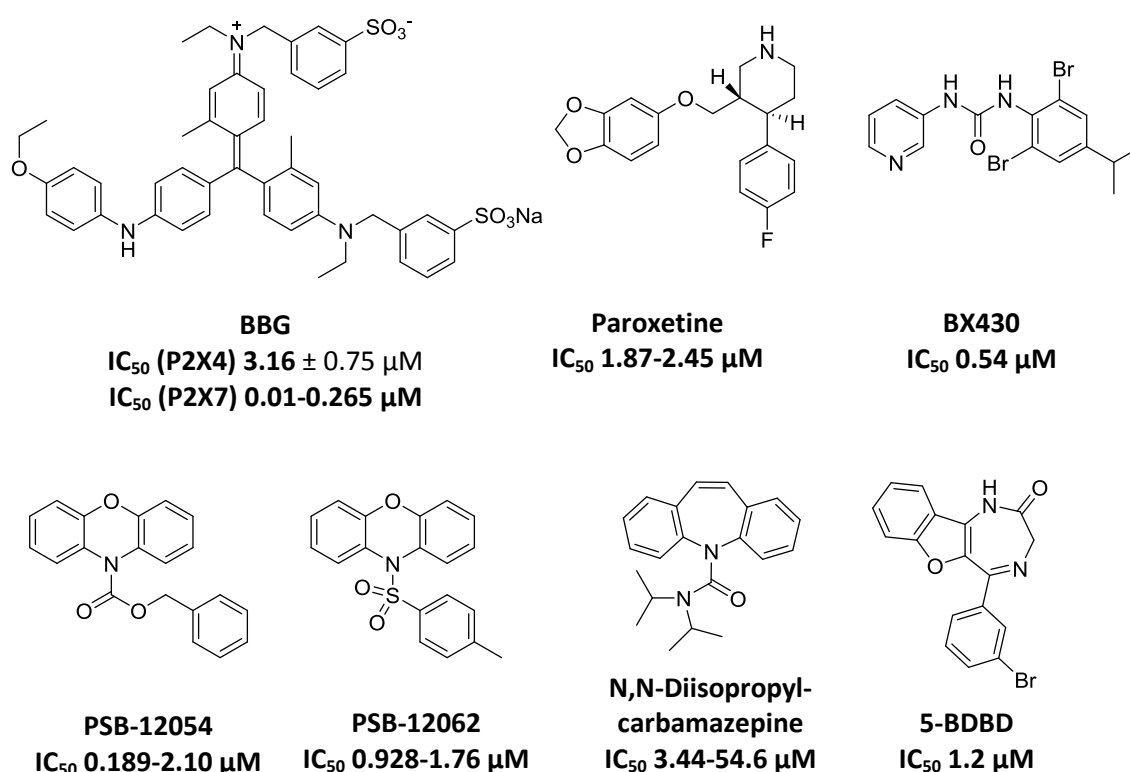
### 1.2.9 The P2X4 receptor subtype

The P2X4 receptor was first cloned from rat hippocampus. Furthermore, the mRNA of the receptor was found ubiquitously in purkinje cells, spinal cord motor neurons and medulla oblongata.<sup>128</sup> It is described to be the widest distributed P2X receptor in the organism, and is expressed in central and peripheral nervous system including activated microglia, epithelia, smooth muscle cells in bladder, intestines and uterus, arteries, uterine endometrium, osteoclasts, kidney, lung, heart, liver, pancreas, B lymphocytes and fat cells.<sup>129, 130</sup> A knockout mouse model tested in different pain and inflammation models showed the association of the P2X4 receptor with genesis and forwarding of neuropathic pain, inflammatory-associated pain and tactile allodynia.<sup>131</sup> Furthermore, it was found to be upregulated in case of neuronal injury or inflammation caused by various transcriptional and translational controlling factors, e. g. the CC chemokine receptor (CCR2), CC chemokine CCL21, fibronectin and the transcription factor interferon regulatory factor 8 (IRF8).<sup>132</sup> CCR2 was further identified as a regulator of P2X4 receptors trafficking from lysosomes to the cell surface via exocytosis. Stimulation of CCR2 with endogenous ligands CCL2 or CCL12 increased the levels of cell surface-located P2X4 receptors. A decrease was observed under the influence of CCR2 antagonist RS-504393.<sup>133</sup> Neuropathic pain is a debilitating pain condition and mainly caused not by noxious stimuli, but by neuronal damage. Pain treatment as applied for pain caused by external stimuli (e. g. NSAIDs and opioids) is ineffective for neuropathic pain. The lack of potent drugs makes it an interesting field for scientific research and the design of novel, selective and effective drug-like ligands.

Furthermore, P2X4 receptors were found to be associated with the enzyme endothelial nitric oxide synthase (eNOS) in murine ventricular myocytes. The stimulation of P2X4 receptors was found to stimulate the activity of eNOS, resulting in increased levels of cardiac NO, demonstrating cardioprotection in heart failure and improvement of cardiac function.<sup>134</sup>

### 1.2.9.1 P2X4 receptor antagonists

The rat P2X4 receptor is not inhibited by classic standard antagonists such as suramin and PPADS in concentrations up to 300  $\mu\text{M}$ . In contrast, the mouse and human orthologues have a weak sensitivity to PPADS, and Coomassie Brilliant Blue G (BBG) is also a weak antagonist, as well as RB-2.<sup>28</sup> TNP-ATP is the most potent competitive, though non-selective antagonist (see Table 1.1). Since antidepressants have been proven to be effective against neuropathic pain states, a selection of antidepressant compounds have been tested for inhibitory potency at the P2X4 receptor. Paroxetine was identified as a potent allosteric antagonist of rat and human P2X4 receptors with low micromolar potency. Furthermore, it was demonstrated to be an effective drug in a neuropathic pain model. The antinociceptive effect could not be attributed to the serotonin receptor pathway.<sup>135</sup> Amitriptyline, a tricyclic antidepressant clinically approved for the treatment of neuropathic pain, is only a weak inhibitor of P2X4 receptors. Due to its lack of potency, P2X4 receptor inhibition is not considered as the defining factor for efficacy against neuropathic pain.<sup>136</sup>



**Figure 1.16:** Structure and potency of P2X4 antagonists BBG, paroxetine, BX430, PSB-12054, PSB-12062, N,N-diisopropylcarbamazepine and 5-BDBD. The potency of BBG at the P2X7 receptor is further discussed in chapter 1.2.12.1.<sup>64, 135, 137-140</sup>

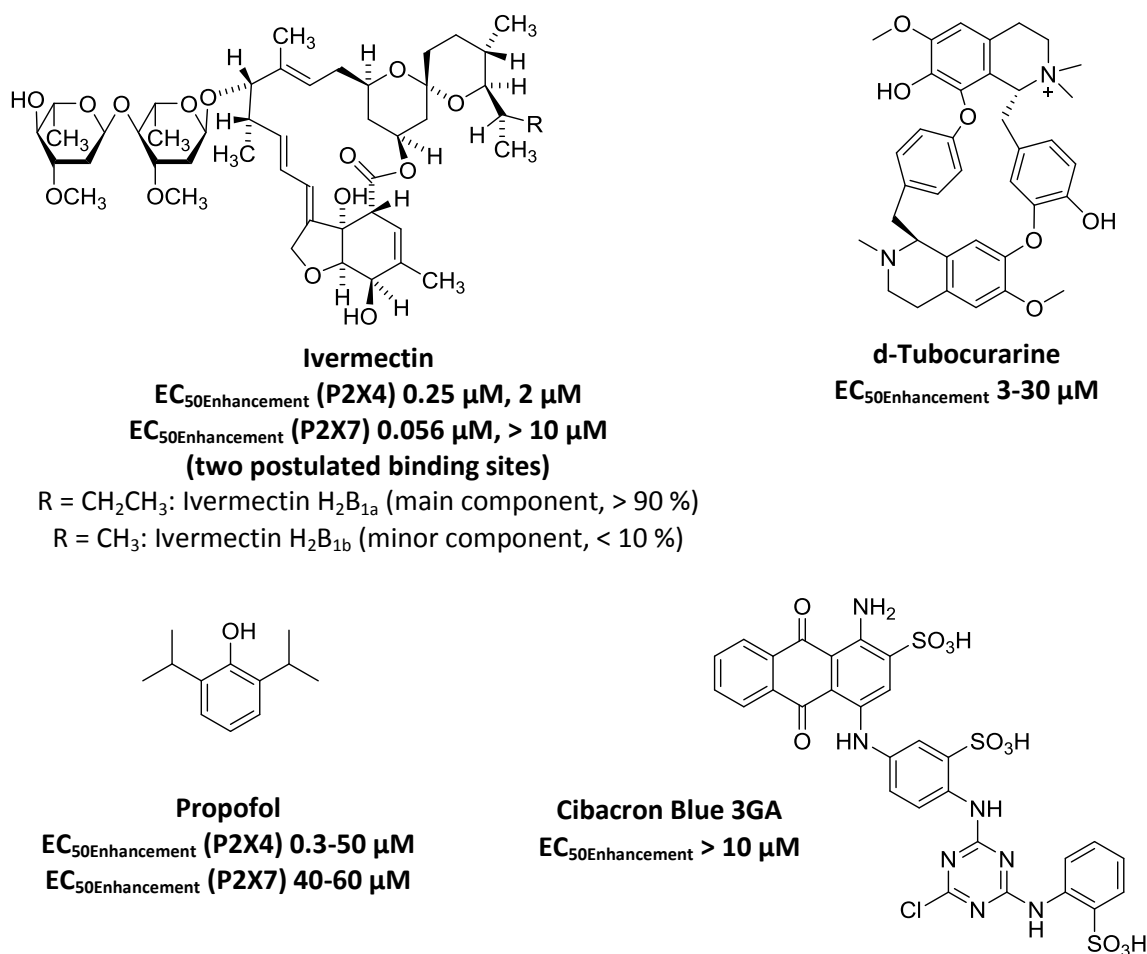
Benzodiazepine derivative 5-BDBD is a selective antagonist of the P2X4 receptor. The information of its mode of action is inconclusive. References for competitive and allosteric binding of 5-BDBD are known.<sup>137, 141</sup> Another lead structure for successful and selective P2X4 antagonism is phenoxazine. A compound library of effective N-substituted derivatives was synthesized. They enabled structure-activity relationships at the P2X4 receptor for the first time. The structure of the most active compound PSB-12054 inhibited the P2X4 receptor with nanomolar potency and was at least tenfold selective towards human P2X1, P2X2, P2X3, and P2X7 receptors. One disadvantage of the compound is its poor water solubility. The closely related derivative PSB-12062 is more water-soluble with potency and selectivity similar to PSB-12054.<sup>64</sup> Structurally distantly related anticonvulsant drug carbamazepine and derivatives were identified as potent P2X4 receptor antagonists as well. The most effective compound of the series was N,N-diisopropylcarbamazepine. The compound was fairly selective towards human P2X2 and P2X7, but not P2X1 and P2X3 receptors ( $IC_{50}$  P2X1  $5.32 \pm 1.91 \mu\text{M}$  and P2X7  $7.18 \pm 2.86 \mu\text{M}$ , respectively).<sup>138</sup> The newest P2X4 receptor-selective phenylurea antagonist BX430 was recently discovered by screening the Canadian Chemical Biology Network library using calcium imaging and whole cell patch clamp experiments. BX430 inhibited the P2X4 receptor with high nanomolar potency. The compound is described to be soluble in physiological solutions and stable at room temperature, and to be selective towards human P2X1-3, P2X5 and P2X7 receptors.<sup>139</sup>

### **1.2.9.2 P2X4 receptor allosteric modulators**

Ethanol was identified as an allosteric antagonist of the P2X4 receptor. The inhibitory effect can only be seen at high concentrations (100 mM), which makes ethanol not very interesting as a P2X4 receptor antagonist. However, there are several genomic findings including the decrease of P2X4 receptor mRNA expression in the brain of alcohol-preferring rats indicating that P2X4 receptor activation may play a role as a reducer of alcohol intake and preference.<sup>142</sup> Therefore, the activated P2X4 receptors may contribute to sobriety and reduction of alcohol use disorders. The broad-spectrum antiparasitic drug ivermectin has been identified as a positive allosteric modulator of the P2X4 receptor with high nanomolar to low micromolar potency in 1999 (see Figure 1.17).<sup>143</sup> Ivermectin is a macrolide drug isolated from *Streptomyces avermectinius* as a mixture of two compounds Ivermectin H<sub>2</sub>B<sub>1a</sub> and ivermectin H<sub>2</sub>B<sub>1b</sub>, and is approved for the treatment of onchocerciasis and in a topical form for rosacea. Further investigations identified ivermectin as an effective drug to reduce alcohol intake and preference by antagonizing ethanol-induced inhibition of P2X4 receptors, which could be verified in an animal model.<sup>144-146</sup> The

positive allosteric modulation can be observed at other ion channels like the glutamate-gated chloride channel,  $\gamma$ -aminobutyric acid type-A receptor, glycine receptor or neuronal  $\alpha$ 7-nicotinic receptor.<sup>147</sup> Ivermectin is perorally bioavailable, widely distributed in the body, especially in cell membranes due to its high lipophilicity. It also penetrates past the blood brain barrier into the CNS.<sup>148</sup> Low concentrations of ivermectin increase the ATP-induced signal at the P2X4 receptor, higher concentrations retard channel closing and receptor desensitization during sustained ATP presence and thereby temporarily induce pore dilation.<sup>147, 149</sup> Those different effects were explained by the existence of two different binding sites for ivermectin at the P2X4 receptor, one with high affinity in the high nanomolar and one with lower affinity in the lower micromolar range.<sup>147, 150</sup> This theory is not proven since binding site of ivermectin has not yet been fully identified. There is evidence that the transmembrane domains are involved in ivermectin recognition. Several residues apparently involved in ivermectin recognition could be identified by side-directed mutagenesis.<sup>151</sup>

Other PAMs of the P2X4 receptor are d-tubocurarine, a muscle relaxant first isolated from *Chondrodendron tomentosum*, RB-2, the standard antagonist at the P2X2 receptor, and i.v. anesthetic propofol. The allosteric effects of d-tubocurarine were identified while characterizing the rat P2X4 receptor using the radioligand [<sup>35</sup>S]ATP $\gamma$ S. D-tubocurarine increased radioligand binding when used in concentrations above 10  $\mu$ M.<sup>152</sup> Cibacron Blue 3GA is a weak inhibitor especially at the P2X2 receptor. The compound is derived from anthraquinone, and was selected as the lead structure for the development of a broad variety of P2X receptor ligands (see chapter 3.1). The positive allosteric modulation is expressed in increased responses of rat P2X4 receptors to ATP. Cells were preincubated with 3-30  $\mu$ M Cibacron Blue 3GA prior to ATP stimulation. The increase could be attributed to enhanced ATP potency without affecting the maximum signal.<sup>153</sup> Propofol is known as an allosteric enhancer at the GABA<sub>A</sub> receptor, which is considered responsible for its general anesthetic and anticonvulsant effect. It was found to enhance ATP-evoked signal at rat P2X4 receptors when used in concentrations higher than 50  $\mu$ M, and was selective towards rat P2X2 and P2X2/3 receptors.<sup>154</sup> Hasaka et al. confirmed this observation, but enhancement of ATP-induced signal was observed at much lower propofol concentrations (0.3-3  $\mu$ M). Higher concentrations were observed to inhibit ATP-induced P2X4 receptor currents in mouse microglia cells.<sup>155</sup> The activity of propofol at the P2X4 receptor was deemed responsible for excitatory side effects of propofol administration.<sup>154</sup>



**Figure 1.17:** Structure and potency of positive allosteric P2X4 modulators. The potency of ivermectin and propofol at the P2X7 receptor is discussed in chapter 1.2.12.2.<sup>143, 152, 154-156</sup>

### 1.2.10 The P2X5 receptor subtype

The P2X5 receptor was first discovered in rat celiac ganglia along with the P2X6 receptor.<sup>157</sup> In humans, it was first discovered in the fetal brain in a truncated form.<sup>158</sup> It was later identified to miss exon 10, which encodes for the major part of the second transmembrane domain.<sup>159</sup> When compared to the other P2X receptor subtypes, the expression of P2X5 receptors in the body is limited. It was found in mesencephalic nucleus of the trigeminal nerve, cervical spinal cord, purkinje cells of the cerebellum, heart, adrenal gland and retina.<sup>28, 157, 160, 161</sup> There is evidence that the P2X5 receptor is found in epithelial cancer cells and in the immune system, especially thymus.<sup>158, 162</sup> The receptor presentation on the membrane is usually poor. The function of the receptor is not yet fully cleared in humans.

The P2X5 receptor shows fast rapid currents and slow desensitization upon prolonged exposure to ATP. The recovery from the desensitized state is also very slow.<sup>159</sup> The receptor is sensitive to



standard agonists ATP and 2-meSATP with low micromolar potency. The rat receptor does not react to  $\alpha,\beta$ -meATP, and the potency at the human orthologue is comparable to the other agonists, although  $\alpha,\beta$ -meATP and BzATP act as a partial agonist.<sup>67, 159</sup>

Standard antagonists PPADS, TNP-ATP, suramin and RB-2 are active at the rat P2X5 receptor with diminishing potency. The human variety was inhibited by PPADS, Brilliant Blue G and suramin.<sup>28</sup> The P2X5 receptor was found to form a heteromeric receptor together with the P2X1 subunit. The so-called P2X1/5 receptor displays properties of both subtypes. The current desensitizes slowly and the ATP potency is similar to the P2X1 receptor. The potency of agonist  $\alpha,\beta$ -meATP is increased to the level of the P2X1 receptor.<sup>163</sup> Furthermore, the P2X1/5 heteromer was found to be highly sensitive to the P2X1 antagonist NF449 (see Figure 1.11), while the inhibitory potency of TNP-ATP was reduced in comparison to its potency at the homomeric P2X1 receptor.<sup>28, 67, 164</sup>

Recently, heteromeric receptors of P2X2 and P2X5 subunits in various stoichiometry were discovered. The identified functional properties include pore dilation, membrane blebbing and phosphatidylserine exposure. All features were previously associated solely with the P2X7 receptor.<sup>165</sup> The sensitivity to ATP and BzATP was slightly reduced in comparison to the homomeric P2X2 receptor, while the inhibitory potency of TNP-ATP was found to be increased, and  $\alpha,\beta$ -meATP had no effect.<sup>46, 165</sup>

### 1.2.11 The P2X6 receptor subtype

The P2X6 subunit was identified along with the P2X5 receptor in 1996 in rat celiac ganglia, a protein of 379 amino acids.<sup>157</sup> High mRNA expression was found in cerebellar Purkinje cells, ependymal, CA1 region of hippocampus, spinal motor neurons, uterus, ovary and bronchial epithelia.<sup>28, 157, 166</sup> The first characterization after discovery via patch clamp experiments showed quick currents after stimulation with ATP, 2-MeSATP and ADP,  $\alpha,\beta$ -meATP was not active.<sup>157</sup> Another study at recombinant P2X6 receptors transfected in human embryonic kidney cells reported sensitivity to ATP and  $\alpha,\beta$ -meATP with low nanomolar potency in the absence of any other P2X receptor subunit ( $EC_{50}$  0.5  $\mu$ M and 0.6  $\mu$ M, respectively). Standard antagonists TNP-ATP and PPADS were also active ( $IC_{50}$  0.8  $\mu$ M and 22  $\mu$ M, respectively), but not suramin.<sup>167</sup> Currents upon stimulation were observed only in a small fraction of the cells. Membrane-located P2X6 receptors were confirmed by western blot analysis in ATP-responsive cells, but the protein was more heavily glycosylated than in non-responsive cells.<sup>168</sup> The receptor shows poor membrane presentation and accumulates in the endoplasmic reticulum.<sup>169</sup> The P2X6 subunit is

unable to oligomerize to build a functional homomeric receptor, which was attributed to an uncharged sequence of 14 amino acids in the N-terminal region that is unique among P2X receptors.<sup>169</sup> While evidence of homomeric P2X6 receptors is inconclusive, heteromeric assembly with P2X2 or P2X4 subunits is documented.<sup>46, 170, 171</sup> The P2X2/6 receptor has lower ATP potency and lower pH tolerance than the homomeric P2X2 receptor and shows slow desensitization kinetics.<sup>170</sup> One functional receptor contains two P2X2 and one P2X6 subunits, respectively.<sup>96</sup>

The P2X6 receptor also easily forms heteromers with the P2X4 receptor. The functional properties of the heteromer closely resemble those of the P2X4 receptor, including weak potency of  $\alpha,\beta$ -meATP, similar potency of ATP and 2-meSATP and inhibition by suramin and RB-2.<sup>171</sup>

### 1.2.12 The P2X7 receptor subtype

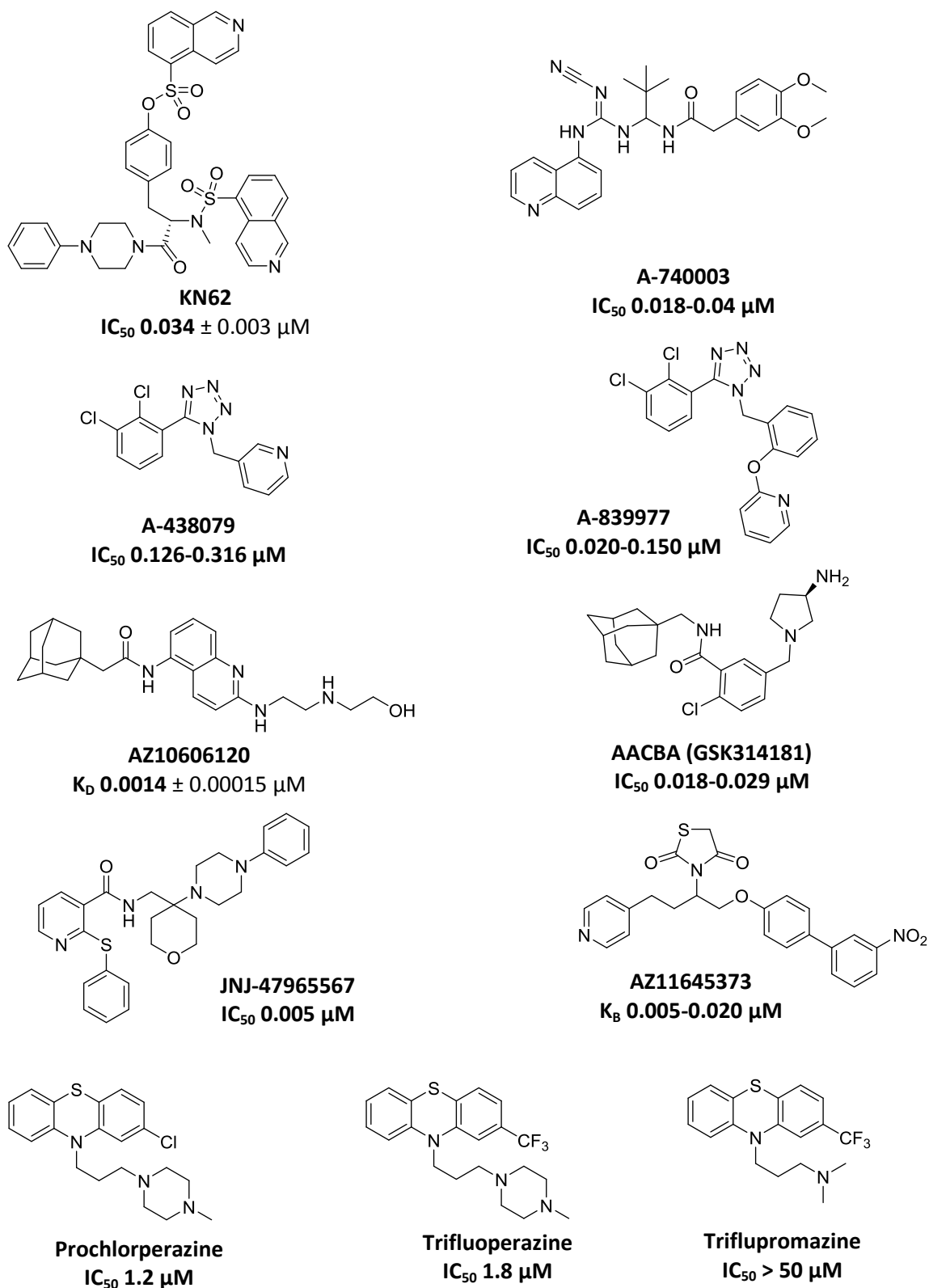
The P2X7 receptor was originally cloned from rat brain. It is identical to the previously described P2XZ receptor, which was found responsible for the formation of membrane pores in macrophages upon exposure to high ATP concentrations.<sup>172</sup> The human orthologue was discovered shortly after in monocytes.<sup>173</sup> The topology of the receptor matches all previously discovered P2X subunits. However, the amino acid sequence, specifically the C-terminal region, is much longer than in all other subtypes. The complete subunit is 595 amino acids long. The C-terminal domain is important for correct oligomerization and posttranslational modification of the receptor, and contains several motifs for protein- and lipid interaction and a cysteine-rich amino acid section.<sup>174</sup> It is orientated solely intracellularly and does not possess any length of hydrophobic residues spanning through the membrane.<sup>172</sup> The mRNA is excessively found in bone marrow cells including granulocytes, monocytes, B-lymphocytes, spleen, heart, placenta, testes, liver, epithelial cells, osteoblasts, microglia and several neuronal cells.<sup>28, 173, 175</sup> The receptor is further differentiated from the other P2X subtypes by its low sensitivity to the physiological agonist ATP. The rat receptor is activated by 0.1 to 100  $\mu$ M ATP, while the human receptor requires higher concentrations (see Table 1.1).<sup>28</sup> BzATP is around 100-fold more potent at the P2X7 receptor than ATP (see Table 1.1). 2-MeSATP is also a weak agonist, while  $\alpha,\beta$ -meATP and  $\beta,\gamma$ -meATP are not active. Prolonged exposure to agonist also induces a higher permeation pathway in the cell membrane, which can induce cell death. It also enables permeability of compounds of high molecular mass like YO-PRO1, a fluorescent dye, or cations like N-methyl-D-glucamine or quinolinium.<sup>173, 176</sup> It is not yet fully cleared how the higher

permeability is achieved. The most likely explanation is a dilation of the ion channel, building a pore-like structure with high conducting ability.<sup>28, 172</sup>

The P2X7 receptor is highly expressed in cells of the immune system. It is associated with inflammatory processes and promotes the release of several proinflammatory interleukins including IL-1 $\beta$  and IL-18.<sup>177, 178</sup> This process is caused by high amounts of ATP released passively by cell death or by cells under extreme stress. High extracellular ATP concentrations are known to cause cell death via activation of P2X7 receptors. A participation of P2X7 receptor, in some cases even its overexpression, could be demonstrated for several inflammatory diseases like Crohn's disease, ulcerative colitis, neuroinflammatory processes or necrosis.<sup>177, 179-181</sup> An orally available antagonist of the P2X7 receptor, AZD9056, was recently assessed in a phase IIa study for efficacy and safety against Crohn's disease. The drug was found to significantly improve pain and general well-being of patients suffering from Crohn's disease.<sup>182</sup> The receptor is also involved in cancer progression, though its role remains inconclusive.<sup>178</sup>

#### **1.2.12.1 P2X7 receptor antagonists**

Several antagonists of the P2X7 receptor are known. A selection is presented in Figure 1.18. Brilliant Blue G is a weak non-competitive antagonist at human P2X7 as well as at P2X4, with an at least threefold preference for rat P2X7 receptor.<sup>140, 183</sup> KN-62 is a very potent non-competitive antagonist at the human, but not the rat P2X7 receptor.<sup>184, 185</sup> Triazole- and tetrazole-based compounds were also identified as potent more drug-like P2X7 inhibitors, namely A-438079 and A-839977. A-438079 was identified as the most potent compound out of a 1-benzyl-5-aryltetrazol library at both human and rat P2X7 receptors. The efficacy was verified in a model of neuropathic pain.<sup>186</sup> A-839977 inhibited human, rat and mouse P2X7 receptors at nanomolar concentrations. The antihyperalgesic effect could be confirmed *in vivo* in the CFA model of inflammatory pain.<sup>187</sup> AZ10606120 was developed as a radioligand for P2X7 and labeled with [<sup>3</sup>H]. The compound binds to P2X7 in a non-competitive way. It is reversible, saturable and could be influenced by addition of classic P2X7 receptor antagonists.<sup>188</sup> AACBA, also known as GSK314181, is an adamantane derivative that inhibits both rat and human P2X7 at low nanomolar concentrations. The effect was found to be more prophylactic than therapeutic in chronic pain models.<sup>189</sup>



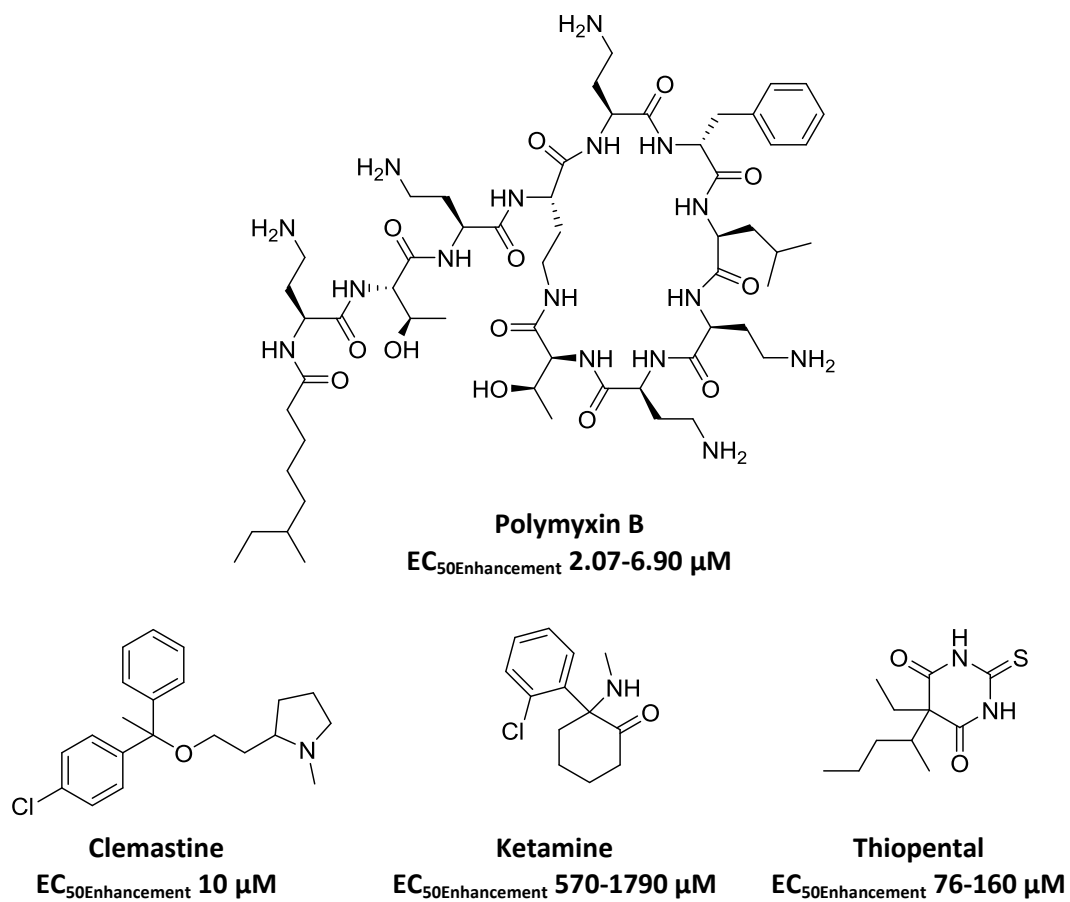
**Figure 1.18:** Structure and potency of P2X7 receptor antagonists KN-62, MRS2540, A-438079, A-839977, A-740003, AZ10606120, AACBA, JNJ-47965567, AZ11645373, prochlorperazine, trifluoperazine and trifluopromazine. Structure and potency of BBG is presented in Figure 1.16.<sup>140, 184, 186-193</sup>

AACBA and AZ10606120 both contain an adamantane amide partial structure. The potency of cyanoguanidine derivative A740003 is comparable to AACBA at human and rat P2X7 receptors. It is also described to be selective towards P2 and other cell surface receptors, e. g. 5-HT, adenosine, adrenergic, dopamine, acetylcholine and opioid receptors. The orthosteric P2X7 antagonist also potently reduces the release of IL-1 $\beta$  in human macrophage THP-1 cells.<sup>190</sup> Cyclic imide P2X7 antagonist AZ116453373 is very selective towards human P2X1, P2X3, P2X4, P2X5 as well as rat P2X2 and P2X2/3 receptors. It inhibits P2X7 receptors in THP-1 cells in nanomolar concentrations. In contrast to the previously discussed antagonists, it is selective towards the rat P2X7 receptor.<sup>191</sup> N-(cyclohexylmethyl)-benzamides were identified as weak P2X7 antagonists by high-throughput screening. JNJ-47965567 is the product of a series of structural modifications. It inhibited human P2X7 receptors in low nanomolar concentrations and was six-to tenfold selective towards rat and mouse orthologues.<sup>192</sup> Further pharmacological characterization demonstrated good permeability into the central nervous system. The efficacy against mania and neuropathic pain could be elucidated in an animal model.<sup>194</sup>

Inhibitory potency is also demonstrated for already approved drugs like antipsychotics prochlorperazine, trifluoperazine and trifluopromazine. The first two inhibit P2X7 receptors in low micromolar concentrations, the latter is less potent. All three are allosteric antagonists at the P2X7 receptor.<sup>193</sup>

### **1.2.12.2 P2X7 receptor allosteric modulators**

Several positive allosteric modulators of the P2X7 receptor have been characterized so far. Polymyxin B was identified as an enhancer of P2X7 activity when the receptor was stimulated with ATP. The effect expressed itself in increased membrane permeabilization and elevated cytotoxicity by otherwise nontoxic ATP concentrations.<sup>195</sup> Another drug reported to enhance ATP-induced human but not murine P2X7 receptor signaling is ivermectin, which has already been discussed as a PAM at the P2X4 receptor in chapter 1.2.9.2. The antiparasitic drug potentiated P2X7 receptor signaling at saturating and subsaturating ATP concentrations.<sup>156</sup> Injectable narcotics like propofol (see chapter 1.2.9.2), ketamine and thiopental reversibly increase P2X7 receptor activity. Their potency could not be correlated with lipophilicity, and thiopental showed inhibition when used in low concentrations.<sup>196</sup> The antihistamine clemastine was recently identified as another PAM at P2X7 receptors. Clemastine was found to bind from the extracellular site. A facilitated pore dilation and increased sensitization to the physiological agonist ATP were reported as responsible for clemastine-induced allosteric enhancement.<sup>197</sup>



**Figure 1.19:** Structures of positive allosteric P2X7 modulators polymyxin B, clemastine, ketamine and thiopental. Structure and potency of ivermectin and propofol are presented in Figure 1.17.<sup>156, 195-197</sup>

### 1.3 Objective

Not many potent and selective inhibitors with drug-like properties are known for any of the P2X receptor subtypes. Such tools are necessary for the *in vivo* study of respective P2X receptors, and for the development of new and potent drugs for the broad variety of diseases P2X receptors are associated with. Many of the identified compounds have several disadvantages concerning solubility, polarity, metabolism or toxicity, exacerbating their suitability of being valid drug candidates. Recently, Dr. Ralf Hausmann succeeded in stabilizing the rat P2X3 receptor by one single mutation that did not affect ATP binding. The first aim of this study was demonstrating that the stably transfected rat P2X3 receptor mutant is suitable for high throughput screening by determination of the Z' factor and the screening an anthraquinone library and further characterizing of hit compounds. Following the successful transfection of all human P2X receptors except the P2X5 and P2X6 subtypes by Dr. Aliaa Abdelrahman and Stefanie Weyer, the establishment of an assay measuring calcium influx, high throughput screening and hit selectivity studies was possible. The search for novel and selective ligands includes the screening of a 440 compound approved drug and inorganic polyoxometalate library at all readily cloned P2X receptor subtypes. The hits are further characterized by determination of potency and for some by determination of inhibition mechanism. The general aim of this study is the identification of novel potent hits at P2X receptors out of different compound libraries, their characterization and assessment with regard to their suitability as potential drugs.

## 2 Material and methods

### 2.1 Material

#### 2.1.1 Chemicals

ATP	Carl Roth GmbH & Co. KG, Karlsruhe
Calcium chloride [CaCl <sub>2</sub> ]	Sigma Aldrich Chemie GmbH, Taufkirchen
Carbachol	Sigma Aldrich Chemie GmbH, Taufkirchen
D-glucose	Sigma Aldrich Chemie GmbH, Taufkirchen
DMSO	AppliChem GmbH, Darmstadt
DMSO for cell culture	AppliChem GmbH, Darmstadt
Dulbecco's Modified Eagle Medium (DMEM)	Gibco® Invitrogen GmbH, Darmstadt
EDTA-sodium	Carl Roth GmbH & Co. KG, Karlsruhe
Ethanol absolute	VWR International GmbH, Darmstadt
FCS	Sigma Aldrich Chemie GmbH, Taufkirchen
FLIPR® Calcium-4 Explorer Kit	Molecular Devices Corporation, Sunnyvale CA (USA)
FLIPR® Calcium-5 Bulk Kit (10 x 10)	Molecular Devices Corporation, Sunnyvale CA (USA)
FLIPR® Calcium-5 Explorer Kit	Molecular Devices Corporation, Sunnyvale CA (USA)
Fluo-4 AM cell permanent dye 10 x 50 µg	Invitrogen GmbH, Darmstadt
Geneticin® (G 418) 100 mg/ml	Invitrogen GmbH, Darmstadt
Glacial acetic acid	Carl Roth GmbH & Co. KG, Karlsruhe
HEPES	Carl Roth GmbH & Co. KG, Karlsruhe
Hydrochloric acid 37 %	AppliChem GmbH, Darmstadt
Isopropanol absolute	ZVE Universität Bonn
Magnesium chloride [MgCl <sub>2</sub> ]	Sigma Aldrich Chemie GmbH, Taufkirchen
Magnesium sulfate [MgSO <sub>4</sub> ]	Sigma Aldrich Chemie GmbH, Taufkirchen
MTT	AppliChem GmbH, Darmstadt
Penicillin-streptomycin (10 000 I.E./ml, 10 mg/ml)	Gibco® Invitrogen GmbH, Darmstadt
Phenol red solution 0.5 %	Sigma Aldrich Chemie GmbH, Taufkirchen
Plasmocin 2.5 mg/ml	Invitrogen GmbH, Darmstadt
Pluronic F-127	Sigma Aldrich Chemie GmbH, Taufkirchen
Potassium chloride [KCl]	Fluka, Sigma Aldrich Chemie GmbH, Taufkirchen



Potassium dihydrogen orthophosphate [KH <sub>2</sub> PO <sub>4</sub> ]	Sigma Aldrich Chemie GmbH, Taufkirchen
Purelab® Plus water	ELGA LabWater, Celle
Sodium bicarbonate [NaHCO <sub>3</sub> ]	Sigma Aldrich Chemie GmbH, Taufkirchen
Sodium chloride [NaCl]	Carl Roth GmbH & Co. KG, Karlsruhe
Sodium dihydrogen phosphate [NaH <sub>2</sub> PO <sub>4</sub> ]	Carl Roth GmbH & Co. KG, Karlsruhe
Sodium hydroxide solution 1 M	Sigma Aldrich Chemie GmbH, Taufkirchen
TRIS-HCl	Carl Roth GmbH & Co. KG, Karlsruhe
Trypsin 2.5 % in HBSS	Lonza Group Ltd., Schweiz

### 2.1.2 Consumable supplies

Corning® 3340 CellBind 96 well plates, sterile	Sigma Aldrich Chemie GmbH, Taufkirchen
Combitips advanced® for Eppendorf Multipette® E3 5 ml, 2.5 ml and 1 ml	Eppendorf AG, Hamburg
Disposable pipettes 1, 5, 10 and 25 ml	Sarstedt, Nümbrecht
Falcons 15 ml, 120 x 17 mm	Sarstedt, Nümbrecht
Falcons 50 ml, 114 x 28 mm	Sarstedt, Nümbrecht
Microtubes 2 ml	Axygen Scientific, Union City
Pipette tips 10, 100 and 1000 µl	Sarstedt, Nümbrecht
Pipette tips 5000 µl	Sarstedt, Nümbrecht
TipOne filter tips sterile 10, 100 and 1000 µl	STARLAB GmbH, Hamburg
Reservoirs, nonsterile 50 ml	VWR International GmbH, Darmstadt
Reservoirs, sterile 50 ml	VWR International GmbH, Darmstadt
Ritips® 0.5 ml, 1 ml, 2.5 ml and 5 ml	Ritter GmbH Medical, Schwabmünchen
Rotilabo® microtest plates, V profile, 96 Well	Carl Roth GmbH & Co. KG, Karlsruhe
Safe Seal® microtubes 1.5 and 5 ml	Eppendorf AG, Hamburg
Tissue culture 96 well plates, sterile	Greiner Bio-one GmbH, Frickenhausen
Tissue Culture Flask 25, 75 und 175 cm <sup>2</sup>	Sarstedt, Nümbrecht

### 2.1.3 Devices

Accu-Jet® pipetting controller	Brand, Wertheim
Analytical balance 440-47N (max. 2000 g)	Kern & Sohn GmbH, Balingen-Frommern
Analytical balance CP225D	Sartorius, Göttingen
Axiovert 25 microscope	Carl Zeiss AG, Oberkochen
Biometra® Thermocycler	Biometra GmbH, Göttingen

## 2 Material and Methods

---

Neubauer Counting chamber 10 mm <sup>2</sup> /0,0025 mm <sup>2</sup>	Paul Marienfeld GmbH & Co. KG, Lauda Königshofen
Eppendorf Easypet®3 pipetting aid	Eppendorf AG, Hamburg
Eppendorf Multipette® E3	Eppendorf AG, Hamburg
Eppendorf Multipette® plus	Eppendorf AG, Hamburg
Eppendorf Research® plus pipettes 0.5-10 µl, 2-20 µl, 10-100 µl, 20-200 µl, 100-1000 µl and 500-5000 µl	Eppendorf AG, Hamburg
Eppendorf Xplorer® electronic pipettes 0.5- 10 µl, 10-100 µl and 30-300 µl	Eppendorf AG, Hamburg
FlexStation® 3 multi-mode microplate reader	Molecular Devices Corporation, Sunnyvale CA (USA)
Freezer -20°C	Bosch GmbH, Stuttgart
Sanyo Ultra Low Freezer -80°C	Ewald Innovationstechnik GmbH, Bad Nenndorf
Fridge	Bosch GmbH, Stuttgart
Hund microscope	Helmut Hund GmbH, Wetzlar
IKA® Vortex 3 vortexer	IKA®-Werke GmbH & Co. KG, Staufen
Jouan IG 650 incubator	Thermo Fisher Scientific, Waltham
Micro 200 centrifuge	Hettich Holding GmbH & Co.oHG, Kirchlingern
NOVOstar® fluorescence plate reader	BMG Labtech GmbH, Ortenberg
NUNC® BIOFLOW workbench	Nunc GmbH & Co. KG, Langenselbold
NUNC® Safe flow 1.2 workbench	Nunc GmbH & Co. KG, Langenselbold
pH 197 measuring instrument	Wissenschaftlich-Technische Werkstätten GmbH, Weilheim
pH electrode SenTix 41	Wissenschaftlich-Technische Werkstätten GmbH, Weilheim
Purelab® Plus water purification plant	ELGA LabWater, Celle
RCT Basic hot plate stirrer	IKA Labortechnik, Staufen
Rotofix 32 centrifuge	Hettich, Tuttlingen
Scaltec SBC 42 balance (min. 0,02 g, max. 120 g)	Scaltec Instruments GmbH, Göttingen
Systemec 3850 ELV autoclave	Systemec, Wettenberg
Ultrasonic bath	Bandelin electronic, Berlin

## 2.1.4 Compounds and compound libraries

Anthraquinone derivatives	synthesized by Dr. Younis Baqi in the group of Prof. Dr. Müller, University of Bonn
Drug library	Internal compound library ( <a href="http://mueller-group.pharma.uni-bonn.de/bibliothek">http://mueller-group.pharma.uni-bonn.de/bibliothek</a> )
Polyoxometalate library (polyoxotungstates, PEGylated polyoxotungstates, rhenium cluster compounds, vanadium clusters)	Synthesized in the group of Prof. Dr. Kortz, University of Bremen, Prof. Dr. Wang, University of Tianjin, Prof. Dr. Stephan, Research Center Dresden-Rossendorf, or purchased from Sigma Aldrich Chemie GmbH
TNP-ATP	Tocris Bioscience, Bristol, UK
RB-2	Sigma Aldrich Chemie GmbH, Taufkirchen
AF-353	Afferent Pharmaceuticals, Inc., San Mateo, CA, USA
BBG	Sigma Aldrich Chemie GmbH, Taufkirchen

## 2.1.5 Solutions and reagents

<b>Calcium-4/Calcium-5 dilution ready for use (Explorer kit)</b>	Component A (dye)	1 vial	Solution is prepared according to company instruction
	Component B (buffer)	10 ml	
<b>Calcium-5 dilution ready for use (Bulk kit)</b>	Calcium-5 stock solution (Bulk kit)	1 ml	Prepared directly before use according to company instruction
	HBSS	ad 10 ml	
<b>Calcium-5 stock dilution (Bulk kit)</b>	Component A (dye)	1 vial	Solution is prepared according to company instruction, stored at -20°C
	HBSS	10 ml	
<b>Carbachol solution 100 µM</b>	Carbachol stock solution	0.01 ml	Stored at -20°C
	HBSS buffer	ad 0.1 ml	
<b>Carbachol stock solution 1 mM</b>	Carbamoylcholine chloride	1.83 mg	Stored at -20°C
	HBSS buffer	1 ml	
<b>Cell culture medium for 1321N1 astrocytoma cells transfected with plasmid pQCXIP</b>	FCS	50 ml	Stored at 4°C
	Penicillin-streptomycin (10.000 I.E./ml, 10 mg/ml)	5 ml	
	Puromycin 10mg/ml	0.11 ml (2 µg/ml)	
	DMEM®	500 ml	
<b>Cell culture medium for 1321N1 astrocytoma cells transfected with plasmid pLXSN</b>	FCS	50 ml	Stored at 4°C
	Penicillin-streptomycin (10.000 I.E./ml, 10 mg/ml)	5 ml	
	G418 (100 mg/ml)	2 ml (200 µg/ml)	
	DMEM®	500 ml	

## 2 Material and Methods

<b>Cell culture medium for non-transfected 1321N1 astrocytoma cells</b>	FCS	50 ml	Stored at 4°C
	Penicillin-streptomycin (10.000 I.E./ml, 10 mg/ml)	5 ml	
	DMEM®	500 ml	
<b>EDTA 0.1 M stock solution</b>	EDTA Purelab® Plus	3.7 g ad 100 ml	pH is adjusted to 7.6, stored at room temperature
<b>EDTA 0.6 mM solution</b>	PBS	2000 ml	Autoclave at 120°C and 2 bar pressure, then leave to cool down to room temperature
	EDTA 0.1 M stock solution	12 ml	
<b>Fluo-4 AM 3 µM dilution ready for use</b>	Fluo-4 AM 1 mM stock solution	0.012 ml	Prepared directly before use
	Pluronic F127 stock solution 25 %	0.012 ml	
	HBSS buffer	ad 4.0 ml	
<b>Fluo-4 AM stock solution 1 mM</b>	Fluo-4 AM (M <sub>r</sub> 1097 g/mol)	50 µg (1 aliquot)	Stored at -20°C, protected from light
	DMSO	45.6 µl	
<b>Hank's buffered salt solution (HBSS)</b>	CaCl <sub>2</sub> (anhyd.)	0.14 g	pH is adjusted to 7.3 using NaOH 1 M or HCl 1 M, stored at 4°C
	MgCl <sub>2</sub>	0.0476 g	
	MgSO <sub>4</sub>	0.0494 g	
	KCl	0.4 g	
	KH <sub>2</sub> PO <sub>4</sub>	0.06 g	
	NaHCO <sub>3</sub>	0.35 g	
	NaCl	8 g	
	Na <sub>2</sub> HPO <sub>4</sub>	0.048 g	
	D-Glucose	1 g	
	Autoclaved Purelab® Plus water	1000 ml	
<b>Medium for freezing at -176°C in liquid nitrogen</b>	DMSO for cell culture	1 ml	Stored at -20°C
	FCS	ad 10 ml	
<b>MTT solution</b>	MTT	5 mg	dissolved using ultrasonic bath, protected from light, prepared directly before use
	PBS	1 ml	
<b>Phosphate-buffered saline (PBS)</b>	NaCl	8,0 g	pH is adjusted to 7.4 using NaOH 1 M or HCl 1 M, autoclaved at 121°C and 2 bar pressure, then stored at 4°C
	Na <sub>2</sub> HPO <sub>4</sub> ·2 H <sub>2</sub> O	1,4 g	
	KH <sub>2</sub> PO <sub>4</sub>	0,2 g	
	KCl	0,2 g	
	Purelab®Plus	1000 ml	

<b>Pluronic® F127 stock solution 25 %</b>	Pluronic® F127 DMSO	0.2 g 0.8 ml	Dissolved at 37°C, then stored at room temperature
<b>Trypsin 0.05 %/EDTA 0.6 mM solution</b>	EDTA 0.6 mM solution Trypsin 2.5 % solution Phenol red indicator 0.5 % solution	2000 ml 40 ml 1.5 ml	aliquoted in 50 ml falcons, stored at 4°C

## 2.1.6 Pipetting schemes

### 2.1.6.1 ATP solutions used for determination of inhibitory potency

	<b>P2X1</b>	<b>P2X2</b>	<b>P2X3</b>	<b>P2X4</b>	<b>P2X7</b>	
<b>ATP amount weighed [mg]</b>	0.5511	0.5511	0.5511	0.5511	5.511	11.022
<b>HBSS [ml]</b>	1	1	1	1	1	1
<b>Concentration [mM]</b>	1	1	1	1	10	20
<b>Dilution</b>	0.1 ml (1 mM) + 0.9 ml HBSS (100 µM)	0.1 ml (1 mM) + 0.9 ml HBSS	0.1 ml (1 mM) + 0.9 ml HBSS (100 µM)	0.1 ml (1 mM) + 0.9 ml HBSS	-	-
<b>Final dilution</b>	0.01 ml (100 µM) + 0.99 ml HBSS	-	0.01 ml (100 µM) + 0.99 ml HBSS	-	-	-
<b>Final concentration in the well [µM]</b>	0.1	1	0.1	1	1000	2000

## 2 Material and Methods

### 2.1.6.2 ATP solutions used for determination of enhancing potency

	P2X1	P2X2	P2X3	P2X4	P2X7
ATP amount weighed [mg]	-	-	0.5511	-	55.11
HBSS [ml]	-	-	1	-	1
Concentration [mM]	-	-	1	-	50
Dilution 1 (full receptor stimulation)	-	-	0.1 ml (1 mM) + 0.9 ml HBSS	-	-
Final concentration in the well 1 [μM]	-	-	10	-	-
Dilution 2 (EC <sub>50</sub> receptor stimulation)	-	-	0.005 ml (100 μM) + 0.995 ml HBSS	-	50 μl (50 mM) + 50 μl HBSS
Final concentration in the well 2 [μM]	-	-	0.1	-	2500

### 2.1.6.3 Standard dilution scheme of ATP (50 mM stock solution)

Dilution	Real concentration [μM]	Final concentration in the well [μM]	Production
All dilutions produced from 5 mM stock solution			
D1	50 000	5000	20 μl stock/well
D2	25 000	2500	50 μl stock + 50 μl HBSS
D3	20 000	2000	40 μl stock + 60 μl HBSS
D4	15 000	1500	30 μl stock + 70 μl HBSS
D5	10 000	1000	20 μl Stock + 80 μl HBSS
D6	8000	800	16 μl stock + 84 μl HBSS
D7	7000	700	14 μl stock + 86 μl HBSS
D8	5000	500	10 μl stock + 90 μl HBSS
D9	4000	400	8 μl stock + 92 μl HBSS
D10	3000	300	6 μl stock + 94 μl HBSS
D11	1000	100	10 μl D5 + 90 μl HBSS

**2.1.6.4 Standard dilution scheme of P2X receptor agonists (1 mM stock solution)**

Dilution	Real concentration [ $\mu\text{M}$ ]	Final concentration in the well [ $\mu\text{M}$ ]	Production
All dilutions produced from 1 mM stock solution			
<b>D1</b>	1000	100	10 $\mu\text{l}$ stock + 90 $\mu\text{l}$ HBSS
<b>D2</b>	300	30	30 $\mu\text{l}$ D0 + 70 $\mu\text{l}$ HBSS
<b>D3</b>	100	10	10 $\mu\text{l}$ D0 + 90 $\mu\text{l}$ HBSS
<b>D4</b>	30	3	10 $\mu\text{l}$ D2 + 90 $\mu\text{l}$ HBSS
<b>D5</b>	10	1	10 $\mu\text{l}$ D3 + 90 $\mu\text{l}$ HBSS
<b>D6</b>	5	0.5	5 $\mu\text{l}$ D3 + 95 $\mu\text{l}$ HBSS
<b>D7</b>	6	0.6	6 $\mu\text{l}$ D3 + 94 $\mu\text{l}$ HBSS
<b>D8</b>	3	0.3	10 $\mu\text{l}$ D4 + 90 $\mu\text{l}$ HBSS
<b>D9</b>	1	0.1	10 $\mu\text{l}$ D5 + 90 $\mu\text{l}$ HBSS
<b>D10</b>	0.5	0.05	10 $\mu\text{l}$ D6 + 90 $\mu\text{l}$ HBSS
<b>D11</b>	0.3	0.03	10 $\mu\text{l}$ D8 + 90 $\mu\text{l}$ HBSS
<b>D12</b>	0.1	0.01	10 $\mu\text{l}$ D9 + 90 $\mu\text{l}$ HBSS
<b>D13</b>	0.03	0.003	10 $\mu\text{l}$ D11 + 90 $\mu\text{l}$ HBSS
<b>D14</b>	0.01	0.001	10 $\mu\text{l}$ D12 + 90 $\mu\text{l}$ HBSS
<b>D15</b>	0.003	0.0003	10 $\mu\text{l}$ D13 + 90 $\mu\text{l}$ HBSS
<b>D16</b>	0.001	0.0001	10 $\mu\text{l}$ D14 + 90 $\mu\text{l}$ HBSS

**2.1.6.5 Dilutions of standard antagonists for the determination of Z'-factor**

	<b>P2X1</b>	<b>P2X2</b>	<b>P2X3</b>	<b>P2X4</b>	<b>P2X7</b>
<b>Antagonist</b>	TNP-ATP	RB-2	AF-353	BBG	BBG
<b>Mr [g/mol]</b>	1123.04	840.10	436.68	854.02	854.02
<b>Amount weighed for 10 mM stock solution [mg]</b>	predissolved in water, 10 mM	8.401	4.367	8.540	8.540
<b>DMSO added for 10 mM stock solution [ml]</b>	-	1	1	1	1
<b>Dilution</b>	2 $\mu\text{l}$ stock solution/well, supplemented with 2 $\mu\text{l}$ DMSO	2 $\mu\text{l}$ stock solution/well	1 $\mu\text{l}$ stock solution + 9 $\mu\text{l}$ DMSO	2 $\mu\text{l}$ stock solution/well	2 $\mu\text{l}$ stock solution/well
<b>Final concentration in the well [<math>\mu\text{M}</math>]</b>	100	100	10	100	100

**2.1.6.6 Standard dilution scheme for test compounds (10 mM stock solution)**

Dilution	Real concentration [ $\mu\text{M}$ ]	Final concentration in the well [ $\mu\text{M}$ ]	Production
All dilutions produced from 10 mM stock solution			
<b>D1</b>	10 000	100	2 $\mu\text{l}$ stock solution/well
<b>D2</b>	5000	50	4 $\mu\text{l}$ stock solution + 4 $\mu\text{l}$ DMSO
<b>D3</b>	3000	30	3 $\mu\text{l}$ stock solution + 7 $\mu\text{l}$ DMSO
<b>D4</b>	1000	10	1 $\mu\text{l}$ stock solution + 9 $\mu\text{l}$ DMSO
<b>D5</b>	500	5	1 $\mu\text{l}$ D2 + 9 $\mu\text{l}$ DMSO
<b>D6</b>	300	3	1 $\mu\text{l}$ D3 + 9 $\mu\text{l}$ DMSO
<b>D7</b>	100	1	1 $\mu\text{l}$ D4 + 9 $\mu\text{l}$ DMSO
<b>D8</b>	50	0.5	1 $\mu\text{l}$ D5 + 9 $\mu\text{l}$ DMSO
<b>D9</b>	30	0.3	1 $\mu\text{l}$ D6 + 9 $\mu\text{l}$ DMSO
<b>D10</b>	10	0.1	1 $\mu\text{l}$ D7 + 9 $\mu\text{l}$ DMSO
<b>D11</b>	1	0.01	1 $\mu\text{l}$ D10 + 9 $\mu\text{l}$ DMSO
<b>D12</b>	0.1	0.001	1 $\mu\text{l}$ D11 + 9 $\mu\text{l}$ DMSO
<b>D13</b>	0.01	0.0001	1 $\mu\text{l}$ D12 + 9 $\mu\text{l}$ DMSO

**2.1.6.7 Standard dilution scheme for test compounds (1 mM stock solution)**

Dilution	Real concentration [ $\mu\text{M}$ ]	Final concentration in the well [ $\mu\text{M}$ ]	Production
All dilutions produced from 1 mM stock solution			
<b>D1</b>	1000	100	20 $\mu\text{l}$ stock solution/well
<b>D2</b>	500	50	40 $\mu\text{l}$ stock solution + 40 $\mu\text{l}$ HBSS
<b>D3</b>	300	30	30 $\mu\text{l}$ stock solution + 70 $\mu\text{l}$ HBSS
<b>D4</b>	100	10	10 $\mu\text{l}$ D1 + 90 $\mu\text{l}$ HBSS
<b>D5</b>	50	5	10 $\mu\text{l}$ D2 + 90 $\mu\text{l}$ HBSS
<b>D6</b>	30	3	10 $\mu\text{l}$ D3 + 90 $\mu\text{l}$ HBSS
<b>D7</b>	10	1	10 $\mu\text{l}$ D4 + 90 $\mu\text{l}$ HBSS
<b>D8</b>	5	0.5	10 $\mu\text{l}$ D5 + 90 $\mu\text{l}$ HBSS
<b>D9</b>	3	0.3	10 $\mu\text{l}$ D6 + 90 $\mu\text{l}$ HBSS
<b>D10</b>	1	0.1	10 $\mu\text{l}$ D7 + 90 $\mu\text{l}$ HBSS
<b>D11</b>	0.1	0.01	10 $\mu\text{l}$ D10 + 90 $\mu\text{l}$ HBSS
<b>D12</b>	0.01	0.001	10 $\mu\text{l}$ D11 + 90 $\mu\text{l}$ HBSS



**2.1.6.8 Standard dilution scheme for test compounds (0.1 mM stock solution)**

Dilution	Real concentration [ $\mu\text{M}$ ]	Final concentration in the well [ $\mu\text{M}$ ]	Production
All dilutions produced from 0.1 mM stock solution			
<b>D1</b>	1000	10	20 $\mu\text{l}$ stock solution/well
<b>D2</b>	500	5	40 $\mu\text{l}$ stock solution + 40 $\mu\text{l}$ HBSS
<b>D3</b>	300	3	30 $\mu\text{l}$ stock solution + 70 $\mu\text{l}$ HBSS
<b>D4</b>	100	1	10 $\mu\text{l}$ D1 + 90 $\mu\text{l}$ HBSS
<b>D5</b>	50	0.5	10 $\mu\text{l}$ D2 + 90 $\mu\text{l}$ HBSS
<b>D6</b>	30	0.3	10 $\mu\text{l}$ D3 + 90 $\mu\text{l}$ HBSS
<b>D7</b>	10	1	10 $\mu\text{l}$ D4 + 90 $\mu\text{l}$ HBSS
<b>D8</b>	5	0.5	10 $\mu\text{l}$ D5 + 90 $\mu\text{l}$ HBSS
<b>D9</b>	3	0.3	10 $\mu\text{l}$ D6 + 90 $\mu\text{l}$ HBSS
<b>D10</b>	1	0.1	10 $\mu\text{l}$ D7 + 90 $\mu\text{l}$ HBSS
<b>D11</b>	0.1	0.01	10 $\mu\text{l}$ D10 + 90 $\mu\text{l}$ HBSS
<b>D12</b>	0.01	0.001	10 $\mu\text{l}$ D11 + 90 $\mu\text{l}$ HBSS

All dilutions were freshly prepared before each experiment.

**2.2 Methods****2.2.1 Cell culture**

All experiments discussed in the following paragraph were performed in human 1321N1 astrocytoma cells stably transfected with human P2X1, P2X2, P2X4 P2X7 or rat P2X3 receptor, via retroviral vector system, respectively. The cells were cultured at 37°C and 5 % CO<sub>2</sub> in tissue culture flask 25, 75 und 175 cm<sup>2</sup>, respectively, using Dulbecco's Modified Eagle Medium (DMEM) supplemented with 10 % FCS, 100 U/ml penicillin G, 100  $\mu\text{g}/\text{ml}$  streptomycin, and a selection antibiotic dependent on the retroviral system used for receptor transfection (G418 800  $\mu\text{g}/\text{ml}$  for human P2X1, P2X2, P2X4 and P2X7 receptor and Puromycin 2  $\mu\text{g}/\text{ml}$  for P2X3 receptor).

The transfection of 1321N1 astrocytoma cells with P2X1, P2X2, P2X4 and P2X7 was performed by Dr. Aliaa Abdelrahman, Scarlett Weigel and Stefanie Weyer. Briefly, the cDNA of the respective receptor was cloned into the retroviral vector pLXSN, which was then cotransfected into GP+envAM12 mouse fibroblast packaging cells together with the viral expression vector pVSV-G. Afterwards, the packaging cells produce retroviruses carrying the desired receptor DNA, which are capable of infecting 1321N1 astrocytoma cells, and insert the receptor gene into its genome. Due to the lack of viral replicating enzymes and proteins, the viruses cannot replicate after cell infection. Successfully transfected cells were selected by supplementing the cell culture medium with selection antibiotic (G418 800  $\mu\text{g}/\text{ml}$ ). The P2X3 receptor was transfected by PD

Dr. Ralf Hausmann. The protocol used for the transfection was the same as for the other P2X receptors. Instead of pLXSN, the retroviral vector pQCXIP, containing the gene for puromycin resistance, was used. For the selection of successfully transfected cells, puromycin 6 µg/ml was added to the cell culture medium.

Since the human P2X1 and P2X3 receptors both desensitize rapidly after stimulation with agonist (see chapters 1.2.6 and 1.2.8), chimeras of both receptors were used to enable their characterization using functional experiment setups. For the P2X1 receptor, the first transmembrane domain was exchanged to the analog of the P2X2 receptor, while one amino acid of the P2X3 receptor, serine in position 15, was exchanged to valine. In both cases, a stabilization of the receptor without a change of its respective binding properties was obtained. Both chimera cell lines (human P2X1 and rat P2X3) were used in all described experiments.

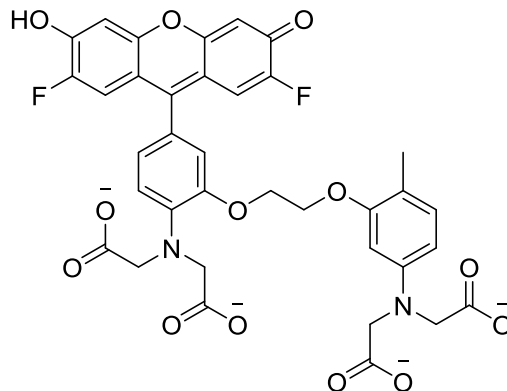
To provide good and stable results in experiments, monoclones with high receptor expression of each cell line were selected. The original cell pool was diluted to a final cell count of 1 cell/200 µl and seeded in sterile tissue culture 96 well plates with a final count of 1 cell/well. Cells were incubated at 37°C and 5 % CO<sub>2</sub> for several days. Only wells containing one colony were transferred to sterile tissue culture 24 well plates. The level of receptor expression was determined by calcium influx measurement after ATP injection. Buffer and carbachol injection served as negative and cell viability control, respectively. Only the monoclonal with the highest fluorescence signal was selected for further experiments, as high fluorescence signal is associated with high receptor expression.

Backups of all cell lines were frozen at -80°C and -176°C in liquid nitrogen. For the latter, a mixture of pure FCS supplemented with 10 % DMSO was used as a cryoprotector. Cells were splitted at least once a week to prevent overgrowth, also before each experiment, using 0.5-2 ml of trypsin-EDTA solution to detach the cells from the bottom of the flask. The amount depends on the size of the flask, 0.5 ml for 25 cm<sup>2</sup>, 1 ml for 75 cm<sup>2</sup> and 2 ml for 175 cm<sup>2</sup>. Since most of the experiments required exact cell amounts, cells were counted using a counting chamber before seed in respective assay plates.

### **2.2.2 Measurement of calcium influx in transfected 1321N1 astrocytoma cells**

P2X receptors are transmembrane ion channels permeable for divalent cations, especially Ca<sup>2+</sup> ions. This feature was utilized to perform functional experiments characterizing the influence of potential ligands on transmembrane calcium influx in transfected 1321N1 astrocytoma cells after agonist stimulation.

All experiments are conducted in living cells. Special fluorescent dyes are utilized to measure the intracellular calcium concentration. The fluorescence intensity of these dyes is enhanced upon formation of complexes with  $\text{Ca}^{2+}$  ions. Fluo-4 as acetoxymethyl ester for cells transfected with human P2X2, P2X4 and P2X7, and Calcium-4 and Calcium-5 for cells transfected with human P2X1 and P2X3, respectively, were used. Fluo-4 AM is cleaved after entering the cell by nonspecific esterases. The negatively charged cleaved form is presented in Figure 2.1.



**Figure 2.1:** Structure of  $\text{Ca}^{2+}$ -complexing fluorescent dye Fluo-4 in its dissociated, negatively charged form.

Calcium-4 and Calcium-5 are  $\text{Ca}^{2+}$ -sensitive fluorescent dyes provided in form of ready for use assay kits developed by Molecular Devices. The company does not provide any information about the structure of the dye. The system includes a masking agent, which blocks any fluorescence of Calcium-4 and Calcium-5 molecules, who did not cross the cell membrane. This leads to reduction of background fluorescence, fluorescence interference caused by spontaneous calcium influxes and loss of cells, since any washing steps are no longer necessary.

### 2.2.2.1 Experimental setup

#### 2.2.2.1.1 Testing for inhibitory and enhancing activity

##### Day 1

Transfected 1321N1 astrocytoma cells were seeded in Corning 3340 black 96 well plates with clear bottom at a concentration of 40 000 cells/well. In order to let the cells attach to the bottom, the plate was incubated overnight at 37°C and 5 %  $\text{CO}_2$ .

### Day 2

Calcium-4 and Calcium-5 dye is prepared according to the instructions provided by Molecular Devices. The explorer kit requires the dilution of component A (dye) with 10 ml of component B (assay buffer). The bulk kit needs the dilution of the dye in 10ml HBSS buffer to prepare a stock solution of Calcium-5 dye. 1 ml of the stock solution is then diluted ad 10 ml with HBSS buffer for the final assay dye. The solutions were mixed thoroughly for at least two minutes. The medium of the cells in the assay plate is removed and cells are incubated with 100  $\mu$ l dye/well at 37°C in the dark for one hour.

Fluo-4 AM 3  $\mu$ M solution is prepared as described in chapter 2.1.5. Cells are incubated with 40  $\mu$ l dye/well for one hour in the dark at room temperature while shaking at 200 rpm. After discarding the dye and washing with 50  $\mu$ l HBSS, cells were incubated with 180  $\mu$ l HBSS buffer/well supplemented with various concentrations of test compounds at room temperature for 30 minutes. The compound dilutions were freshly prepared for each experiment. The pipetting scheme for preparation of compound dilutions is presented in chapter 2.1.4. 178  $\mu$ l of HBSS and 2  $\mu$ l of each compound dilution were added to the respective well, rendering a final DMSO concentration of 1 %/well.

The EC<sub>50</sub> and EC<sub>80</sub> values of ATP were determined prior to any testing of potential antagonists every time a freshly defrozed cell line was used. This is necessary to compensate for any changes in receptor expression due to the stress cells have to endure because of the freezing process. The EC<sub>50</sub> and EC<sub>80</sub> values of ATP remained unchanged for P2X1, P2X2, P2X3 and P2X4, but a decrease was observed after defreezing for cells transfected with the P2X7 receptor. The ATP concentration used for stimulation was increased from 1 mM to 2 mM. The former concentration was used for the POM experiments, the latter for the drug library experiments and the selectivity experiments of anthraquinone derivatives.

The 10 mM stock solutions of POMs, except the five polyoxotungstates from Prof. Wei Wang from University of Tianjin, China, were prepared in HBSS buffer due to insufficient solubility in organic solvents. The stock solutions of the polyoxotungstate derivatives from China were prepared in DMSO. PV5, P<sub>8</sub>W<sub>48</sub>, KB1 and KB2, could not be dissolved completely neither in buffer nor in DMSO at such high concentrations, therefore less concentrated stock solutions in HBSS were prepared for those compounds (1 mM for PV5, KB1 and KB2, and 0.1 mM for P<sub>8</sub>W<sub>48</sub>). The respective pipetting schemes are presented in chapters 2.1.6.6, 2.1.6.7 and 2.1.6.8.

Each well was incubated with 20  $\mu$ l of respective solution on top of 160  $\mu$ l of buffer supplemented with 2  $\mu$ l of DMSO to reach the final DMSO concentration of 1 %/well to allow the testing of higher compound concentrations of these stock solutions.

Each well incubated with test compound was stimulated with the same agonist concentration for determination of inhibitory potency. The physiological agonist ATP was the used agonist for all P2X receptor subtypes. The concentration prepared for stimulation matched the  $EC_{80}$  value determined previously for each receptor cell line by injecting various concentrations of ATP after incubating with 1 % DMSO instead of test compounds. The ATP dilutions used for determination of  $EC_{50}$  and  $EC_{80}$  depended on the transfected receptor tested. Dilution concentrations and preparation for each receptor are summarized in chapter 2.1.6.1. At least seven different concentrations were tested for dose-response experiments.

Pure HBSS buffer was injected as negative control. All solutions for injection were provided in a V-profile microtest plate loaded with 40  $\mu$ l/well to prevent loss of volume. Further control solutions tested in duplicates in each experiments are ATP (positive control, standard stimulation concentration, preincubation with 1 % DMSO instead of test compound), carbachol 100  $\mu$ M (preincubation with 1 % DMSO) and a standard antagonist provided in high enough concentrations to guarantee complete inhibition of the receptor (added for preincubation instead of test compound). The antagonist used depended on the receptor cell line tested in the respective experiment. The used antagonists and their preparation are summarized in chapter 2.1.6.5. Carbachol is an agonist at muscarinic acetylcholine receptors. These receptors are physiologically expressed in 1321N1 astrocytoma cells and impart the release of  $Ca^{2+}$  ions from intracellular storage organs. This provides an increase of  $Ca^{2+}$ -dependent fluorescence independent from the transfected P2X receptor and renders a positive control to prove the functionality of the assay principle and the vitality of the cells.

Fluorescence intensity was measured after 30 minutes incubation with test compound or DMSO before and after injection of agonist using the fluorescent imaging plate reader NOVOstar®. 20  $\mu$ l of agonist were injected into each well, rendering a total assay volume of 200  $\mu$ l/well. The fluorescence in each well is measured for a total time of 35.6 seconds. In between injection of two wells, the injection needle is flushed with Purelab® Plus water to prevent contamination. The program settings used in each experiment are summarized in Table 2.1.

**Table 2.1:** Advanced settings of NOVOstar® for measurement of calcium influx using fluorescent dyes Fluo-4, Calcium-4 and Calcium-5.

Measurement parameter	Fluo-4, Calcium-4 and Calcium-5
Excitation wavelength	485 nm, bandwidth 25 nm
Emission wavelength	520 nm, bandwidth, 20 nm
Number of flashes (Validation)	10 (10)
Gain	variable
Timeframe 1 (2)	0-4 s (11.6-35.6 s)
Number of intervals	60 (4)
Time interval	0.4 (1.0)
Injection time	11.6 s
Injection volume	20 µl
Pump speed	65 µl/s
Position delay	0.2 s
Temperature	RT
Basic fluorescence	22 000-28 000 fluorescent counts
Washing steps after injection	3
Washing solution	Purelab® Plus

Some compounds showed ATP-induced receptor enhancing properties during initial experiments. The concentration-dependency of the effect was determined analog to the determination of inhibitory potency by preincubating cells with various concentrations of test compounds for 30 minutes prior to the stimulation by one single concentration of agonist ATP. The concentration selected for cell stimulation represents the respective EC<sub>50</sub> concentration of ATP. Additional experiments with fully stimulated receptors were conducted for P2X<sub>3</sub> receptors for further characterization. The ATP concentration used in these experiments was 10 µM. All concentrations and preparation of solutions are summarized in chapter 2.1.6.2.

### 2.2.2.1.2 Testing for agonistic activity

Most of the test compounds were examined for their inhibitory potency, but some indicated agonistic properties during initial screening experiments. The experimental setup was modified for further investigation. Cells were incubated without test compound for 30 minutes and then injected with various concentration of test compound as agonist, instead of preincubating with the test compound and then stimulating with agonist. ATP was used as a positive control.

### 2.2.2.1.3 Determination of inhibition mechanism

The determination of inhibition mechanism became of great interest for several potent hits. Cells were incubated for 30 minutes with a single concentration of selected test compound based on the previously determined inhibitory dose-response curves. Five different concentrations of test compound were tested in duplicates on one 96 well plate of cells, plus duplicates DMSO 1 % as positive control. Cells were stimulated with various ATP concentrations to create shift curves. The nature of the shift provides an indication how the test compounds affects receptor activation upon agonist presence. When full activation of receptor is reached even under influence of high inhibitor concentration, and the EC<sub>50</sub> value of agonist is shifted to higher concentrations than the control, competitive receptor inhibition is indicated. The same EC<sub>50</sub> value, but a decrease of agonist potency upon full stimulation points to an allosteric inhibition mechanism of the antagonist.

### 2.2.2.2 Data analysis

Data evaluation required a two-step completion. The first step was executed in Microsoft® Excel. The first four measurement points of each calcium assay were taken prior to agonist injection and therefore discarded for the determination of fluorescence signal increase. Since ion channels provide a very fast response upon agonist stimulation, the very first fluorescence value measured after agonist stimulation was taken as starting point and subtracted from each following figure. This feature was programmed in Microsoft® Excel to be executed for each value obtained for each well. Only the sheer fluorescence increase was used for further data analysis. It was calculated by subtraction of the basic fluorescence out of each value. The mean was calculated out of all values obtained for one well. It was used for further dose-response analysis using GraphPad® Prism 4.02 for Windows (GraphPad® Software, San Diego, California, USA). All means obtained for test compounds were set in relation to the negative control (buffer) posing as 0 % receptor activity and the positive control (ATP), posing as 100 % receptor activity. Compound concentration values were then logarithmized, and curve fitting analysis was conducted, using sigmoidal dose response with variable slope, based on the logistic equation:

$$Y = Bottom + \frac{Top - Bottom}{1 + 10^{((logEC_{50} - X) \times Hill\ slope)}}$$

Top and Bottom represent 100 and 0 % receptor activation, respectively, while X represents the concentration of the used ligand. No constraints were selected. Each experiment was repeated three times. The mean curve was calculated by averaging the mean data of each experiment, followed by sigmoidal dose response analysis with variable slope. This calculation was selected for every dose-response experiment, including testing for inhibitory potency and enhancement dose-dependency.

The bell-shaped curve analysis was selected for compounds showing inhibition in high and enhancement in low concentrations, using GraphPad® Prism 5.03 (GraphPad® Software, San Diego, California, USA). It follows the equation:

$$Y = Dip + \frac{Plateau1 - Dip}{1 + 10^{((LogEC_{50\_1} - X) \times nH1)}} + \frac{Plateau2 - Dip}{1 + 10^{((logEC_{50\_2} - X) \times nH2)}}$$

Plateau1 and Plateau2 are the plateaus at the left and right end of the curve. Dip represents the plateau level in the middle of the curve, LogEC<sub>50\_1</sub> and LogEC<sub>50\_2</sub> are the concentrations that give half-maximal stimulatory and inhibitory effects, and nH1 and nH2 represent the unitless Hill slopes.

ATP shift curves were conducted in order to gain more insight in the inhibition mechanism of the most interesting hits. The Gaddum/Schild analysis was selected for determination whether the shift of the ATP curve fits with competitive antagonism. The equations are:

$$EC_{50} = 10^{\log EC_{50}}$$
$$\log EC = \log \left[ EC_{50} \times \left( 1 + \left( \frac{B}{10^{(-1 \times pA_2)}} \right)^{\text{Schild Slope}} \right) \right]$$
$$Y = Bottom + \frac{Top - Bottom}{1 + 10^{((\log EC - X) \times Hill\ slope)}}$$

Bottom and top represent the minimum and maximum responses, and X is the concentration of the used ligand in both sigmoidal dose response and Gaddum/Schild equations, respectively. The calculation of the dose ratio (DR) was needed for the linear regression. The dose ratio is defined as the quotient of the agonist EC<sub>50</sub> concentration influenced by antagonist and the control



agonist EC<sub>50</sub> concentration. The concentration of antagonist is then plotted against DR-1 to create the linear regression of the Schild plot.

Some compounds tested in ATP shift curve experiment did not show a shift of EC<sub>50</sub> value, but a concentration-dependent reduction of the maximal ATP effect. The fluorescence signal induced by the highest ATP concentration used in the experiment was calculated for those compounds. The buffer control was based as 0 % and the respective highest ATP concentration as 100 %. The unpaired Student's t-test of the respective means was conducted in order to determine whether the influence of the compound on the maximal ATP effect was statistically significantly different from the fluorescence increase caused by the highest ATP concentration of the control. The difference between mean pEC<sub>50</sub> of ATP control and mean pEC<sub>50</sub> of ATP influenced by respective test compound concentration was deemed significant, when the calculated P value was lower than 0.05. For all experiments, the two-tailed P value was selected. The same analysis was used to determine significance of maximal ATP effect of the control and after preincubation with respective test compound. Significant differences of the mean (P < 0.05) were marked with (\*), very significant differences (p < 0.01) with (\*\*), and highly significant differences (p < 0.001) with (\*\*\*)).

The unpaired Student's t-test was also selected for the analysis of the data collected for the fluorescence signal enhancement caused by some test compounds. The pEC<sub>50Enhancement</sub> values and the enhancement of maximal ATP effect were analyzed with the same protocol as described for pEC<sub>50</sub> values and maximal ATP effect determined out of ATP shift curves for inhibitory compounds. The ATP control was calculated from the results of the highest ATP concentration used in the respective experiment. It was perched at 100 % for the calculation of enhancement, the buffer control as 0 %. The ATP control was subtracted from the values of each sample to demonstrate the magnitude of enhancement.

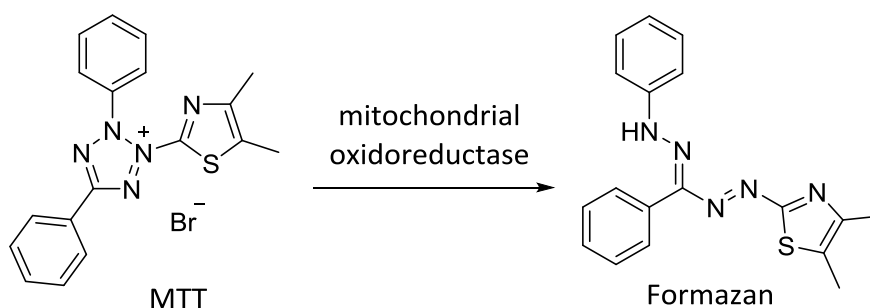
The validity of each experiment at each receptor was determined by calculation of Z'-factor as described by Zhang et al. in 1999.<sup>198</sup> The Z' factor is calculated by the following equation, with  $\sigma$  representing the standard deviation and  $\mu$  the mean of the positive (index p) and negative control (index n), respectively.

$$Z' = 1 - \frac{|3 \times \sigma_p + 3 \times \sigma_n|}{|\mu_p - \mu_n|}$$

The ATP values without addition of any inhibitor or test component were used as positive control. The negative control was calculated from the data obtained by preincubation with a standard antagonist. The concentration was selected high enough to completely block any receptor activity. When it was not possible to apply a standard antagonist on the assay plate, the buffer control was taken as the negative control instead. The Z'-factors from all experiments were averaged for each receptor and the standard error of the mean was calculated. At a Z'-factor higher than 0.5, the separation band between positive and negative control is large and the assay is deemed as suitable for high-throughput screening.

### 2.2.3 Measurement of compound toxicity and cell viability

Cell viability experiments were conducted to determine cytotoxicity of potent test compounds and to eliminate the possibility of positive calcium influx results due to cell toxicity. The experiment is based upon 3-(4,5-Dimethylthiazol-2-yl)-2,5-diphenyltetrazolium bromide (MTT), a yellow tetrazolium salt, being reduced to purple formazan, as illustrated in Figure 2.2.



**Figure 2.2:** Conversion of MTT to formazan.

The reduction is catalyzed by oxidoreductase enzymes that are primarily expressed in cellular mitochondria. Since the enzyme is only active in living cells, the amount of purple dye produced is directly proportional to the quantity of living cells in the well.

#### 2.2.3.1 Experimental setup

##### Day 1

Non-transfected 1321N1 astrocytoma cells were seeded in sterile tissue culture 96 well plates with a concentration of 2000 cells/well in a final volume of 180  $\mu$ l (POMs) or 99  $\mu$ l (all other compounds) and incubated overnight at 37°C and 5 % CO<sub>2</sub>.

Day 2

The dilutions of test compounds were prepared as discussed in chapter 2.2.2.1. The pipetting schemes can be found in chapters 2.1.6.6, 2.1.6.7 and 2.1.6.8. The dilutions for POMs were prepared in cell culture medium containing 10 % DMSO. All other compounds were diluted in pure DMSO. 5-Fluorouracil, a known cytotoxic cancer drug, was included in each experiment as a positive control. Cells were then supplemented with 20  $\mu$ l (POMs) or 1  $\mu$ l test compound, or pure DMSO (negative control), respectively, and then incubated for 72 hours at 37°C and 5 % CO<sub>2</sub>. The final DMSO concentration in the well never exceeded 1%. Each compound concentration was measured in duplicates in three independent experiments.

Day 5

One hour prior to the end of the 72 hour incubation period, each well was supplemented with 40  $\mu$ l (POMs) or 20  $\mu$ l (all other compounds) of freshly prepared MTT solution 5 mg/ml in PBS. Incubation was then continued to the end at 37°C and 5 % CO<sub>2</sub>, so that still alive cells could transform the yellow tetrazolium salt to purple formazan. The medium was removed and 100  $\mu$ l of DMSO was added to each well to lyse the cells. The plate was shaken at 200 rpm for 2 minutes to dissolve the formazan crystals produced in mitochondria. UV absorbance of the purple formazan was measured using FlexStation 3 at 570 nm. A second measurement was conducted directly afterwards to eliminate background absorbance. The full settings of the measurement are summarized in Table 2.2.

**Table 2.2:** Advanced settings of FlexStation3 for measurement UV absorbance of produced purple Formazan during MTT cell viability experiment

Measurement parameter	Settings
Read mode	Absorbance
Wavelength	LM1: 570 nm LM2: 690 nm
Assay plate	96 well standard clear bottom
Wells to read	Entire plate
Compound transfer	None
Automix	No
Calibration	On
Settle time	Off
Priority: wavelength or column	column

### **2.2.3.2 Data analysis**

Data analysis was performed analog to results of calcium influx measurement using Microsoft® Excel and GraphPad® Prism 4.02. The EC<sub>50</sub> value was determined using sigmoidal dose-response analysis with variable slope. No constraints were defined. The results of each well obtained via UV measurement at 690 nm were subtracted from the respective results obtained at 570 nm to eliminate background fluorescence of residual medium and cell components. The data was then transferred to GraphPad® Prism 4.02. The EC<sub>50</sub> value is here defined as the concentration of test compound, at which half of the cells are dead after 72 hours exposure.

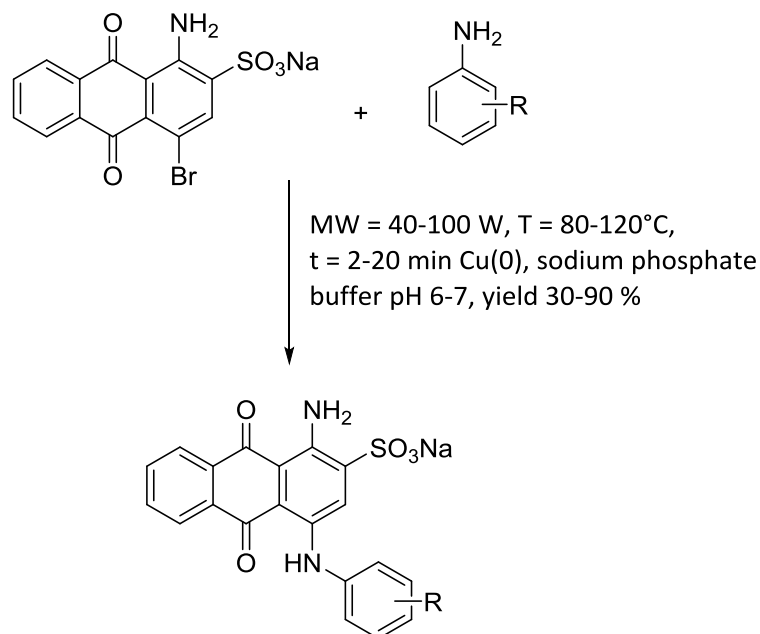
### 3 Characterization of the S15V mutant of rat P2X3 receptor

#### 3.1 Introduction

Antraquinones are chemical derivatives of anthracene and represent a class of natural products. They are either produced by the polyketide or the shikimate pathway. Anthraquinones synthesized by the latter often carry hydroxyl residues in positions 1 and 8 as well as methyl in position 3. The hydroxyl residues also represent glycosylation sites. Anthraquinones and dianthrones are important contents of plants including senna, frangula, aloe and rhubarb, and have been known for their laxative purposes for a long time.<sup>199</sup> Naturally glycosylated, the glycosides behave as prodrugs and are metabolized in the colon. This leads to the release of the aglycones that are responsible for the laxative effect by causing an increase of secretion and motility in the colon.

Antraquinone derivatives are also used as anticancer drugs. The most prominent representative is mitoxantrone, an alkaline substituted anthracendione, which is utilized in the therapy of lymphoma, leukemia, breast and prostate cancer.<sup>200</sup> It acts as an intercalate substance and inhibits the activity of topoisomerase II. Alongside cancer, it is also approved for the treatment of multiple sclerosis.<sup>201</sup> The use in both indications is limited by cardiotoxicity.<sup>200, 202</sup>

The anthraquinone derivative RB-2 is a weak antagonist and allosteric modulator at P2 receptors.<sup>66, 203</sup> RB-2 is an anthraquinone-chlorotrizinyl reactive dye and was formerly used in textile industry and in the purification process of proteins by affinity chromatography.<sup>204</sup> A truncated version of RB-2 was selected as a lead structure for the development of new potent antagonists of P2 receptors. The library contains 165 amino and 26 desamino derivatives. It was originally developed for the pharmacological testing at the P2Y<sub>2</sub> and the P2Y<sub>12</sub> receptors.<sup>205, 206</sup> The aim was the identification of a new and potent ligand with antithrombotic efficacy. P2Y<sub>12</sub>, a G<sub>i</sub>-coupled GPCR, plays an important role in blood platelet function and regulation.<sup>207</sup> All investigated compounds display an aminoanthraquinone- or desaminoanthraquinone core with a sulfonic acid group in position 2 and various residues with great structural differences in position 4 linked via an amino bridge. The synthesis of the compounds has been described in detail.<sup>208-210</sup> Briefly, 4-bromo-substituted anthraquinone derivatives are coupled with the appropriate amine by microwave-assisted Ullmann reaction in phosphate buffer (pH 6-7) in the presence of Cu<sup>0</sup>. The synthesis scheme is presented in Figure 3.1, and Figure 3.2 gives an overview of the different basic structures of the tested compounds.

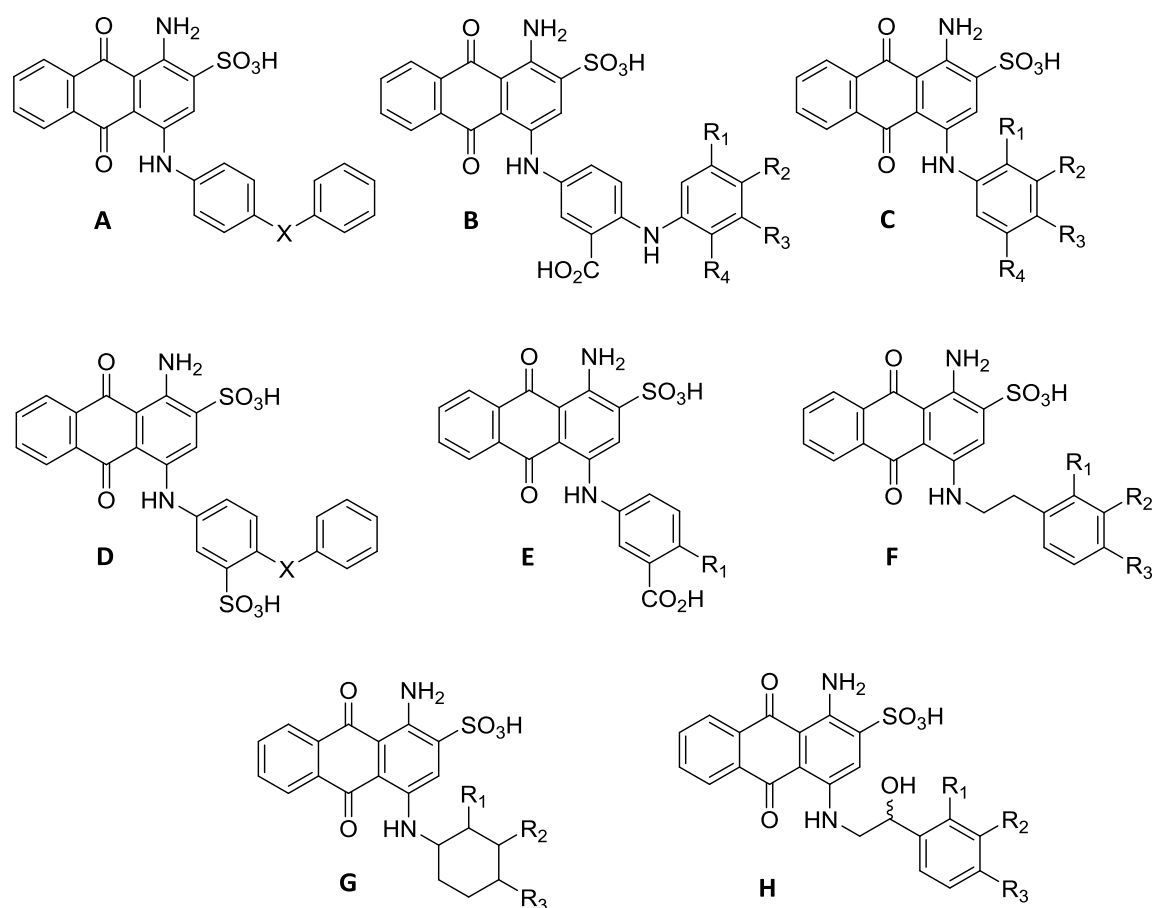


**Figure 3.1:** Microwave-assisted Cu(0)-catalyzed synthesis of 4-phenylamino-substituted 1-amino-2-sulfoanthraquinone derivatives in phosphate buffer.<sup>208</sup>

A variety of different substitutions is available, which facilitates the study of structure-activity relationships. This compound library has previously been identified to contain potent antagonists of P2X<sub>2</sub>, P2Y<sub>2</sub>, P2Y<sub>12</sub> receptors, ecto-5'-nucleotidase and ectonucleoside triphosphate diphosphohydrolases. They display high inhibitory potency with nanomolar IC<sub>50</sub> and K<sub>i</sub> concentrations, respectively.<sup>103, 205, 206, 211-214</sup>

A total of 26 compounds are available in their deaminated form, where the amino residue in position 1 was replaced with hydrogen. Most of them are derivatives displaying scaffold C. The purpose of eliminating the amino function in position 1 was to characterize its influence on compound binding and efficacy.

Hausmann et al. succeeded in creating a stable non-desensitizing rat P2X<sub>3</sub> receptor mutant by exchanging serine in position 15 to valine, as is described in detail in chapter 1.2.8.<sup>118</sup> The receptor was transfected retrovirally into 1321N1 astrocytoma cells, creating a stably expressing cell line. The aim of this study was to evaluate the created cell line and determine its suitability for high-throughput screening by testing the anilinoanthraquinone library via measurement of calcium influx. Since Cibacron Blue 3GA is an identified PAM of the P2X<sub>3</sub> receptor, the effect of structural derivatization on compound activity was also evaluated.<sup>127</sup>



**Figure 3.2:** Basic scaffolds of tested aminoanthraquinone derivatives. Residues are presented in chapters 3.4.1 and 3.4.2.

### 3.2 Z'-factor for determination of assay quality

The Z'-factor was calculated to determine assay quality and therefore the accuracy of the results. When the Z'-factor is higher than 0.5, the assay system is considered acceptable for high-throughput screening.<sup>198</sup> The Z'-factor was calculated for each experiment, using the mean and standard deviation of all positive and all negative controls. The data obtained of all experiments was used to calculate the average Z'-factor. A total number of 75 values were included in this analysis. The average Z'-factor for the measurement of calcium influx in the 1321N1 astrocytoma cell line stably transfected with the P2X3 receptor was  $0.64 \pm 0.02$ . Therefore, the assay is suitable for high-throughput screening.

## 3.3 Potency of standard agonists and antagonists

The affinity and potency of several standard agonists and antagonists towards the S15V mutant of the rat P2X3 receptor (P2X3) stably expressed in 1321N1 astrocytoma cell lines were determined as a first step. Eleven cell monoclonal lines were successfully selected and cultured to find cells with high receptor expression. Two different concentrations (0.1  $\mu\text{M}$  and 1  $\mu\text{M}$ ) of the physiological agonist ATP were used for initial stimulation experiments. Carbachol and HBSS buffer were used as positive and negative controls, respectively. Three of those monoclonal lines showed high fluorescence signal increase between 6000 and 18 000 fluorescence counts. The monoclonal line giving the highest signal (monoclonal 7) was used in all further experiments.

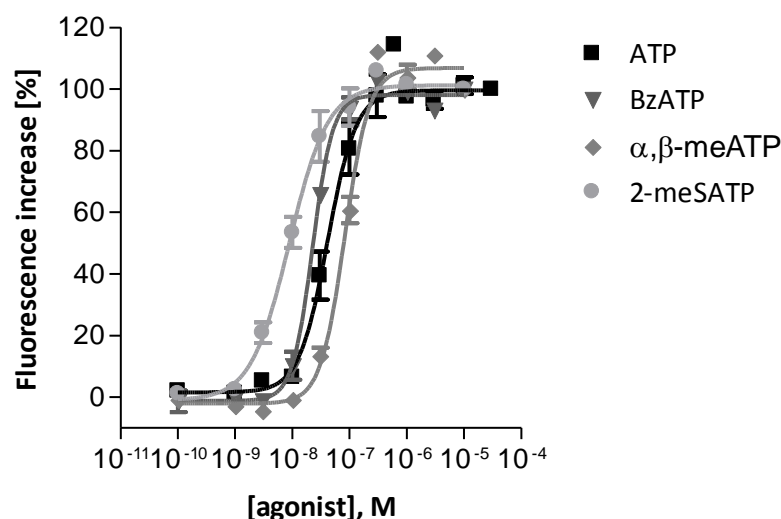
### 3.3.1 Standard agonists

Several standard agonists,  $\alpha,\beta$ -meATP, BzATP and 2-meSATP (structures see Figure 1.9), whose affinity and potency is well described at P2X receptors, were selected for further receptor characterization.

The physiological agonist ATP showed an  $\text{EC}_{50}$  value of  $0.0514 \pm 0.0096 \mu\text{M}$ . The results indicate a higher affinity as previously determined via patch clamp experiments (1.2  $\mu\text{M}$ ,<sup>68</sup>  $1.6 \pm 0.1 \mu\text{M}$ <sup>69</sup> or  $4.1 \pm 0.53 \mu\text{M}$ <sup>70</sup> at human and  $2.6 \pm 0.9 \mu\text{M}$ <sup>69</sup> at rat P2X3). However, they are lower than those obtained in radioligand binding studies ( $\text{IC}_{50}$  0.00316 against [<sup>35</sup>S]ATP $\gamma$ S).<sup>215</sup> Both human and rat P2X3 wild type receptors show rapid desensitization milliseconds after agonist stimulation, so the adequate estimation of agonist affinity by functional experiments like measurement of calcium influx or patch clamp experiments proves to be difficult.<sup>216</sup> The high affinity data of radioligand binding experiments suggest a very high potency of ATP at wild type P2X3 receptors. Pratt et al. suggest the possibility of two classes of binding sites, a low-affinity activator and a high-affinity inhibitory site on the receptor as an explanation for this phenomenon.<sup>69</sup> According to this theory, the high affinity of ATP to the latter and its slow dissociation traps the receptor in its desensitized state and defines the unusually slow recovery rate.

The  $\text{EC}_{50}$  value of ATP determined with the P2X3 receptor mutant lies below the reported functional and binding data of the P2X3 receptor wild type and was determined to be around five times more potent than reported by Hausmann et al. by measurement of calcium influx. The same is true for the potent ATP analog  $\alpha,\beta$ -meATP.<sup>118</sup>





**Figure 3.3:** Mean dose-response curves of standard agonists at the P2X3 receptor (mean  $\pm$  SEM,  $n = 3-7$ ).

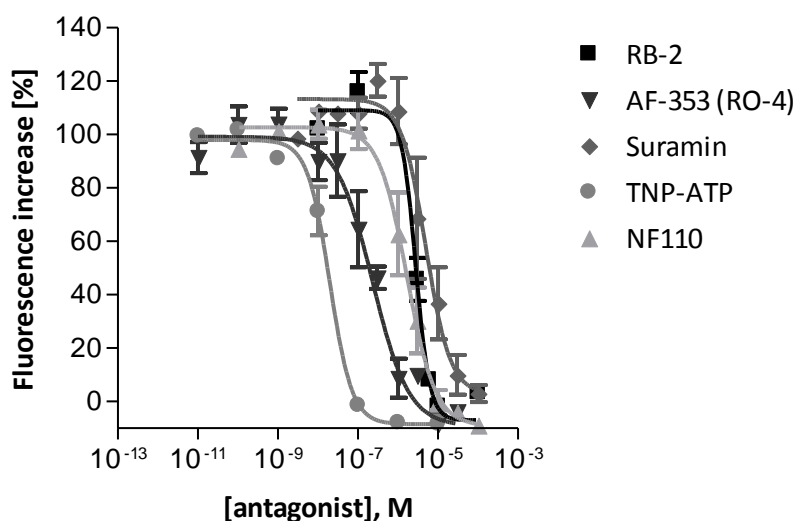
Additionally, BzATP and 2-meSATP, further potent standard agonists at wild type P2X3 receptors, were tested. BzATP proved to be slightly more potent at the P2X3 receptor than ATP. This was previously reported by Bianchi et al., although again with higher values (see Table 3.1).<sup>63</sup> The most active agonist was 2-meSATP with an  $EC_{50}$  value of  $0.00925 \pm 0.00109 \mu\text{M}$ . It was almost 30 times more potent than reported previously for the wild type receptor.<sup>28</sup> Discrepancies like this could be attributed to receptor desensibilization distorting its sensitivity to stimulation. Despite the high potency of 2-meSATP, ATP was selected as standard agonist for stimulation experiments due to lower cost.

**Table 3.1:** Agonistic potency of standard agonists (mean  $\pm$  SEM,  $n = 3-7$ ) and described in the literature at the P2X3 receptor.<sup>28, 63, 118</sup>

Agonist	$EC_{50} \pm \text{SEM} [\mu\text{M}]$	$EC_{50} [\mu\text{M}]$ from literature
ATP	<b><math>0.0514 \pm 0.0096</math></b>	<b>0.280-0.339</b>
BzATP	<b><math>0.0241 \pm 0.0024</math></b>	<b>0.03-0.08</b>
$\alpha,\beta$ -meATP	<b><math>0.0859 \pm 0.0064</math></b>	<b>0.354-2</b>
2-meSATP	<b><math>0.00925 \pm 0.00109</math></b>	<b>0.3</b>

### 3.3.2 Standard antagonists

Several well-known standard antagonists were tested at the P2X3 receptor. Suramin, RB-2, TNP-ATP and the P2X3 receptor-selective compounds AF-353 and NF110 were available for testing. The results are presented in Figure 3.4. The most potent standard antagonist was TNP-ATP, which was capable of blocking calcium flux in low nanomolar concentrations (see Table 3.2). This result correlates to previously reported data of patch clamp experiments at rat P2X3 receptors, where an  $IC_{50}$  value of  $\sim 0.002 \mu\text{M}$  was determined.<sup>28</sup> RB-2 and Suramin were proven to be relatively weak antagonists. The results for suramin are comparable to the ones already reported, but RB-2 was previously identified as a weak allosteric modulator.<sup>28, 63</sup> RB-2 is a mixture of meta/para sulfonate substitution at the last phenyl residue. The substitution pattern at the last ring is most likely responsible for the diversion, since only the *ortho*-isomer acts as a PAM at the P2X3 receptor.



**Figure 3.4:** Mean dose-response curves of standard antagonists at the P2X3 receptor stimulated with ATP  $0.1 \mu\text{M}$  (mean  $\pm$  SEM,  $n = 3-7$ ).

Gever et al described AF-353 as a potent and selective non-competitive P2X3 receptor antagonist.<sup>121</sup> The results at the P2X3 receptor indicate a lower  $IC_{50}$  value ( $0.389 \pm 0.100 \mu\text{M}$ ). Since the compound is described to inhibit the receptor in a non-competitive way, it is possible that the amino acid exchange to stabilize the receptor lead to an alteration of the antagonist binding pocket, resulting in a loss of potency.

NF110 was initially described as the first suramin-derived antagonist who preferably inhibits the P2X3 receptor over the P2X1 receptor in a competitive manner with an  $IC_{50}$  value of  $0.090 \pm 0.018 \mu\text{M}$ .<sup>125</sup> In our experiments, the compound was found to be approximately tenfold less potent. The mode of inhibition of NF110 was determined via patch clamp experiments at the heteromeric P2X2/3 receptor subtype due to its non-desensitizing properties upon ATP stimulation. The different pharmacology of the heteromeric receptor (see chapter 1.2.8) could explain the observed discrepancy.

**Table 3.2:** Inhibitory potency of standard antagonists (mean  $\pm$  SEM, n = 3-7) and described in the literature at the P2X3 receptor.<sup>28, 121, 125</sup>

Antagonist	$IC_{50} \pm \text{SEM} [\mu\text{M}]$	$IC_{50} \pm \text{SEM} [\mu\text{M}]$ from literature
RB-2	<b>2.88</b> $\pm$ 0.12	<b>1.4</b> <sup>a, b</sup>
AF-353 (RO-4)	<b>0.389</b> $\pm$ 0.100	<b>0.00891</b>
Suramin	<b>4.41</b> $\pm$ 2.04	<b>3</b>
TNP-ATP	<b>0.0190</b> $\pm$ 0.0036	<b>0.001</b>
NF110	<b>1.57</b> $\pm$ 0.55	<b>0.090</b> $\pm$ 0.018

<sup>a</sup>:  $EC_{50}$ Enhancement of positive allosteric modulation

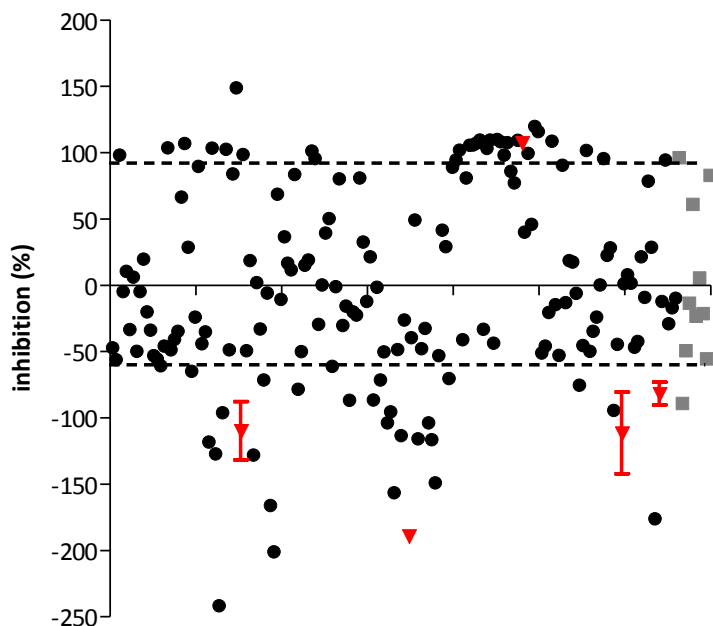
<sup>b</sup>: Enhancement only by the *ortho*-isomer (Cibacron Blue 3GA)

### 3.4 Potency of amino- and desaminoanthraquinone derivatives

The next step in the characterization of the P2X3 receptor represented the screening of a comprehensive compound library to prove its suitability for high-throughput screening via measurement of calcium influx. The selected derivatives were already identified to be potent inhibitors of the P2X2 receptor and they contain a high variety of structural modifications for extensive structure-activity-relationship studies.<sup>103</sup> A compound library of 165 anthraquinone- and 26 desaminoanthraquinone derivatives was selected for screening and determination of dose-response curves.

The first step was a screening experiment, where a single concentration (10  $\mu\text{M}$ ) was tested at least three times in duplicates. The results are presented in Figure 3.5. Since many compounds seemed to be highly active, dose-response curves to determine the  $IC_{50}$  concentration were conducted for all compounds which inhibited the P2X3 receptor more than 80 %. Moreover, a lot of compounds apparently enhanced the maximal ATP effect, resulting in receptor inhibition mathematically lower than zero. Both effects were examined further in additional experiments.

In the following chapters, structure-activity relationships of compounds with inhibitory and ATP-enhancing potency demonstrated.



**Figure 3.5:** Inhibition of the P2X3 receptor by 165 anthraquinone (●) and 26 desaminoanthraquinone compounds (■) in a single concentration of 10  $\mu$ M (mean,  $n = 3-5$ ). Compounds YB038, YB087, YB120, YB149 and YB160 are marked (▼), since they were selected for further experiments (mean  $\pm$  SEM,  $n = 3-5$ ). Dashed line: compounds with an inhibition value  $\geq 80\%$  or  $\leq -100\%$  were submitted to dose-response curve determination.

### 3.4.1 Inhibitory potency

During the initial screening experiments, 39 anthraquinone- and 5 desaminoanthraquinone derivatives were found to inhibit the P2X3 receptor to over 80% at a final concentration of 10  $\mu$ M (see Figure 3.5). For of those hits, concentration-response curves were conducted.

#### 3.4.1.1 Scaffold C, D and E of aminoanthraquinones

The results of the screening and dose-response experiments are summarized in Table 3.3 for compounds based on scaffold C, Table 3.4 for scaffold D and Table 3.5 for scaffold E. Smaller substituents introduced in position 4 of the aminoanthraquinone core proved to be suitable for inhibitors of the P2X3 receptor.

**Table 3.3:** Inhibitory potency of aminoanthraquinone derivatives with basic scaffold C at the P2X3 receptor (mean  $\pm$  SEM, n = 3-5).

Compound	R <sub>1</sub>	R <sub>2</sub>	R <sub>3</sub>	R <sub>4</sub>	IC <sub>50</sub> $\pm$ SEM [ $\mu$ M]
<b>YB025 (Acid Blue 25)</b>	H	H	H	H	> 10 (-24 %)
<b>YB022</b>	H	H	Cl	H	n. c. <sup>a</sup> (106 %)
<b>YB034</b>	H	H	Br	H	<b>5.89</b> $\pm$ 2.01 <sup>b</sup>
<b>YB036</b>	H	H	CH <sub>3</sub>	H	n. c. <sup>a</sup> (83 %)
<b>YB073</b>	H	H	CH <sub>2</sub> CH <sub>3</sub>	H	<b>8.90</b> $\pm$ 1.12 <sup>b</sup>
<b>YB011</b>	H	H	OH	H	> 10 (-21 %)
<b>YB045</b>	H	H	SO <sub>3</sub> H	H	> 10 (-72 %)
<b>YB015</b>	H	H	OCH <sub>3</sub>	H	> 10 (-61 %)
<b>YB019</b>	H	H	NH <sub>2</sub>	H	> 10 (-42 %)
<b>YB054</b>	H	CH <sub>3</sub>	OH	H	<b>7.04</b> $\pm$ 1.43 <sup>b</sup>
<b>YB037</b>	H	COOH	NH <sub>2</sub>	H	n. c. <sup>a</sup> (148 %)
<b>YB059</b>	H	CH <sub>3</sub>	H	CH <sub>3</sub>	n. c. <sup>a</sup> (101 %)
<b>YB005</b>	COOH	H	H	H	> 10 (10 %)
<b>YB009</b>	SO <sub>3</sub> H	H	H	H	> 10 (-5 %)
<b>YB004</b>	COOH	H	H	Cl	> 10 (-5 %)
<b>YB007</b>	COOH	H	Cl	H	> 10 (6 %)
<b>YB006</b>	H	COOH	H	H	> 10 (-34 %)
<b>YB008</b>	H	H	COOH	H	> 10 (-50 %)
<b>YB010</b>	OH	H	H	H	> 10 (19 %)
<b>YB016 (PSB-0716)</b>	OCH <sub>3</sub>	H	H	H	> 10 (-46 %)
<b>YB020</b>	NH <sub>2</sub>	H	H	H	> 10 (-36 %)

<sup>a</sup>: n. c. no convergence (nonlinear regression fit of the data was not possible)

<sup>b</sup>: curve was extrapolated

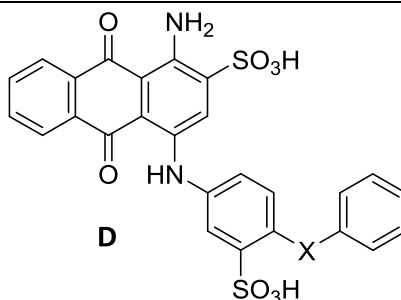
The sole aniline derivative YB025 was not active, but the introduction of several residues in different positions of scaffold C lead to an increase of inhibitory potency. Small residues like halogen (chlorine in YB022 and bromine in YB034), a methyl (YB036) or an ethyl group (YB073) were tolerated in the *para*-position, whereas compounds with a hydroxyl (YB011), a sulfonic acid (YB045), a methoxy (YB015), an amino (YB019) or a carboxymethyl substituent in this position showed no inhibitory activity. The concentration-response curves for the active compounds confirmed the initial results for the bromine residue (YB034, IC<sub>50</sub> 5.89  $\pm$  2.01  $\mu$ M). The determination of the IC<sub>50</sub> value for the chlorine substituent was not successful. A fluorine

residue in the *para*-position displayed a very different effect, which will be discussed in detail later on in chapter 3.4.2.

**Table 3.4:** Inhibitory potency of aminoanthraquinone derivatives with basic scaffold D at the P2X3 receptor (mean  $\pm$  SEM, n = 3-5).

Compound	X	IC <sub>50</sub> $\pm$ SEM [ $\mu$ M]
YB030	O	7.92 $\pm$ 1.74 <sup>a</sup>
YB039 (PSB-0739)	NH	n. c. <sup>b</sup> (98 %)

Scaffold

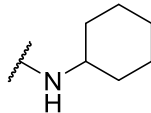
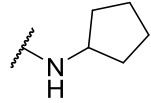
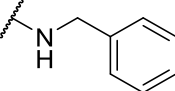
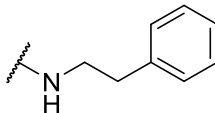
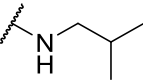
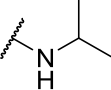
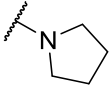
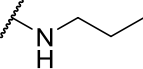


<sup>a</sup>: curve was extrapolated

<sup>b</sup>: n.c. no convergence (nonlinear regression fit of the data was not possible)

The combination of two different substituents in different positions on the aniline residue of scaffold C led to inhibitory potency at the P2X3 receptor. When the previously proven inactive hydroxyl group in the *para*-position is combined with a methyl residue in the *meta*-position, inhibition of the P2X3 receptor can be observed (YB054, IC<sub>50</sub> 7.04  $\pm$  1.43  $\mu$ M). Its potency is similar to the introduction of an amino- and a carboxylic acid function in the same positions. The introduction of those residues in *meta*-position of each other was tolerated as well (YB037). Two methyl substituents in *meta*-position (YB059) also led to inhibition of the receptor at 10  $\mu$ M screening concentration, but these results could not be confirmed in concentration-response experiments. Positioning a carboxylic acid (YB005) or a sulfonic acid function (YB009) in the *ortho*-position of the aniline ring abolished any inhibitory effect of the compounds. This result was consistent in combination with chlorine in different positions (see compounds YB004 and YB007). The transposition of the carboxylic acid residue in the *meta*- or *para*-position of the aniline ring did not improve these results (see compounds YB006 and YB008). Generally, the introduction of small hydrophilic residues (compounds YB010, YB016 and YB020) in the *ortho*-position was not tolerated by the P2X3 receptor.

**Table 3.5:** Inhibitory potency of aminoanthraquinone derivatives with basic scaffold E at the P2X3 receptor (mean  $\pm$  SEM, n = 3-5).

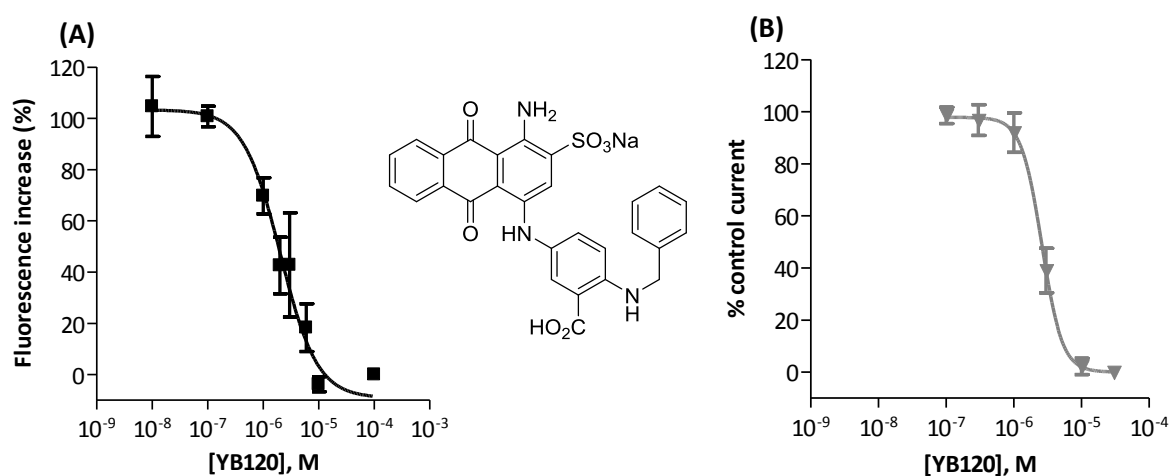
Compound	R	IC <sub>50</sub> $\pm$ SEM [ $\mu$ M]
<b>YB117</b>		<b>7.71 <math>\pm</math> 0.17<sup>a</sup></b>
<b>YB118</b>		> 10 (77 %)
<b>YB120</b>		<b>2.39 <math>\pm</math> 1.00<sup>a</sup></b>
<b>YB119</b>		<b>5.99 <math>\pm</math> 0.52<sup>a</sup></b>
<b>YB121</b>		> 10 (40 %)
<b>YB123</b>		> 10 (45 %)
<b>YB126</b>		> 10 (-52 %)
<b>YB122</b>		<b>6.89 <math>\pm</math> 0.79<sup>a</sup></b>

<sup>a</sup>: curve was extrapolated

The linker between the sulfoaniline and the second benzene moiety was varied in scaffold D. Both nitrogen and oxygen showed high inhibitory potency during initial screening at 10  $\mu$ M, but only for the oxygen linker IC<sub>50</sub> values could be calculated.

Scaffold E was varied by introducing different residues in the *para*-position of the carboxyaniline moiety in position 4 of the aminoanthraquinone core. The cyclohexylamino residue (YB117) was more potent than its cyclopentyl analog (YB118). No inhibitory activity could be observed for the pyrrolidin-1-yl group (YB126) in the initial screening experiments. The exchange of the cyclohexyl residue to a benzyl function (YB120) led to a slight increase in potency, but still in the lower micromolar range. This proved to be the most active compound of all of these three scaffolds.

The concentration-response curves measured via calcium influx experiment and via patch clamp (thanks to PD Dr. Ralf Hausmann from the Institute of Toxicology and Pharmacology, University of Aachen) of three independent experiments are presented in Figure 3.6 as an example for all conducted dose-response curves with active compounds based on scaffold C, D and E. The respective  $IC_{50}$  values were  $2.39 \pm 1.00 \mu\text{M}$  for measurement of calcium influx and  $2.60 \mu\text{M}$  for patch clamp experiments. The results are reproducible by different methods, and it seems unlikely that any fluorescence of the compounds themselves interfered with the calcium influx experiment.



**Figure 3.6:** Mean dose-response curves and structure of YB120 at the P2X3 receptor (mean  $\pm$  SEM,  $n = 3$ ), determined by (A) measurement of calcium influx (■, curve was extrapolated) and (B) by patch clamp experiments (▼). The patch clamp-derived data was provided by PD Dr. Ralf Hausmann. Data is presented as mean  $\pm$  SEM from 5-6 independent experiments.

The elongation to a phenylethyl moiety (YB119) did not improve the inhibitory effect. Non-cyclic aliphatic residues like an isobutyl (YB121) or isopropyl (YB123) function attached via N to the carboxyaniline residue showed weak to no activity. Only the non-branched short ethyl group weakly inhibited the P2X3 receptor similar to the other active aminoanthraquinone derivatives.

#### 3.4.1.2 Scaffold A and B of aminoanthraquinones

The addition of a second phenyl residue in the *para*-position of the aminoaniline moiety was the first step to a series of compounds displaying constant inhibitory activity at the P2X3 receptor. The results are presented in Table 3.6.



**Table 3.6:** Inhibitory potency of aminoanthraquinone derivatives with basic scaffold A at the P2X3 receptor (mean  $\pm$  SEM, n = 3).

Compound	X	IC <sub>50</sub> $\pm$ SEM [ $\mu$ M]
YB017	CH <sub>2</sub>	5.98 $\pm$ 2.09 <sup>a</sup>
YB018	O	> 10 (-49 %)
YB027	S	> 10 (-44 %)
YB026	NH	6.28 $\pm$ 2.31 <sup>a</sup>

<sup>a</sup>: curve was extrapolated

First, the influence of the linker between the two phenyl residues in scaffold A was investigated. A methylene group (YB017), nitrogen (YB026), oxygen (YB018) and sulfur (YB027) were tested. Only the methylene and the amino linker showed suitable inhibitory potency at the P2X3 receptor.

Scaffold B was obtained by introducing a carboxyl group in position 3 of the first aniline ring. It was the starting point for a whole series of compounds displaying various residue patterns on the second aniline moiety. All compounds except YB103 were shown to be full antagonists of the P2X3 receptor with IC<sub>50</sub> values between 2 and 8  $\mu$ M, respectively. Short residues like chlorine, fluorine, methyl, methoxy or ethoxy groups were tolerated in all positions of the second aniline ring, but did not lead to an improvement of inhibitory activity below the micromolar range. The only residue not tolerated was an ethyl function in position 2 (YB103). Since the ethoxy residue in the same position did not abolish inhibitory potency, it is possible that anything bulkier than a methyl residue needs a polar structure like oxygen for full inhibition of the P2X3 receptor.

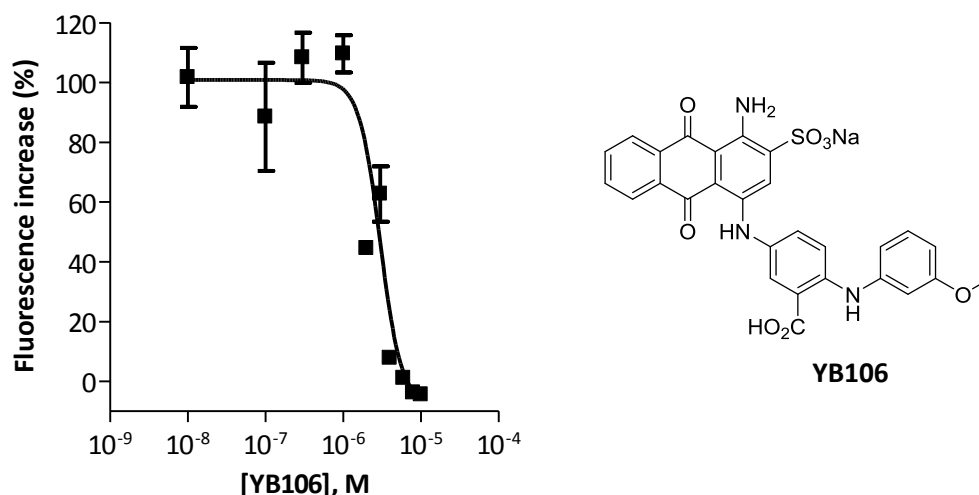
**Figure 3.7:** Inhibitory potency of aminoanthraquinone derivatives with basic scaffold B at the P2X3 receptor (mean  $\pm$  SEM, n = 3).

Scaffold

Compound	R <sub>1</sub>	R <sub>2</sub>	R <sub>3</sub>	R <sub>4</sub>	IC <sub>50</sub> $\pm$ SEM [ $\mu$ M]
YB100	H	H	H	H	<b>3.29</b> $\pm$ 0.37
YB103	H	H	H	CH <sub>2</sub> CH <sub>3</sub>	> 10 (-42 %)
YB101	H	CH <sub>3</sub>	H	H	<b>7.56</b> $\pm$ 0.90 <sup>a</sup>
YB102	H	H	CH <sub>3</sub>	H	<b>3.50</b> $\pm$ 0.20
YB104	H	H	Cl	H	<b>2.62</b> $\pm$ 0.37
YB105	H	H	H	OCH <sub>3</sub>	<b>2.47</b> $\pm$ 0.25
YB106	H	H	OCH <sub>3</sub>	H	<b>2.81</b> $\pm$ 0.41
YB107	H	H	H	Cl	<b>2.38</b> $\pm$ 0.30
YB108	H	F	H	H	<b>2.82</b> $\pm$ 0.12
YB110	CH <sub>3</sub>	H	CH <sub>3</sub>	H	<b>5.35</b> $\pm$ 2.30 <sup>a</sup>
YB111	CH <sub>3</sub>	H	H	CH <sub>3</sub>	<b>3.41</b> $\pm$ 0.77
YB113	H	CH <sub>3</sub>	H	CH <sub>3</sub>	<b>3.33</b> $\pm$ 0.78
YB114	H	H	CH <sub>3</sub>	CH <sub>3</sub>	<b>3.48</b> $\pm$ 0.50
YB115	H	H	H	OCH <sub>2</sub> CH <sub>3</sub>	<b>6.33</b> $\pm$ 0.11 <sup>a</sup>
YB116	H	OCH <sub>2</sub> CH <sub>3</sub>	H	H	<b>3.52</b> $\pm$ 0.90
YB124	H	H	H	F	<b>3.62</b> $\pm$ 0.54 <sup>a</sup>
YB125	H	H	F	H	<b>7.12</b> $\pm$ 1.07 <sup>a</sup>
YB139	H	H	Cl	H	<b>6.83</b> $\pm$ 1.17 <sup>a</sup>

<sup>a</sup>: curve was extrapolated

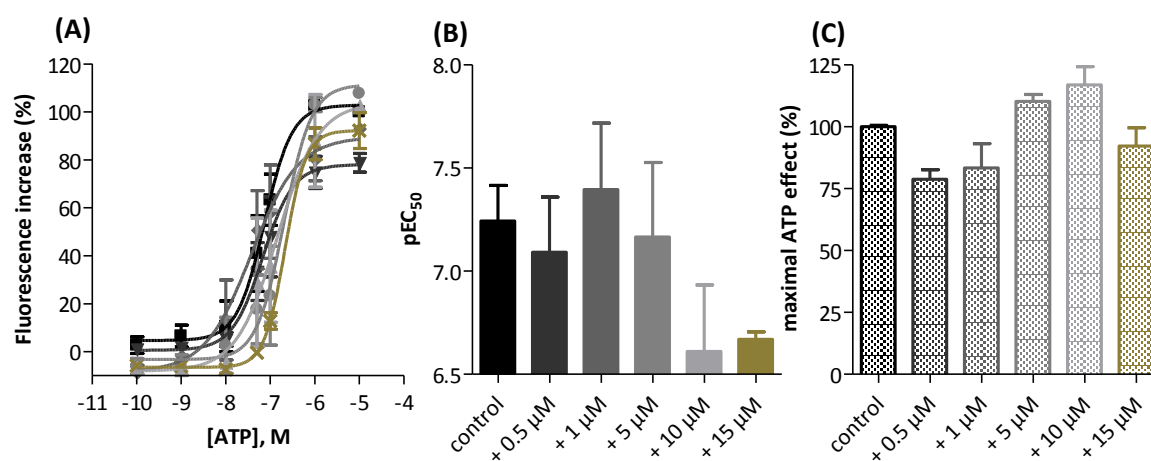
One of the most active compounds was YB106 with an IC<sub>50</sub> value of 2.81  $\pm$  0.41  $\mu$ M (see Figure 3.8). Small residues in various positions of the second aniline ring did not further improve the inhibitory potency. No compounds with larger residues like phenyl or benzyl or longer aliphatic groups were available for testing. With the exception of position 2, the introduction of such functions in other positions of the second aniline ring might further improve inhibition potency. Nonetheless, scaffold B was proven to be a successful lead structure for the development of potent aminoanthraquinone-based inhibitors of the P2X3 receptor.



**Figure 3.8:** Mean dose-response curve and structure of scaffold B anthraquinone derivative YB106 at the P2X3 receptor (mean  $\pm$  SEM,  $n = 3$ ).

#### 3.4.1.3 Determination of inhibition mechanism

The inhibitory potency of anthraquinone derivatives proved to be weak, but in order to determine the mechanism of inhibition, ATP concentration-response experiments with and without various concentrations of an anthraquinone-based inhibitor were conducted. One of the most active compounds, scaffold E-based compound YB120, was selected as an example for the whole series of anthraquinone derivatives. The results are presented in Figure 3.9.



**Figure 3.9:** (A) Mean ATP dose-response curves, (B) ATP  $pEC_{50}$  values and (C) maximal ATP effect (%) at 10  $\mu$ M ATP characterizing the influence of most active inhibitory scaffold E derivative YB120 0.5  $\mu$ M ( $\blacktriangledown$ ), 1  $\mu$ M ( $\blacklozenge$ ), 5  $\mu$ M ( $\bullet$ ), 10  $\mu$ M ( $\blacktriangle$ ) and 15  $\mu$ M ( $\times$ ) at the P2X3 receptor. Cells were incubated with compounds prior to stimulation with ATP 0.0001-10  $\mu$ M, respectively. Buffer containing 1% DMSO without compound was used as control ( $\blacksquare$ ). Data is presented as mean  $\pm$  SEM from 3-6 independent experiments.

Before testing the high concentration of 15  $\mu\text{M}$  YB120, a fluorescence test was necessary to eliminate any interfering fluorescence signal. No increase of basic fluorescence prior to ATP injection could be detected. The obtained results were therefore included in the data analysis and interpretation.

The concentrations of YB120 used in this experiment were selected based on the previously determined  $\text{IC}_{50}$  value of  $2.39 \pm 1.00 \mu\text{M}$ . None of the concentrations tested affected the maximal ATP effect with statistical significance (see Figure 3.9). However, the  $\text{pEC}_{50}$  values of ATP were slightly shifted towards higher concentrations.

Since the maximal ATP effect is sparsely affected, the shift of  $\text{EC}_{50}$  value indicates YB120 to be a competitive antagonist of the P2X3 receptor. A Schild plot was conducted to further analyze the effect. The results are presented in Table 3.7.

**Table 3.7:**  $\text{pA}_2$ , Hill slope and Schild slope of Gaddum/Schild  $\text{EC}_{50}$  shift analysis for anthraquinone derivative YB120 at the P2X3 receptor. Data was calculated from the mean of 3-6 independent experiments.

	<b><math>\text{pA}_2</math></b>	<b>Hill slope</b>	<b>Schild slope</b>
<b>YB120</b>	4.98	1.20	3.95

$\text{PA}_2$  is defined as the logarithm of the concentration of antagonist needed to shift the ATP dose-response curve by a factor of 2. The Schild slope quantifies how well the shifts match the prediction of competitive interaction. When the inhibitor binds in a competitive mode, the Schild slope is 1.0. If the shift of ATP dose-response curve to the right is greater than predicted, the Schild slope is greater than 1, when it is less than predicted, it is less than 1. Here, the Schild slope is greater than 1. The lack of fluorescence signal decrease and the slight shift of  $\text{EC}_{50}$  to the right are hints for orthosteric antagonism, but the analysis was inconclusive. The lack of fluorescence signal decrease and the slight shift of  $\text{EC}_{50}$  values to the right are hints for competitive receptor inhibition, but the results of the analysis did not confirm the initial observation. In the literature, a competitive mode of inhibition for the anthraquinone derivatives at P2X2 receptors has been determined previously via patch clamp experiments in *Xenopus oocytes*.<sup>103</sup> Since aminoanthraquinone derivative Cibacron Blue 3GA is postulated as an allosteric modulator of P2X3 receptor, it is possible that YB120 is capable of interacting with the P2X3 receptor by different binding sites.<sup>127</sup> This could be a cause for the inconclusive Schild plot data.

### 3.4.1.4 Desaminoanthraquinone derivatives

A series of deaminated anthraquinone compounds was tested in order to determine the importance of the amino function in position 1 of the anthraquinone core. Not all anthraquinone compounds were available in the deaminated form. Table 3.8 and Table 3.9 contain the results of the most interesting substitutes.

**Table 3.8:** Inhibitory potency of desaminoanthraquinone derivatives with basic scaffold C at the P2X3 receptor (mean  $\pm$  SEM, n = 3-5). The data of the aminated derivative is repeated for better comparison.

Compound	R <sub>1</sub>	R <sub>2</sub>	IC <sub>50</sub> $\pm$ SEM [ $\mu$ M] of aminated compound	IC <sub>50</sub> $\pm$ SEM [ $\mu$ M] of deaminated compound
daYB025	H	H	> 10 (-24 %)	> 10 (-24 %)
daYB016	CH <sub>3</sub>	H	> 10 (-46 %)	> 10 (-14 %)
daYB010	OH	H	> 10 (19 %)	<b>4.86 <math>\pm</math> 0.64<sup>a</sup></b>
daYB022	H	Cl	n. c. <sup>b</sup> (106 %)	> 10 (61 %)
daYB034	H	Br	<b>5.89 <math>\pm</math> 2.01<sup>a</sup></b>	<b>7.69 <math>\pm</math> 0.80<sup>a</sup></b>
daYB036	H	CH <sub>3</sub>	n. c. <sup>b</sup> (83 %)	> 10 (32 %)

<sup>a</sup>: curve was extrapolated

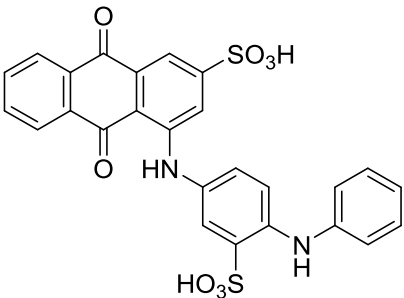
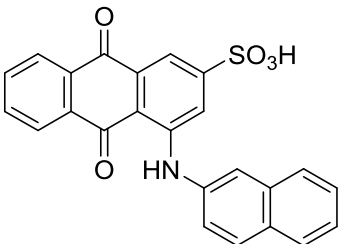
<sup>b</sup>: n. c. no convergence

When comparing the results of deaminated compounds available with their respective aminated counterpart (see chapters 3.4.1.1 and 3.4.1.2, respectively), most of them remained inactive at the P2X3 receptor. The deamination seemed to have no effect on the compound's potency. A distinct affinity improvement could be observed upon deamination only for compounds daYB010 and daYB041 (inhibition values for YB010 and YB041 were  $19 \pm 18$  and  $18 \pm 36$  %, respectively).

The subsequently determined IC<sub>50</sub> value of the deaminated compounds remained in the same range between 1 and 10  $\mu$ M as observed for all other active anthraquinone derivatives. By contrast, the activity of YB034 remained unaffected by the loss of the amino function. Unlike the aminated form, concentration-response curves for deaminated daYB039 could be generated,

but the potency of the compound was comparable to the rest of the anthraquinone series. These observations indicate that the amino group in position 1 of the anthraquinone core seems not to be essential for antagonistic potency, since neither presence nor absence have a significant influence on compound affinity to the P2X3 receptor. Position 1 could be a suitable position for the introduction of other residues to improve activity and selectivity towards the P2X3 receptor.

**Table 3.9:** Inhibitory potency of desaminoanthraquinone derivatives at the P2X3 receptor. Compound daYB039 is based on scaffold D (mean  $\pm$  SEM, n = 3-5). The data of the aminated derivative is repeated for better comparison.

Compound	Structure	IC <sub>50</sub> $\pm$ SEM [ $\mu$ M] of aminated compound	IC <sub>50</sub> $\pm$ SEM [ $\mu$ M] of deaminated compound
daYB039		n. c. <sup>a</sup> (98 %)	<b>3.62 <math>\pm</math> 0.57</b>
daYB041		> 10 (18 %)	<b>10.0 <math>\pm</math> 0.7</b>

<sup>a</sup>: n. c. no convergence

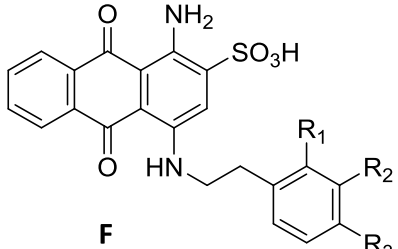
### 3.4.2 Enhancement of ATP potency

An increase of the maximum fluorescence increase of the agonist effect was noticed for several compounds during the initial screening experiments. This observation manifested itself in the form of negative inhibition values calculated after data analysis. The concerned compounds are visible as black dots located below the X-axis in Figure 3.5. Since for some compounds, a twofold fluorescence increase of the ATP control was observed, further tests were initiated to determine whether this phenomenon was actually caused by an interaction of the compound with the receptor or just an artefact of fluorescence measurement.

### 3.4.2.1 Anthraquinone derivatives

All compounds which displayed an increase by more than 100 % at 10  $\mu\text{M}$  in the initial screening experiment were further investigated. The first step was the determination whether the observed enhancement of maximal ATP effect was concentration-dependent. The ATP concentration injected in these experiments was lowered to the  $\text{EC}_{50}$  value (0.05  $\mu\text{M}$ ) to better characterize the magnitude of the enhanced maximal ATP effect. The results are presented in Table 3.10. The occurrence of enhancement could not clearly be linked to a common structural element. Nevertheless, some basic structural features could be identified who seem to facilitate the appearance of enhancement of maximal ATP effect at the P2X3 receptor. The most prominent residue was a phenylethylamino function added to the anthraquinone core in position 4 (YB094), defining scaffold F.

**Table 3.10:** Enhancing potency of anthraquinone derivatives with scaffold F at the P2X3 receptor stimulated with ATP  $\text{EC}_{50}$  concentration 0.05  $\mu\text{M}$ , and enhancement of maximal ATP effect. ATP control signal is based as 0 % for the calculation of the percental increase. Data is presented as mean  $\pm$  SEM from 3-5 independent experiments.

Scaffold				$\text{EC}_{50}$ Enhancement $\pm$ SEM [ $\mu\text{M}$ ] or ATP signal enhancement at 10 $\mu\text{M}$ (%)	Enhancement of maximal ATP 0.05 $\mu\text{M}$ effect $\pm$ SEM [%]
	$\text{R}_1$	$\text{R}_2$	$\text{R}_3$		
YB094	H	H	H	<b>3.29</b> $\pm$ 0.83 <sup>a</sup>	90 $\pm$ 21
YB029	H	OCH <sub>3</sub>	OCH <sub>3</sub>	> 10 (118 %)	n. d. <sup>b</sup>
YB081	H	H	OH	<b>2.28</b> $\pm$ 0.33 <sup>a</sup>	41 $\pm$ 0
YB087	H	H	Cl	<b>2.59</b> $\pm$ 0.60 <sup>a</sup>	111 $\pm$ 27
YB093	H	H	F	<b>4.21</b> $\pm$ 0.94 <sup>a</sup>	87 $\pm$ 17
YB080	H	H	OCH <sub>3</sub>	> 10 (51 %)	n. d. <sup>b</sup>
YB147	H	H	Br	> 10 (95 %)	n. d. <sup>b</sup>
YB112	Cl	H	H	> 10 (44 %)	n. d. <sup>b</sup>
YB148	H	F	H	> 10 (45 %)	n. d. <sup>b</sup>
YB149	H	Cl	H	<b>2.17</b> $\pm$ 0.16	95 $\pm$ 21

<sup>a</sup>: curve was extrapolated

<sup>b</sup>: n. d. not determined

The introduction of various residues in different positions also led to compounds displaying enhancement of maximal ATP effect. A concentration-response relationship with  $EC_{50\text{Enhancement}}$  values between 2 and 5  $\mu\text{M}$  could be seen for compounds YB094, YB081, YB087, YB093 and YB149. The potency was similar to previously discussed compounds with inhibitory effect of the P2X3 receptor, respectively. Small residues like a hydroxyl function or halogen in the *para*-position of the phenyl moiety were tolerated. A larger methoxy residue or bromine in the same position showed a much lesser enhancement of maximal ATP effect and were not further investigated. The combination of two methoxy groups in the *para*- and the *meta*-position did show a massive increase of ATP signal during the initial screening experiment, but a successful concentration-response relationship could not be generated. The magnitude of signal increase varied distinctively between the compounds. While fluorine in the *para*-position lead to the same and chlorine to the highest detected signal increase of all compounds (YB087  $111 \pm 27\%$ ), the hydroxyl function reduced the enhancement by almost 50% although no difference between the  $EC_{50\text{Enhancement}}$  concentrations could be observed. The average dose-response curve for compound YB087 is shown in Figure 3.10.

**Table 3.11:** Enhancing potency of anthraquinone derivatives with scaffold G at the P2X3 receptor stimulated with ATP  $EC_{50}$  concentration 0.05  $\mu\text{M}$ , and enhancement of maximal ATP effect. ATP control signal is based as 0% for the calculation of the percental increase. Data is presented as mean  $\pm$  SEM from three independent experiments.

Compound	Scaffold G			$EC_{50\text{Enhancement}} \pm$ SEM [ $\mu\text{M}$ ] or ATP signal enhancement at 10 $\mu\text{M}$ (%)	Enhancement of maximal ATP 0.05 $\mu\text{M}$ effect $\pm$ SEM [%]
	$R_1$	$R_2$	$R_3$		
YB032	H	H	H	$2.43 \pm 0.38$	$57 \pm 13$
YB042	H	H	OH	$2.56 \pm 0.90^a$	$33 \pm 7$

<sup>a</sup>: curve was extrapolated

A cyclohexylamino moiety in the same position (YB032) represents another scaffold of compounds with enhancing properties and was named scaffold G. Its derivatives increased the maximal ATP effect. The  $EC_{50\text{Enhancement}}$  value obtained from concentration-response experiments



for YB032 and the derivative supplied with a hydroxyl function in position 4 of the cyclohexyl ring (YB042) lay in the same range as those of previously discussed compounds. However, the observed enhancement of ATP effect however was significantly reduced from 90 % to 57 % and 33 %, respectively.

**Table 3.12:** Enhancing potency of anthraquinone derivatives with scaffold C at the P2X3 receptor stimulated with ATP EC<sub>50</sub> concentration 0.05  $\mu$ M and enhancement of maximal ATP effect. ATP control signal is based as 0 % for the calculation of the percental increase. Data is presented as mean  $\pm$  SEM from three independent experiments.

Compound	Scaffold			EC <sub>50</sub> Enhancement $\pm$ SEM [ $\mu$ M] or ATP signal enhancement at 10 $\mu$ M (%)	Enhancement of maximal ATP 0.05 $\mu$ M effect $\pm$ SEM [%]
	R <sub>1</sub>	R <sub>2</sub>	R <sub>3</sub>		
YB031	H	H	CH <sub>2</sub> PO(OCH <sub>2</sub> CH <sub>3</sub> ) <sub>2</sub>	1.43 $\pm$ 0.49 <sup>a</sup>	44 $\pm$ 6
YB038	H	H	CH <sub>2</sub> COOH	0.897 $\pm$ 0.296	24 $\pm$ 7
YB047	H	H	NHCOCH <sub>3</sub>	1.50 $\pm$ 0.24 <sup>a</sup>	76 $\pm$ 16
YB048	CH <sub>3</sub>	NH <sub>2</sub>	H	1.82 $\pm$ 0.40 <sup>a</sup>	66 $\pm$ 22
YB085	H	CH <sub>3</sub>	Cl	2.07 $\pm$ 0.34 <sup>a</sup>	48 $\pm$ 8
YB095	F	H	H	1.22 $\pm$ 0.12 <sup>a</sup>	68 $\pm$ 32
YB159	H	CHOHCH <sub>2</sub> CH <sub>3</sub>	H	> 10 (77 %)	n. d. <sup>b</sup>
YB160	H	COCH <sub>2</sub> CH <sub>3</sub>	H	2.22 $\pm$ 0.45	83 $\pm$ 27

<sup>a</sup>: curve was extrapolated

<sup>b</sup>: n. d. not determined

Derivatives obtained from scaffold C were already discussed as forwarding P2X3 receptor antagonists. Some compounds based on this scaffold showed enhancing properties instead. In particular, when bulky residues like diethoxyphosphorylmethyl (YB031), carboxymethyl (YB038) or acetamido (YB047) are introduced in *para*-position of the aniline moiety, enhancement instead of inhibition can be observed. The most potent enhancing compound of all proved to be YB038 with an EC<sub>50</sub>Enhancement value of 0.897  $\pm$  0.296  $\mu$ M. The respective concentration-response curve is presented in Figure 3.11. The magnitude of ATP 0.05  $\mu$ M-induced enhancement though was much smaller than observed for other anthraquinone derivatives. A 1-hydroxypropyl

(YB159) or propranoyl residue (YB160) in the *meta*-position encouraged enhancement as well, but did improve neither affinity nor magnitude of fluorescence signal.

Scaffold H was obtained by attaching a phenyl residue to carbon 3 of the 1-hydroxypropyl side chain of compound YB159. Neither the lead compounds (enantiomeric mixture YB088, (R)-enantiomer YB151 and (S)-enantiomer YB152) nor the introduction of various small residues in different positions of the newly introduced phenyl ring showed any ATP signal-enhancing properties. This modification apparently represents a possibility to repress any enhancement, but at the same time does not provide any inhibitory potency.

Figure 3.10 and Figure 3.11 demonstrate the concentration-response relationship of four enhancement-showing compounds. Compounds YB087 and YB149 were selected for displaying enhancement-facilitating scaffold I, and YB038 and YB160 as variations of scaffold K. YB038 was selected because of its high affinity, the other three for the particularly strong enhancement of ATP 0.5  $\mu$ M-induced fluorescence increase.

**Table 3.13:** Enhancing potency of anthraquinone derivatives with scaffold H at the P2X3 receptor stimulated with ATP EC<sub>50</sub> concentration 0.05  $\mu$ M and enhancement of maximal ATP effect. ATP control signal is based as 0 % for the calculation of the percental increase. Data is presented as mean  $\pm$  SEM from three independent experiments.

Compound	Scaffold H			EC <sub>50</sub> Enhancement $\pm$ SEM [ $\mu$ M] or ATP signal enhancement at 10 $\mu$ M (%)	Enhancement of maximal ATP 0.05 nM effect $\pm$ SEM [%]
	R <sub>1</sub>	R <sub>2</sub>	R <sub>3</sub>		
YB088	H	H	H	< 10 (40 %)	n. d. <sup>a</sup>
YB151 <sup>b</sup>	H	H	H	< 10 (-7 %)	n. d. <sup>a</sup>
YB152 <sup>c</sup>	H	H	H	< 10 (-1 %)	n. d. <sup>a</sup>
YB150	H	H	F	< 10 (-1 %)	n. d. <sup>a</sup>
YB153	H	H	Cl	< 10 (48 %)	n. d. <sup>a</sup>
YB154	H	H	Br	< 10 (43 %)	n. d. <sup>a</sup>

<sup>a</sup>: n. d. not determined

<sup>b</sup>: (R)-enantiomer

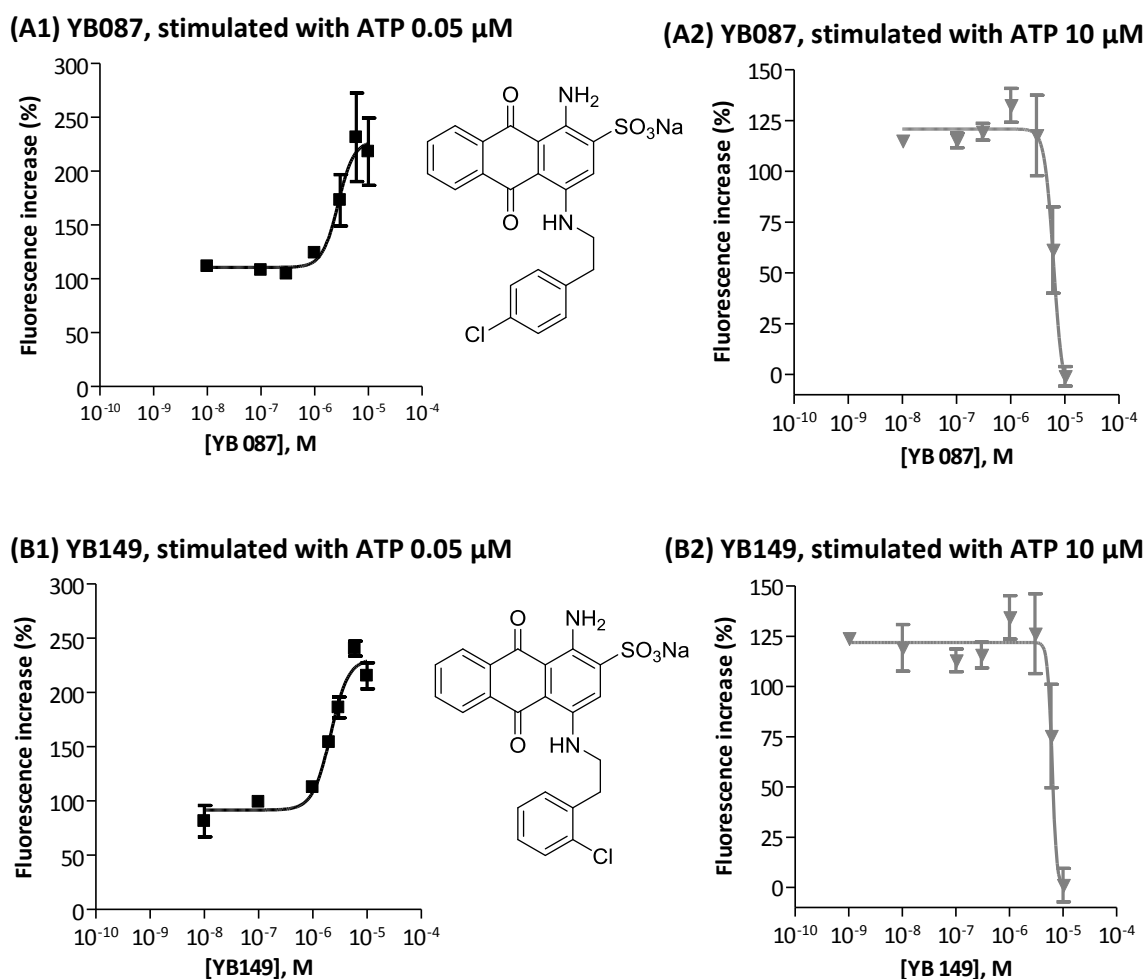
<sup>c</sup>: (S)-enantiomer

#### 3.4.2.2 Further investigations of enhancement effect of anthraquinone derivatives

The enhancement of ATP-induced effect seemed dependent on the compound concentration. Further experiments were conducted for compounds YB038, YB087, YB149 and YB160 in representation of the whole series. As the experiment is based on the detection of fluorescence, any interference of the colored test compound would distort the results, especially since the enhancement of fluorescence increased with enhanced compound concentration. As already described in chapter 2.2.2, each test plate was validated prior to agonist injection after the incubation time with test compound ended. Therefore, any increase of basic fluorescence due to the added test compound could be determined *in situ* by comparison to the control wells which did not contain any test compounds. As summarized in Table 2.1 and Table 2.2, the respective maxima for the fluorescent dyes are 494 nm and 516 nm for Fluo-4 and range between 470 and 495 nm and 515 to 575 nm, respectively. Both fluorophores were excited at 485 nm, and the emission was measured at 520 nm. Wells with higher basic fluorescence than controls were marked for further investigation. An increase of basic fluorescence cannot only be caused by an interference of test compound and the dye, but also by cell toxicity, which causes leakage of dye from damaged cells into the calcium-containing buffer. A significant increase of basic fluorescence was observed using anthraquinone compound concentrations higher than 10  $\mu\text{M}$ . All testing was therefore limited to a maximal concentration of 10  $\mu\text{M}$  anthraquinone or desaminoanthraquinone derivative.

In an attempt to finally exclude any distortion of the results, each anthraquinone derivative with enhancing properties was tested for agonistic activity by injecting various compound concentrations instead of ATP. No fluorescence signal increase for any compound was detected. Anthraquinone-based compounds therefore did not have any agonistic property at the P2X3 receptor. All results described were conducted by stimulating the P2X3 receptor with the previously determined  $\text{EC}_{50}$  concentration of ATP. This concentration was selected in order to prove if the selected compounds were capable of increasing the activation state starting from the half maximal agonist concentration. The experiments were repeated using ATP 10  $\mu\text{M}$ , a concentration causing maximal receptor stimulation, to determine whether these anthraquinone derivatives were capable of enhancing the maximal ATP effect past the maximal possible ATP response. The results are presented in Figure 3.10 and Figure 3.11 A2 to B2 for compounds YB038, YB087, YB149, and YB160. An increase of maximal ATP effect could be determined only for compound YB038, displaying scaffold C. This anthraquinone-based compound therefore is capable of enhancing the ATP effect at the P2X3 receptor even past the

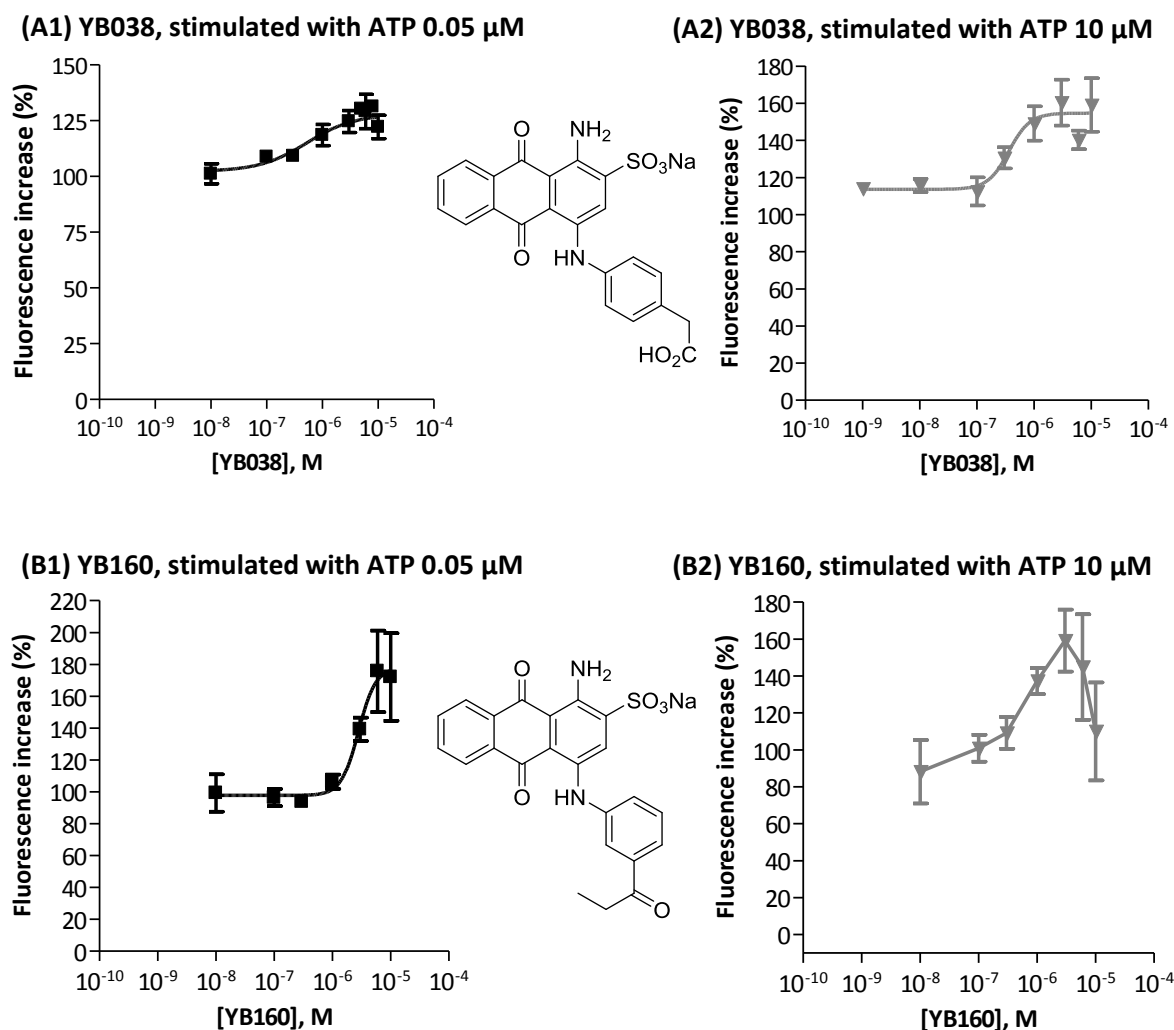
physiologically possible level. The same effect is indicated for YB160, but a successful concentration-response relationship could not be obtained.



**Figure 3.10:** Structures and mean dose-response curves (mean  $\pm$  SEM,  $n = 3-4$ ) of (A) YB087 and (B) YB149 stimulated with either (1)  $\text{EC}_{50}$  ( $\blacksquare$ , 0.05  $\mu\text{M}$ ) or (2) maximal response concentration of ATP ( $\blacktriangledown$ , 10  $\mu\text{M}$ ).

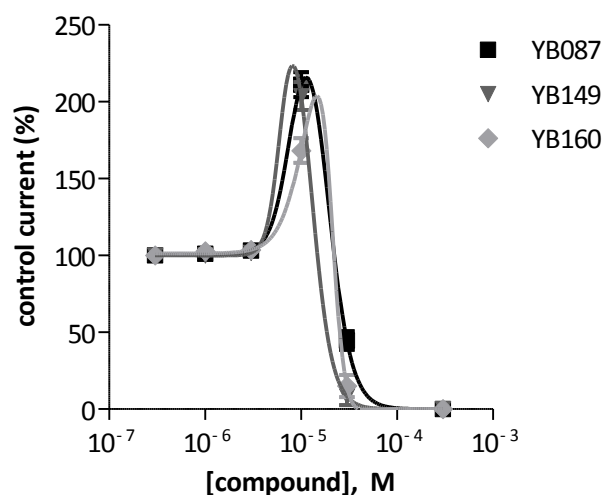
Contrary to expectations and to the first experiments with ATP 0.05  $\mu\text{M}$ , YB087 and YB149 showed inhibition at concentrations higher than 5  $\mu\text{M}$  at the P2X3 receptor when stimulated with 10  $\mu\text{M}$  ATP. A similar effect can be seen for YB160 to a lesser extent. This indicates that the compound seemed to inhibit the P2X3 receptor when used in higher concentrations. It is possible that all three ATP binding pockets are occupied by test compound when high concentrations of YB087, YB149 and YB160 are used. This would prevent ATP from binding and subsequently activating the receptor. As the concentration and occupancy of binding pockets decreases, the remaining anthraquinone molecules bound to the receptor enhance the affinity

of ATP and therefore may cause the observed enhancement of maximal ATP effect. If the concentration is decreased further, it becomes too low to enhance the ATP-induced fluorescence, and the maximal ATP effect returns to the normal level. It is possible that the ATP concentration used for receptor stimulation somehow altered the receptor function, since this described phenomenon was not observed under receptor stimulation by the  $EC_{50}$  concentration of ATP.



**Figure 3.11:** Structures and mean dose-response curves (mean  $\pm$  SEM,  $n = 3-4$ ) of (A) YB038 and (B) YB160 stimulated with either (1)  $EC_{50}$  ( $\blacksquare$ , 0.05  $\mu$ M) or (2) maximal response concentration of ATP ( $\blacktriangledown$ , 10  $\mu$ M)

Compounds YB087, YB149 and YB160 were used in a patch clamp experiment in the group of PD Dr. med. Ralf Hausmann from the Institute of Toxicology and Pharmacology in Aachen in order to verify these observations. The results of these experiments are presented in Figure 3.12 and Table 3.14.



**Figure 3.12:** Mean dose response curves of YB087, YB149 and YB160 at the P2X3 receptor obtained by patch clamp experiments ( $MW \pm SEM$ ). The data was provided by PD Dr. Ralf Hausmann. Each concentration was measured at 4-6 times.

The bell-shaped regression was selected for data analysis. The first  $EC_{50}$  value ( $EC_{50\text{Enhancement}}$ ) describes the first inflection point on the left side, the  $IC_{50}$  value represents the second inflection point on the right side of the bell curve. The effect of each concentration was measured between four to six times. The same observation can be seen as already described for Figure 3.10 and Figure 3.11 A1-B1, respectively. It also supports the theory that not only the compound concentration but also the ATP amount used for cell stimulation has influence on the conducted fluorescence signal.

**Table 3.14:** Results of bell-shaped non-linear regression analysis and respective confidence intervals of concentration-response experiments using patch clamp experiments at the P2X3 receptor. Each data point used in the analysis was measured 4-6 times.

	$EC_{50\text{Enhancement}}$ [ $\mu\text{M}$ ]	$IC_{50}$ [ $\mu\text{M}$ ]	Maximal current increase (%)	Concentration of maximal current increase [ $\mu\text{M}$ ]
<b>YB087</b>	8.00	18.8	116	11.2
<b>YB149</b>	6.12	12.7	123	8.07
<b>YB160</b>	11.9	21.2	104	14.7

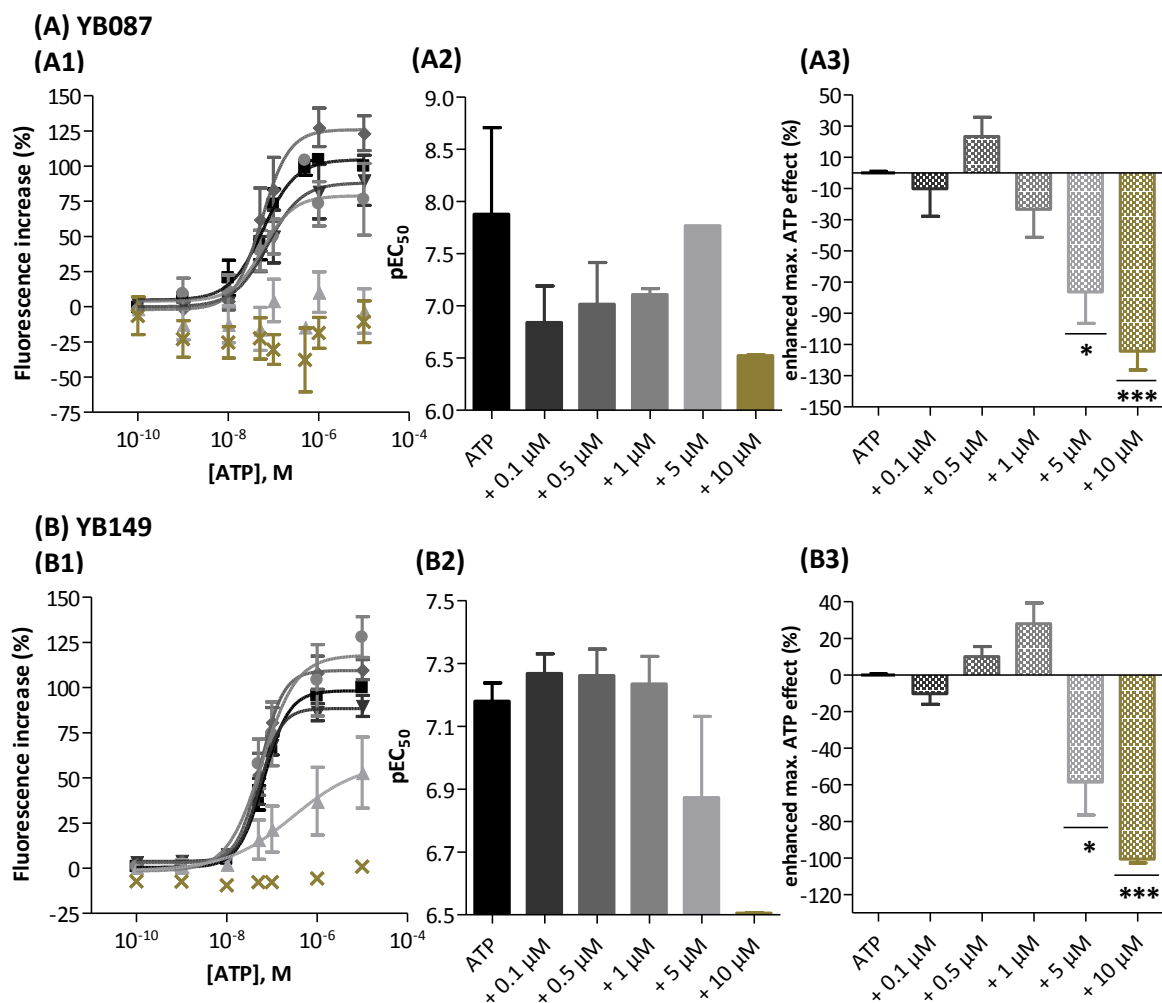
An increase of maximal receptor stimulation possible under ATP influence could only be observed for YB038 (see Figure 3.11 A1 and A2). This indicates that YB038 somehow interacts differently with the P2X3 receptor than the other compounds YB087, YB149 and YB160. In an

attempt to get further insight in the mechanism of action, all four compounds were tested in another experiment analog to the determination of inhibition mechanism for antagonists, where cells were preincubated with certain concentrations of anthraquinone derivative selected based on their  $EC_{50\text{Enhancement}}$  values, and subsequently stimulated with various concentrations of ATP (for experimental setup see chapter 2.2.2.1.3). The results are presented in Figure 3.13 and Figure 3.14.

It was expected that under the influence of different concentrations of the respective anthraquinone compound, either the maximal level of fluorescence increase reached by full receptor stimulation would be enhanced or the  $EC_{50}$  value of ATP would be shifted to the left towards lower concentrations.

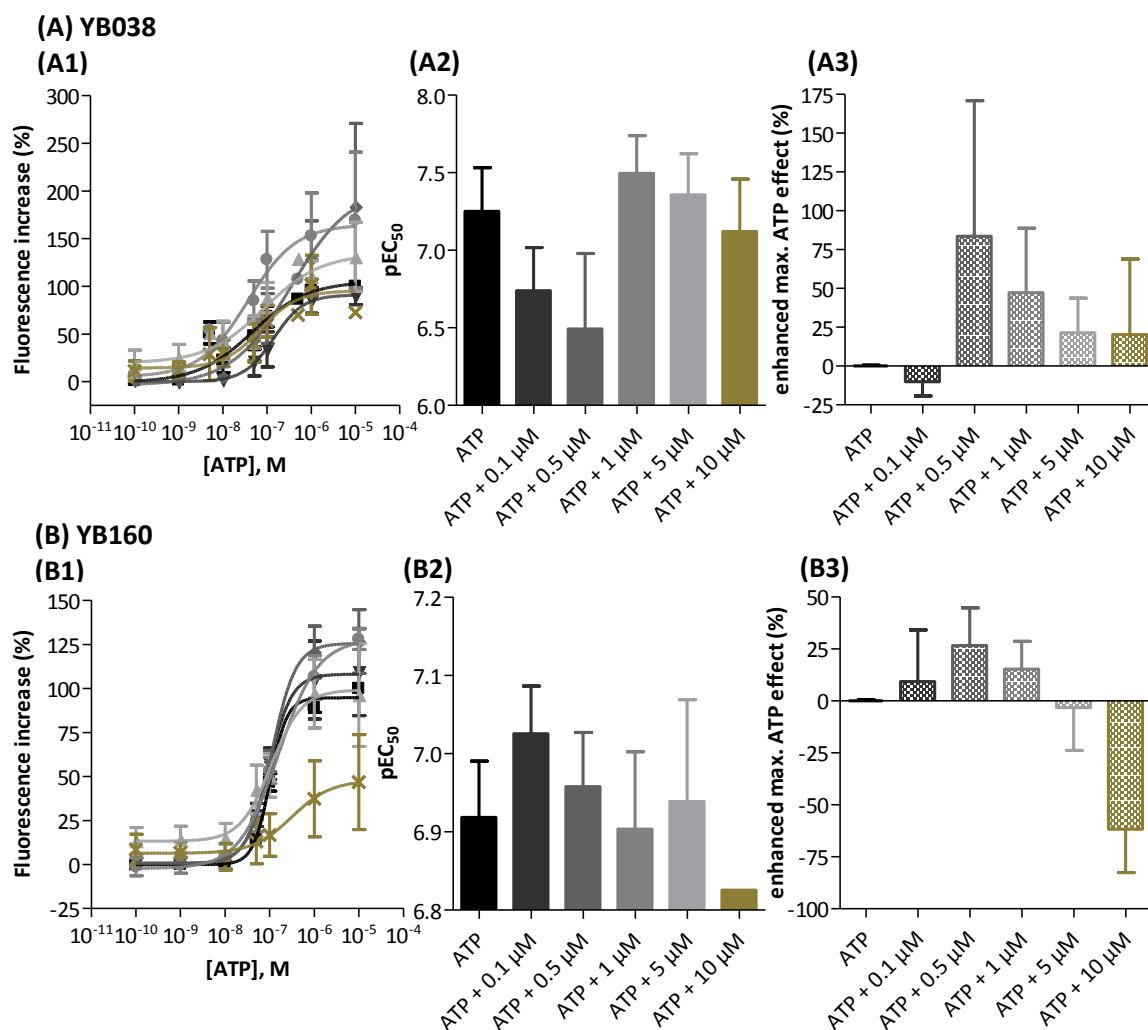
As already observed in the previous experiments, the addition of high concentrations (10  $\mu\text{M}$  and 5  $\mu\text{M}$ ) of YB087, YB149 and YB160 abolished any agonistic ATP activity (YB087) or visibly lowered it (YB149 and YB160, see Figure 3.13 and Figure 3.14). The decrease was statistical significant for YB087 and YB149. A slight enhancement of maximal ATP effect could be observed at concentrations lower than 5  $\mu\text{M}$ , but it was nowhere nearly as high as detected in the initial concentration-response experiments (see Figure 3.10 A1 and B1 and Figure 3.11 B1). None of the slight increases were statistically significant, same as for the  $EC_{50}$  values of ATP. The results indicate that the enhancement of the ATP effect does not repose on an increase of ATP affinity to the P2X3 receptor, and seems to be dependent on the ATP concentration used for receptor stimulation, as observed previously (see again Figure 3.10 and Figure 3.11). Since high concentrations of anthraquinone enhancer lead to inhibition of the receptor, it is possible that this effect only occurs when not all binding pockets are occupied.

A decrease of  $EC_{50}$  value could be observed for YB038, but the difference was not statistically significant from the  $EC_{50}$  value of the ATP control curve, and it could only be detected for the YB038 concentrations 5  $\mu\text{M}$  and 1  $\mu\text{M}$  (see higher  $pEC_{50}$  values in Figure 3.14 A2). Under the influence of YB038 0.5  $\mu\text{M}$ , the  $EC_{50}$  value increased contrary to expectations, but the enhancement of fluorescence increase was the highest detected for all four compounds in this experiment. Due to the inconsistency of the results, a final conclusion about the mechanism how YB038 increases the ATP-induced fluorescence signal was still not possible, although all experiments indicate that the mechanism of action is different from the other three compounds used for further examination. A possible explanation would be the alteration of the ion pore by so that more calcium ions are capable of passing and therefore increasing the maximal ATP effect. This could also explain the further increase of maximum possible ATP-induced fluorescence signal demonstrated in Figure 3.10 and Figure 3.11.



**Figure 3.13:** (1) Mean ATP dose-response curves, (2) ATP pEC<sub>50</sub> values and (3) enhancement of maximal ATP effect characterizing the influence scaffold G anthraquinone derivatives (A) YB038 and (B) YB160. Cells were stimulated with ATP 0.0001-10  $\mu$ M after preincubation with 0.1  $\mu$ M (▼), 0.5  $\mu$ M (◆), 1  $\mu$ M (●), 5  $\mu$ M (▲) or 10  $\mu$ M (×) of test compound, respectively. Buffer containing 1 % DMSO without compound was used as control (■). The unpaired Student's t-test for determination of significant differences of means was conducted for pEC<sub>50</sub> and enhanced maximal ATP effect. Statistical significance ( $p < 0.05$ ) is marked with (\*), highly statistical significant differences ( $p < 0.001$ ) with (\*\*\*). Data is presented as mean  $\pm$  SEM from 3-8 independent experiments.





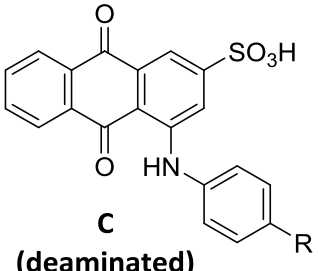
**Figure 3.14:** (1) Mean ATP dose-response curves, (2) ATP pEC<sub>50</sub> values and (3) enhancement of maximal ATP effect characterizing the influence scaffold G anthraquinone derivatives (C) YB038 and (D) YB160. Cells were stimulated with ATP 0.0001-10  $\mu$ M after preincubation with 0.1  $\mu$ M ( $\blacktriangledown$ ), 0.5  $\mu$ M ( $\blacklozenge$ ), 1  $\mu$ M ( $\bullet$ ), 5  $\mu$ M ( $\blacktriangle$ ) or 10  $\mu$ M ( $\times$ ), respectively. Buffer containing 1% DMSO without compound was used as control ( $\blacksquare$ ). The unpaired Student's t-test for determination of significant differences of means was conducted for EC<sub>50</sub> and enhanced maximal ATP effect ( $p < 0.05$ ). Statistical significance ( $p < 0.05$ ) is marked with (\*). Data is presented as mean  $\pm$  SEM from 3-8 independent experiments.

### 3.4.2.3 Desaminoanthraquinone derivatives

The initial screening experiments showed that the amino function in position 1 of the anthraquinone core is not essential for inhibitory activity (see chapter 3.4.1.4). Since certain structural elements of the anthraquinone series were identified to enhance the ATP-induced fluorescence signal increase (see chapters 3.4.2.1 and 3.4.2.2), special focus was laid on the deaminated versions of the most interesting compounds as far as they were available. The results are presented in Table 3.15.

**Table 3.15:** Enhancing potency of scaffold C desaminoanthraquinone derivatives at the P2X3 receptor stimulated with ATP  $EC_{50}$  concentration 0.05  $\mu$ M, and enhancement of maximal ATP effect. ATP control signal is based as 0 % for the calculation of the percental increase. Data is presented as mean  $\pm$  SEM from 3-4 independent experiments. The data of the aminated derivatives is repeated for better comparison.

**Scaffold**



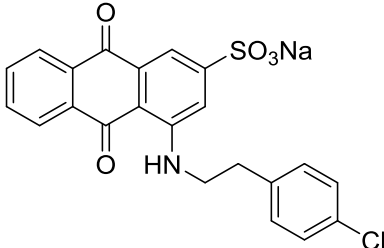
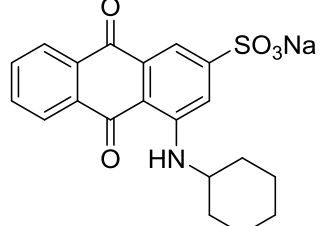
Compound	R	$EC_{50}$ Enhancement $\pm$ SEM [ $\mu$ M] or ATP signal enhancement at 10 $\mu$ M (%) of aminated compound	$EC_{50}$ Enhancement $\pm$ SEM [ $\mu$ M] or ATP signal enhancement at 10 $\mu$ M (%) of deaminated compound	Enhancement of maximal ATP 0.05 $\mu$ M effect $\pm$ SEM [%] of deaminated compound
daYB047	NHCOCH <sub>3</sub>	1.50 $\pm$ 0.24	> 10 (29 %)	n. d. <sup>a</sup>
daYB011	OH	> 10 (21 %)	n. c. (90 %) <sup>b</sup>	n. d. <sup>a</sup>

<sup>a</sup>: n. d. not determined

<sup>b</sup>: n. c. no convergence

None of the 26 desaminoanthraquinones showed any inhibition value below -100 % (see Figure 3.5). Since daYB011 came close, it was nonetheless tested in concentration-response experiments under stimulation with  $EC_{50}$  concentration of ATP. It was not possible to successfully create a dose-response relationship. The estimated  $EC_{50}$  value of three independent experiments exceeded 10  $\mu$ M by far, so no further experiments were conducted. Any enhancement of compounds available as deaminated derivatives was abolished by removing the amino function. It seems that the residue is not important for inhibitory potency but plays an essential role for conducting enhancing properties. An interesting step would be the exchange to other polar or bulky residues in order to determine whether polarity or occupancy of the position are the important features for enhancement of the P2X3 receptor.

**Table 3.16:** Enhancing potency of scaffold F desaminoanthraquinone derivative daYB087 and scaffold G desaminoanthraquinone derivative daYB032 at the P2X3 receptor stimulated with ATP EC<sub>50</sub> concentration 0.05 μM, and enhancement maximal ATP effect. ATP control signal is based as 0 % for the calculation of the percental increase. Data is presented as mean ± SEM from three independent experiments. The data of the aminated derivatives is repeated for better comparison.

Compound	Structure	EC <sub>50</sub> Enhancement ± SEM [μM] or ATP signal enhancement at 10 μM (%) of aminated compound	EC <sub>50</sub> Enhancement ± SEM [μM] or ATP signal enhancement at 10 μM (%) of deaminated compound	Enhancement of maximal ATP 0.05 μM effect ± SEM [%] of deaminated compound
daYB087		2.28 ± 0.36 <sup>a</sup>	< 10 (28 %)	n. d. <sup>b</sup>
daYB032		2.43 ± 0.38	< 10 (22 %)	n. d. <sup>b</sup>

<sup>a</sup>: curve was extrapolated

<sup>b</sup>: n. d. not determined

### 3.4.3 Cytotoxicity

An increase of basic fluorescence could be observed for some compounds when used in higher concentrations over 6-8 μM. In order to eliminate any possibility that this could be caused by lysed cells leaking the loaded dye reacting with calcium ions in the buffer, five anthraquinone compounds, enhancers YB038, YB087, YB149 and YB160 and antagonist YB120 were tested for cytotoxicity by cell viability experiment using 3-(4,5-dimethylthiazol-2-yl)-2,5-diphenyl-tetrazolium bromide (MTT). The results are presented in Table 3.17.

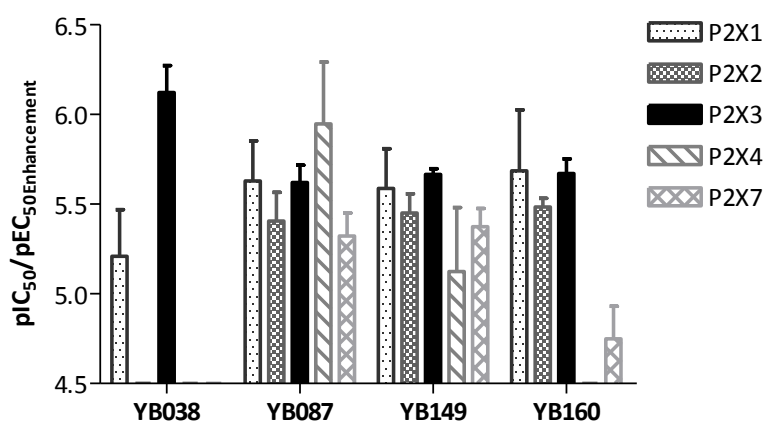
None of the tested anthraquinone derivatives caused any detectable cell toxicity when used in concentrations up to 100 μM. It was therefore estimated to be unlikely that any inhibitory action determined using calcium influx experiments is attributable to cytotoxicity of the anthraquinone test compounds.

**Table 3.17:** Cytotoxicity EC<sub>50</sub> values of anthraquinone derivatives and positive control 5-FU at non-transfected 1321N1 astrocytoma cells (mean ± SEM, n = 4).

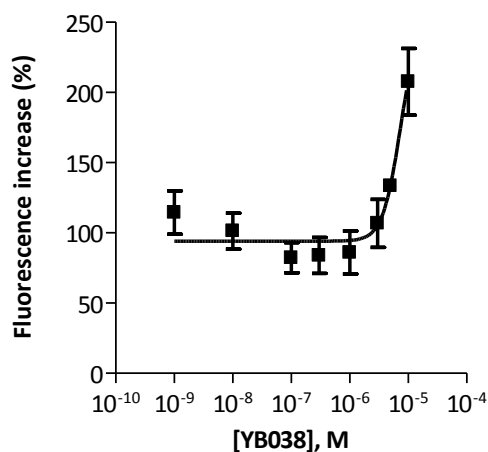
	5-FU	YB038	YB087	YB120	YB149	YB160
<b>Cytotoxicity EC<sub>50</sub> [μM]</b>	1.29 ± 0.62	> 100	> 100	> 100	> 100	> 100

### 3.4.4 Selectivity towards other P2X receptor subtypes

Among other things, anthraquinone derivatives were reported to be potent inhibitors at least at the closely related P2X<sub>2</sub> receptor, the P2Y<sub>12</sub> receptor and the enzymes NTPDase and CD73.<sup>103, 206, 212, 213</sup> The potency of the four enhancement showing anthraquinone compounds YB038, YB087, YB149 and YB160 and the antagonist YB120 were tested at the P2X receptor subtypes P2X<sub>1</sub>, P2X<sub>2</sub>, P2X<sub>4</sub> and P2X<sub>7</sub> in order to determine selectivity and whether the phenomenon of enhancement is only prominent at the P2X<sub>3</sub> receptor. The results are shown in Figure 3.15.

**Figure 3.15:** pEC<sub>50Enhancement</sub> (YB038 at P2X<sub>1</sub>, all compounds at P2X<sub>3</sub> receptor) and pIC<sub>50</sub> values of anthraquinone derivatives at P2X receptors (mean ± SEM, n = 3-4).

Enhancement of maximal ATP effect could only be detected for YB038 at the P2X<sub>1</sub> receptor with an EC<sub>50Enhancement</sub> value of 9.09 ± 5.70 μM. That is tenfold less than for the P2X<sub>3</sub> receptor (0.897 ± 0.296 μM). The graph for YB038 enhancement at the P2X<sub>1</sub> receptor is presented in Figure 3.16. YB038 was not active at the other P2X receptor subtypes, neither as an enhancing agent nor as a receptor antagonist. The observed enhancement of maximal ATP effect was much higher than at the P2X<sub>3</sub> receptor (108 ± 24 %), but occurred at much higher concentrations.



**Figure 3.16:** Mean dose-response curve of YB038 at the human P2X1 receptor (mean  $\pm$  SEM,  $n = 5$ ).

Since the  $EC_{50\text{Enhancement}}$  value at the P2X1 receptor is almost tenfold higher, YB038 can be viewed as a moderately selective positive enhancer of ATP potency at the P2X3 receptor, whereas the enhancing potency is much higher at the P2X1 receptor. YB038 acted as an antagonist at the other P2X receptor subtypes, with  $IC_{50}$  values in the micromolar range (see Table 3.18) and around three- to ninefold preference of the P2X3 receptor. The other three compounds YB087, YB149 and YB160, if active, all acted as antagonists at the other subtypes, with  $IC_{50}$  values comparable to the  $EC_{50\text{Enhancement}}$  values seen at P2X3 receptor.

**Table 3.18:** Enhancing potency (all compounds at the P2X3 and YB038 at the P2X1 receptor) and inhibitory potency of selected anthraquinone compounds at P2X receptors (mean  $\pm$  3,  $n = 3-4$ ).

	P2X1	P2X2	P2X3	P2X4	P2X7
<b>YB038</b>	<b>9.07 <math>\pm</math> 5.70</b> ( $EC_{50\text{Enhancement}}$ )	< 10 (20 %)	<b>0.897 <math>\pm</math> 0.296</b> ( $EC_{50\text{Enhancement}}$ )	< 10 (23 %)	< 10 (46 %)
<b>YB087</b>	<b>3.01 <math>\pm</math> 1.42</b>	<b>4.48 <math>\pm</math> 1.57</b> (remaining receptor activity 21 %)	<b>2.59 <math>\pm</math> 0.60</b> ( $EC_{50\text{Enhancement}}$ )	<b>1.51 <math>\pm</math> 1.00</b> (remaining receptor activity 13 %)	<b>4.98 <math>\pm</math> 1.44</b>
<b>YB149</b>	<b>3.26 <math>\pm</math> 1.43</b>	<b>3.74 <math>\pm</math> 0.82</b> (remaining receptor activity 24 %)	<b>2.17 <math>\pm</math> 0.16</b> ( $EC_{50\text{Enhancement}}$ )	<b>10.2 <math>\pm</math> 6.9</b> (remaining receptor activity 23 %)	<b>4.48 <math>\pm</math> 1.10</b>
<b>YB160</b>	<b>3.18 <math>\pm</math> 1.43</b>	<b>3.32 <math>\pm</math> 0.37</b> (remaining receptor activity 64 %)	<b>2.22 <math>\pm</math> 0.45</b> ( $EC_{50\text{Enhancement}}$ )	< 10 (48 %)	< 10 (30 %)

YB087 and YB149 were not able to completely inhibit the P2X2 and P2X4 receptor. Both receptors retained a residual activity of nearly 20 % at the highest concentration used in the experiment (10  $\mu$ M). This effect was also observed for YB160 at the P2X2 receptor. Furthermore, YB160 did show no concentration-dependent activity at the P2X4 and P2X7 receptor.

### 3.5 Discussion

Anilinoanthraquinone derivatives were originally synthesized for pharmacological evaluation of P2 receptors. The lead structure RB-2 has previously been identified as a weak nonselective purinergic P2 and ectonucleotidase antagonist.<sup>66, 203</sup> In order to study structure-activity relationships, the lead structure was truncated and various residues in different positions of the aniline moiety were introduced, as well as the replacement of the aniline ring itself against several aliphatic, polar or lipophilic structures. The pharmacological evaluation at mouse and human P2Y<sub>2</sub> receptors showed inhibitory potency with IC<sub>50</sub> values between 3  $\mu$ M and 30  $\mu$ M for several of the 4-phenylamino-substituted 1-amino-2-sulfoanthraquinone derivatives, which were also potent antagonists at the P2X3 receptor.<sup>205</sup> The most potent compound at the P2Y<sub>2</sub> receptor was YB033 with an IC<sub>50</sub> value of  $3.04 \pm 0.58 \mu$ M. The phenyl moiety was described to be essential for P2Y<sub>2</sub> receptor activity.

At ecto-5'-nucleotidase, YB052 and YB063 were the two most potent inhibitors with K<sub>i</sub> concentrations of  $0.260 \pm 0.010 \mu$ M and  $0.150 \pm 0.020 \mu$ M, respectively. YB052 is based on scaffold C with a carboxyl group in position 2 and fluorine in position 4 of the aniline ring. In YB063, the aniline in position 4 of the 1-amino-2-sulfoanthraquinone core is exchanged to 2-aminoanthracene. The naphthyl derivatives YB040 ( $\alpha$ -naphthalene) and YB041 ( $\beta$ -naphthalene) were also potent ecto-5'-nucleotidase inhibitors with potency in the high nanomolar to low micromolar range (K<sub>i</sub>  $0.53 \pm 0.03 \mu$ M and  $1.47 \pm 0.33 \mu$ M). The mechanism of inhibition was determined to be competitive. YB052 was further characterized as selective towards NTPDases, P2Y<sub>2</sub>, P2Y<sub>4</sub>, P2Y<sub>6</sub> and P2Y<sub>12</sub>.<sup>212</sup> Both compounds were not active at the P2X3 receptor. Some anthraquinone derivatives were also identified as NTPDase inhibitors. YB022, also a scaffold C derivative with chlorine in position 4 of the aniline ring, was the most potent nonselective antagonist at NTPDase1, 2 and 3 with K<sub>i</sub> values between 16  $\mu$ M and 18  $\mu$ M. The 2-naphthalene derivative YB041 also inhibited NTPDase1 (K<sub>i</sub>  $0.328 \pm 0.110 \mu$ M) and 3 (K<sub>i</sub>  $2.22 \pm 1.03 \mu$ M) with preference over NTPDase2.<sup>213</sup>

As already discussed in chapter 1.2.7.1, the 1,3,5-triazine derivatives of scaffold C, PSB-10211 and PSB-1011, were synthesized as potent antagonists of the P2X2 receptor with nanomolar

potency. The two compounds descend from the same library, but were not available for testing at the P2X3 receptor. Their selectivity towards P2X1 and P2X3 was described as moderate. The mechanism of action was again described as being competitive.<sup>103</sup>

The anthraquinone library was extended and also evaluated for inhibitory potency at the human P2Y<sub>12</sub> receptor. The aim was the development of a potent non-nucleotide antagonist with more drug-like properties like lower molecular weight and better subtype selectivity.<sup>206</sup> The attached aniline ring in position 4 of the 1-amino-2-sulfoanthraquinone core was extended by a second phenyl ring via a one atom linker. The exchange of the linker to nitrogen, oxygen or sulfur did not decrease the potency as P2Y<sub>12</sub> receptor antagonists, with IC<sub>50</sub> values between 0.0249 (YB039, the most active inhibitor at P2Y<sub>12</sub>, also called PSB-0739) and 1.85 μM (YB026). For the most active compound YB039, the inhibition mechanism was determined as being competitive. The compounds were also expected to be selective towards other P2 receptors.

The 4-phenylamino-3-carboxyphenylamino derivatives of PSB-0739 were the most active inhibitory compounds at the P2X3 receptor. An acidic function in position 3 of the aniline ring D is required for inhibitory activity, as well as an extension by a second aniline ring in position 4. Small residues like chlorine, fluorine, methyl, methoxy or ethoxy are tolerated in all positions of ring E, but without increasing the inhibitory potency of the compound.

The enhancing properties of the anthraquinone derivatives is not surprising, since Cibacron Blue 3GA has previously been identified as a PAM of the P2X3 receptor (see chapter 1.2.8.2). The characterization of a scaffold causing enhancement of maximal ATP effect is much more complicated. The results at the P2X3 receptor indicate that the effect of respective substitution cannot be predicted. Scaffold F could be identified to facilitate enhancement, but it was not an essential structural feature. A lot of other compounds not based on scaffold F also showed enhancing properties. The structures were very heterogenic, and the structural differences between inhibiting and enhancing compounds were sometimes very small. The only structural feature that seemed to be necessary for enhancing properties is the amino residue in position 1 of the 2-sulfoanthraquinone core. Its removal abolished any enhancing properties of the compound. Cibacron Blue 3GA is also described as a positive allosteric modulator of P2X4 (see chapter 1.2.9.2). So far, no data of the potency of anthraquinone derivatives at P2X4 receptor has been published, so structure-activity relationship at this P2X receptor subtype cannot be conducted. The results at the P2X3 receptor though indicate that allosteric modulation by anthraquinone derivatives could also be important at the P2X4 receptor.

The mechanism of inhibition at the targets known so far has been described as competitive. The results conducted for YB120 at the P2X3 receptor indicate the same. Since negative charge is favorable for competitive binding due to the negative charge of ATP and its fixation by positively charged amino acids in the agonist binding pocket, the conclusion seems valid.

The functional evaluation of the P2X3 receptor stably transfected in 1321N1 astrocytoma cells via fluorescent measurement of calcium influx was successful. The results demonstrate that the single point mutant of rat P2X3 receptor is suitable for high throughput screening, and new active compounds, lead structures and pharmacological effects could be demonstrated.

In general, it can be said that 1-amino-2-sulfoanthraquinone derivatives are also potent inhibitors at the P2X3 receptor. The compound class does not solely contain antagonists, positive modulation leading to enhanced receptor activity was also observed and does not seem to follow any common structural feature.



## 4 Inhibitory potency of polyoxometalates at P2X receptors

### 4.1 Introduction

Polyoxometalates (POMs) are inorganic, negatively charged complexes consisting of metal ions in their highest oxidation state connected by oxygen atoms. The most frequently used ions are early transition metals such as tungsten (W), molybdenum (Mo), vanadium (V), niobium (Nb) and antimony (Sb), but many other elements, including noble metals, can be incorporated into the POM framework as heteroatoms. This enables a high variety of three-dimensional structures bearing different polarity, redox potential, surface area properties and acidity.<sup>217-219</sup> The most common basic three-dimensional structures are octahedra linked together through shared corner atoms and edges, but also square-planar and hexagonal-bipyramidal assemblies have been reported.<sup>220</sup> For the present experimental series, 23 POMs were available, 17 with tungsten, four with rhenium and two with vanadium as the main metal ion. Most polyoxotungstates also contained further elements like titanium, cobalt or phosphorus. The compounds were provided by Dr. Holger Stephan from the Institute of Radiopharmaceutical Cancer Research of the Helmholtz Center, Dresden, Prof. Dr. Ulrich Kortz from the School of Engineering of the Jacobs University, Bremen and Prof. Dr. Wei Wang from the Center for Synthetic Soft Materials, Nankai University, China. Both vanadium salts were purchased from Sigma Aldrich Chemie GmbH. Basic information on all compounds including charge and stability are summarized in Table 4.1.

PV2 and PW<sub>12</sub> are basically the same compounds, though crystallized either as sodium salt (PW<sub>12</sub>) or as the free acid (PV2). Both compounds, as well as P<sub>6</sub>W<sub>18</sub>, show limited stability.<sup>221, 222</sup> All results concerning those compounds therefore have to be interpreted with caution, since one experiment lasts nearly two hours, and it cannot be guaranteed that the compounds remain unaltered over that time period.

The available compounds display variable three-dimensional shapes. The most common one is the Keggin structure of PV2 and PW<sub>12</sub>, PV3 and PV4 and the closely related Weakley and double-Keggin shape. The complex consists of a central tetrahedron, circled by four trimetallic groups. The Weakley structure is also called a Keggin-derived sandwich. The higher the molecular weight, the more complicated the three-dimensional structure. These range from HPA-23, a cryptate encapsulating a sodium ion in its central cavity to the plate-like Pope-Jeannin-Preyssler, the wheel-shaped Contant-Tézé or the cylindrical Wells-Dawson structure. For better illustration, the different shapes of the compounds are demonstrated in Figure 4.1.

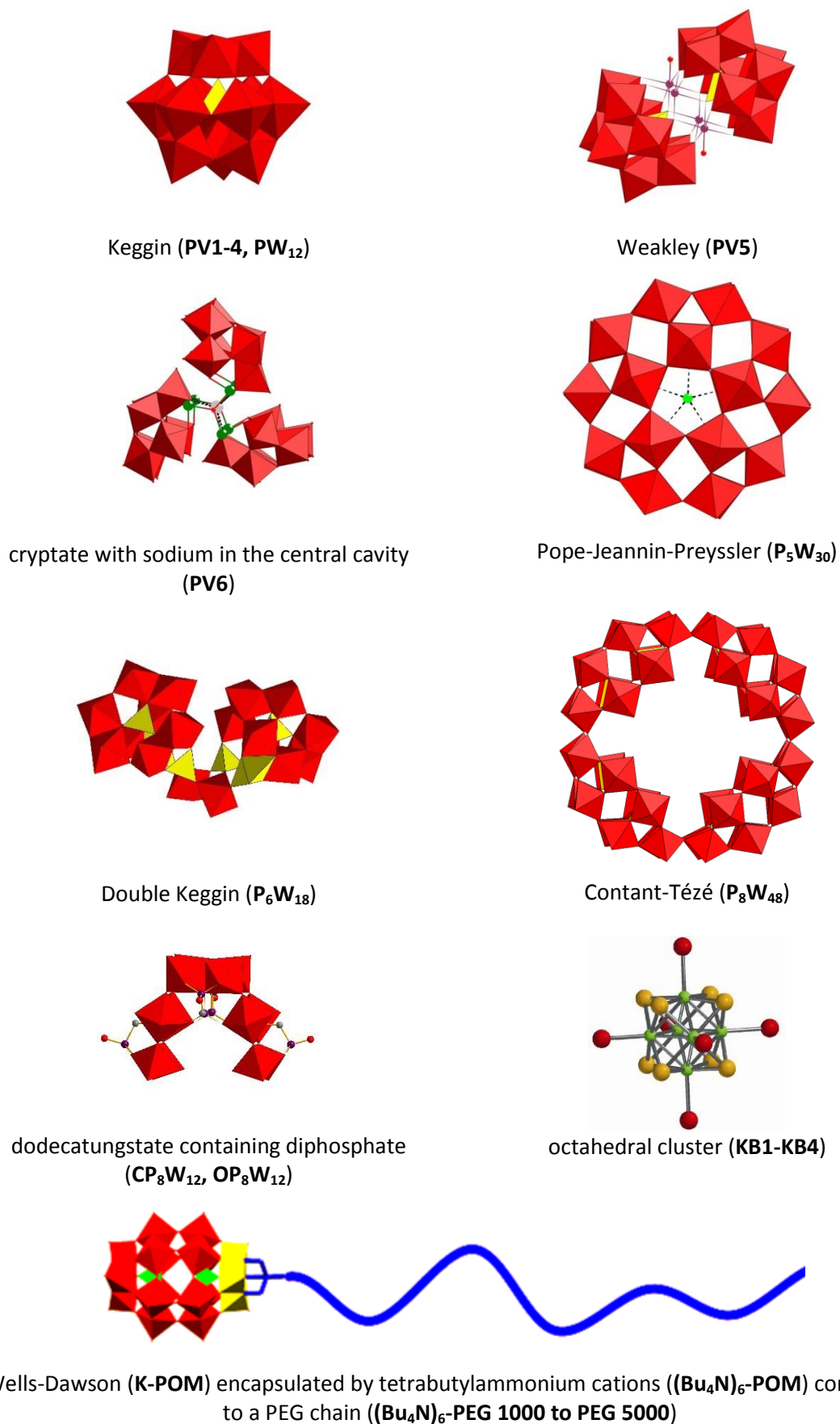
**Table 4.1:** General information of polyoxotungstates, rhenium and vanadate clusters available for calcium influx experiments at P2X receptors.<sup>221-242</sup>

Name	Formula	Structure type	Molecular weight [g/mol]	Charge at pH 7.4	Stability in aqueous solution
PV1	Na <sub>6</sub> [H <sub>2</sub> W <sub>12</sub> O <sub>40</sub> ]	Metatungstate of corner- and edge-sharing WO <sub>6</sub> -octahedrons	2986	-6	++
PV2	H <sub>3</sub> [PW <sub>12</sub> O <sub>40</sub> ]	plenary Keggin	2862	-3	±
PV3	K <sub>7</sub> [Ti <sub>2</sub> W <sub>10</sub> PO <sub>40</sub> ]	disubstituted Keggin	2879	-7	++
PV4	K <sub>6</sub> [H <sub>2</sub> TiW <sub>11</sub> CoO <sub>40</sub> ]	monosubstituted Keggin	3006	-8	+
PV5	K <sub>10</sub> [CO <sub>4</sub> (H <sub>2</sub> O) <sub>2</sub> (PW <sub>9</sub> O <sub>34</sub> ) <sub>2</sub> ]	Weakley	5122	-10	++
PV6 (HPA-23)	(NH <sub>4</sub> ) <sub>18</sub> [NaSb <sub>9</sub> W <sub>21</sub> O <sub>86</sub> ]	Cryptate encapsulating a sodium ion in its central cavity	6680	-18	++
P <sub>5</sub> W <sub>30</sub>	Na <sub>15</sub> [P <sub>5</sub> W <sub>30</sub> O <sub>110</sub> ]	Pope-Jeannin-Preyssler	7780	-15	++
P <sub>6</sub> W <sub>18</sub>	Na <sub>20</sub> [P <sub>6</sub> W <sub>18</sub> O <sub>79</sub> ]	Double Keggin	5222	-20	-
P <sub>8</sub> W <sub>48</sub>	Na <sub>33</sub> [H <sub>7</sub> P <sub>8</sub> W <sub>48</sub> O <sub>184</sub> ]	Contant-Tézé	12790	-33	++
PW <sub>12</sub>	Na <sub>3</sub> [PW <sub>12</sub> O <sub>40</sub> ]	Keggin	2948	-3	-
OP <sub>8</sub> W <sub>12</sub>	Na <sub>16</sub> [(O <sub>3</sub> POPO <sub>3</sub> ) <sub>4</sub> W <sub>12</sub> O <sub>36</sub> ]	Folded macrocyclic dodecatungstate with diphosphate complex	3848	-16	++
CP <sub>8</sub> W <sub>12</sub>	Na <sub>16</sub> [(O <sub>3</sub> PCH <sub>2</sub> PO <sub>3</sub> ) <sub>4</sub> W <sub>12</sub> O <sub>36</sub> ]	Folded macrocyclic dodecatungstate with diphosphate complex	3840	-16	++
K-POM	K <sub>8</sub> [H <sub>3</sub> P <sub>2</sub> W <sub>15</sub> V <sub>3</sub> O <sub>62</sub> ]	Wells-Dawson type	4278	-9	*
(Bu <sub>4</sub> N) <sub>6</sub> -POM	(Bu <sub>4</sub> N) <sub>6</sub> [H <sub>3</sub> P <sub>2</sub> W <sub>15</sub> V <sub>3</sub> O <sub>62</sub> ]	Wells-Dawson encapsulated by 6 tetrabutyl-ammonium groups	5422	-9	*
(Bu <sub>4</sub> N) <sub>6</sub> -PEG 1000	(Bu <sub>4</sub> N) <sub>6</sub> [H <sub>3</sub> P <sub>2</sub> W <sub>15</sub> V <sub>3</sub> O <sub>62</sub> ]-PEG 1000	Added PEG chain with MW of 1000 Da	6672	-9	*

Continuation of Table 4.1

(Bu <sub>4</sub> N) <sub>6</sub> - PEG 2000	(Bu <sub>4</sub> N) <sub>6</sub> [H <sub>3</sub> P <sub>2</sub> W <sub>15</sub> V <sub>3</sub> O <sub>62</sub> ]- PEG 2000	Added PEG chain with MW of 2000 Da	7571	-9	*
(Bu <sub>4</sub> N) <sub>6</sub> - PEG 5000	(Bu <sub>4</sub> N) <sub>6</sub> [H <sub>3</sub> P <sub>2</sub> W <sub>15</sub> V <sub>3</sub> O <sub>62</sub> ]- PEG 5000	Added PEG chain with MW of 5000 Da	10568	-9	*
KB1	K <sub>4</sub> [(Re <sub>6</sub> S <sub>8</sub> )(OH) <sub>6</sub> ]	Octahedral cluster chalcogenide anionic complex with terminal hydroxo ligands	1632	0 to -2 due to formation of hydroxo complexes	+
KB2	K <sub>4</sub> [(Re <sub>6</sub> Se <sub>8</sub> )(OH) <sub>6</sub> ]	Octahedral cluster chalcogenide anionic complex with terminal hydroxo ligands	2007	0 to -2 due to formation of hydroxo complexes	+
KB3	K <sub>4</sub> [Re <sub>6</sub> S <sub>8</sub> (CH <sub>3</sub> COO) <sub>6</sub> ]	Octahedral hexaacetate cluster complex	1884	-4	+
KB4	K <sub>4</sub> [(Re <sub>6</sub> S <sub>8</sub> )(HCOO) <sub>6</sub> ]	Octahedral cluster complex with monodentate coordinated formate ions	1800	-4	++
NaVO <sub>3</sub>	NaVO <sub>3</sub>	Metavanadate	122	-1	+
Na <sub>3</sub> VO <sub>4</sub>	Na <sub>3</sub> VO <sub>4</sub>	Orthovanadate	184	-3	+

++: very stable, +: stable, ±: stability not guaranteed during experiment, -: unstable, \*: no information available about stability in aqueous solution, but thermostable up to 160°C.



**Figure 4.1:** Structures of investigated polyoxotungstates and rhenium cluster compounds.

The charge of the compound increases along with the complexity of the three-dimensional shape. All compounds are negatively charged in solution. The solubility of some compounds is low, namely PV5, KB1, KB2 and  $P_8W_{48}$ , despite their high charge, so that the concentration of the prepared stock solutions had to be reduced from 10 mM to 1 mM or 0.1 mM, respectively.

The structural diversity of the available rhenium cluster compounds was lower than that of the available polyoxotungstates. All four compounds possess an octahedral shape with the basic formula  $[Re_6Q_8L_6]$  containing sulfur, selenium or tellur in position of Q and OH, acetate or formate in position of L (see Figure 4.1).

Several POMs were shown to have antitumoral, antibacterial, antiviral and antidiabetic properties.<sup>243-259</sup> The anticancer effect is attributed to DNA ladder formation, induction of apoptosis and inhibition of histone deacetylase (HDAC).<sup>243, 246, 247</sup> The effect was also proven in *in vivo* cancer models.<sup>244, 245</sup> The antibacterial effect could be demonstrated particularly for polyoxotungstates with Keggin shape. The combination with  $\beta$ -lactam antibiotics oxacillin, piperacillin or cefazolin showed a synergistic effect in MRSA, which was attributed to a reduced formation of penicillin-binding protein 2'.<sup>248, 250</sup> Antiviral properties were found against RNA-viruses like influenza A, anti-respiratory syncytial virus (RSV), Dengue virus, Hepatitis B and SARS.<sup>251, 254</sup> Particularly interesting is the activity against HIV-1, which was connected to inhibition of DNA polymerase activity.<sup>252, 253</sup> Antidiabetic properties were proven for tungsten and vanadium-based Dawson structures *in vivo* in a mouse model.<sup>256</sup> Vanadium-based compounds displayed insulin-mimetic features.<sup>257</sup> The insulin-mimetic effect was associated with improvement of glucose homeostasis, reduction of insulin resistance and improvement of insulin sensitivity in liver and muscle.<sup>258</sup>

Due to their high negative charge at physiological pH value, POMs were considered to not be able to cross cell membranes and enter intracellular compartments. It was therefore suggested that the pharmacological potency of POMs is conveyed through inhibition of structures presented on the extracellular site. Despite the fact that the high negative charge does hinder the entry of the compound into cells, measurable concentrations of various POMs inside cells were reported.<sup>217</sup> An example is HPA-23, which is also part of this experimental setting (PV6). Intracellular crystals of HPA-23 were detected using Raman spectroscopy.<sup>260</sup> Furthermore, the uptake of several polyoxotungstates in macrophages could be confirmed. Intracellular uptake and extracellular interaction were both assumed to be vital for antiviral activity.<sup>261</sup>

Recently, POMs were identified as potent inhibitors of nucleotide-degrading enzymes, especially NPPs and NTPDases, in rodents and humans. These results indicate that many of the described pharmacological properties of POMs can be associated with inhibition of this enzyme class.<sup>221, 262-265</sup> Their potency was ascribed to their negative charge and their similarity to the physiological ectonucleotidase substrates ATP and ADP.<sup>221</sup> Since nucleoside-degrading enzymes are not the only nucleotide-binding proteins expressed on the cell surface, polyoxometalates were tested at further structures activated by nucleotides. In 2011, Ramona Malek investigated POMs at G protein-coupled nucleotide-activated P2Y receptors.<sup>266</sup> The aim of the present study was to determine whether POMs are also interacting with P2X receptor ion channels. The results are discussed in the following chapters.

## 4.2 Z'-factor for determination of assay quality

The Z'-factor was calculated for all experiments conducted with POMs tested at P2X receptor subtypes. The results are presented in Table 4.2.

**Table 4.2:** Z'-factors of experiments conducted for testing the inhibitory potency of polyoxometalates at P2X receptors. Data is presented as mean  $\pm$  SEM.

	<b>P2X1</b> (n = 28)	<b>P2X2</b> (n = 27)	<b>P2X3</b> (n = 28)	<b>P2X4</b> (n = 28)	<b>P2X7</b> (n = 15)
<b>Z'-factor <math>\pm</math> SEM</b>	<b>0.61 <math>\pm</math> 0.05</b>	<b>0.57 <math>\pm</math> 0.05</b>	<b>0.62 <math>\pm</math> 0.12</b>	<b>0.64 <math>\pm</math> 0.04</b>	<b>0.68 <math>\pm</math> 0.10</b>

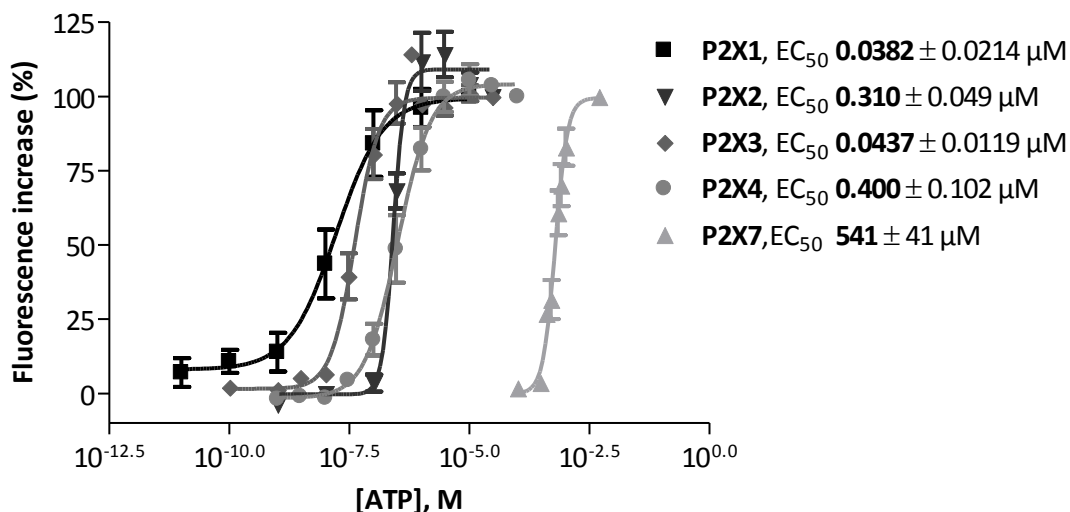
All standard antagonists used as negative control for all P2X receptor subtypes are summarized in chapter 2.1.6.5. During the first experiments, the comparability of Z'-factors obtained using standard inhibitor and the derived Z'-factors using buffer as negative control were tested. Since no significant difference could be detected, buffer-derived Z'-factors were also included, when the use of standard antagonists was not possible due to space conflict on the measuring plate.

All determined means of Z'-factors were higher than 0.50, therefore the assays for all receptor subtypes can be concluded to be useful for high-throughput screening.

### 4.3 Inhibitory potency of polyoxotungstates, vanadates and rhenium clusters at P2X receptors

The inhibitory potency of 17 polyoxotungstates, two vanadates and four rhenium cluster compounds was determined at the human P2X receptor subtypes P2X1, P2X2, P2X4, P2X7 and the rat P2X3. All compounds were tested by measurement of calcium influx in stably transfected 1321N1 astrocytoma cells. In order to exclude any interference by potential toxicity of the compounds cell viability experiments were performed.

Prior to these experiments, the  $EC_{80}$  value of the physiological agonist ATP was determined for each receptor subtype. The corresponding concentration-response curves and  $EC_{50}$  concentrations are shown in Figure 4.2.



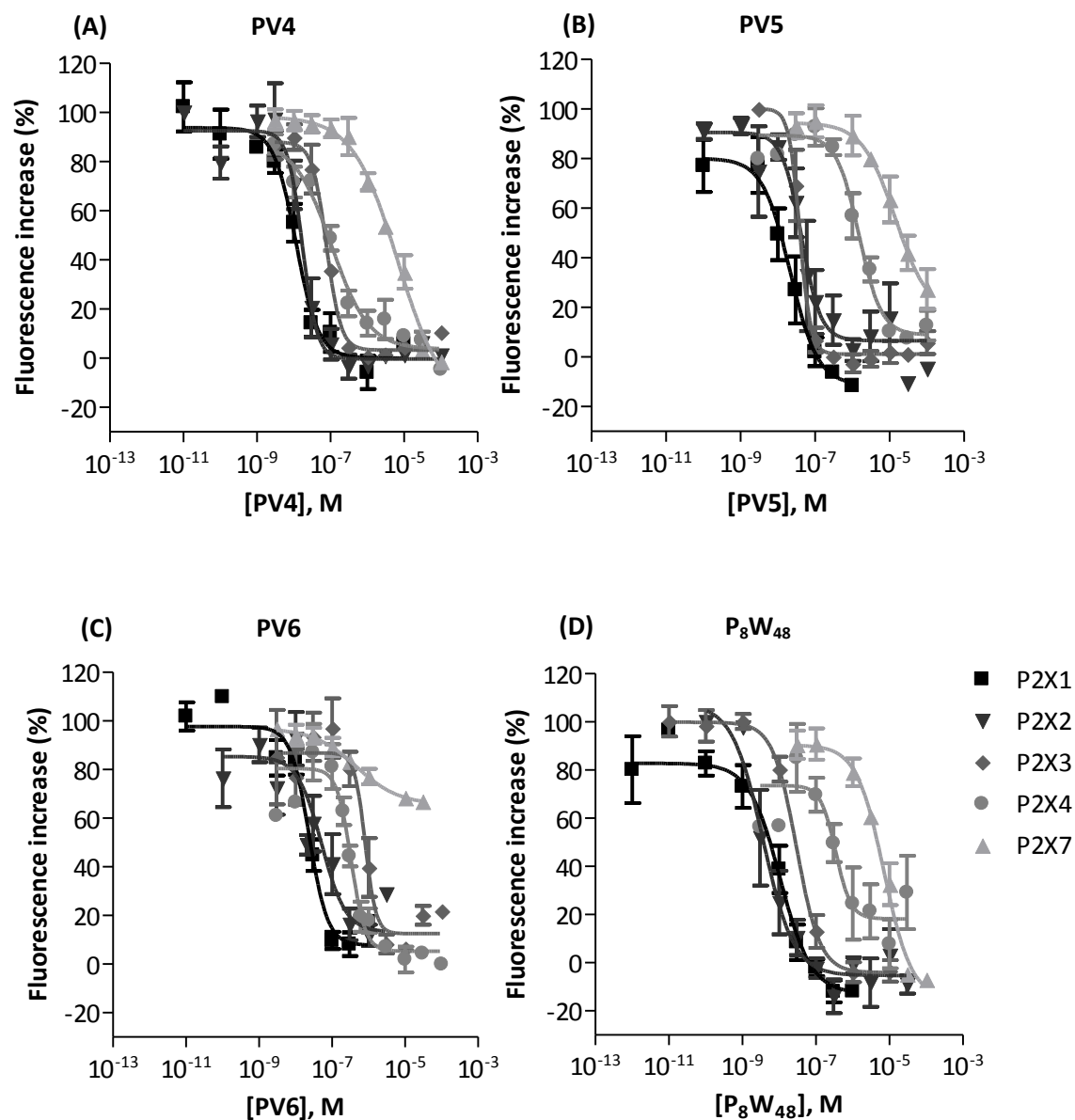
**Figure 4.2:** Mean dose-response curves and  $EC_{50}$  values of ATP at P2X receptors, presented as mean  $\pm$  SEM, n = 3-7.

Based on these results, the ATP concentrations selected for testing for inhibitory potency of POMs were the  $EC_{80}$  concentrations (0.1  $\mu$ M for P2X1 and P2X3, 1  $\mu$ M for P2X2 and P2X4 and 1 mM for P2X7 receptor) in all experiments described in the following chapters.

#### 4.3.1 Polyoxotungstates

Polyoxotungstates of different shape, order and charge were available for testing. Four of those are based on the same polyoxotungstate core. Those are  $(Bu_4N)_6$ -POM, to which a PEG-chain of

different length, 1000 Dalton in  $(\text{Bu}_4\text{N})_6\text{-PEG 1000}$ , 2000 Dalton in  $(\text{Bu}_4\text{N})_6\text{-PEG 2000}$  and 5000 Dalton in  $(\text{Bu}_4\text{N})_6\text{-PEG 5000}$ , was attached. The results of these PEGylated polyoxotungstates are presented in chapter 4.3.2. The results of the remaining polyoxotungstates are presented in Table 4.3. Four compounds, PV4, PV5, PV6 and  $\text{P}_8\text{W}_{48}$  were active at all tested P2X receptor subtypes with different potencies. The corresponding concentration-response curves are shown in Figure 4.3.



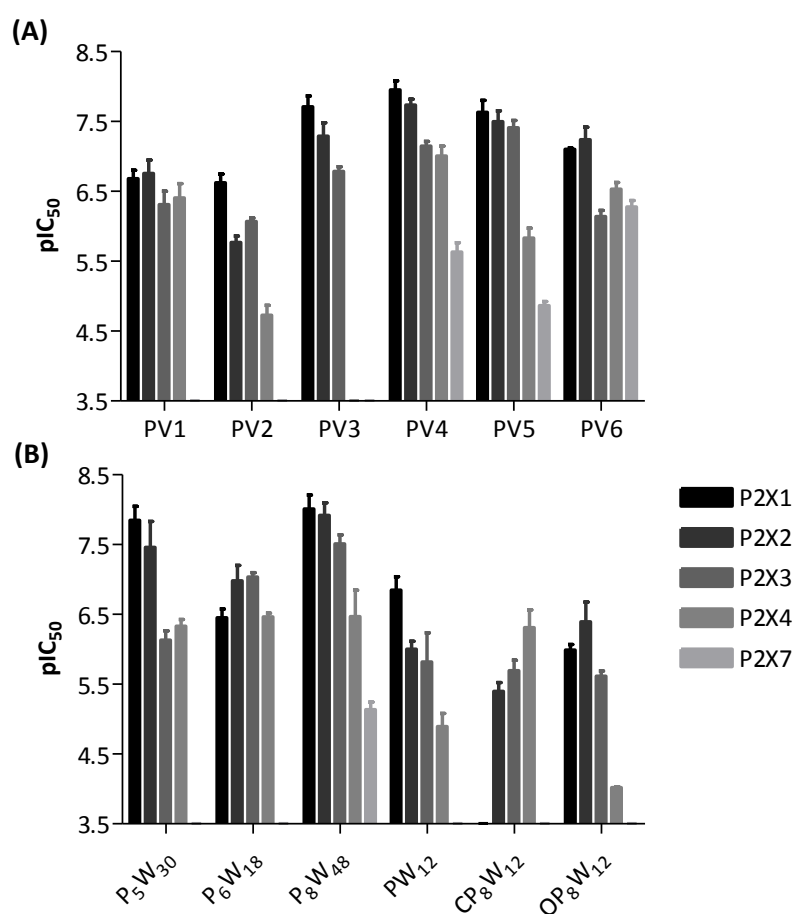
**Figure 4.3:** Mean dose response curves of polyoxotungstates (A) PV4, (B) PV5, (C) PV6 and (D)  $\text{P}_8\text{W}_{48}$  at P2X receptors. Data is presented as mean  $\pm$  SEM,  $n = 3-8$ .



**Table 4.3:** Inhibitory potency of polyoxotungstates and remaining receptor activity at human P2X receptors (mean  $\pm$  SEM, n = 3-8).

Name	Formula	IC <sub>50</sub> $\pm$ SEM [ $\mu$ M] or inhibition (%)				
		P2X1	P2X2	P2X3	P2X4	P2X7
PV1	Na <sub>6</sub> [H <sub>2</sub> W <sub>12</sub> O <sub>40</sub> ]	<b>0.231</b> $\pm$ 0.053	<b>0.246</b> $\pm$ 0.074	<b>0.579</b> $\pm$ 0.218	<b>0.542</b> $\pm$ 0.258	> 10 (2 %)
PV2	H <sub>3</sub> [PW <sub>12</sub> O <sub>40</sub> ]	<b>0.260</b> $\pm$ 0.072	<b>1.83</b> $\pm$ 0.33	<b>0.862</b> $\pm$ 0.102	<b>22.1</b> $\pm$ 4.8	> 10 (14 %)
PV3	K <sub>7</sub> [Ti <sub>2</sub> W <sub>10</sub> PO <sub>40</sub> ]	<b>0.0243</b> $\pm$ 0.008	<b>0.0766</b> $\pm$ 0.0245	<b>0.167</b> $\pm$ 0.025	> 10 (-13 %)	> 10 (-10 %)
PV4	K <sub>6</sub> [H <sub>2</sub> TiW <sub>11</sub> CoO <sub>40</sub> ]	<b>0.0126</b> $\pm$ 0.0031	<b>0.0196</b> $\pm$ 0.0033	<b>0.0724</b> $\pm$ 0.0111	<b>0.108</b> $\pm$ 0.028	2.77 $\pm$ 0.69
PV5	K <sub>10</sub> [Co <sub>4</sub> (H <sub>2</sub> O) <sub>2</sub> (PW <sub>9</sub> O <sub>34</sub> ) <sub>2</sub> ]	<b>0.0317</b> $\pm$ 0.0119	<b>0.0382</b> $\pm$ 0.0123	<b>0.0410</b> $\pm$ 0.0103 (remaining receptor activity 13 %)	<b>1.61</b> $\pm$ 0.42	<b>13.9</b> $\pm$ 1.9 (remaining receptor activity 27 %)
PV6	(NH <sub>4</sub> ) <sub>18</sub> [NaSb <sub>9</sub> W <sub>21</sub> O <sub>86</sub> ]	<b>0.0792</b> $\pm$ 0.0031 (remaining receptor activity 18 %)	<b>0.0803</b> $\pm$ 0.0316 (remaining receptor activity 23 %)	<b>0.757</b> $\pm$ 0.139	<b>0.309</b> $\pm$ 0.062	<b>0.572</b> $\pm$ 0.143 (remaining receptor activity 65 %)
P <sub>5</sub> W <sub>30</sub>	Na <sub>15</sub> [P <sub>5</sub> W <sub>30</sub> O <sub>110</sub> ]	<b>0.0173</b> $\pm$ 0.0066 (remaining receptor activity 22 %)	<b>0.0716</b> $\pm$ 0.0560	<b>0.806</b> $\pm$ 0.223	<b>0.519</b> $\pm$ 0.090	> 10 (4 % (100 nM))
P <sub>6</sub> W <sub>18</sub>	Na <sub>20</sub> [P <sub>6</sub> W <sub>18</sub> O <sub>79</sub> ]	<b>0.420</b> $\pm$ 0.125	<b>0.186</b> $\pm$ 0.076	<b>0.0941</b> $\pm$ 0.0138 (remaining receptor activity 39 %)	<b>0.349</b> $\pm$ 0.04	> 10 (24 %)
P <sub>8</sub> W <sub>48</sub>	Na <sub>33</sub> [H <sub>7</sub> P <sub>8</sub> W <sub>48</sub> O <sub>184</sub> ]	<b>0.0165</b> $\pm$ 0.0062	<b>0.0144</b> $\pm$ 0.0065	<b>0.0335</b> $\pm$ 0.0086 (remaining receptor activity 33 %)	<b>0.723</b> $\pm$ 0.571	<b>7.78</b> $\pm$ 1.91
PW <sub>12</sub>	Na <sub>3</sub> [PW <sub>12</sub> O <sub>40</sub> ]	<b>0.192</b> $\pm$ 0.089	<b>1.16</b> $\pm$ 0.361	<b>3.37</b> $\pm$ 2.03	<b>15.6</b> $\pm$ 7.1	> 10 (19 %)
CP <sub>8</sub> W <sub>12</sub>	Na <sub>16</sub> [(O <sub>3</sub> PCH <sub>2</sub> PO <sub>3</sub> ) <sub>4</sub> W <sub>12</sub> O <sub>36</sub> ]	> 10 (49 %)	<b>4.51</b> $\pm$ 1.38	<b>2.26</b> $\pm$ 0.64 (remaining receptor activity 22 %)	<b>0.765</b> $\pm$ 0.357	> 10 (-5 %)
OP <sub>8</sub> W <sub>12</sub>	Na <sub>16</sub> [(O <sub>3</sub> POPO <sub>3</sub> ) <sub>4</sub> W <sub>12</sub> O <sub>36</sub> ]	<b>1.06</b> $\pm$ 0.20	<b>0.727</b> $\pm$ 0.270	<b>2.50</b> $\pm$ 0.41	<b>96.1</b> $\pm$ 3.0	> 10 (-8 %)

The most active compound of this series was cobalt- and titanium-containing monosubstituted Keggin structure PV4. It completely inhibited all P2X receptor subtypes tested with  $IC_{50}$  values ranging from 0.0126 to 2.77  $\mu M$  (see Table 4.3). It was the most active compound at P2X1 and P2X4 receptors, and showed almost the same inhibitory potency at P2X2 and P2X3 receptors as  $P_8W_{48}$  (see Figure 4.3). PV1-3,  $P_5W_{30}$ ,  $P_6W_{18}$ ,  $PW_{12}$ ,  $CP_8W_{12}$  and  $OP_8W_{12}$  inhibited P2X1 to P2X4 receptors, but showed no activity at the P2X7 receptor. PV2, provided by Prof. Dr. Ulrich Körtz, and  $PW_{12}$ , provided by Dr. Holger Stephan, showed the same activity at all respective subtypes, due to being the same compound crystallized as different salts (see Table 4.1). All compounds of this POM series were shown to be potent antagonists of the P2X1, P2X2 and P2X3 receptor with  $IC_{50}$  values in the low nanomolar to low micromolar range. Only  $CP_8W_{12}$  was not active at the P2X1 receptor, despite the fact that structurally it is almost identical to active compound  $OP_8W_{12}$ . Except for PV1, PV4,  $P_5W_{30}$ ,  $P_6W_{18}$  and  $CP_8W_{12}$  at the P2X4 receptor, a significantly lower potency of the compounds towards P2X4 and P2X7 receptors than for the remaining P2X subtypes was observed, while their activity at the other subtypes tested was comparable.



**Figure 4.4:**  $pIC_{50}$  values of polyoxotungstates (A) PV1-6 and (B)  $P_5W_{30}$ ,  $P_6W_{18}$ ,  $P_8W_{48}$ ,  $PW_{12}$ ,  $CP_8W_{12}$  and  $OP_8W_{12}$  at human P2X receptors. Data is presented as mean  $\pm$  SEM (n = 3-8).

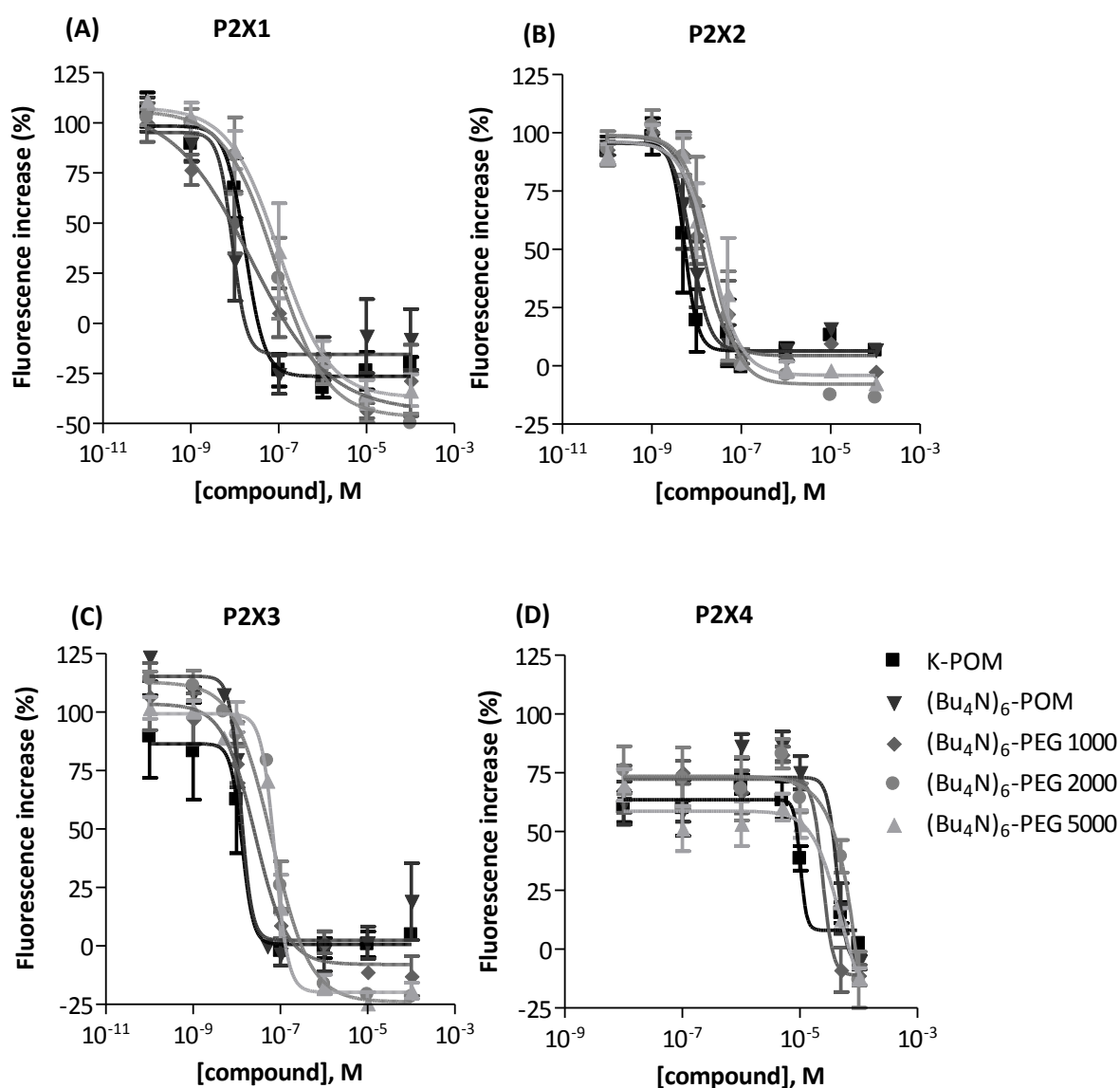
PV2 and  $PW_{12}$  have the same structure and charge, but were crystallized with different cations. Both compounds show at least tenfold less activity compared to the other polyoxotungstates at P2X1, P2X2 and P2X3, except for PV1. Since PV2 and  $PW_{12}$  bear the lowest negative charge in solution, closely followed by PV1, it is possible that the negative charge could be a defining factor for potency of receptor inhibition at these three subtypes. The selectivity data presented in Figure 4.4 combined with the structural information in Table 4.1 suggest that a certain amount of negative charge has to be present in the respective polyoxotungstate compound in order to inhibit those receptor subtypes with nanomolar potency. However, the relationship does not appear to be linear. An increase in charge does not further enhance the inhibitory potency of the polyoxotungstate (see Table 4.3). No such relationship between charge and affinity could be observed for P2X4 and P2X7 receptors. The determined potencies of all polyoxotungstates were significantly lower at P2X4 and P2X7 receptors than at the other subtypes P2X1, P2X2 and P2X3. The only exception was  $CP_8W_{12}$  at the P2X4 receptor. The dodecatungstate cluster compound was identified to be the most active one at the P2X4 receptor with an almost three-fold selectivity versus the P2X3 receptor, where it showed its second highest affinity. The similar compound  $OP_8W_{12}$  was considerably less potent, despite the high structural similarity and same charge.

The activity profile of polyoxotungstates at the P2X7 receptor was different from the other subtypes. As already mentioned, most compounds showed no inhibitory activity at this subtype, and the potency of the active structures PV4, PV5 and  $P_8W_{48}$  was moderate in comparison to the other P2X receptors. Although PV6 showed the lowest  $IC_{50}$  value and therefore seemed the most potent polyoxotungstate antagonist of P2X7 receptors, the inhibition was not complete and the receptor activity was only diminished by 35 % at the highest concentration tested.

Next to the charge of the complex, the influence of the three-dimensional structure was considered for characterization of activity. PV2, PV3, PV4 and  $PW_{12}$  are all Keggin-derived structures,  $P_6W_{18}$  displays the double-Keggin shape. All compounds were potent antagonists of P2X1, P2X2 and P2X3 receptors. A slight increase in potency can be observed for all compounds when charge and molecular weight increased from PV2 to PV4. The double-Keggin structure did not further enhance the respective potency. Since the other, more complicated and heavier structures like Weakley (PV5), Pope-Jeannin-Preyssler ( $P_5W_{30}$ ), or Contant-Tézé ( $P_8W_{48}$ ) were also effective antagonists of these P2X receptor subtypes, molecular weight and shape, like charge, cannot be the solely defining parameters for characterization of inhibitory potency of polyoxotungstates.

### 4.3.2 PEGylated polyoxotungstates

Five polyoxotungstates displaying the Wells-Dawson structure with or without an attached linker connected to a polyethylene glycol chain of varying length were kindly provided by Prof. Dr. Wei Wang from the Nankai University in Tianjin, China. PEGylation of compounds is used as an attempt to prolong its biological half-life and to direct drug delivery.<sup>267, 268</sup> The Wells-Dawson basic structure K-POM, its derivative attached to a linker  $(\text{Bu}_4\text{N})_6\text{-POM}$  and the same structure with different PEG chains were available for testing. The results at human P2X receptors P2X1, P2X2, P2X4 and P2X3 receptor are presented in Figure 4.5 and Figure 4.4.

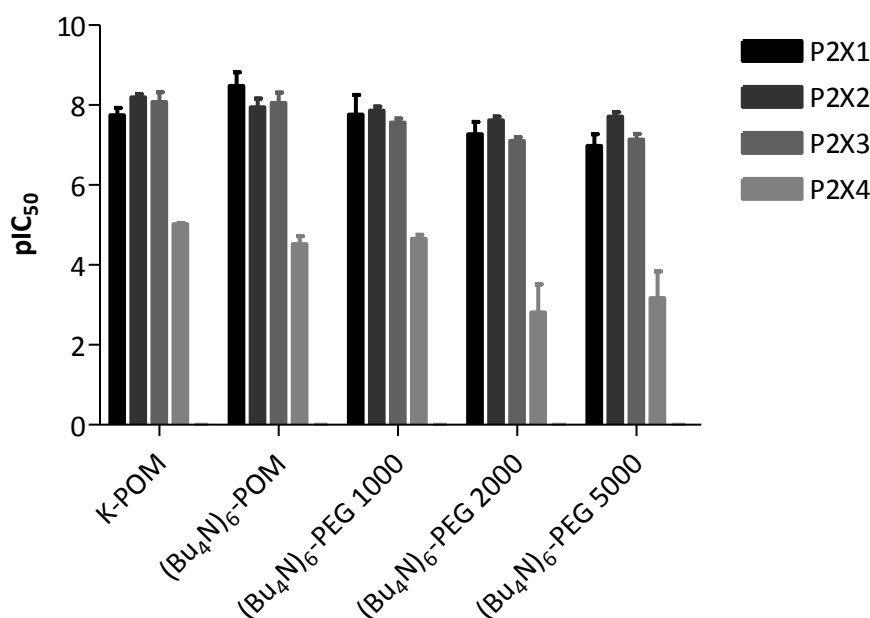


**Figure 4.5:** Mean dose-response curves of PEGylated and non-PEGylated Wells-Dawson polyoxotungstates at P2X receptors. Data is presented as mean  $\pm$  SEM ( $n = 3-5$ ).

**Table 4.4:** Inhibitory potency of PEGylated and non-PEGylated Wells-Dawson polyoxotungstates at P2X receptors. (mean  $\pm$  SEM, n = 3-6)

Name	Formula	IC <sub>50</sub> $\pm$ SEM [ $\mu$ M] or inhibition (%)				
		P2X1	P2X2	P2X3	P2X4	P2X7
K-POM	K <sub>8</sub> [HP <sub>2</sub> W <sub>15</sub> V <sub>3</sub> O <sub>62</sub> ]	0.0216 $\pm$ 0.0097	0.00660 $\pm$ 0.00117	0.0106 $\pm$ 0.0042	9.65 $\pm$ 0.59	
(Bu <sub>4</sub> N) <sub>6</sub> <sup>-</sup> POM	(Bu <sub>4</sub> N) <sub>6</sub> [H <sub>3</sub> P <sub>2</sub> W <sub>15</sub> V <sub>3</sub> O <sub>62</sub> ]	0.0104 $\pm$ 0.0074	0.0170 $\pm$ 0.0095	0.0128 $\pm$ 0.0043	35.6 $\pm$ 11.8	see chapter 4.3.3
(Bu <sub>4</sub> N) <sub>6</sub> <sup>-</sup> PEG 1000	(Bu <sub>4</sub> N) <sub>6</sub> [H <sub>3</sub> P <sub>2</sub> W <sub>15</sub> V <sub>3</sub> O <sub>62</sub> ]- PEG 1000	0.0731 $\pm$ 0.0413	0.0148 $\pm$ 0.0034	0.0288 $\pm$ 0.0063	23.4 $\pm$ 5.8	
(Bu <sub>4</sub> N) <sub>6</sub> <sup>-</sup> PEG 2000	(Bu <sub>4</sub> N) <sub>6</sub> [H <sub>3</sub> P <sub>2</sub> W <sub>15</sub> V <sub>3</sub> O <sub>62</sub> ]- PEG 2000	0.0892 $\pm$ 0.0374	0.0257 $\pm$ 0.0052	0.0846 $\pm$ 0.0195	> 100 (-36 %)	
(Bu <sub>4</sub> N) <sub>6</sub> <sup>-</sup> PEG 5000	(Bu <sub>4</sub> N) <sub>6</sub> [H <sub>3</sub> P <sub>2</sub> W <sub>15</sub> V <sub>3</sub> O <sub>62</sub> ]- PEG 5000	0.168 $\pm$ 0.072	0.0213 $\pm$ 0.00562	0.0840 $\pm$ 0.0231	> 100 (-47 %)	

K-POM was proven to be the most active POM of all at the P2X2 receptor with an IC<sub>50</sub> value of 6.60  $\pm$  1.17 nM. The inhibitory potency at P2X1 and P2X3 receptors was comparable to the other very potent polyoxotungstates with IC<sub>50</sub> values in the low nanomolar range as well. All derivatives were again significantly less active at the P2X4 receptor than at the before mentioned receptor which is further demonstrated in Figure 4.6.

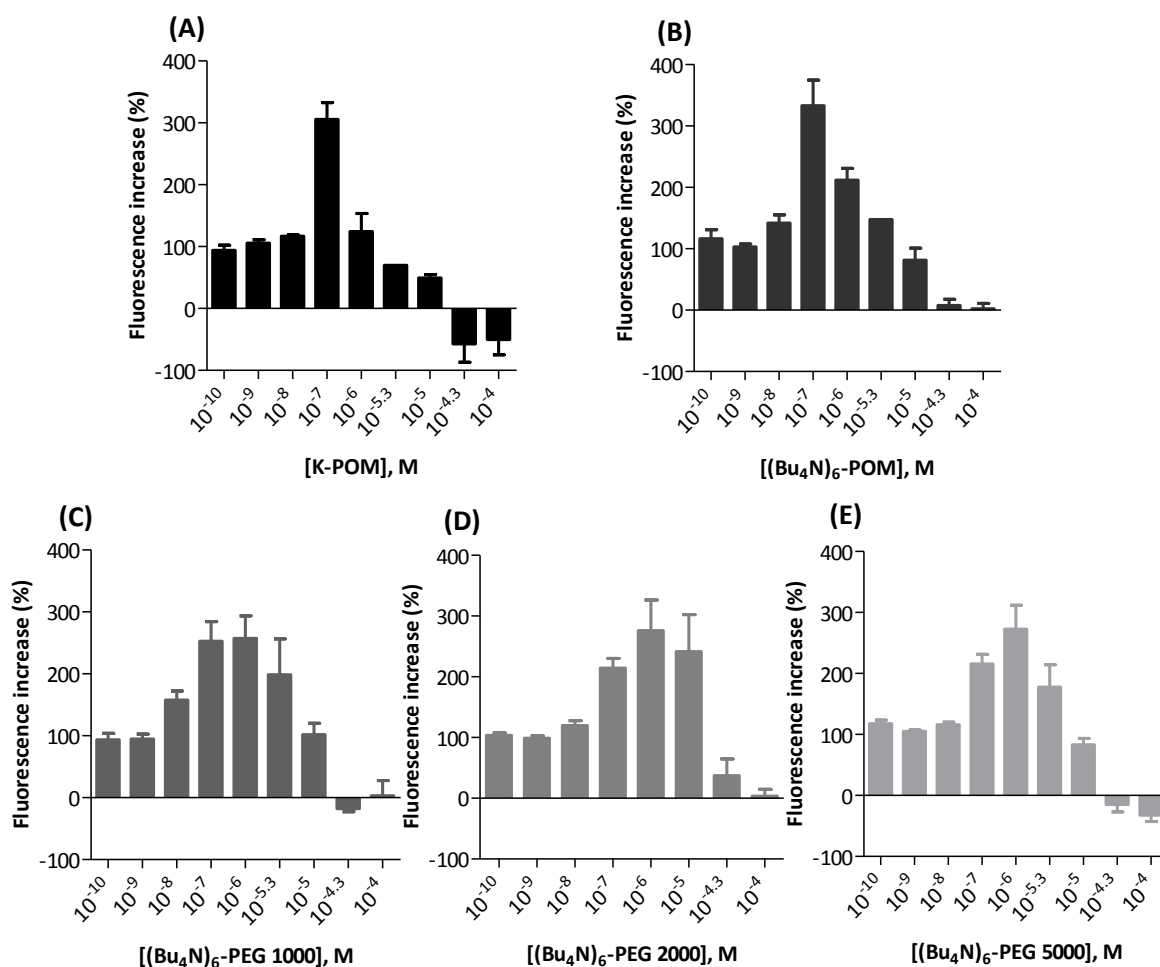
**Figure 4.6:** The pIC<sub>50</sub> values of polyoxotungstates at P2X receptors subtypes P2X1-4. Data is presented as mean  $\pm$  SEM (n = 3-5).

All five compounds showed comparable potency at P2X1, P2X2 and P2X3 receptors, as was already seen with the previous series of polyoxotungstates. A very small decrease in  $IC_{50}$  values could be observed upon PEGylation and with increase in the PEG chain length. Thus, PEGylation of the compound did not seem to have much effect on the potency of the Wells-Dawson compound. It can be concluded that PEGylation is well tolerated and may therefore be a means to increase the half-life of POMs used as P2X receptor antagonists for *in vivo* studies.

At the P2X4 receptor however, PEGylation resulted in a decrease of inhibitory potency, which was already low for the parent POM.

### 4.3.3 PEGylated POMs at P2X7

The results at the P2X7 subtype were proven to be more complex than at the other P2X receptors, as can be seen in Figure 4.7 and Table 4.5.



**Figure 4.7:** Mean dose response data of PEGylated Wells-Dawson POMs and the non-PEGylated versions at the human P2X7 receptor. The concentrations of respective antagonist [M] on the X-axis are plotted against the fluorescence increase (%) on the Y-axis. (MW  $\pm$  SEM, n = 3-5).

At first, it was considered that the enhancement of ATP-induced fluorescence increase might have been due to a pipetting error during the experiment, but the phenomenon occurred at the same concentrations in all experiments conducted for all five compounds. The inhibitory potency is expressed in  $IC_{50}$ , while the enhancing concentration is described in the concentration at which the maximal enhancement of ATP-induced fluorescence increase is observed. The PEG chain seemed to slightly decrease the inhibitory potency, although the effect was not proportional to the chain length. The same can be observed for the concentration of fluorescence signal enhancement. Due to a lack in sufficient amount of compound, it was not possible to conduct further experiments. The data available for the non-PEGylated derivatives K-POM and  $(Bu_4N)_6$ -POM indicated that the concentration window in which enhancement of ATP-induced signal occurred was small and peaked in a sharply defined maximum, while the addition of a PEG chain seemed to broaden the concentration range for enhancement and decrease the maximum of enhancement. The length of the chain did not appear to have any influence; the inhibitory  $IC_{50}$  value shifted with elongation from 1000 to 2000 Dalton, but then reduced again when extending to 5000 Dalton. The same was observed for the  $EC_{50\text{Enhancement}}$  and the maximal ATP effect.

**Table 4.5:** Inhibitory and enhancing potency of PEGylated POMs and the non-PEGylated derivatives at human P2X7 receptor, calculated by bell-shaped non-linear regression analysis of concentration-response experiments. Data is presented as mean  $\pm$  SEM from 3-5 independent experiments.

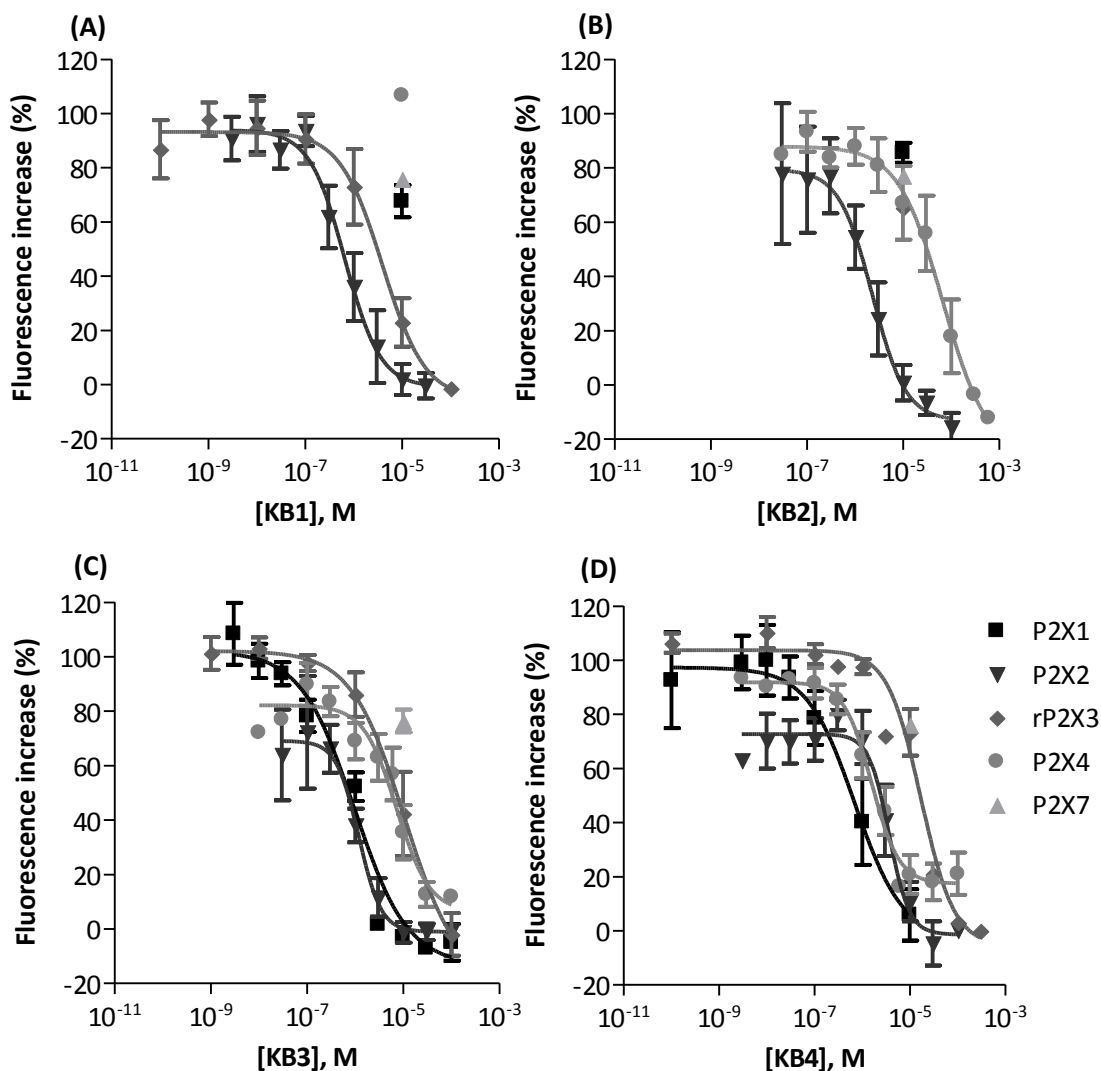
	K-POM	$(Bu_4N)_6$ -POM	$(Bu_4N)_6$ -PEG 1000	$(Bu_4N)_6$ -PEG 2000	$(Bu_4N)_6$ -PEG 5000
$EC_{50\text{Enhancement}}$ [ $\mu\text{M}$ ]	<b>0.0241</b> $\pm$ 0.0087	<b>0.0362</b> $\pm$ 0.0090	<b>0.0251</b> $\pm$ 0.0143	<b>0.167</b> $\pm$ 0.148	<b>0.113</b> $\pm$ 0.045
$IC_{50}$ [ $\mu\text{M}$ ]	<b>0.230</b> $\pm$ 0.059	<b>0.714</b> $\pm$ 0.463	<b>8.84</b> $\pm$ 1.05	<b>21.5</b> $\pm$ 5.9	<b>6.58</b> $\pm$ 1.80
Enhancement of fluorescence signal (%)	<b>271</b> $\pm$ 27	<b>261</b> $\pm$ 48	<b>164</b> $\pm$ 34	<b>191</b> $\pm$ 68	<b>181</b> $\pm$ 38
Concentration of peak enhancement [ $\mu\text{M}$ ]	<b>0.0333</b> $\pm$ 0.0112	<b>0.0738</b> $\pm$ 0.0367	<b>1.32</b> $\pm$ 0.62	<b>3.61</b> $\pm$ 1.39	<b>1.25</b> $\pm$ 0.45

No fluorescence enhancement could be detected at any concentration for any of the remaining POMs at any target. Since those five compounds are the only ones displaying the Wells-Dawson structure, but contain the same elements as the remaining polyoxotungstates, it is possible that

enhancement at the P2X7 receptor is associated with the three-dimensional shape of the compound.

#### 4.3.4 Rhenium cluster compounds

Four rhenium cluster polyoxometalates were available for testing next to the polyoxotungstates. In contrast to the tungstate-based compounds, the rhenium cations are not connected by oxygen, but by other chalcogenide elements such as tellurium, selenium (KB2) or sulfur (KB1, KB3 and KB4). The results of calcium influx experiments are presented in Figure 4.8 and Table 4.6.



**Figure 4.8:** Mean dose response curves of rhenium clusters at P2X receptors. Data is presented as mean  $\pm$  SEM,  $n = 3-5$ .



In general, the inhibitory potency of rhenium cluster compounds at different P2X receptors is less than that of polyoxotungstates. None of the compounds available was capable of inhibiting the P2X7 receptor, but all of them were active at the P2X2 subtype. The most active compound was KB3 with an  $IC_{50}$  value of  $843 \pm 138$  nM (see also Figure 4.8), closely followed by KB1 with  $1.11 \pm 0.58$   $\mu$ M. Neither KB1 nor KB2 were active at P2X1 or P2X4 receptors. KB2 inhibited the P2X4 receptor only when used in high micromolar concentrations. KB3 and KB4 inhibited both subtypes at low micromolar concentrations, but not even upon increase of test compound concentration, the ATP-induced P2X4 receptor activity was reduced completely to 0 %.

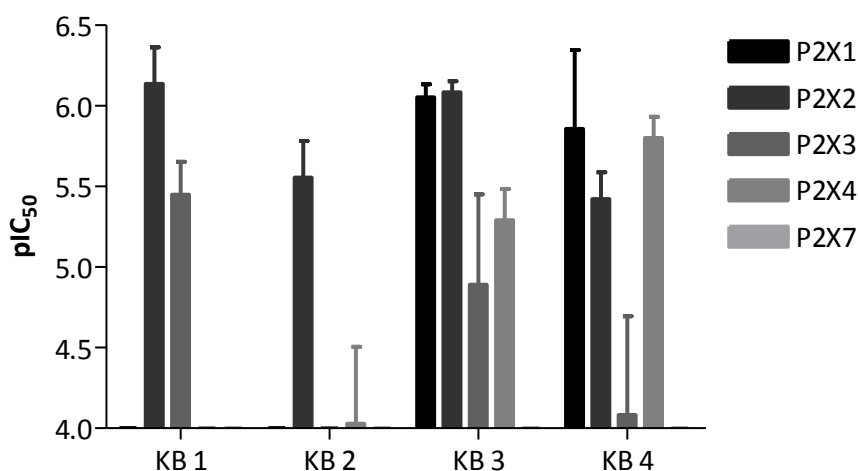
**Table 4.6:** Inhibitory potency of rhenium cluster compounds at P2X receptors (mean  $\pm$  SEM, n = 3-5).

Compound	Formula	$IC_{50} \pm SEM$ [ $\mu$ M] or inhibition $\pm$ SEM (%) at 10 $\mu$ M				
		P2X1	P2X2	P2X3	P2X4	P2X7
KB1	$K_4[Re_6S_8(OH)_6]$	> 10 (32 %)	<b>1.11</b> $\pm$ 0.58	<b>4.28</b> $\pm$ 1.49	> 10 (-7 %)	> 10 (14 %)
KB2	$K_4[(Re_6Se_8)(OH)_6]$	> 10 (14 %)	<b>4.09</b> $\pm$ 1.97	> 10 (35 %)	<b>48.8</b> $\pm$ 16.4	> 10 (13 %)
KB3	$K_4[Re_6S_8(CH_3COO)_6]$	<b>0.933</b> $\pm$ 0.177	<b>0.843</b> $\pm$ 0.138	<b>39.5</b> $\pm$ 30.3	<b>6.21</b> $\pm$ 2.73 (remaining receptor activity 12 %)	>10 (8 %)
KB4	$K_4[(Re_6S_8)(HCOO)_6]$	<b>4.33</b> $\pm$ 3.78	<b>4.52</b> $\pm$ 1.27	<b>17.8</b> $\pm$ 3.51	<b>1.80</b> $\pm$ 0.50 (remaining receptor activity 21 %)	> 10 (24 %)

All of the compounds showed weak potency in comparison to polyoxotungstates at the P2X3 receptor. Despite the high structural similarity to KB1, the most active compound, KB2 was not capable of inhibiting the P2X3 receptor. The addition of acetate (KB3) or formate residues (KB4) to the KB1 basic structure reduced its inhibitory potency.

Although the potency of rhenium cluster compounds is lower, they appear to be more P2X subtype selective. For a better overview, the results are highlighted in Figure 4.9. KB2 was active at the P2X2 receptor with a tenfold higher potency in comparison to the P2X4 receptor and no activity at the other receptor subtypes. KB1 was inactive at P2X1, P2X4 and P2X7 receptors, but inhibited P2X2 and P2X3 receptors with similar potency. KB3 and KB4 were sparsely to moderately active at all subtypes except P2X7. Although the compounds appear to show a

preference for certain receptor subtypes, they are not likely to play an important role as P2X antagonists due to low potency.



**Figure 4.9:** pIC<sub>50</sub> values of rhenium clusters at P2X receptors. Data is presented as mean ± SEM (n = 3-4).

#### 4.3.5 Vanadium-based polyoxometalates

Two vanadium salts were purchased and tested at human P2X subtypes P2X1, P2X2, P2X4, P2X7 and P2X3 to determine the activity of vanadium-based metal clusters. The results are presented in Table 4.7.

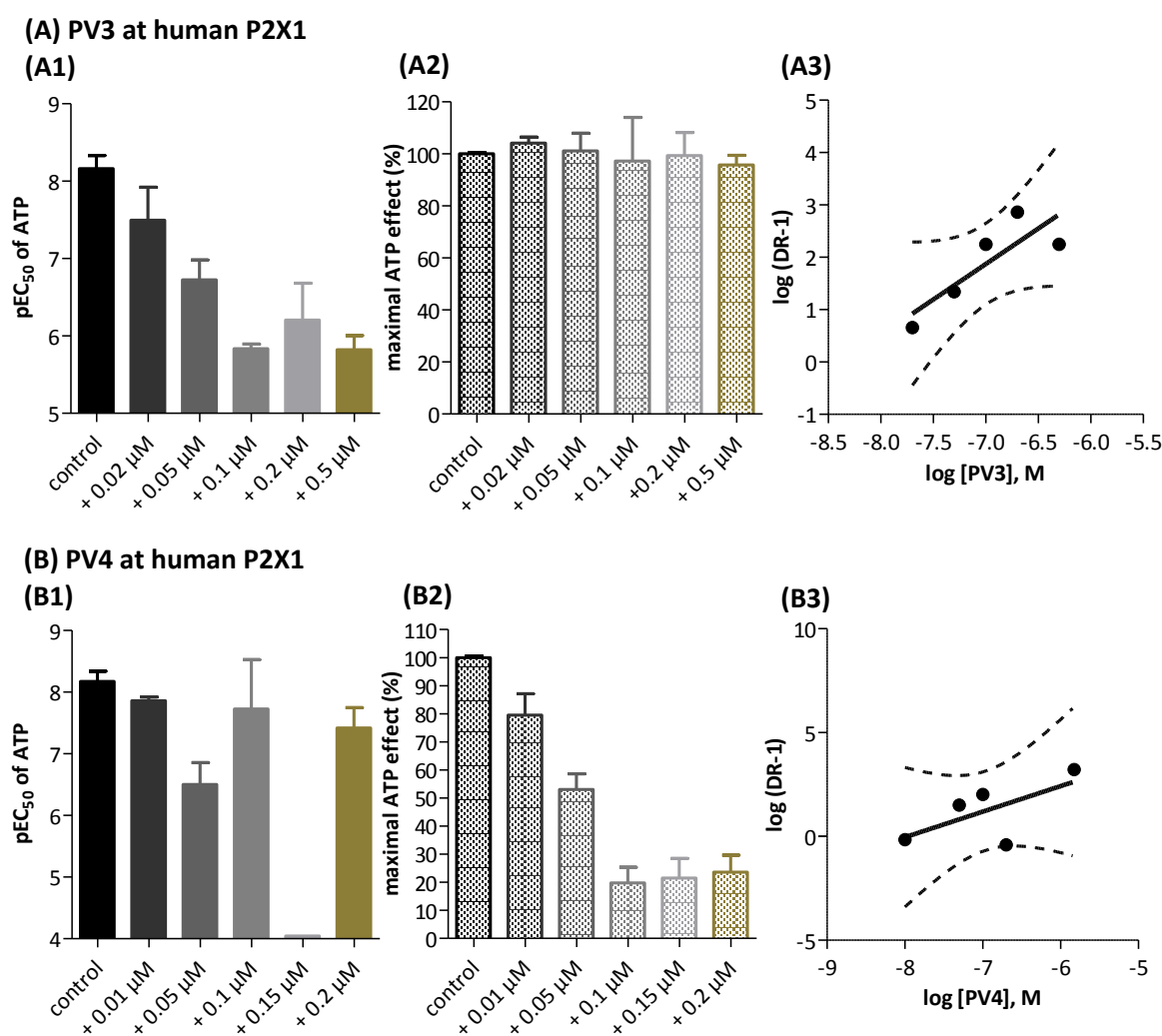
**Table 4.7:** Inhibitory potency of vanadium-based complexes at P2X receptors (mean ± SEM, n = 3).

Name	IC <sub>50</sub> ± SEM [μM] or inhibition at 10 μM or 1 μM (%)				
	P2X1	P2X2	P2X3	P2X4	P2X7
NaVO <sub>3</sub>	> 10 (-30 %)	3.15 ± 0.56	> 10 (43 %)	> 10 (23 %)	< 10 (12 %)
Na <sub>3</sub> VO <sub>4</sub>	> 10 (-3 %)	> 10 (1 %)	> 1 (30 %)	> 10 (25 %)	> 10 (17 %)

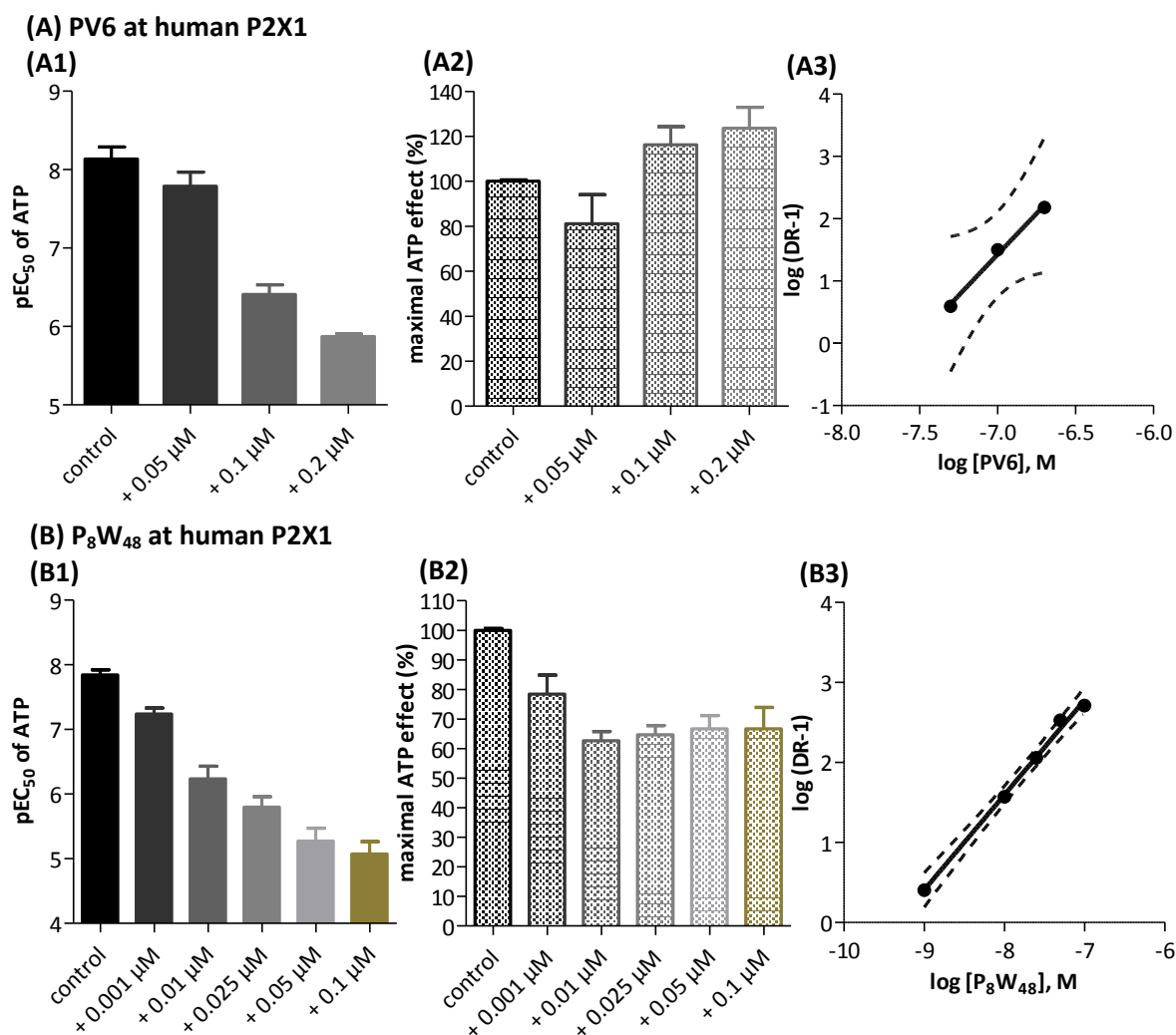
Compared to the remaining polyoxometalates, both vanadium salts had little to no inhibitory potency at most of the P2X receptor subtypes. The most potent compound was metavanadate sodium salt NaVO<sub>3</sub> at the human P2X2 receptor with an IC<sub>50</sub> value of 3.15 ± 0.56 μM. Since both compounds are significantly smaller than the other POMs, it is possible that a certain three-dimensional size is needed for successful inhibition of P2X receptors.

### 4.3.6 Determination of inhibition mechanism of selected polyoxometalates

Single concentrations of selected compounds were tested by determining their effect on the  $EC_{50}$  value of ATP in order to understand how POMs inhibit P2X receptors. The human P2X1 receptor was initially selected for this experiment. It was incubated with four of the most active compounds at concentrations that were based on the determined  $IC_{50}$  values. The selected compounds showed different three-dimensional structures: Keggin structures PV3 and PV4, cryptate PV6 and Contant-Tézé  $P_8W_{48}$ . The selected compounds were also tested at the P2X3 receptor to determine whether the species has an influence on the inhibition mechanism. The results determined at both receptors are presented in Figure 4.10 to Figure 4.13.



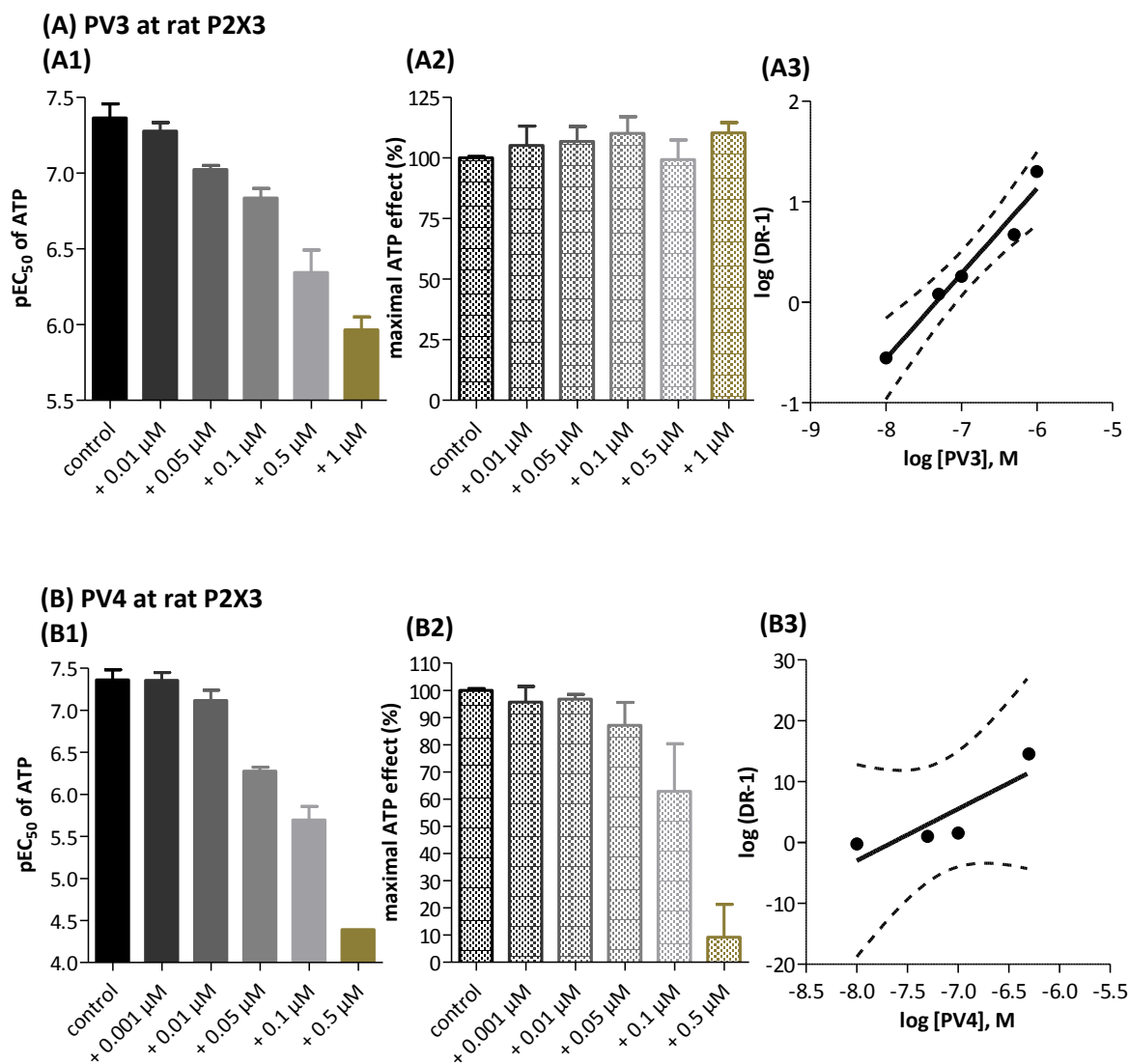
**Figure 4.10:** (1)  $pEC_{50}$  concentrations, (2) maximal ATP effect with or without addition of a defined concentration of polyoxotungstates (A) PV3 and (B) PV4, and (3) the respective Schild plots at the human P2X1 receptor. Buffer containing 1 % DMSO without compound was used as control. Data is presented as mean  $\pm$  SEM from 3-10 independent experiments. The Schild plots are presented as mean  $\pm$  95 % confidence interval.



**Figure 4.11:** (1) pEC<sub>50</sub> concentrations, (2) maximal ATP effect with or without addition of a defined concentration of polyoxotungstates (A) PV6 and (B) P<sub>8</sub>W<sub>48</sub>, and (3) the respective Schild plots at the human P2X1 receptor. Buffer containing 1 % DMSO without compound was used as control. Data is presented as mean ± SEM from 3-10 independent experiments. The Schild plots are presented as mean ± 95 % confidence interval.

PV6 at the human P2X1 receptor was the first compound to be tested. Only three different concentrations were selected for the experiment. Five to six concentrations of the remaining compounds were tested in all following experiments, since three concentrations were insufficient for a valid analysis. Every compound caused the ATP curve to shift to the right. Higher ATP concentrations have to be used to reach the full level of receptor activity. This indicates a competitive inhibition mechanism for PV6, where the antagonist competes with the agonist for the binding cavity. An increase in agonist concentration prevents the antagonist from binding to the receptor. If an antagonist does not inhibit by binding to the agonist binding site, but to another binding site, it is called an allosteric antagonist. The inhibition mechanism of an

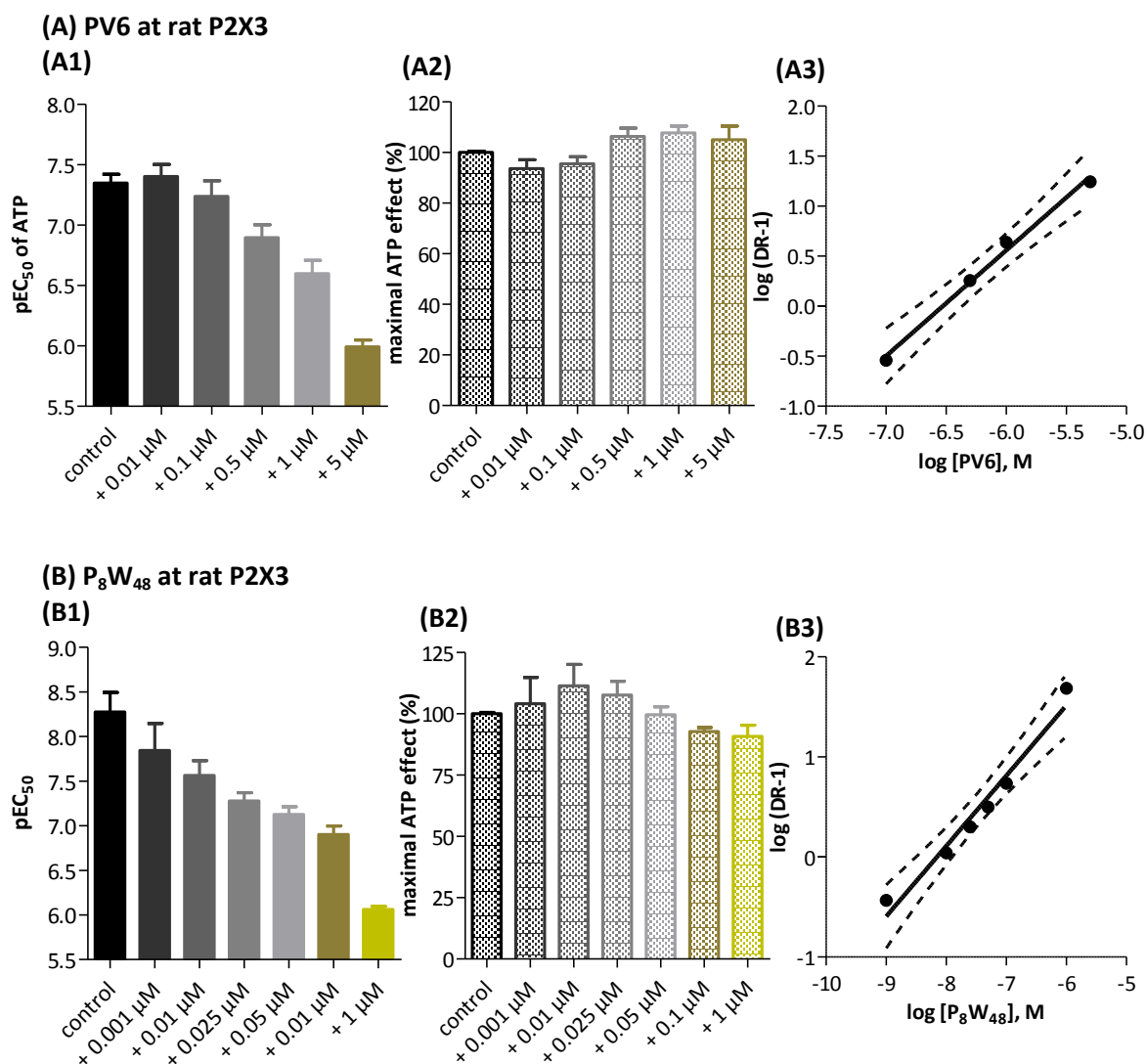
allosteric antagonist is an alteration of receptor conformation induced by the allosteric modulator which reduces the efficacy of the agonist. In that case, the  $EC_{50}$  value of the agonist is not affected by the antagonist independent of its concentration. Upon an increase in agonist concentration, it is no longer capable of activating the receptor to full level.



**Figure 4.12:** (1) pEC<sub>50</sub> concentrations, (2) maximal ATP effect with or without addition of a defined concentration of polyoxotungstates (A) PV3 and (B) PV4, and (3) the respective Schild plots at the P2X3 receptor (mean ± SEM, n = 3-6). Buffer containing 1% DMSO without compound was used as control. Data is presented as mean ± SEM from 3 to 6 independent experiments. The Schild plots are presented as mean ± 95% confidence interval.

A shift of the agonist curve to the right side can be observed for all four compounds at both receptors. This indicates that these compounds are orthosteric antagonists. However, the

shifted curves for PV4 and to some extent for  $P_8W_{48}$  also show a decrease in maximal fluorescence, which cannot be restored upon increase in ATP concentration. For PV3 and PV6, the shift of the ATP dose-response curves indicates a competitive mechanism of inhibition at both receptor subtypes. The results were further examined using the Gaddum/Schild analysis. The results are summarized in Table 4.8.



**Figure 4.13:** (1) pEC<sub>50</sub> concentrations, (2) maximal ATP effect with or without addition of a defined concentration of polyoxotungstates (A) PV6 and (B)  $P_8W_{48}$ , and (3) the respective Schild plots at the rat P2X3 receptor. Buffer containing 1% DMSO without compound was used as control. Data is presented as mean  $\pm$  SEM from 3 to 6 independent experiments. The Schild plots are presented as mean  $\pm$  95% confidence interval.

PA<sub>2</sub> represents the negative logarithm of antagonist needed to shift the dose response curve to the right by a factor of 2. The higher the pA<sub>2</sub> value the lower the respective concentration needed to shift the curve and the more effective the antagonist is. The highest pA<sub>2</sub> value of the

series was featured by  $P_8W_{48}$  at the P2X1 receptor. Generally, the  $pA_2$  values were higher at P2X1 than at P2X3 receptors. These results correspond with the previously determined  $IC_{50}$  concentrations of the compounds, which were all more potent at P2X1 than at P2X3 receptors (see Table 4.3).

**Table 4.8:**  $pA_2$ , Schild slope and Hill slope of Gaddum/Schild  $EC_{50}$  shift analysis for determination of competitive mechanism of inhibition of selected POMs at P2X1 and P2X3 receptors.

	$pA_2$	Hill slope	Schild slope
<b><u>P2X1</u></b>			
<b>PV3</b>	8.65	0.775	1.27
<b>PV4</b>	8.37	0.472	3.12
<b>PV6</b>	7.73	1.00	2.18
<b><math>P_8W_{48}</math></b>	10.3	0.533	1.06
<b><u>P2X3</u></b>			
<b>PV3</b>	7.42	2.85	0.929
<b>PV4</b>	7.77	1.62	2.51
<b>PV6</b>	6.58	2.01	0.972
<b><math>P_8W_{48}</math></b>	7.81	2.07	0.920

The Schild slope represents the slope of the linear regression of the log (DR-1) versus the logarithm of tested antagonist concentration. The mechanism of inhibition is deemed competitive when the Schild slope matches unity. The slopes of linear regression of PV3 and PV6 at P2X3 receptors and  $P_8W_{48}$  at both receptor subtypes lied closely to unity and can be considered as orthosteric antagonists at the respective receptors. The data of PV3 and PV6 at the P2X1 receptor is inconclusive, since the Schild slopes did not exactly match unity. For PV6, it can probably be attributed to the fact that only three antagonist concentrations were tested. Since the decrease of ATP  $EC_{50}$  concentrations is clearly visible (see Figure 4.13), a competitive mechanism of inhibition is assumed. The slope of linear regression of PV4 at both receptor subtypes definitely differed from unity. A competitive mode of inhibition cannot not be confirmed for PV4, even though its three-dimensional structure is the same as PV3. Additionally, a concentration-dependent decrease of maximal ATP effect was observed, which is a sign for allosteric interaction of PV4 with both P2X receptors. It is possible that PV4 can interact with P2X receptors by two different binding sites.

In conclusion, it can be said that POMs inhibit P2X receptors predominantly by competitive interaction. Since other influences on the receptors were observed for PV4, the determined

mode of inhibition cannot be transferred to the whole group of POMs and seemed to be influenced even by small structural changes.

### 4.3.7 Cytotoxicity of polyoxometalates

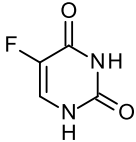
Since all compounds mainly consist of heavy metal ions, cytotoxicity was a possible factor not to be underestimated. Cytotoxicity can be mistaken for inhibition in a functional experiment like measurement of calcium influx. Cell viability assays using MTT were conducted. 1321N1 astrocytoma cells were incubated with various concentrations of polyoxometalates starting from 300  $\mu\text{M}$  or 100  $\mu\text{M}$ , respectively, and incubated for 72 hours. One hour before reading point, MTT was added. Only still live cells were capable of converting yellow MTT to purple formazan. Cells were lysed with DMSO to dissolve produced formazan, and UV absorbance was measured. The results are presented in Table 4.9.

Most of the polyoxotungstates and all of the rhenium cluster were slightly cytotoxic when used in high concentrations above 50  $\mu\text{M}$ , respectively. Since all of them had inhibitory activity at low nanomolar to low micromolar concentrations, it is unlikely that the results are biased by cytotoxicity. The same can be said for PV1, PV4, and PV6, for whom dose-response relations for cytotoxicity could be detected. The  $\text{EC}_{50}$  values of  $\text{P}_8\text{W}_{48}$ , K-POM,  $(\text{Bu}_4\text{N})_6\text{-POM}$  and the PEGylated versions  $(\text{Bu}_4\text{N})_6\text{-PEG 1000}$  and  $(\text{Bu}_4\text{N})_6\text{-PEG 2000}$  were shown to be cytotoxic in concentrations close to the detected  $\text{IC}_{50}$  values at human P2X4 or P2X7 receptor, respectively (see Table 4.3 and Table 4.4). Based on the results for both PEGylated POMs, it is possible that  $(\text{Bu}_4\text{N})_6\text{-PEG 5000}$  is also cytotoxic. Due to lack of compound, it was not possible to test it in a cell viability assay.

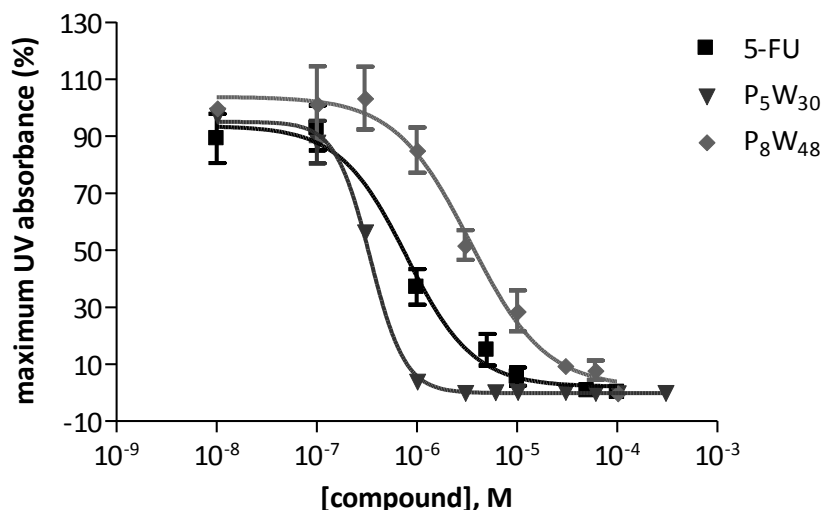
The most cytotoxic compound was  $\text{P}_5\text{W}_{30}$ , which was already toxic when used in concentrations in the nanomolar range (cytotoxicity  $\text{EC}_{50}$   $0.283 \pm 0.055 \mu\text{M}$ ). The respective concentration-response curve can be seen in Figure 4.14 along with the positive control 5-FU and  $\text{P}_8\text{W}_{48}$ . The detected cytotoxic concentrations are higher than the  $\text{IC}_{50}$  values determined for human P2X1, P2X2 and rat P2X3 receptors. Therefore, the detected receptor inhibition is unlikely to be affected by compound toxicity. It is unlikely that the observed reduced calcium influx at the human P2X4 receptor can be attributed to actual receptor inhibition, because the  $\text{IC}_{50}$  values determined to characterize the inhibitory potency and the cytotoxicity values are almost the same.



**Table 4.9:** Cytotoxicity EC<sub>50</sub> values of polyoxotungstates, rhenium cluster compounds and positive control 5-FU at non-transfected 1321N1 astrocytoma cells (mean ± SEM, n = 4).

Name	Formula	Cytotoxicity EC <sub>50</sub> ± SEM [μM] non-transfected 1321N1 astrocytoma cells
5-FU		1.29 ± 0.62
PV1	Na <sub>6</sub> [H <sub>2</sub> W <sub>12</sub> O <sub>40</sub> ]	170 ± 35
PV2	H <sub>3</sub> [PW <sub>12</sub> O <sub>40</sub> ]	> 300
PV3	K <sub>7</sub> [Ti <sub>2</sub> W <sub>10</sub> PO <sub>40</sub> ]	> 50
PV4	K <sub>6</sub> [H <sub>2</sub> TiW <sub>11</sub> CoO <sub>40</sub> ]	125 ± 9
PV5	K <sub>10</sub> [Co <sub>4</sub> (H <sub>2</sub> O) <sub>2</sub> (PW <sub>9</sub> O <sub>34</sub> ) <sub>2</sub> ]	> 50
PV6	(NH <sub>4</sub> ) <sub>18</sub> [NaSb <sub>9</sub> W <sub>21</sub> O <sub>86</sub> ]	9.50 ± 0.64
P <sub>5</sub> W <sub>30</sub>	Na <sub>15</sub> [P <sub>5</sub> W <sub>30</sub> O <sub>110</sub> ]	0.283 ± 0.055
P <sub>6</sub> W <sub>18</sub>	Na <sub>20</sub> [P <sub>6</sub> W <sub>18</sub> O <sub>79</sub> ]	> 100
P <sub>8</sub> W <sub>48</sub>	Na <sub>33</sub> [H <sub>7</sub> P <sub>8</sub> W <sub>48</sub> O <sub>184</sub> ]	3.48 ± 0.56
PW <sub>12</sub>	Na <sub>3</sub> [PW <sub>12</sub> O <sub>40</sub> ]	> 100
OP <sub>8</sub> W <sub>12</sub>	Na <sub>16</sub> [(O <sub>3</sub> PCH <sub>2</sub> PO <sub>3</sub> ) <sub>4</sub> W <sub>12</sub> O <sub>36</sub> ]	> 200
CP <sub>8</sub> W <sub>12</sub>	Na <sub>16</sub> [(O <sub>3</sub> POPO <sub>3</sub> ) <sub>4</sub> W <sub>12</sub> O <sub>36</sub> ]	> 100
K-POM	K <sub>8</sub> [HP <sub>2</sub> W <sub>15</sub> V <sub>3</sub> O <sub>62</sub> ]	10.4 ± 1.4
(Bu <sub>4</sub> N) <sub>6</sub> -POM	(Bu <sub>4</sub> N) <sub>6</sub> [H <sub>3</sub> P <sub>2</sub> W <sub>15</sub> V <sub>3</sub> O <sub>62</sub> ]	6.46 ± 0.39
(Bu <sub>4</sub> N) <sub>6</sub> -PEG 1000	(Bu <sub>4</sub> N) <sub>6</sub> [H <sub>3</sub> P <sub>2</sub> W <sub>15</sub> V <sub>3</sub> O <sub>62</sub> ]-PEG 1000	5.79 ± 1.10
(Bu <sub>4</sub> N) <sub>6</sub> -PEG 2000	(Bu <sub>4</sub> N) <sub>6</sub> [H <sub>3</sub> P <sub>2</sub> W <sub>15</sub> V <sub>3</sub> O <sub>62</sub> ]-PEG 2000	6.42 ± 0.68
(Bu <sub>4</sub> N) <sub>6</sub> -PEG 5000	(Bu <sub>4</sub> N) <sub>6</sub> [H <sub>3</sub> P <sub>2</sub> W <sub>15</sub> V <sub>3</sub> O <sub>62</sub> ]-PEG 5000	n. d. <sup>a</sup>
KB1	K <sub>4</sub> [Re <sub>6</sub> S <sub>8</sub> (OH) <sub>6</sub> ]	> 100
KB2	K <sub>4</sub> [(Re <sub>6</sub> Se <sub>8</sub> )(OH) <sub>6</sub> ]	> 60
KB3	K <sub>4</sub> [Re <sub>6</sub> S <sub>8</sub> (CH <sub>3</sub> COO) <sub>6</sub> ]	> 70
KB4	K <sub>4</sub> [(Re <sub>6</sub> S <sub>8</sub> )(HCOO) <sub>6</sub> ]	> 70

<sup>a</sup>: n. d. not determined, due to lack of compound



**Figure 4.14:** Mean dose-response cytotoxicity curves of polyoxotungstates P<sub>5</sub>W<sub>30</sub>, P<sub>8</sub>W<sub>48</sub> and known cytotoxic agent 5-FU at non-transfected 1321N1 astrocytoma cells determined via MTT cell viability experiment (mean  $\pm$  SEM, n = 3-4).

#### 4.4 Discussion

POMs were identified previously as potent modulators of various targets. The antitumoral effect was of particular interest. Keggin and Dawson-derived polyoxotungstates and germanotungstates were identified as potent inhibitors of HDAC, a protein closely connected to cell cycle progression. The loss of functionality of these enzymes is associated with several cancers.<sup>243</sup> Furthermore, polyoxotungstates were found to generally inhibit the growth of rats infected with cancer cell lines including cervical HeLa, liver SSMC-7721, leukemia HL-60 and colon HLC cancer cells.<sup>244, 245</sup> The detailed mechanisms of cytotoxicity by POMs in these cancer cells were not described. Antitumoral activity in osteosarcoma cell lines was determined for copper-containing K<sub>7</sub>Na<sub>3</sub>[Cu<sub>4</sub>(H<sub>2</sub>O)<sub>2</sub>(PW<sub>9</sub>O<sub>34</sub>)<sub>2</sub>]20H<sub>2</sub>O. The cytotoxic effect was higher in tumorous than in normal cells, and was associated with an increase of reactive oxygen species, a decrease of the glutathione/glutathione disulfide (GSH/GSSG) ration and cell cycle arrest in the G2/M phase, which progressively lead to apoptosis.<sup>269</sup> Furthermore, three Keggin-shaped POMs containing cobalt and titanium were identified as cytotoxic agents in breast and kidney cancer cell lines. The binding to ctDNA and the penetration of the compound into the cell were named as contributing factors of antitumoral activity of POMs.<sup>270</sup> In all these cases, the cytotoxicity was determined by MTT cell viability assay. The respective values ranged from low to high micromolar concentrations and are comparable to the cytotoxic concentrations determined for POMs in this experimental setting. Only the most toxic POM P<sub>5</sub>W<sub>30</sub> showed higher toxicity. The

inhibitory activity at P2X1, P2X2 and P2X3 receptors of almost all compounds was proven to be 10-100fold higher than their cytotoxic activity.

POMs were previously identified to be potent inhibitors especially of ATP/ADP-degrading enzymes: rat ecto-5'-nucleotidases, human and rat NTPDase subtypes 1, 2, 3 and human NTPDase8, human NPP subtypes 1, 2 and 3 and human TNAP.<sup>221, 271</sup> These enzymes were found to play an important role in cancer growth and progression.<sup>272</sup> In 2011, Ramona Malek determined the inhibitory potency of polyoxotungstates and rhenium cluster compounds at purinergic P2Y receptor subtypes P2Y<sub>1</sub>, P2Y<sub>2</sub>, P2Y<sub>4</sub>, P2Y<sub>6</sub> and P2Y<sub>11</sub> receptor.<sup>266</sup>

PW<sub>12</sub> and PV2 showed little to no activity at the P2Y receptors tested; only at the human P2Y<sub>2</sub> receptor, an IC<sub>50</sub> value could be determined for PW<sub>12</sub>. At human NTPDases and NPPs, both compounds showed comparable activity to P2X receptors. Most polyoxotungstate compounds were as potent at human P2X receptor subtypes P2X1, P2X2 and rat P2X3 as determined at NPP1, with the exception of CP<sub>8</sub>W<sub>12</sub> and OP<sub>8</sub>W<sub>12</sub>. Both were more than 20 or 30-fold selective for NPP1 (K<sub>i</sub> 0.02 or 0.041 μM, respectively), and PV4 and PV5 displayed a tenfold preference for NPP1 (K<sub>i</sub> 0.00146 and 0.00498 μM). The potency of polyoxotungstates at all NTPDases was either comparable or lower than at P2X receptors. The only exception was PV5, which was around ten times more potent at NTPDase1 (K<sub>i</sub> 0.00388 ± 0.00140 μM) than at all P2X receptor subtypes. All compounds were only moderately active at the P2Y receptors, in most cases in the same range of potencies shown at P2X4 and P2X7 receptors.<sup>266, 271</sup> P<sub>5</sub>W<sub>30</sub> can only be assessed as an antagonist when used in concentrations below 0.2 μM due to its toxicity (see chapter 4.3.7). Since all IC<sub>50</sub> values of POMs determined for the P2Y receptors were either equal or higher than that, the observed decrease of calcium influx-induced fluorescence is more likely ascribed to toxicity than receptor inhibition, as was already discussed for P2X4 and P2X7 receptors. At NTPDases and NPPs, P<sub>5</sub>W<sub>30</sub> acted as a very potent inhibitor with K<sub>i</sub> values between 0.0218 (NTPDase2) and 0.0777 μM (NTPDase3), which was comparable to its activities at the P2X receptor subtypes P2X1 and P2X3.

All rhenium cluster compounds did not show any inhibitory potency at the P2Y receptors tested, with the exception of KB1 at the rat P2Y<sub>6</sub> receptor, for which an IC<sub>50</sub> value of 21.0 ± 10.9 μM was determined.<sup>266</sup> At the human NTPDase subtypes 1, 2 and 3, only KB4 was active. It was almost tenfold more potent at the latter two subtypes than at all P2X receptors (K<sub>i</sub> 0.680 ± 0.151 μM for NTPDase2 and 0.582 ± 0.050 μM for NTPDase3, respectively). All four rhenium cluster compounds were even more potent at the human nucleotide pyrophosphatase NPP1 with K<sub>i</sub> values between 0.100 and 0.537 μM.<sup>271</sup>

The PEGylated compounds and corresponding non-PEGylated forms K-POM and (Bu<sub>4</sub>N)<sub>6</sub>-POM were not tested previously, so no comparison of activity is possible. Since all compounds were proven to be exceedingly active at all P2X receptor subtypes except for P2X7, it would be of interest to test their inhibitory potency at NTPDases and NPPs as well. Further experiments are planned.

In conclusion, it can be said that POMs are potent inhibitors at P2X1, P2X2 and P2X3 receptors, and fairly selective towards P2X4 and P2X7. The potency of most compounds is comparable or lower than at most of the ATP- and ADP-degrading enzymes. The most notable exception was NPP1, at which several POMs showed around ten-fold higher potency than at P2X receptors. It could be demonstrated that high inhibitory potency is not limited to nucleotide-degrading enzymes, but can also be found at other nucleotide-binding receptors.

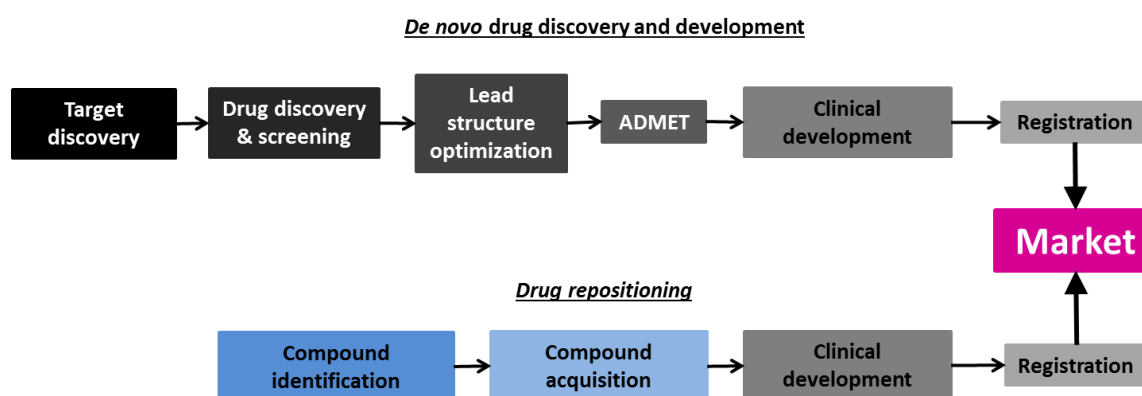
## 5 Interaction of approved drugs with P2X receptors

### 5.1 Introduction

The rediscovery of already approved drugs for new pharmacological targets and medical indications is referred to as drug repurposing, repositioning, reprofiling or redirecting.<sup>273</sup> It was proven to be a powerful and effective tool for the development of new cures for complicated and tricky diseases. The procedure is used especially by pharmaceutical companies to reduce the existing gap between the economical investments in research and development, including structure-based drug design, combinatorial chemistry, genomics and high-throughput screening, and the number of newly approved drugs.<sup>274</sup> There are several benefits to the repurpose approach:

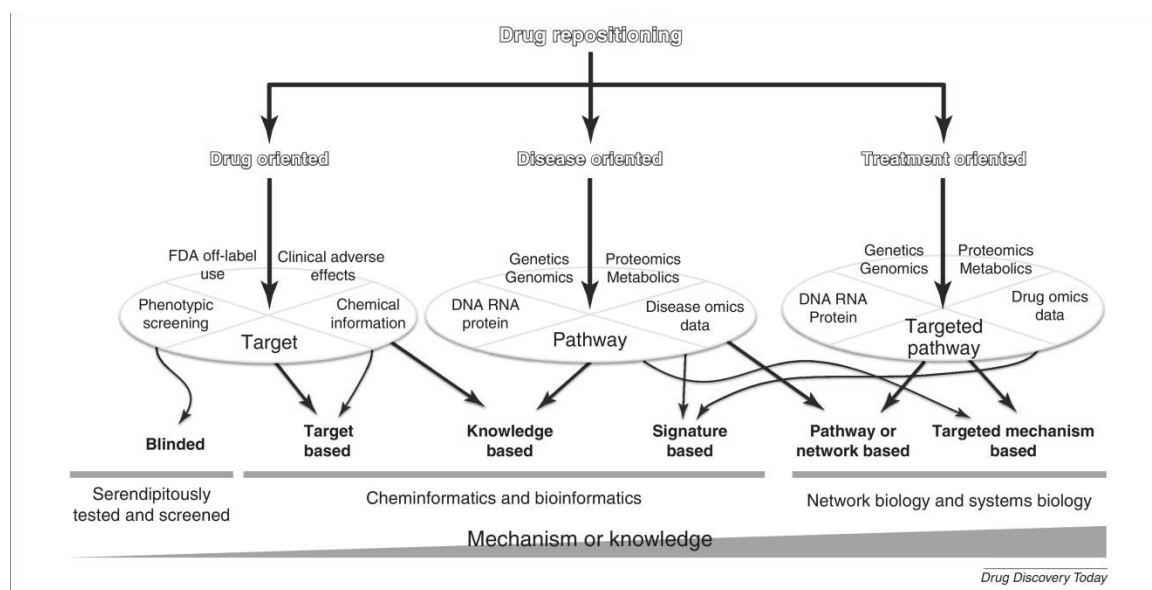
- 1) known pharmacological safety profiles and pharmacokinetics in humans
- 2) reduction of time between discovery and approval of the drug
- 3) cost effectiveness due to no longer required early drug development
- 4) easier attracted investments due to close proximity to market authorization.<sup>274, 275</sup>

One of the most important aspects for the rediscovery of known drugs is cost effectiveness, which can be attributed to a shortcut of several important steps during drug development. The initial years required for drug development are not needed. This advances the process directly to preclinical testing or even clinical trials, reducing the developmental process from 10 to 17 years to 3 to 12 years next to risk and cost reduction (see Figure 5.1).



**Figure 5.1:** Comparison of de novo drug discovery and drug repositioning (modified from Ashburn et al.)<sup>274</sup>

The successful repositioning of drugs needs careful considerations in order to enhance the probability of matching for various medical problems. The process can be facilitated considerably by application of computational methods e.g. biology, chemo- and bioinformatics in order to combine the information about known targets, drugs, disease biomarkers and pathways (see Figure 5.2). The starting point for a drug repositioning study can be a drug itself, a certain target or a specific disease. The method of choice depends on the starting point and the available information.



**Figure 5.2:** Flowchart demonstrating existing drug repositioning methods.<sup>276</sup>

In a target-based drug repositioning approach, the affinity and/or activity of drug library compounds at a known target structure like a protein (e.g. receptor or enzyme) or a biomarker is determined via actual screening (HTS) or virtual docking experiments. A successfully validated assay system or a good virtual target fit allows fast screening of large compound libraries. Depending on the selected method, valuable hits with minimal effort and low cost can be identified. A disadvantage is that high potency at the target structure may not automatically be relevant for disease pathogenesis. It may also not be sufficient enough to be applied as therapy. Since the target-based drug repositioning approach does not render much information about new mechanisms beyond the known target, a method using knowledge is much more useful for predicting e. g. unknown drug targets, drug-drug similarities, interactions or new disease biomarkers. Specific genetic signatures are further aspects considered in computational methods for drug repurposing. These signatures include any genetic altering responsible for

complicated metabolic or signaling pathways. The inclusion of genetic signatures enables the connection of different disease alterations and known protein interactions for better characterization of the mechanism of action of drugs.<sup>276-278</sup>

It is reported that out of the 75 first-in-class drugs approved between 1999 and 2008, containing 50 small molecules (67 %) and 25 biologics (33 %), 28 of the small molecule drugs were discovered by phenotypic drug screening and 17 by target-based methods. Both methods do not require pharmaceutical or biological information, and can easily be applied to a large number of drugs and diseases.<sup>279</sup> Phenotypic screening is the oldest and most important method applied for the search of new and rediscovering drugs. It often starts with clinical observations rendering a certain hitherto unknown pharmacological effect. The general alteration of an entire phenotype to a desired state and knowledge about the mechanistic insight of a specific drug are very useful tools in the discovery of first-in-class drugs for unknown disease patterns and orphan diseases.<sup>280-283</sup>

The use of large publically accessible drug libraries like the National Center for Advancing Translational Sciences (NCATS) or the Open Innovation Drug Discovery program (OIDD) at Lilly is a useful tool for strategical organization of drug repurposing.<sup>273, 283-286</sup> NCATS contains the largest public repository of approved drugs including those in clinical trials. Both allow access to large small molecule libraries directly applicable to *in vitro* screening assays for fast and effective determination of potency. A library of 600 compounds from NCATS was recently used in a study to identify potential drugs capable of inhibiting the entry of Ebola virus-like particles in HeLa cells. The screening identified 53 hits.<sup>287</sup> Another screening experiment of 2600 FDA-approved drugs to find anti-Ebola-active compounds rendered 80 Ebola inhibitors, with matching hits like selective estrogen receptor modulator toremifene, antihistamines bupropion and clemastine, tricyclic and tetracyclic antidepressants clomipramine and maprotiline and microtubule inhibitor vinorelbine.<sup>287, 288</sup>

Drug repurposing is preferably used for discovery of new agents for orphan, particularly dangerous and acute diseases lacking proper and effective drugs. Efforts to discover new cancer therapies are also exceptionally strong. For example, next to their capability of blocking Ebola virus entry into cells, tricyclic antidepressants like imipramine and promethazine were identified to be potent growth inhibitors of small cell lung cancer and other neuroendocrine tumors via inhibition of caspase 3, among other targets.<sup>289</sup> Ion channels proven to be involved in oncogenesis, like potassium and voltage-gated calcium channels, were recently the focus of a study investigating the anticancer effect of approved drugs on these targets.<sup>275</sup>

Another very prominent example of successful drug repurposing is sildenafil, a PDE-5 inhibitor. Originally designed as an antihypertensive drug, the blood pressure-lowering effect in early studies was proven to be only moderate. Simultaneously, the positive effect on penile erectile dysfunction due to the involvement of PDE-5 in the incurrence of an erection was discovered, and clinical studies with a new outcome were designed, leading to the approval of sildenafil (Viagra®) as the first orally available drug to treat penile erectile dysfunction in 1998 by Pfizer Inc., New York, NY, USA. Since then, due to the strong and selective inhibition of PDE-5, sildenafil has been approved for the treatment of pulmonary hypertension (Revatio®) by the FDA.<sup>290</sup> The drug is not recommended for children in this indication.<sup>291</sup>

Another very prominent example for successful drug repositioning is thalidomide. It was originally approved as a sedative in 1957 under the tradename Contergan® by German company Grünenthal, with recommended use particularly for pregnant women.<sup>292</sup> This indication was based on the lack of toxicity in rodents when used in high doses.<sup>293</sup> The discovery of the direct association between the intake of thalidomide during early pregnancy and infantile congenital abnormalities led to the retraction of the drug from the market and to a complete change of procedure of therapeutic drug approval.<sup>294, 295</sup> However, in the past years, thalidomide was rediscovered as an active and potent agent against multiple myeloma in combination with dexamethasone<sup>296</sup> and against erythema nodosum leprosum. The latter was already discovered in 1965.<sup>297</sup> In Germany it has been available since 2009 only by submission of the so-called T-prescription. It is part of the T register, which supervises the prescription and emission of thalidomide and its derivatives lenalidomide and pomalidomide.<sup>298, 299</sup> Both derivatives are also approved for the treatment of multiple myeloma. The strict control of prescription serves the prevention of deformities in newborn children. Strict safety measures were demanded from all EU member states by the European Commission.

Since the rediscovering of approved drugs for new indications, diseases and targets can be a successful strategy, we tested a small library of 440 drugs for inhibitory potency at purinergic P2X receptors. The aim of this study was the discovery of new potent and selective ligands for various P2X subtypes. The library was screened at each receptor subtype expressed in 1321N1 astrocytoma cells in a final concentration of 20 µM via measurement of calcium influx. Subsequently, concentration-response curves were generated for active compounds. The results are discussed in the following chapter.



## 5.2 Determination of Z'-factor

As already discussed in the previous chapter, the Z'-factor was calculated for every experiment and each receptor subtype. The Z'-factor is described as a suitable statistical parameter to assess assay quality. When it was not possible to use the standard antagonist as negative control due to space conflict, the buffer data was taken instead. The results are presented in Table 5.1.

**Table 5.1:** Z'-factors of all experiments conducted for testing the inhibitory potency of approved drugs and structurally related derivatives at P2X receptors. Data is presented as mean  $\pm$  SEM.

	<b>P2X1</b> (n = 52)	<b>P2X2</b> (n = 35)	<b>P2X3</b> (n = 100)	<b>P2X4</b> (n = 7)	<b>P2X7</b> (n = 100)
<b>Z'-factor <math>\pm</math> SEM</b>	<b>0.58 <math>\pm</math> 0.06</b>	<b>0.77 <math>\pm</math> 0.03</b>	<b>0.61 <math>\pm</math> 0.06</b>	<b>0.63 <math>\pm</math> 0.07</b>	<b>0.53 <math>\pm</math> 0.02</b>

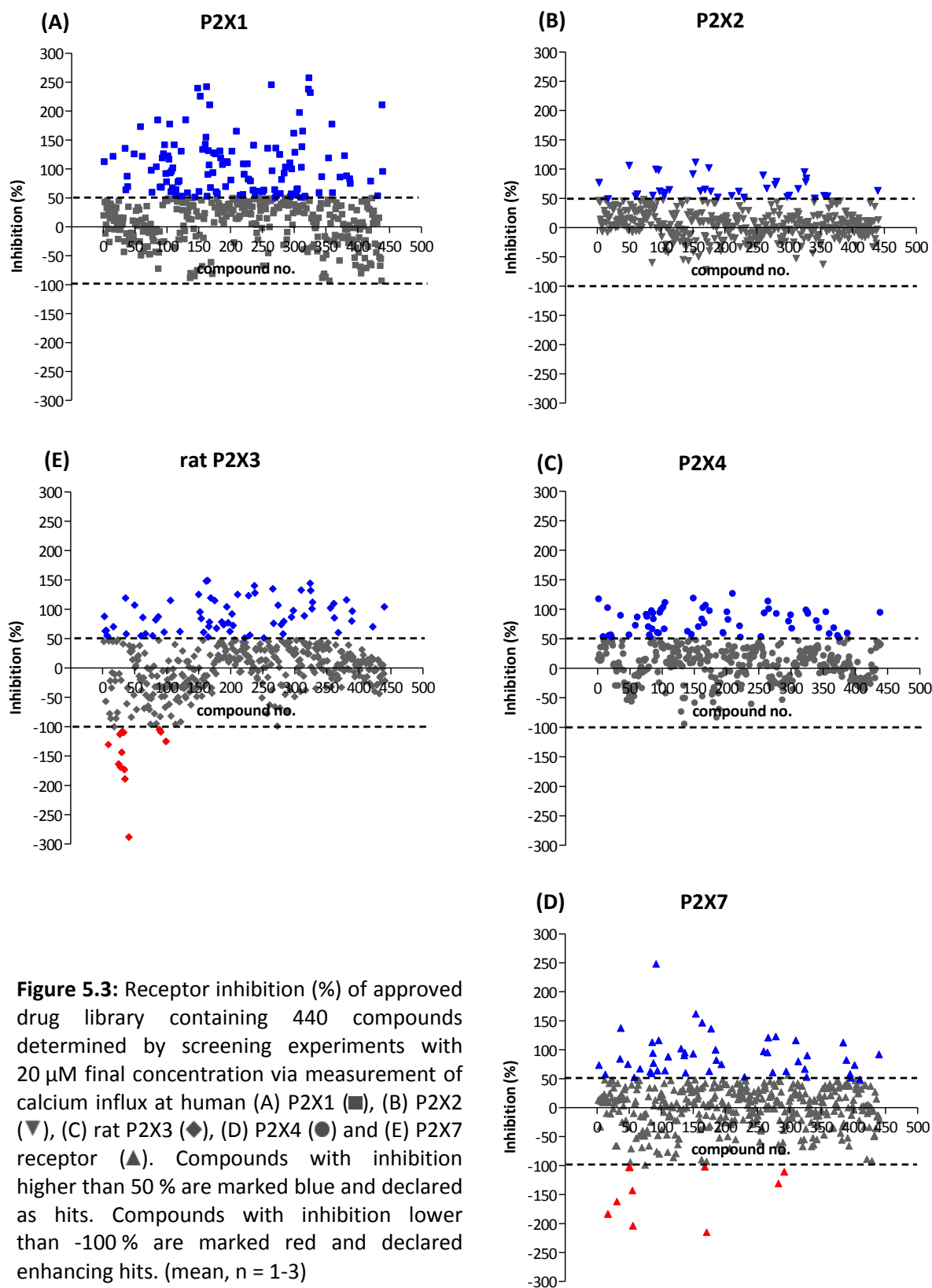
When the Z'-factor is higher than 0.5, the assay is considered as suitable for high-throughput screening. Since all Z'-factors determined were higher than 0.5, the experiments are suitable for high-throughput screening and the determined results can be considered as valid.

## 5.3 Inhibitory potency of approved drugs at P2X receptors

### 5.3.1 Screening

A library of 440 already approved drugs was tested at the human P2X receptor subtypes P2X1, P2X2, P2X7 and the rat P2X3 in order to identify new lead structures for the synthesis of selective agonists and antagonists. Dr. Aliaa Abdelrahman and Stefanie Weyer generated the data at the human P2X4 receptor using the same experimental setup. The results are presented in Figure 5.3.

All compounds were screened once at a final concentration of 20  $\mu$ M. It was planned to further investigate all drugs showing an inhibition of the respective receptor higher than 50 %. Since a lot of compounds exceeded this limit, especially at the P2X1 and the P2X3 receptor, it was decided to test those hits at the receptors P2X1, P2X3 and P2X7 once again at lower final concentration of 1  $\mu$ M. When the detected inhibition was again higher than 50 %, dose-response experiments were conducted. Only a small amount of drugs were identified to inhibit the P2X2 receptor by more than 50 % at 20  $\mu$ M final concentration. All hits were tested in concentration-response experiments. The potency and importance of the detected hits are discussed in detail in the following chapters, categorized in different subgroups based on their structure, with special focus on the human P2X1, P2X7 and the rat P2X3 receptor.



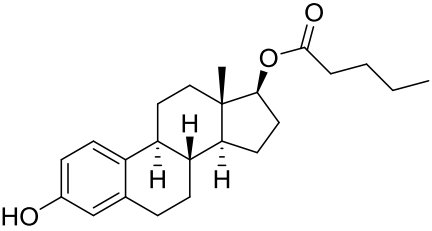
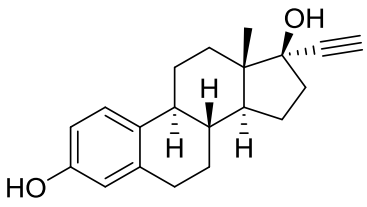
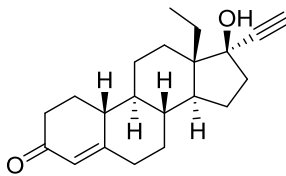
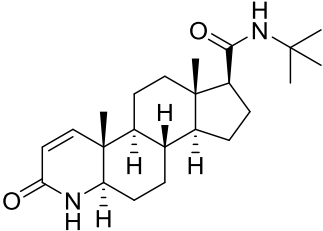
### 5.3.1.1 Steroids

Several compounds bearing a steroidal basic structure were among the hits detected in the initial screenings. The results of the subsequently determined concentration-response experiments are presented in Table 5.2.

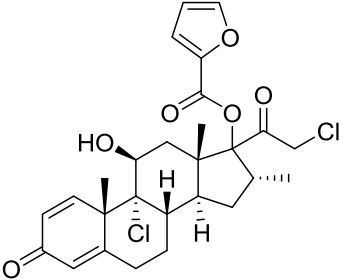
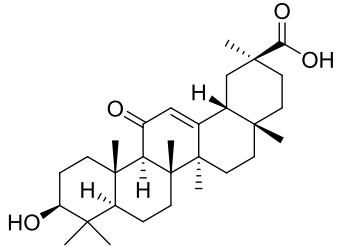
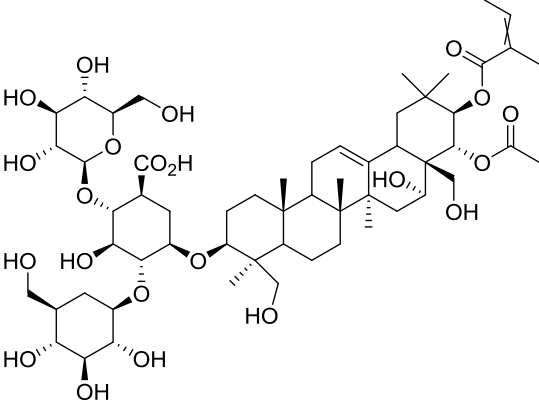
Next to female sexual hormones like estrogen derivatives estradiol valerate and ethinyl estradiol, the 4-azasteroid finasteride, the 19-nortestosteron-derived norgestrel, the class III glucocorticoid mometasone furoate and natural steroids including glycosides digitonin, lanatoside C, saponine  $\beta$ -escin and pentacyclic triterpene  $18\beta$ -glycyrrhetic acid were able to diminish calcium influx in P2X receptor-transfected cells.

Estradiol is the primary female sex hormone belonging to the estrogens. It plays an important role in reaching sexual maturity and the induction of the female cycle proliferation phase. Signal transduction follows a translocation of the hormone receptor into the nucleus, where the transcription of respective genes is regulated upon binding of the hormone-receptor-complex to DNA segments. The initially detected inhibitory potency could not be confirmed for all compounds. Estradiol valerate was identified as a potential antagonist at the P2X1 receptor. However, it did not show any dose-response relation at this P2X receptor subtype. Ethinyl estradiol, the metabolically stable  $17\alpha$ -ethinyl-derivative of estradiol, was found to be capable of inhibiting the P2X2 receptor at micromolar concentrations. High inhibitory potency was also detected at the P2X1 receptor at  $20\ \mu\text{M}$ , but since this could not be observed any longer upon reduction of the concentration to  $1\ \mu\text{M}$ , no concentration-response experiments were conducted. As estradiol valerate did not show any dose-response relation at this receptor, it was to be expected that the inhibitory potency of ethinyl estradiol at P2X1 receptors would be comparable to the one detected for the P2X2 receptor or weaker.

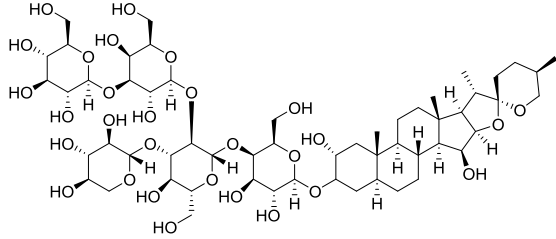
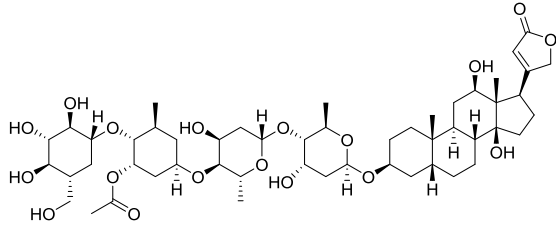
**Table 5.2:** Inhibitory potency of steroids and steroid-derived drugs at P2X receptors (mean  $\pm$  SEM, n = 3-4).

Compound	Structure	IC <sub>50</sub> $\pm$ SEM [ $\mu$ M] or inhibition at 20 $\mu$ M or 1 $\mu$ M (%)				
		P2X1	P2X2	P2X3	P2X4	P2X7
Estradiol valerate		> 100 (n. c.) <sup>a</sup>	> 20 (1 %)	> 20 (-1 %)	> 1 (12 %)	> 20 (-76 %)
Ethinyl estradiol		> 1 (-36 %)	15.0 $\pm$ 3.0	> 20 (41 %)	> 1 (2 %)	> 20 (-10 %)
Norgestrel		> 1 (-12 %)	> 100 (n. c.) <sup>a</sup>	> 1 (-28 %)	> 20 (17 %)	> 20 (-36 %)
Finasteride		> 100 (n. c.) <sup>a</sup>	> 20 (-18 %)	> 20 (-32 %)	> 20 (17 %)	> 20 (-78 %)

Continuation of Table 5.2

<b>Mometasone furoate</b>		> 1 (8 %)	<b>7.16 ± 1.37</b> remaining receptor activity 30 %	> 1 (-48 %)	> 1 (-11 %)	<b>1.27 ± 0.41</b>
<b>18β-Glycyrrhetic acid</b>		> 1 (4 %)	<b>10.2 ± 0.1</b> Remaining receptor activity 40 %	> 1 (24 %)	> 1 (-21 %)	> 1 (13 %)
<b>β-Escin</b>		> 100 (n. c.) <sup>a</sup>	<b>0.700 ± 0.176</b> Remaining receptor activity 26 %	> 1 (29 %)	<b>0.643 ± 0.094</b>	> 1 (37 %)

Continuation of Table 5.2

<b>Digitonine</b>		<b>0.133 ± 0.005</b> Remaining receptor activity 23 %	<b>0.380 ± 0.021</b> Remaining receptor activity 54 %	<b>0.483 ± 0.092</b>	<b>0.540 ± 0.013</b>	> 1 (-34 %)
<b>Lanatoside C</b>		<b>0.355 ± 0.109</b> Remaining receptor activity 43 %	> 20 (24 %)	<b>0.282 ± 0.139</b>	> 20 (20 %)	> 20 (21 %)

<sup>a</sup>: n. c. no convergence of sigmoidal dose-response analysis in three independent experiments

Finasteride is a 5 $\alpha$ -reductase inhibitor which blocks the conversion of testosterone to dihydrotestosterone and is approved for the treatment of benign prostatic hypertrophy and androgenetic alopecia. It was active at the P2X1 receptor, but like for estradiol valerate, no IC<sub>50</sub> value could be determined. The same was observed for norgestrel, whose (S)-enantiomer is used in the morning after pill and the so-called mini pill, at the P2X2 receptor. It could be assumed that sexual hormones and closely related derivatives are capable of inhibiting P2X1 and P2X2 receptors at high concentrations. However, for other derivatives (5 $\alpha$ -androstan-17 $\beta$ -ol-3-one, medroxyprogesterone acetate, testosterone, methyltestosterone, norethindrone acetate and estradiol), which are closely related to the detected hits, no such observation could be made. Since a successful dose-response relationship could only be detected for ethinyl estradiol at the P2X2 receptor, it is possible that the observed reduction of calcium influx by the other hits was not related to P2X receptor inhibition, but other effects due to poor solubility or cell toxicity.

Closely related glycosylated steroids digitonin, lanatoside C and  $\beta$ -escin were also capable of inhibiting P2X receptors at both concentrations tested, respectively. The detected IC<sub>50</sub> values for digitonin at the P2X1, P2X4 and P2X3 receptor were comparable in the high nanomolar range. The same was observed for lanatoside C at P2X1 and P2X3. Both drugs are cardiac glycosides, lanatoside C of the group of cardenolides, a steroid associated to a five-membered unsaturated lactone ring, and digitonin, a triterpene saponine detergent from foxglove. Although the two compounds appeared to be potent antagonists of P2X receptors, there were doubts whether the observed reduced calcium influx was due to a receptor inhibition. High basic fluorescence values were detected for digitonin during the assay validation previous to ATP injection. This indicates either strong autofluorescence of the compound or cytotoxic effects. Since both compounds were described as being cytotoxic before, with IC<sub>50</sub> values comparable to the ones determined in these experiments, it is more likely that the supposed inhibitory potency detected via measurement of calcium influx was caused by cytotoxicity.<sup>300</sup>

18 $\beta$ -Glycyrrhetic acid is a triterpenoid derivative of the  $\beta$ -amyrin type and one of the main ingredients of liquorice. It is used in traditional Chinese medicine and as a herbal remedy against respiratory diseases. Furthermore, 18 $\beta$ -glycyrrhetic acid was identified to have anti-mycobacterial, anti-rotaviral and anti-inflammatory effects against *Mycobacterium bovis* infections and rheumatoid arthritis, respectively.<sup>301-303</sup> The compound was capable of inhibiting the P2X2 receptor subtype with an IC<sub>50</sub> value of 10.2  $\pm$  0.1  $\mu$ M. At 20  $\mu$ M, the compound also showed affinity to the remaining P2X receptor subtypes tested. Since no subtype was blocked more than 50 % in the second screening at 1  $\mu$ M final concentration, no concentration-response

experiments were conducted. Due to the decrease of inhibitory potency, the IC<sub>50</sub> values at the remaining receptors were estimated between 20 μM and 1 μM.

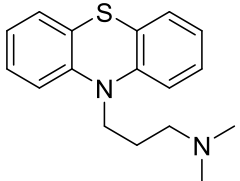
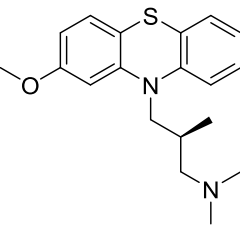
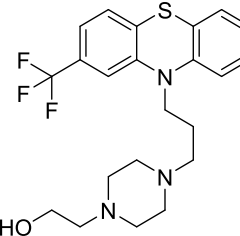
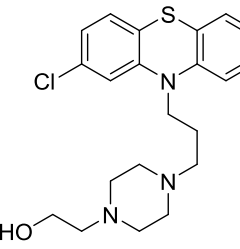
Despite the primarily observed activity of several steroid-based drugs, the suitability of steroids as potential lead structures for new P2X receptor ligands does not appear to be promising. The glucocorticoid compounds are approved for their immunosuppressive and anti-inflammatory properties. Only mometasone furoate, a class III glucocorticoid agent, was identified as a hit at the P2X2 and P2X7 receptor. The subsequent dose-response experiments yielded IC<sub>50</sub> values in the low micromolar range ( $7.16 \pm 1.37 \mu\text{M}$  and  $1.27 \pm 0.41 \mu\text{M}$ , respectively). Since none of the other corticosteroids showed any inhibitory activity at any P2X receptor subtype, the steroid moiety did not seem to be a suitable starting point for the development of new P2X receptor ligands.

### **5.3.1.2 Tricyclic antidepressants and phenothiazines**

Several tricyclic compounds including phenothiazine derivatives were identified as potential ligands especially at the human P2X2 and P2X4 receptor. Phenothiazines are one of the oldest classes of antipsychotic drugs whose basic structure was not obtained from natural products.<sup>304</sup> Furthermore, they also have antimicrobial and antihelminthic properties.<sup>305</sup> Their antipsychotic effects can mainly be attributed to their affinity for dopamine receptors, but phenothiazines are also known to bind to a variety of other targets, e.g. histamine, muscarinic, adrenergic, serotonergic and cholinergic receptors. This widespread binding behavior is regarded as the reason for their broad efficacy for different medical indications. The phenothiazine derivatives prochlorperazine and trifluoperazine were previously identified to be potent modulators of P2X7 receptor.<sup>193</sup> Both compounds were not part of the compound library used in the present experiments. However, the related piperazine-containing derivatives fluphenazine and perphenazine were found to have affinity to all P2X receptors tested when used in high concentrations (see Table 5.3). The results are summarized in Table 5.3. An IC<sub>50</sub> value of  $7.84 \pm 2.32 \mu\text{M}$  was determined at the P2X4 receptor for fluphenazine. Perphenazine was initially active at P2X1, P2X4 and P2X3 receptors at 20 μM. The subsequently measured IC<sub>50</sub> value at the P2X4 receptor was in the same range as the one for fluphenazine ( $5.88 \pm 1.43 \mu\text{M}$ ). Levomepromazine and promazine were also identified as hits with inhibitory potency at the P2X2 receptor. The respective IC<sub>50</sub> values were comparable to those of phenothiazines at the P2X4 receptor ( $5.63 \pm 2.19$  and  $4.61 \pm 1.70 \mu\text{M}$ , respectively).

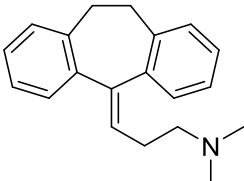
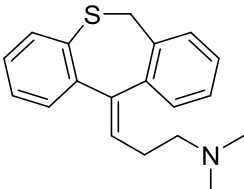


**Table 5.3:** Inhibitory potency of phenothiazine drugs at P2X receptors (mean  $\pm$  SEM, n = 3-4).

Compound	Structure	IC <sub>50</sub> $\pm$ SEM [ $\mu$ M] or inhibition at 20 $\mu$ M or 1 $\mu$ M (%)				
		P2X1	P2X2	P2X3	P2X4	P2X7
Promazine-HCl		> 1 (18 %)	<b>4.61 <math>\pm</math> 1.70</b> Remaining receptor activity 37 %	> 1 (49 %)	<b>5.91 <math>\pm</math> 1.74</b> Remaining receptor activity 26 %	> 20 (27 %)
Levomepromazine-HCl		> 1 (29 %)	<b>5.63 <math>\pm</math> 2.19</b> remaining receptor activity 36 %	> 20 (33 %)	<b>3.77 <math>\pm</math> 0.32</b> Remaining receptor activity 26 %	> 20 (1 %)
Fluphenazine		> 1 (-21 %)	> 1 (19 %)	> 1 (-26 %)	<b>7.84 <math>\pm</math> 2.32</b>	> 1 (9 %)
Perphenazine		> 1 (-10 %)	> 20 (10 %)	> 1 (-44 %)	<b>5.88 <math>\pm</math> 1.43</b>	> 20 (-49 %)

Some of the structurally related tricyclic antidepressants (TCA), amitriptyline and dosulepin, were also identified as P2X receptor antagonists (see Table 5.4). Same as phenothiazines and other antipsychotics, tricyclic antidepressants also show inhibitory potency at a broad variety of targets, including  $\alpha$ -adrenergic and muscarinic acetylcholine receptors. Both TCA were identified as antagonists at the P2X2 receptor with IC<sub>50</sub> values comparable to levomepromazine and promazine. Amitriptyline additionally inhibited the P2X1 receptor in the same concentration range, and was slightly more potent at the P2X4 receptor. The results at the P2X4 receptor are in contrast to previously published data, where amitriptyline was found to have no effect on P2X4.<sup>136</sup> The inhibitory potency of dosulepin at P2X4 receptors was in the low micromolar range, as was determined for levomepromazine, fluphenazine and perphenazine. The results indicate that purinergic ion channels, particularly P2X2 and P2X4, also belong to the broad target spectrum of tricyclic CNS-drugs.

**Table 5.4:** Inhibitory potency of tricyclic antidepressants at P2X receptors (mean  $\pm$  SEM, n = 3-4).

Compound	Structure	IC <sub>50</sub> $\pm$ SEM [ $\mu$ M] or inhibition at 20 $\mu$ M or 1 $\mu$ M (%)				
		P2X1	P2X2	P2X3	P2X4	P2X7
Amitriptyline		17.8 $\pm$ 6.6	30.8 $\pm$ 7.9	> 20 (1 %)	6.87 $\pm$ 1.41	> 20 (-5 %)
Dosulepin		> 1 (-53 %)	11.3 $\pm$ 1.0	> 20 (-66 %)	7.21 $\pm$ 0.70	> 20 (19 %)

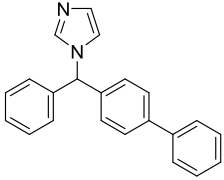
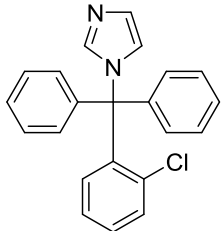
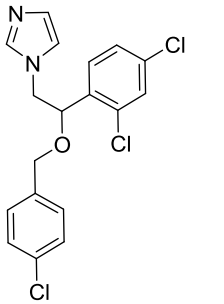
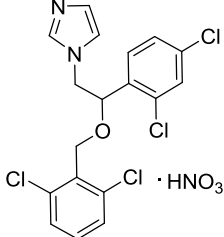
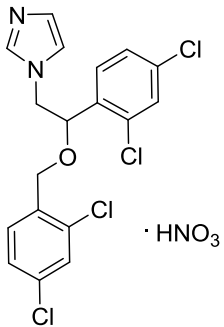
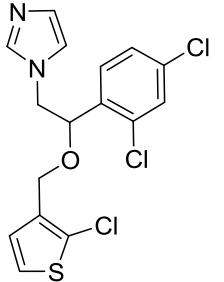
### 5.3.1.3 Imidazole-containing antifungal drugs

Imidazole-based antifungal drugs are broad spectrum fungistatic agents. The antifungal effect is achieved by their binding to the heme iron cation of 14- $\alpha$ -demethylase and thereby preventing the conversion of lanosterol to ergosterol. This causes a lack of ergosterol, which is equivalent to cholesterol in fungal membranes, and inhibits the fungal growth due to membrane instability. The essential structure for this mechanism is the imidazole function of the compounds.

During the initial screening, several of the imidazole antifungals diminished the calcium influx in P2X receptor-transfected 1321N1 astrocytoma cells. The results and respective IC<sub>50</sub> values are summarized in Table 5.5. Inhibitory activity could be detected especially at the P2X1 and the P2X3 receptor, respectively, with comparable IC<sub>50</sub> values in the low micromolar range between 2.05 and 3.00  $\mu$ M. The same was seen for econazole at P2X1 and P2X4 receptors. None of the compounds were active at a final concentration of 1  $\mu$ M at P2X2 and P2X7 receptors, so no dose-response experiments were conducted. All hits led to full inhibition, no remaining receptor activity could be detected. Not all of the imidazole drugs in the library showed affinity for P2X receptors. Ketoconazole, oxiconazole and sertaconazole did not show a decrease in ATP-induced calcium influx. An elongation of the side chain next to the imidazole ring therefore had no positive effect on the affinity towards P2X receptors.

Of the triazole antifungals, only fluconazole was available for testing. No activity at any P2X receptor subtype could be detected.

**Table 5.5:** Inhibitory potency of imidazole antifungal drugs at P2X receptors (mean  $\pm$  SEM, n = 3-4).

Compound	Structure	IC <sub>50</sub> $\pm$ SEM [ $\mu$ M] or inhibition at 20 $\mu$ M or 1 $\mu$ M (%)				
		P2X1	P2X2	P2X3	P2X4	P2X7
Bifonazole		> 1 (-9 %)	> 20 (27 %)	<b>2.78</b> $\pm$ 1.21	> 20 (47 %)	> 1 (9 %)
Clotrimazole		<b>2.09</b> $\pm$ 0.04	> 20 (-19 %)	<b>2.09</b> $\pm$ 0.99	> 20 (40 %)	> 1 (-8 %)
Econazole		<b>3.00</b> $\pm$ 1.21	> 1 (9 %)	> 1 (32 %)	<b>7.60</b> $\pm$ 1.77	> 1 (-8 %)
Isoconazole nitrate		<b>1.65</b> $\pm$ 0.55	> 1 (10 %)	> 1 (7 %)	<b>6.10</b> $\pm$ 1.62	> 20 (25 %)
Miconazole nitrate		> 1 (3 %)	> 1 (15 %)	> 1 (-7 %)	<b>6.36</b> $\pm$ 1.69	> 1 (-42 %)
Tioconazole		> 1 (-7 %)	> 1 (15 %)	<b>4.32</b> $\pm$ 1.01	<b>3.12</b> $\pm$ 0.51	> 1 (19 %)

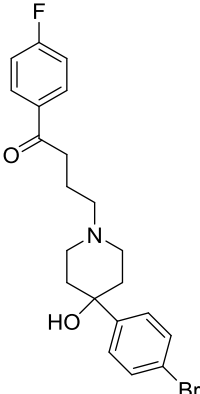
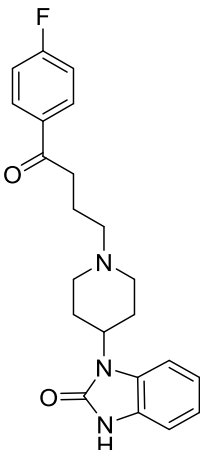
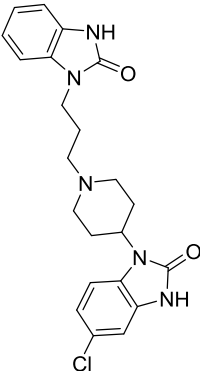
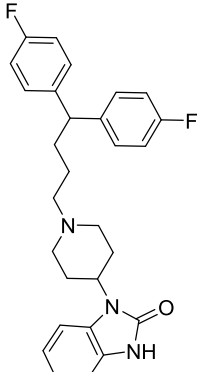
### 5.3.1.4 *Butyrophenones*

Butyrophenone-based drugs also play an important role in the treatment of schizophrenia next to phenothiazines. Their antipsychotic activity was identified after structural modification of phenylpiperidine-based analgesics with a butyrophenone core structure. Haloperidol is the most commonly used butyrophenone antipsychotic in Germany, with high affinity for the dopamine receptor subtype D<sub>2</sub>, next to D<sub>1</sub>, D<sub>3</sub>, D<sub>4</sub> and the  $\alpha$ -adrenergic receptor.<sup>306</sup> Dopamine receptor subtypes D<sub>2</sub>, D<sub>3</sub> and D<sub>4</sub> are members of the so-called D<sub>2</sub>-like family. All members are GPCR coupled to G<sub>i/o</sub>, which inhibits the adenylyl cyclase and reduces the intracellular cAMP concentration upon activation. This leads to opening of potassium channels, stabilizing the resting potential and reducing the excitability of the cell. The antipsychotic effect though cannot be attributed to the drug's affinity at one specific receptor subtype. In fact, the inhibitory potency at various targets like 5-HT, acetylcholine, norepinephrine or histamine receptors was demonstrated to promote the antipsychotic efficacy of a drug against positive and negative symptoms of schizophrenia. The D<sub>2</sub> and 5-HT<sub>3</sub> receptor subtypes are also prominent in the area postrema, a circumventricular organ in the brain that represents the chemoreceptor trigger zone for emesis. Inhibition of the D<sub>2</sub> receptor is associated with relief of nausea and emesis.

Haloperidol was part of the drug library tested, but did not show any inhibitory activity at any P2X receptor subtype in the initial screening at 20  $\mu$ M final concentration. The same was observed for azaperone, a pyridinylpiperazine derivative of haloperidol and mainly used as a sedative in veterinary medicine.

The closely related derivative bromperidol was identified as a hit with low micromolar IC<sub>50</sub> value (3.46  $\pm$  0.33  $\mu$ M) at the P2X1 receptor. It showed no activity any of the other subtypes tested (see Table 5.6). The structurally related benzimidazolone containing derivatives pimozone and the antiemetics domperidone and droperidol were all identified as hits at the P2X2 receptor, but had no longer any inhibitory potency at the P2X1 receptor when tested at 1  $\mu$ M. At P2X4, only pimozone was active, with potency comparable to the results at the P2X2 subtype.

**Table 5.6:** Inhibitory potency of butyrophenone-derived drugs at P2X receptors (mean  $\pm$  SEM, n = 3-4).

Compound	Structure	IC <sub>50</sub> $\pm$ SEM [ $\mu$ M] or inhibition at 20 $\mu$ M 1 $\mu$ M (%)				
		P2X1	P2X2	P2X3	P2X4	P2X7
<b>Bromperidol</b>		<b>3.46 <math>\pm</math> 0.33</b>	> 20 (15 %)	> 20 (-33 %)	> 20 (46 %)	> 20 (15 %)
<b>Droperidol</b>		> 1 (-15 %)	<b>104 <math>\pm</math> 60</b>	> 20 (-28 %)	> 20 (4 %)	> 20 (43 %)
<b>Domperidone</b>		> 1 (-10 %)	<b>14.4 <math>\pm</math> 3.0</b>	> 1 (-31 %)	> 20 (38 %)	> 1 (-11 %)
<b>Pimozide</b>		> 1 (24 %)	<b>3.57 <math>\pm</math> 1.45</b> Remaining receptor activity 27 %	> 1 (-48 %)	<b>2.10 <math>\pm</math> 0.30</b>	> 20 (-34 %)

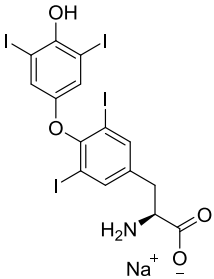
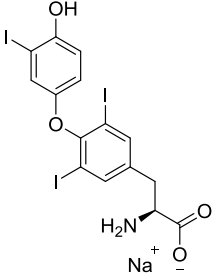
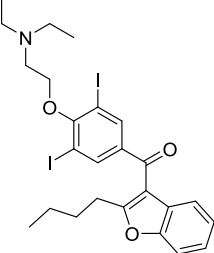
### 5.3.1.5 *Thyroid hormones and related drugs*

Levothyroxine and liothyronine are two homologous iodinated thyronine hormones produced in the thyroid gland which are indispensable for normal metabolism, growth and development.<sup>307</sup>

Both are synthesized starting from L-tyrosine, which is posttranslationally modified after stimulation by thyrotropin, the thyroid regulating hormone secreted from the anterior pituitary gland. Therapeutically, both are indicated for substitution in case of hypothyroidism. Both compounds are distinguished structurally by the number of iodine bound to the thyronine core, which is reflected in the abbreviated term T3 (liothyronine, L-3,5,3'-triiodothyronine) and T4 (levothyroxine, L-3,5,3',5'-tetraiodothyronine). While levothyroxine was identified as an antagonist of P2X1 and P2X3 receptor with IC<sub>50</sub> values in the low micromolar range (see Table 5.7), liothyronine reduced the activity of P2X2 receptors with slightly lesser potency (15.0 ± 1.9 μM). No or weaker inhibitory activity was detected at the other subtypes. Liothyronine appeared to be selective for the P2X2 receptor, but inhibition was seen only when the drug was used in concentrations way above those used normally in a therapeutic context.

Amiodarone is an antiarrhythmic drug with high affinity to potassium ion channels. Due to structural similarity and molecular interference when used in combination with thyroid hormones, it was included into the discussion of inhibitory potency of thyroid hormones at P2X receptors.<sup>308</sup> It blocks the potassium outflow in phase III of the action potential in cardiomyocytes by inhibiting potassium ion channels and selectively prolongs their refractory period and reduces cardiac arrhythmia.<sup>309</sup> The initial screening showed inhibition higher than 50 % of all P2X receptor subtypes except the P2X7 subtype. Concentration-response experiments were conducted at P2X2 and P2X4 receptors, demonstrating IC<sub>50</sub> values in the low micromolar range (10.2 ± 0.5 μM and 4.01 ± 1.02 μM, respectively). The affinity at the P2X2 receptor is comparable to liothyronine. At P2X7 receptors, it was initially demonstrated to be a potential enhancer of ATP potency, which is further discussed in chapter 5.4.3.

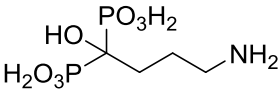
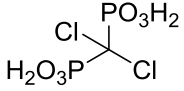
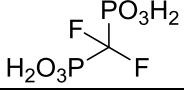
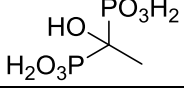
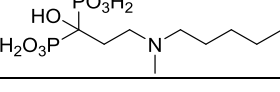

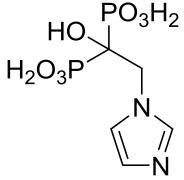
**Table 5.7:** Inhibitory potency of thyroid hormones at P2X receptors (mean  $\pm$  SEM, n = 3-4).

Compound	Structure	IC <sub>50</sub> $\pm$ SEM [ $\mu$ M] or inhibition at 20 $\mu$ M or 1 $\mu$ M (%)				
		P2X1	P2X2	P2X3	P2X4	P2X7
<b>Levo-thyroxine-Na</b>		5.30 $\pm$ 4.08 Remaining receptor activity 11 %	> 20 (46 %)	3.52 $\pm$ 0.44	> 20 (38 %)	> 20 (-10 %)
<b>Liothyronine-Na</b>		> 1 (-55 %)	15.0 $\pm$ 1.9	> 1 (10 %)	> 20 (21 %)	> 20 (34 %)
<b>Amiodarone</b>		> 1 (-29 %)	10.2 $\pm$ 0.5 Remaining receptor activity 23 %	> 1 (7 %)	4.01 $\pm$ 1.02	> 20 (-39 %)

### 5.3.1.6 Bisphosphonates

Since polyoxometalates have been identified as potent inhibitors of all P2X receptors (see chapter 4.3), similar negatively charged drugs were of peculiar interest. Bisphosphonates are small negatively charged inorganic diphosphate analogues approved for the treatment of osteoporosis. Bisphosphonates accumulate in the bone, which is attributed to their high affinity to hydroxyapatite. They inhibit the activity of osteoclasts, which leads to a reduction of bone resorption. None of the compounds tested showed any inhibitory activity at P2X receptors (see Table 5.8). Since the molecular weight is much lower in comparison to POMs, it is possible that the compounds are too small for potent inhibition.

**Table 5.8:** Inhibitory potency of bisphosphonate derivatives at P2X receptors (mean  $\pm$  SEM, n = 3-4).

Compound	Structure	Inhibition $\pm$ SEM at 10 $\mu$ M (%)				
		P2X1	P2X2	P2X3	P2X4	P2X7
<b>Alendronate</b>		> 10 (2 %)	> 10 (1 %)	> 10 (-3 %)	> 10 (14 %)	> 10 (-9 %)
<b>Clodronate</b>		> 10 (13 %)	> 10 (1 %)	> 10 (10 %)	> 10 (10 %)	> 10 (7 %)
<b>Difluoromethylene-diphosphonate</b>		> 10 (-3 %)	> 10 (-2 %)	> 10 (16 %)	> 10 (11 %)	> 10 (2 %)
<b>Etidronate</b>		> 10 (15 %)	> 10 (-8 %)	> 10 (-9 %)	> 10 (27 %)	> 10 (4 %)
<b>Ibadronate</b>		> 10 (1 %)	> 10 (1 %)	> 10 (-12 %)	> 10 (20 %)	> 10 (6 %)
<b>Methylene-diphosphonate</b>		> 10 (1 %)	> 10 (-1 %)	> 10 (7 %)	> 10 (10 %)	> 10 (-14 %)
<b>Zoledronate</b>		> 10 (-2 %)	> 10 (2 %)	> 10 (-6 %)	> 10 (16 %)	> 10 (-20 %)

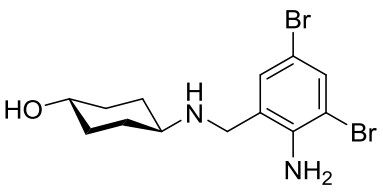
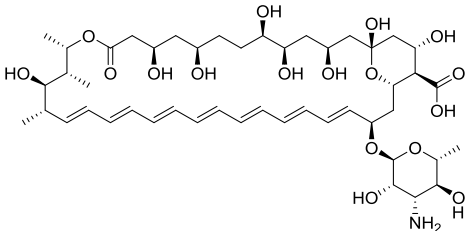
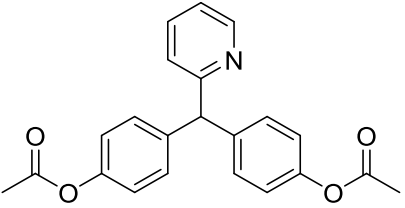
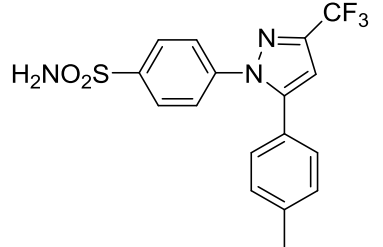
### 5.3.1.7 Various screening hits without structural relation

Not all detected hits could be subdivided into groups with similar structural properties. All compounds with inhibitory potency that were singletons are summarized in Table 5.9.

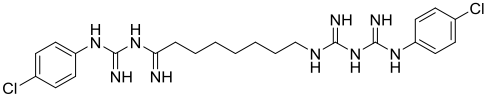
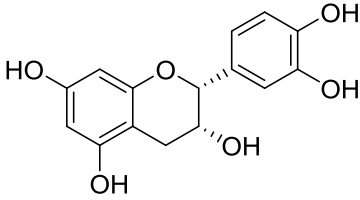
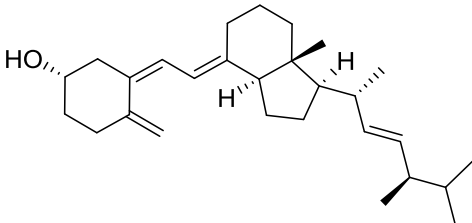
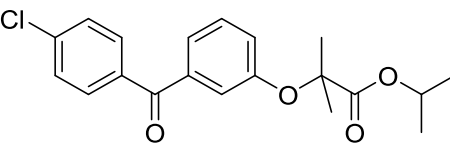
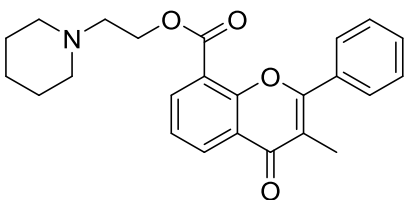
All hits presented in this chapter are structurally non-related drugs with potency ranging from low nanomolar (e.g.  $0.0324 \pm 0.0288 \mu\text{M}$  for amphotericin B at the P2X3 receptor) to micromolar concentrations (e. g.  $48.9 \pm 19.6 \mu\text{M}$  for meclizine at the P2X1 receptor). Most compounds were active at particular P2X subtypes, with low inhibitory potency at the remaining receptors tested when used in high concentrations.



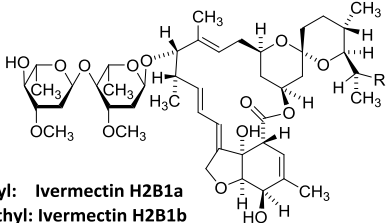
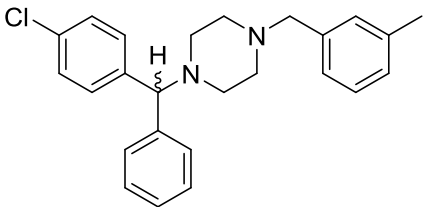
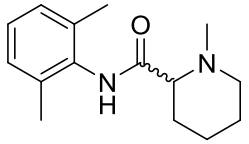
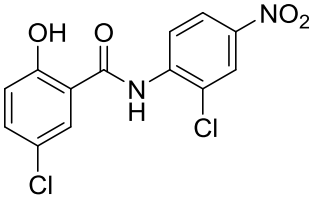
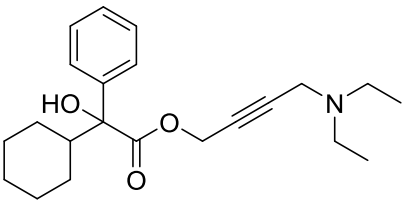
**Table 5.9:** Inhibitory potency of structurally non-related hits at P2X receptors (mean  $\pm$  SEM, n = 3-4).

Compound	Structure	IC <sub>50</sub> $\pm$ SEM [ $\mu$ M] or inhibition at 20 $\mu$ M or 1 $\mu$ M (%)				
		P2X1	P2X2	P2X3	P2X4	P2X7
Ambroxol		> 20 (38 %)	<b>5.69</b> $\pm$ 1.06	> 20 (-29 %)	> 20 (45 %)	> 20 (10 %)
Amphotericin B		> 1 (25 %)	> 20 (-27 %)	<b>0.0324</b> $\pm$ 0.0288 Remaining receptor activity 49 %	> 20 (22 %)	> 20 (-63 %)
Bisacodyl		> 100 (n. c.) <sup>a</sup>	> 20 (21 %)	> 100 (n. c.) <sup>a</sup>	<b>0.711</b> $\pm$ 0.297 Remaining receptor activity 16 %	<b>0.0962</b> $\pm$ 0.0324
Celecoxib		> 1 (21 %)	<b>16.3</b> $\pm$ 2.70 Remaining receptor activity 32 %	> 1 (-17 %)	<b>14.7</b> $\pm$ 3.4 Remaining receptor activity 10 %	> 1 (-4 %)

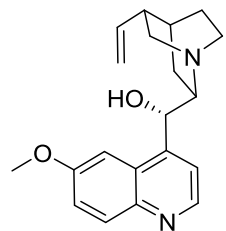
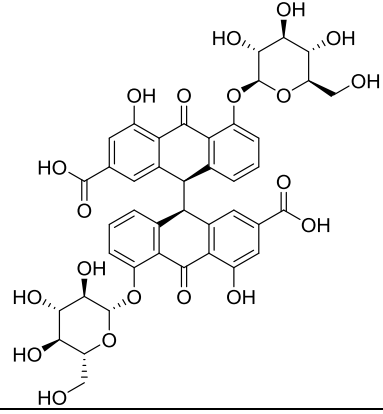
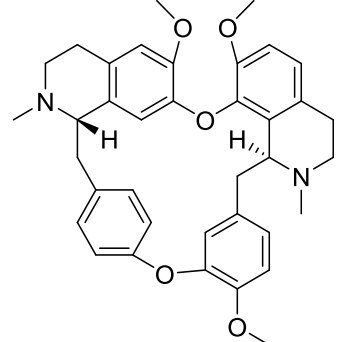
Continuation of Table 5.9

<b>Chlorhexidine</b>		<b>0.302 ± 0.088</b> Remaining receptor activity 26 %	> 1 (11 %)	> 1 (6 %)	> 20 (36 %)	> 20 (12 %)
<b>Epicatechin</b>		> 100 (n. c.) <sup>a</sup>	> 20 (1 %)	> 20 (-15 %)	> 1 (1 %)	> 20 (3 %)
<b>Ergocalciferol</b>		> 100 (n. c.) <sup>a</sup>	> 20 (-28 %)	> 20 (-32 %)	> 1 (14 %)	> 20 (-46 %)
<b>Fenofibrate</b>		<b>5.02 ± 2.46</b> Remaining receptor activity 27 %	> 20 (17 %)	> 1 (9 %)	> 20 (32 %)	> 20 (-21 %)
<b>Flavoxate</b>		<b>35.9 ± 12.2</b>	> 20 (25 %)	> 20 (-10 %)	> 20 (37 %)	> 20 (9 %)

Continuation of Table 5.9

<b>Ivermectin</b>	 <p>R = ethyl: Ivermectin H2B1a R = methyl: Ivermectin H2B1b</p>	<b>1.72 ± 0.23</b> Remaining receptor activity 33 %	> 20 (19 %)	<b>2.73 ± 1.16</b>	> 20 (-63 %)	> 20 (-8 %)
<b>Meclizine</b>		<b>48.9 ± 19.6</b>	<b>12.6 ± 2.2</b> Remaining receptor activity 18 %	> 1 (-21 %)	> 20 (35 %)	> 20 (-32 %)
<b>Mepivacaine</b>		<b>&gt; 10 (n. c.)<sup>a</sup></b>	> 20 (-15 %)	> 20 (-33 %)	> 20 (-14 %)	> 20 (-12 %)
<b>Niclosamide</b>		> 1 (-6 %)	> 20 (-17 %)	<b>0.0134 ± 0.0029</b>	<b>&gt; 100 (n. c.)<sup>a</sup></b>	<b>0.322 ± 0.129</b>
<b>Oxybutynin</b>		<b>50.8 ± 19.6</b>	> 20 (13 %)	> 1 (-34 %)	> 20 (48 %)	> 20 (49 %)

Continuation of Table 5.9

<b>Quinidine sulfate</b>		> 1 (-9 %)	<b>27.1 ± 12.0</b> Remaining receptor activity 17 %	> 1 (-51 %)	> 1 (5 %)	> 1 (14 %)
<b>Senoside A</b>		> 1 (20 %)	> 20 (30%)	<b>14.6 ± 3.3</b>	> 20 (-21 %)	> 20 (-12 %)
<b>Tetrandrine</b>		> 1 (9 %)	<b>8.47 ± 1.21</b> Remaining receptor activity 18 %	> 20 (38 %)	<b>10.4 ± 3.4</b>	> 1 (10 %)

<sup>a</sup>: n. c. no convergence in 3 independent experiments

Ambroxol was identified as a selective antagonist of the P2X2 receptor with an IC<sub>50</sub> value in the low micromolar range ( $5.69 \pm 1.06 \mu\text{M}$ ). No significant inhibition of the other P2X receptors could be detected at  $20 \mu\text{M}$ , which makes ambroxol selective at the P2X2 subtype towards other P2X receptors. It is approved as an expectorant for children and adults. Expectorants generally increase mucin secretion or mucus hydration. Additionally, ambroxol increases the production of surfactant by type II pneumocytes of the alveoli and stimulates the activity of the ciliated epithelium.<sup>310</sup> A local anesthetic effect by inhibition of both tetrodotoxin-sensitive and tetrodotoxin-resistant neuronal voltage-gated sodium channels in rat dorsal root ganglia, as well as inhibition of closely related voltage-gated calcium channels and glutamate receptors also have been reported.<sup>311</sup> Suppression of chronic, inflammatory and neuropathic pain could be confirmed in *in vivo* animal models.<sup>312</sup> Ambroxol itself is an active *N*-desmethyl metabolite of bromhexine, which is also approved as an expectorant drug in respiratory diseases. The bioavailability of a single oral dose of ambroxol 30 mg amounts to 72.9 % and leads to plasma concentrations between  $0.148 \mu\text{M}$  and  $0.257 \mu\text{M}$  ( $1.007\text{-}1.142 \text{ ng/ml}$ ).<sup>313, 314</sup> These concentrations are much lower than necessary for antagonistic activity at the P2X2 receptor. Since a lot of the experiments in the literature were conducted at rat dorsal root ganglia, the efficacy of ambroxol at the heteromeric P2X2/3 receptors would be interesting. Nevertheless, it could be a promising leading structure for the development of selective P2X2 receptor ligands due to its P2X receptor selectivity.

Other hits at the P2X2 receptor with comparable IC<sub>50</sub> values were COX-2-selective NSAID celecoxib (IC<sub>50</sub>  $16.3 \pm 2.70 \mu\text{M}$ ), antiarrhythmic agent quinidine sulfate (IC<sub>50</sub>  $27.1 \pm 12.0 \mu\text{M}$ ) and calcium channel blocker tetrandrine (IC<sub>50</sub>  $8.47 \pm 1.21 \mu\text{M}$ ). Amiodarone and meclizine were also potent inhibitors of the P2X2 receptor, but were also active at P2X1 or P2X4 receptors with comparable potency, respectively.

Tetrandrine and quinidine share remote resemblance due to the bis-benzylisoquinoline (tetrandrine) and quinoline (quinidine) structures. Tetrandrine is an active ingredient in Chinese medicinal herb *Radix Stephanae tetrandrae*, and possesses antiarrhythmic and antihypertensive properties by inhibition of cardiac voltage-dependent calcium- and calcium-activated potassium channels.<sup>315, 316</sup> Calcium influx is also reduced in cells lacking voltage-gated calcium channels. This observation was attributed to a potential inhibition of either the  $\alpha$ -adrenergic receptor or the intracellular pathway of IP<sub>3</sub>-induced calcium release from sarcoplasmic reticulum.<sup>317</sup> Since the P2X2 and P2X4 receptors are also expressed in cardiomyocytes, it is possible that at least part of reduced calcium influx may be attributed to antagonism of both P2X receptor subtypes.<sup>318</sup>

Quinidine is a class Ia antiarrhythmic drug used for the treatment of supraventricular and ventricular arrhythmia. It mainly inhibits the inward sodium current as well as cardiac potassium channels and downregulates the activity of the Na<sup>+</sup>/Ca<sup>2+</sup>-exchanger.<sup>319</sup> In this experimental series, it was moderately potent at the P2X2 receptor, but also showed comparable potency at P2X1 and P2X7 receptors. Since the receptor inhibition at 1 μM final concentration was lower than 50 %, no IC<sub>50</sub> value was determined at those subtypes.

Celecoxib is a COX-2-selective inhibitor and member of the classical NSAID approved for the treatment of rheumatoid arthritis. Inhibitory potency was detected at all P2X receptor subtype at 20 μM. Only the P2X2 receptor was inhibited more than 50 % when the concentration was reduced to 1 μM. The subsequently determined IC<sub>50</sub> concentration was in the moderate micromolar range. The drug was not capable to block the receptor activity completely. A remaining P2X2 receptor activity of 32 % was detected, as was also seen for amiodarone (23 %).

Amphotericin B has strong antifungal properties, like the imidazole derivatives. It belongs to the polyene derivatives and is related to the antibiotic class of macrolides. The mechanism of action though is different; amphotericin B and its closely related derivatives nystatin and natamycin bind to ergosterol. This complex leads to a pore-like formation through the cell membrane with the hydrophobic surface localized on the outer side towards the lipid bilayer and the hydrophilic parts of both structures oriented towards the inside. Due to the high stability of these complexes, the integrity of the cell membrane is compromised leading to an outflow of ions and the destruction of the fungi cells.<sup>320</sup> Amphotericin B has been gold standard in the treatment of systemic fungal infections. The therapeutic use is limited by its poor water solubility at physiological pH and the dose-related nephrotoxicity. In order to improve its pharmacology, amphotericin B is administered mainly as a colloidal solution with sodium desoxycholate, as a lipid formulation (Abelcet®) or encapsulated in liposomes (AmBisome®). The amphotericin B in our compound library was available without any complex or lipid supplement. While the stock solutions and the dilutions were prepared in DMSO and therefore perfectly soluble, this cannot be guaranteed for the assay system, where the compound dilutions are added to an aqueous buffer system. Although a visual control did not yield any anomalies, it is most likely that amphotericin B precipitated onto the cell monolayer on the bottom of the assay plate during the experiment. At the P2X3 receptor, antagonism at nanomolar concentrations (IC<sub>50</sub> 0.0324 ± 0.0288 μM) was observed. The initial screening data at 20 μM at P2X7 receptors implied enhancement of maximal ATP effect, which will be discussed in chapter 5.4.3. No effect was detected at P2X1, P2X2 and P2X4 receptors. Since complete solubility of amphotericin B

during the experiment cannot be guaranteed, it cannot be considered as a P2X receptor ligand based solely on these results.

Fenofibrate, the first member of the fibric acid derivatives, was identified as a selective P2X1 receptor antagonist. It is approved for the treatment of hypertriglyceridemia. The modulation of lipid metabolism is evoked by activation of peroxisome proliferator-activated receptor alpha (PPAR $\alpha$ ). The potency at PPAR $\alpha$  is relatively weak. The receptor is activated by fenofibrate with an EC<sub>50</sub> value of 22.4  $\mu$ M.<sup>321</sup> The inhibitory potency at P2X1 receptors is four times higher (5.02  $\pm$  2.46  $\mu$ M). At the P2X3 receptor, inhibition higher than 50 % at 20  $\mu$ M final concentration was detected, which was reduced to 9 % at 1  $\mu$ M. The closely related bezafibrate was not active at any P2X subtype.

Ivermectin, flavoxate and meclizine were identified as further hits at the P2X1 receptor. Meclizine is a piperazine-based antihistamine drug of the first generation and inhibits the histamine H<sub>1</sub> receptor. Like many other first generation antihistamines, it also binds to muscarinic acetylcholine receptors, constitutive androstane receptors and pregnane X receptors.<sup>322-324</sup> It is mainly used for the prophylactic treatment and management of motion sickness due to its strong antiemetic effects, which exceeds the abilities of other antihistamines such as cetirizine and hydroxyzine. The inhibitory effect of meclizine at the P2X1 receptor was weak. The compound also showed inhibition of the P2X2 receptor with slightly higher potency (IC<sub>50</sub> 12.6  $\pm$  2.2  $\mu$ M vs. 48.9  $\pm$  19.6  $\mu$ M, respectively).

Ivermectin was identified as an inhibitory agent at P2X1 and P2X3 receptors. This was surprising, since ivermectin has previously been described as a PAM of P2X4 and P2X7 receptors.<sup>147, 156</sup> The ATP-enhancing effect at the P2X4 receptor was postulated to be caused by insertion of ivermectin between the transmembrane helices of the receptor trimer, potentially leading to pore-dilation that also diminished receptor desensitization.<sup>149</sup> Ivermectin inhibited P2X1 and P2X3 receptors at micromolar concentrations (IC<sub>50</sub> 1.72  $\pm$  0.23  $\mu$ M and 2.73  $\pm$  1.16  $\mu$ M, respectively), without showing any signs of positive allosteric modulation.

In comparison to ivermectin, flavoxate and oxybutynin were weaker antagonists of the P2X1 receptor with similar activity as meclizine. Both are approved for the treatment of overactive bladder syndrome. Additionally, oxybutynin is used in the treatment of hyperhidrosis. The effect of flavoxate is carried out by inhibition of phosphodiesterases and calcium influx. A local anesthetic effect comparable to lidocaine is known as well.<sup>325</sup> After oral administration, flavoxate is rapidly absorbed and metabolized to 3-methyl-flavone-8-carboxylic acid (MFCA). Only traces of flavoxate are detectable in the blood.<sup>326</sup> Since the activity of flavoxate at the P2X1

receptor is relatively low, the potency of the metabolite MFCA should be determined. Oxybutynin is applied orally, in intravesical or transdermal therapeutic system. The systemic bioavailability of oral formulations is less than 10 % due to high first-pass metabolism in the liver. The primary metabolite is N-desethyloxybutynin.<sup>327</sup> The concentration of the metabolite is significantly higher than of the drug itself upon oral administration of 5 mg (0.0375 – 0.0895  $\mu\text{M}$  for oxybutynin vs. 0.162 – 0.193  $\mu\text{M}$  for N-desoxybutynin).<sup>328</sup> The bioavailable concentrations are too low to activate the P2X1 receptor, and the inhibitory potency of the metabolite could not be determined, since it was not part of the compound library. The application of higher oxybutynin doses is most likely not possible due to higher incidence of anticholinergic adverse events.

Sennoside A is an O-glycoside anthranoid derivatives isolated from Senna plants and widely used for its laxative effect. It was identified as an antagonist with a micromolar  $\text{IC}_{50}$  value at the P2X3 receptor. During the initial screening at 20  $\mu\text{M}$ , high inhibition was also detected at P2X1, P2X4 and P2X7 receptor subtypes, which was, however, less than 50 % at 1  $\mu\text{M}$  concentration. Therefore, no dose-response experiments were conducted. The Senna anthraquinones were the lead structures for the development of the anthraquinone library tested at the P2X3 receptor (see chapter 3), so the inhibitory potency of one of the original structures is not surprising.

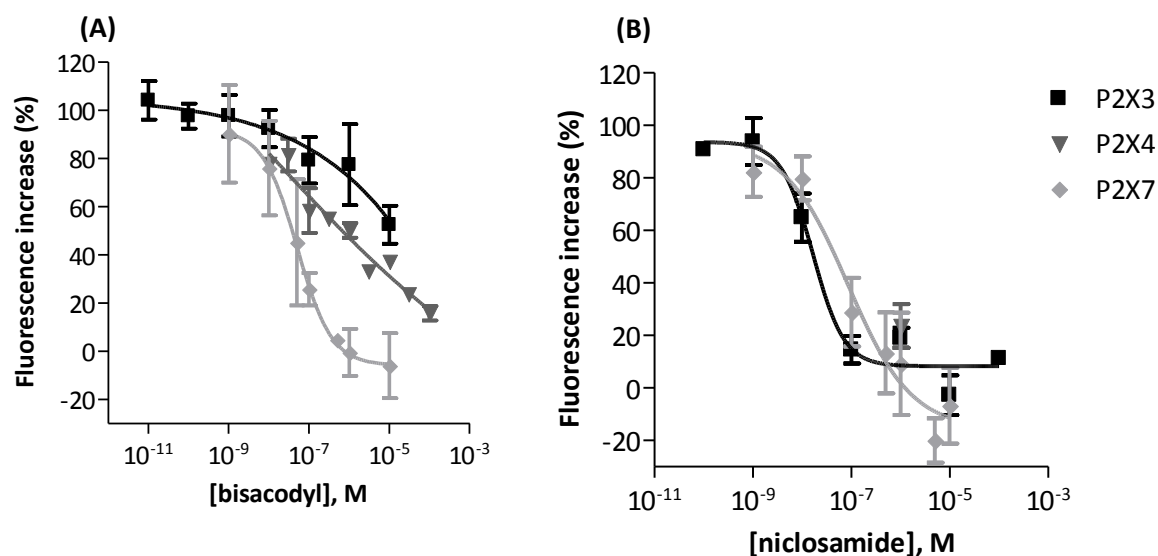
Epicatechin, ergocalciferol and mepivacaine were initially tested as potential hits at the P2X1 receptor, but concentration-dependent effects could not be observed, so inhibitory potency of those drugs could not be proven. None were active at other P2X receptor subtypes tested.

The two most interesting hits detected in the initial screening were bisacodyl and niclosamide. Both were identified to be potent antagonists of both P2X3 and P2X7 receptors. Bisacodyl additionally inhibited the P2X4 receptor. The respective dose-response curves are presented in Figure 5.4.

Bisacodyl was identified as a potent hit at P2X1, P2X3, P2X4 and P2X7 receptors in the initial screening at 20  $\mu\text{M}$ . Concentration-response curves could be generated successfully for the P2X4 and P2X7 receptors. The compound is almost eightfold less potent at the P2X4 than at the P2X7 receptor. Both screening concentrations 20  $\mu\text{M}$  and 1  $\mu\text{M}$  were identified to potently inhibit also the P2X3 receptor, but the subsequent dose-response experiments were not successful. However, niclosamide was potent at both P2X3 and P2X7 receptors in the low (P2X3) and high nanomolar range (P2X7). The drug also blocked the activity of P2X1 and P2X4 receptors at 20  $\mu\text{M}$ , but no inhibitory activity was detected during the repeat at 1  $\mu\text{M}$  final concentration at the P2X1 receptor and no dose-response relation could be generated at the P2X4 receptor.



Weak inhibitory potency at both subtypes therefore has to be taken into account for evaluation of its selectivity.



**Figure 5.4:** Mean dose-response curves of (A) bisacodyl and (B) niclosamide at P2X3, P2X4 and P2X7 receptors. Data is presented as mean  $\pm$  SEM from 3-5 independent experiments.

Both compounds were very interesting hits, since they are not toxic when used in therapeutic concentrations in an animal model, and the potency at the respective targets was very high in comparison to other drugs.<sup>329, 330</sup> Therefore, further investigations were conducted to additionally characterize their activity and their potential as lead structures for drug development.

### 5.3.2 Structure-activity-relationships of bisacodyl and niclosamide derivatives

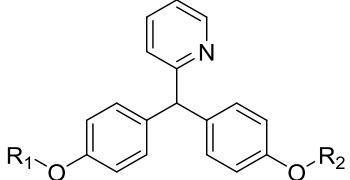
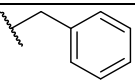
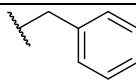
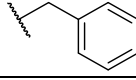
Bisacodyl and niclosamide were identified as potent antagonists at P2X3 and P2X7 receptors, respectively. Both compounds are reported to be non-toxic and have been used as drugs in high concentrations for a long time. Both were selected for further characterization based on their high potency. A small library of nine compounds derived from the bisacodyl structure with aliphatic side chains of varying length were synthesized by M. Sc. The-Hung Vu. Niclosamide bears high structural similarity to *N*-(3,5-bis-trifluoromethylphenyl)-5-chloro-2-hydroxybenzamide, also known as IMD-0354, here MT164, a selective NF $\kappa$ B inhibitor, which has been identified as a potent P2X1 receptor antagonist by M. Sc. Sabrina Densborn and Dr. Aliaa Abdelrahman.<sup>331-334</sup> A series of structural derivatives has been synthesized by Dr. Maoqun Tian.

The whole library was tested at P2X3 and P2X7 receptors. The results of both experiment series are discussed in the following chapters.

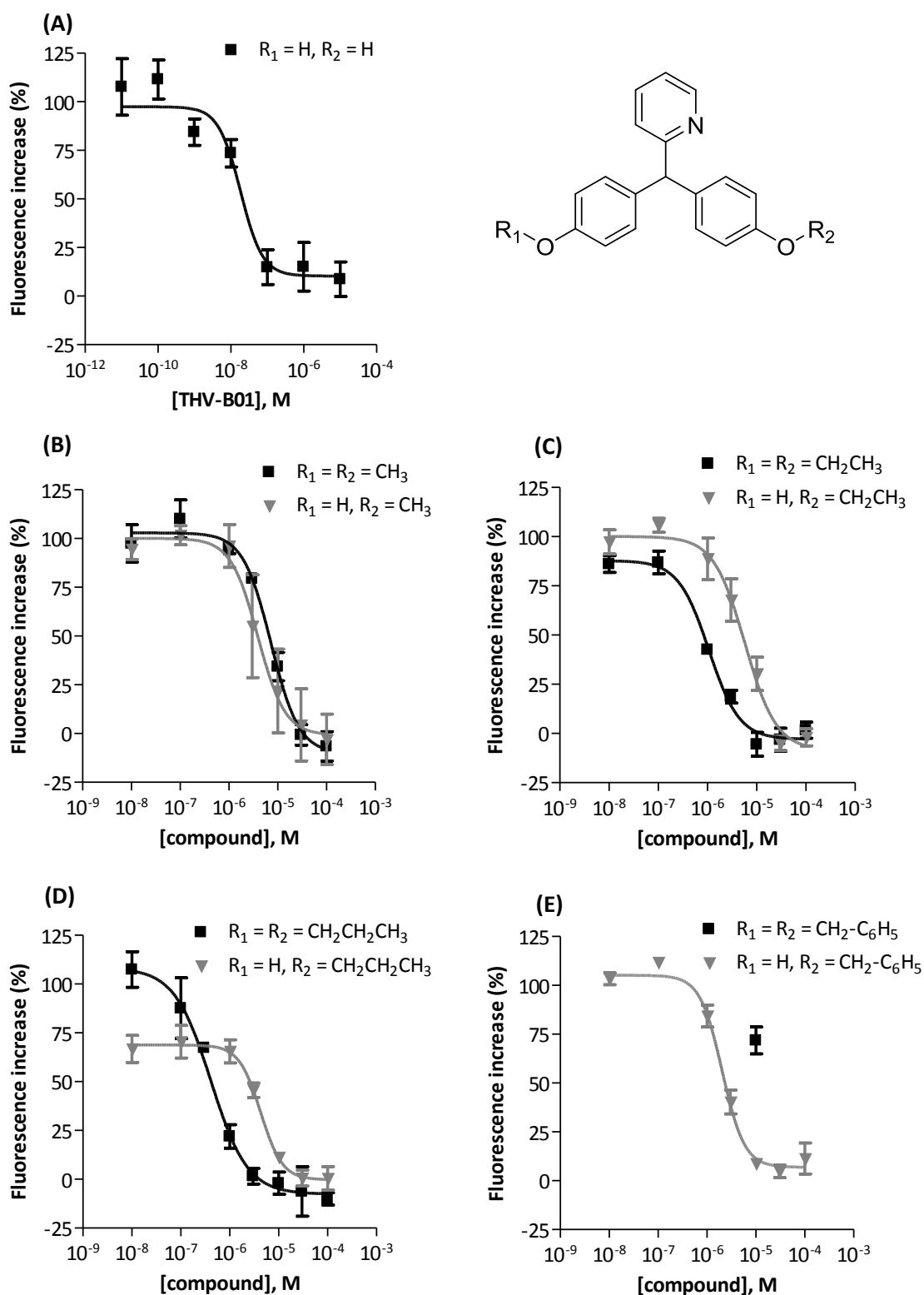
### 5.3.2.1 Bisacodyl derivatives

Bisacodyl is a triarylmethane-based drug approved for the treatment of chronic obstipation. It was identified as a potent and moderately selective antagonist of human P2X7 receptor with an  $IC_{50}$  value of  $0.0962 \pm 0.0324 \mu\text{M}$ . A small library of compounds bearing aliphatic residues of varying length instead of the ester moieties was synthesized by The-Hung Vu. The structures of the derivatives and the corresponding experimental results are presented in Table 5.10.

**Table 5.10:** Inhibitory potency of bisacodyl derivatives at P2X receptors (mean  $\pm$  SEM,  $n = 3-4$ ).

Name	Residues		$IC_{50} \pm \text{SEM} [\mu\text{M}]$ or inhibition at $10 \mu\text{M}$ (%)				
							
	$R_1$	$R_2$	<b>P2X1</b>	<b>P2X2</b>	<b>P2X3</b>	<b>P2X4</b>	<b>P2X7</b>
<b>THV-B01</b>	H	H	> 10 (35 %)	> 10 (41 %)	<b>0.0194</b> $\pm 0.0036$	> 10 (25 %)	> 10 (46 %)
<b>THV -B02-1</b>	CH <sub>3</sub>	CH <sub>3</sub>	> 10 (1 %)	> 10 (28 %)	<b>7.55</b> $\pm$ 1.72	> 10 (16 %)	> 10 (-29 %)
<b>THV -B02-2</b>	H	CH <sub>3</sub>	> 10 (1 %)	> 10 (7 %)	<b>6.43</b> $\pm$ 3.98	> 10 (6 %)	> 10 (-13 %)
<b>THV -B03-1</b>	CH <sub>2</sub> CH <sub>3</sub>	CH <sub>2</sub> CH <sub>3</sub>	> 100 (n. c.) <sup>a</sup>	> 10 (48 %)	<b>1.19</b> $\pm$ 0.29	> 10 (16 %)	> 10 (-17 %)
<b>THV -B03-2</b>	H	CH <sub>2</sub> CH <sub>3</sub>	> 10 (22 %)	> 10 (9 %)	<b>5.97</b> $\pm$ 2.06	> 10 (10 %)	> 10 (-23 %)
<b>THV -B04-1</b>	CH <sub>2</sub> CH <sub>2</sub> CH <sub>3</sub>	CH <sub>2</sub> CH <sub>2</sub> CH <sub>3</sub>	> 10 (41 %)	<b>1.55</b> $\pm$ 0.60 remaining receptor activity 46 %	<b>0.452</b> $\pm$ 0.053	> 10 (33 %)	> 10 (10 %)
<b>THV -B04-2</b>	H	CH <sub>2</sub> CH <sub>2</sub> CH <sub>3</sub>	> 10 (42 %)	> 10 (36 %)	<b>4.14</b> $\pm$ 0.23	> 10 (25 %)	> 10 (-19 %)
<b>THV -B05-1</b>			> 10 (17 %)	> 10 (23 %)	> 10 (28 %)	> 10 (18 %)	> 10 (7 %)
<b>THV -B05-2</b>	H		> 100 (n. c.) <sup>a</sup>	> 10 (38 %)	<b>1.86</b> $\pm$ 0.12	> 10 (32 %)	> 10 (-25 %)

<sup>a</sup>: n. c. no convergence seen in three independent experiments



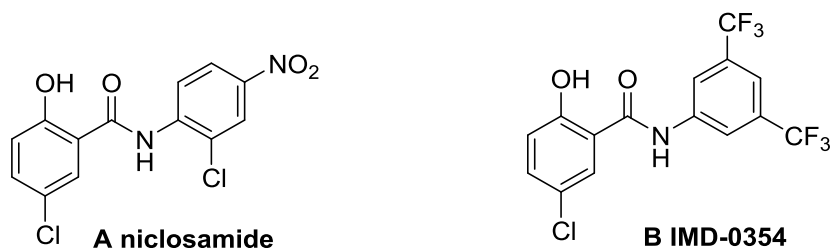
**Figure 5.5:** Mean dose-response curves of bisacodyl derivatives (A) THV-B01, (B) THV-B02-1 (■) and THV-B02-2 (▼), (C) THV-B03-1 (■) and THV-B03-2 (▼), (D) THV-B04-1 (■) and THV-B04-2 (▼) and (E) THV-B05-1 (■) and THV-B05-2 (▼) at the rat P2X3 receptor. (mean  $\pm$  SEM, n = 3-4)

The cleavage of the acetate residues and subsequent etherification of the phenolic hydroxyl residues led to new derivatives and allowed the observation of structure-activity relationships. While bisacodyl was a potent P2X7 antagonist with no concentration-dependent inhibition detectable at the other P2X receptor subtypes except P2X4, the newly synthesized derivatives showed no inhibitory potency higher than 50 % at P2X7, but at the P2X3 receptors. THV-B05-1 was the only compound from this series with less than 50 % inhibitory potency at this target. The symmetrical propyl derivative THV-B04-1 was additionally active at the P2X2 receptor, but only reduced the receptor activity to about 50 %. The symmetric ethyl-substituted THV-B03-1 and the asymmetrical benzyl-substituted compound THV-B05-2 showed P2X1 receptor inhibition higher than 50 % when screened at 10  $\mu$ M final concentration, but no concentration-dependent inhibition was observed. No other derivative was active at any other subtype.

The most active compound of this series at the P2X3 receptor was the hydrolyzed diphenol, which is the active metabolite of bisacodyl and responsible for the intestinal stimulating effect. Elongation of the attached aliphatic side chains did not seem to have any effect on the affinity towards the P2X3 receptor (see also Figure 5.5). The asymmetric propyl compound THV-B04-2 was found to be almost tenfold less active than its symmetric variant THV-B04-1. This was also seen to a lesser extent for the ethyl derivatives THV-B03-1 and THV-B03-1. The observation supports the theory that symmetric substitution of the diphenol is necessary for higher inhibitory potency at the P2X3 receptor, but the effect was not observed for the methyl-substituted derivatives THV-B02-1 and THV-B02-2. Furthermore, the asymmetric benzyl derivative THV-B05-2 was demonstrated as a potent P2X3 antagonist with a low micromolar  $IC_{50}$  value, while symmetric THV-B05-1 did not show any inhibitory potency when screened at 10  $\mu$ M.

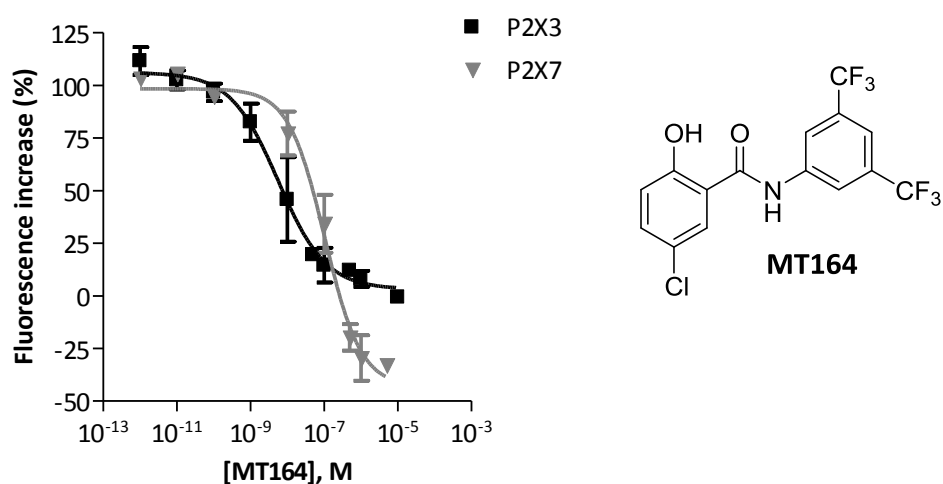
### 5.3.2.2 *Niclosamide derivatives*

Niclosamide was identified as a potent antagonist of both P2X3 and P2X7 receptors. The compound bears high structural similarity to *N*-(3,5-bis-trifluoromethylphenyl)-5-chloro-2-hydroxybenzamide (IMD-0354, also named MT164, see Figure 5.6 B). It is one of 1140 compounds of a commercial TOCRIS library, which has been identified as a lead structure for the development of P2X1 receptor ligands (data not yet published). The whole library of IMD-0354 derivatives, synthesized by Dr. Maoqun Tian, has now been tested at the P2X3 and the P2X7 receptor.



**Figure 5.6:** Structures of (A) niclosamide and (B) *N*-(3,5-bis-trifluoromethylphenyl)-5-chloro-2-hydroxybenzamide (IMD-0354, MT164).

All compounds were initially screened at a final concentration of 10  $\mu\text{M}$ . Every compound except MT205, MT239, MT267, MT273 and MT316 was capable of inhibiting both P2X3 and P2X7 receptors by more than 80 %. The same was seen for MT279 at the P2X3, and for MT232 and MT234 at the P2X7 receptor. The screenings of all compounds were repeated at both receptors at final concentrations of 1  $\mu\text{M}$  and 0.1  $\mu\text{M}$  for further characterization. When the inhibitory potency at 0.1  $\mu\text{M}$  still remained higher than 50 %, concentration-response experiments were conducted. The results are summarized in Table 5.11. The substitution of both phenyl rings named A and B (see structure in Table 5.11) was considered separately to facilitate the discussion of structure-activity relationships, starting with ring A. The lead structure MT164 (IMD-0354) was proven to be a potent antagonist at both receptor subtypes with a slight preference for the P2X3 receptor ( $\text{IC}_{50}$  0.0147  $\pm$  0.0103  $\mu\text{M}$  and 0.128  $\pm$  0.019  $\mu\text{M}$ , respectively, see also Figure 5.7). The compound was almost tenfold more potent at P2X3 than at P2X7 receptors.



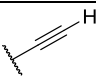
**Figure 5.7:** Mean dose-response curves and structure of MT164 at the P2X3 and the P2X7 receptor. Data is presented as mean  $\pm$  SEM from 3-4 independent experiments.

## 5 Results and Discussion

**Table 5.11:** Inhibitory potency of nicosamide-related *N*-(3,5-bis-trifluoromethylphenyl)-5-chloro-2-hydroxybenzamide derivatives at P2X3 and P2X7 receptors (mean  $\pm$  SEM,  $n = 3-4$ ).

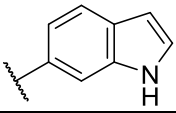
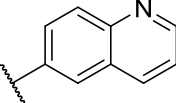
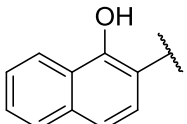
Name	Residues									IC <sub>50</sub> $\pm$ SEM [ $\mu$ M] or inhibition at 10 $\mu$ M, 1 $\mu$ M or 0.1 $\mu$ M (%)	
	R <sub>1</sub>	R <sub>2</sub>	R <sub>3</sub>	R <sub>4</sub>	R <sub>5</sub>	R <sub>6</sub>	R <sub>7</sub>	R <sub>8</sub>	R <sub>9</sub>	P2X3	P2X7
Nicosamide										<b>0.0134</b> $\pm$ 0.0029	<b>0.322</b> $\pm$ 0.129
<b>MT263</b>	H	CF <sub>3</sub>	H	CF <sub>3</sub>	H	Cl	H	H	OH	>0.1	> 1
<b>MT165</b>	H	H	H	Cl	H	CF <sub>3</sub>	H	CF <sub>3</sub>	H	>0.1 (15 %)	> 1 (30 %)
<b>MT166</b>	OH	H	H	H	H	CF <sub>3</sub>	H	CF <sub>3</sub>	H	>0.1 (38 %)	> 0.1 (17 %)
<b>MT169</b>	OH	H	H	CH <sub>3</sub>	H	CF <sub>3</sub>	H	CF <sub>3</sub>	H	<b>0.124</b> $\pm$ 0.039	> 0.1 (13 %)
<b>MT173</b>	OH	Cl	H	H	H	CF <sub>3</sub>	H	CF <sub>3</sub>	H	<b>0.0158</b> $\pm$ 0.0040	> 0.1 (28 %)
										Remaining receptor activity 24 %	
<b>MT175</b>	OH	H	Cl	H	H	CF <sub>3</sub>	H	CF <sub>3</sub>	H	<b>0.0109</b> $\pm$ 0.0052	<b>0.0513</b> $\pm$ 0.0025
<b>MT205</b>	OCH <sub>3</sub>	H	H	Cl	H	CF <sub>3</sub>	H	CF <sub>3</sub>	H	> 10 (10 %)	> 10 (41 %)
<b>MT232</b>	Cl	H	H	H	H	CF <sub>3</sub>	H	CF <sub>3</sub>	H	> 0.1 (42 %)	> 10 (6 %)
<b>MT234</b>	CH <sub>2</sub> OH	H	H	H	H	CF <sub>3</sub>	H	CF <sub>3</sub>	H	> 1 (15 %)	> 1 (8 %)
<b>MT235</b>	H	OH	H	H	H	CF <sub>3</sub>	H	CF <sub>3</sub>	H	> 1 (39 %)	> 1 (17 %)
<b>MT240</b>	OH	F	H	H	H	CF <sub>3</sub>	H	CF <sub>3</sub>	H	<b>0.113</b> $\pm$ 0.024	> 1 (36 %)
<b>MT244</b>	OH	CH <sub>3</sub>	H	H	H	CF <sub>3</sub>	H	CF <sub>3</sub>	H	<b>0.169</b> $\pm$ 0.035	> 0.1 (15 %)
<b>MT246</b>	OH	NO <sub>2</sub>	H	H	H	CF <sub>3</sub>	H	CF <sub>3</sub>	H	> 0.1 (37 %)	> 0.1 (26 %)
<b>MT259</b>	H	H	H	H	H	CF <sub>3</sub>	H	CF <sub>3</sub>	H	> 1 (46 %)	> 1 (39 %)
<b>MT264</b>	OH	H	H	NO <sub>2</sub>	H	CF <sub>3</sub>	H	CF <sub>3</sub>	H	<b>0.0922</b> $\pm$ 0.0054	<b>0.739</b> $\pm$ 0.163
<b>MT265</b>	OH	H	H	OH	H	CF <sub>3</sub>	H	CF <sub>3</sub>	H	> 1 (43 %)	> 1 (2 %)
<b>MT266</b>	H	CF <sub>3</sub>	H	H	H	CF <sub>3</sub>	H	CF <sub>3</sub>	H	> 1 (48 %)	> 1 (29 %)
<b>MT279</b>	NO <sub>2</sub>	H	H	H	H	CF <sub>3</sub>	H	CF <sub>3</sub>	H	> 1 (3 %)	> 1 (24 %)
<b>MT281</b>	NH <sub>2</sub>	H	H	H	H	CF <sub>3</sub>	H	CF <sub>3</sub>	H	> 1 (16 %)	> 1 (46 %)
<b>MT283</b>	OH	H	H	H	OH	CF <sub>3</sub>	H	CF <sub>3</sub>	H	<b>0.0174</b> $\pm$ 0.0040	<b>0.593</b> $\pm$ 0.141

Continuation of Table 5.11

	R <sub>1</sub>	R <sub>2</sub>	R <sub>3</sub>	R <sub>4</sub>	R <sub>5</sub>	R <sub>6</sub>	R <sub>7</sub>	R <sub>8</sub>	R <sub>9</sub>		
<b>MT303</b>	OH	H	H	F	H	CF <sub>3</sub>	H	CF <sub>3</sub>	H	<b>0.0370 ±</b> 0.0171	<b>0.144 ±</b> 0.022
<b>MT305</b>	OH	H	H	OCH <sub>3</sub>	H	CF <sub>3</sub>	H	CF <sub>3</sub>	H	<b>0.127 ±</b> 0.0083	<b>0.572 ±</b> 0.170
<b>MT164</b>	OH	H	H	Cl	H	CF <sub>3</sub>	H	CF <sub>3</sub>	H	<b>0.0147 ±</b> 0.0103	<b>0.128 ±</b> 0.019
<b>MT170</b>	OH	H	H	Cl	H	H	CF <sub>3</sub>	H	H	<b>0.0140 ±</b> 0.0041	> 0.1 (32 %)  Remaining receptor activity 17 %
<b>MT301</b>	OH	H	H	Cl	H	H	Cl	H	H	<b>0.0823 ±</b> 0.0318	<b>1.79 ±</b> 0.043
<b>MT304</b>	OH	H	H	Cl	H	H	NO <sub>2</sub>	H	H	<b>0.0563 ±</b> 0.0098	<b>1.07 ±</b> 0.306  Remaining receptor activity 18 %
<b>MT310</b>	OH	H	H	Cl	H	H	F	H	H	> 1 (33 %)	<b>6.38 ± 0.48</b>
<b>MT341</b>	OH	H	H	Cl	H	H	CN	H	H	> 0.1 (-6 %)	<b>&gt; 1 (n.c.)<sup>a</sup></b>
<b>MT182</b>	OH	H	H	Cl	H	NO <sub>2</sub>	H	H	H	<b>0.104 ±</b> 0.010	> 1 (35 %)
<b>MT184</b>	OH	H	H	Cl	H	CN	H	H	H	> 0.1 (26 %)	> 1 (9 %)
<b>MT167</b>	OH	H	H	Cl	H	H	H	CF <sub>3</sub>	H	<b>&gt; 10 (n.c.)<sup>a</sup></b>	> 1 (41 %)
<b>MT188</b>	OH	H	H	Cl	H	H	H	Cl	H	> 0.1 (40 %)	> 0.1 (40 %)
<b>MT221</b>	OH	H	H	Cl	H	H	H	SO <sub>2</sub> CF <sub>3</sub>	H	> 0.1 (29 %)	<b>1.47 ±</b> 0.340
<b>MT227</b>	OH	H	H	Cl	H	H	H	C(CH <sub>3</sub> ) <sub>3</sub>	H	> 0.1 (-10 %)	<b>0.661 ±</b> 0.274
<b>MT274</b>	OH	H	H	Cl	H	H	H		H	> 0.1 (2 %)	> 1 (2 %)
<b>MT309</b>	OH	H	H	Cl	H	H	H	OCF <sub>3</sub>	H	<b>0.0511 ±</b> 0.0148	<b>0.504 ±</b> 0.175  Remaining receptor activity 16 %
<b>MT171</b>	OH	H	H	Cl	H	H	H	H	CF <sub>3</sub>	> 0.1 (-36 %)	> 1 (17 %)
<b>MT177</b>	OH	H	H	Cl	H	CH <sub>3</sub>	H	CH <sub>3</sub>	H	> 0.1 (19 %)	> 0.1 (-6 %)
<b>MT179</b>	OH	H	H	Cl	H	Cl	H	Cl	H	<b>0.0155 ±</b> 0.0030	<b>0.408 ±</b> 0.022
<b>MT186</b>	OH	H	H	Cl	H	OCH <sub>3</sub>	H	OCH <sub>3</sub>	H	> 1 (46 %)	> 1 (1 %)

## 5 Results and Discussion

Continuation of Table 5.11.

	R <sub>1</sub>	R <sub>2</sub>	R <sub>3</sub>	R <sub>4</sub>	R <sub>5</sub>	R <sub>6</sub>	R <sub>7</sub>	R <sub>8</sub>	R <sub>9</sub>		
<b>MT215</b>	OH	H	H	Cl	H	F	H	F	H	> 0.1 (44 %)	> 10 (n. c.)
<b>MT267</b>	OH	H	H	Cl	H	OH	H	OH	H	> 10 (37 %)	> 1 (30 %)
<b>MT275</b>	OH	H	H	Cl	H	NO <sub>2</sub>	H	NO <sub>2</sub>	H	> 1 (44 %)	> 0.1 (38 %)
<b>MT230</b>	OH	H	H	Cl	H	NO <sub>2</sub>	H	CF <sub>3</sub>	H	<b>0.0690 ±</b> 0.0337	<b>0.340 ±</b> 0.088
<b>MT282</b>	OH	H	H	Cl	H	H	Cl	NO <sub>2</sub>	H	<b>0.0140 ±</b> 0.0023	<b>0.540 ±</b> 0.024
<b>MT177</b>	OH	H	H	Cl	H	CH <sub>3</sub>	H	CH <sub>3</sub>	H	> 0.1 (19 %)	> 0.1 (-6 %)
<b>MT179</b>	OH	H	H	Cl	H	Cl	H	Cl	H	<b>0.0155 ±</b> 0.0030	<b>0.408 ±</b> 0.022
<b>MT186</b>	OH	H	H	Cl	H	OCH <sub>3</sub>	H	OCH <sub>3</sub>	H	> 1 (46 %)	> 1 (1 %)
<b>MT215</b>	OH	H	H	Cl	H	F	H	F	H	> 0.1 (44 %)	> 10 (n. c.)
<b>MT267</b>	OH	H	H	Cl	H	OH	H	OH	H	> 10 (37 %)	> 1 (30 %)
<b>MT275</b>	OH	H	H	Cl	H	NO <sub>2</sub>	H	NO <sub>2</sub>	H	> 1 (44 %)	> 0.1 (38 %)
<b>MT230</b>	OH	H	H	Cl	H	NO <sub>2</sub>	H	CF <sub>3</sub>	H	<b>0.0690 ±</b> 0.0337	<b>0.340 ±</b> 0.088
<b>MT282</b>	OH	H	H	Cl	H	H	Cl	NO <sub>2</sub>	H	<b>0.0140 ±</b> 0.0023	<b>0.540 ±</b> 0.024
<b>MT162</b>	OH	H	H	H	H	CF <sub>3</sub>	H	H	H	> 0.1 (27 %)	> 1 (6 %)
<b>MT239</b>	OH	H	H	H	H	H	H	SO <sub>2</sub> NH <sub>2</sub>	H	> 10 (29 %)	> 10 (-52 %)
<b>MT241</b>	OH	H	H	H	H	H	H	Br	H	> 1 (34 %)	> 1 (21 %)
<b>MT258</b>	OH	Cl	H	H	H	NO <sub>2</sub>	H	CF <sub>3</sub>	H	> 0.1 (8 %)	> 1 (39 %)
<b>MT273</b>	OH	H	H	H	H					> 10 (42 %)	> 10 (25 %)
<b>MT316</b>	OH	H	H	H	H					> 1 (42 %)	> 0.1 (46 %)
<b>MT207</b>						CF <sub>3</sub>	H	CF <sub>3</sub>	H	> 0.1 (14 %)	<b>0.896 ±</b> 0.122

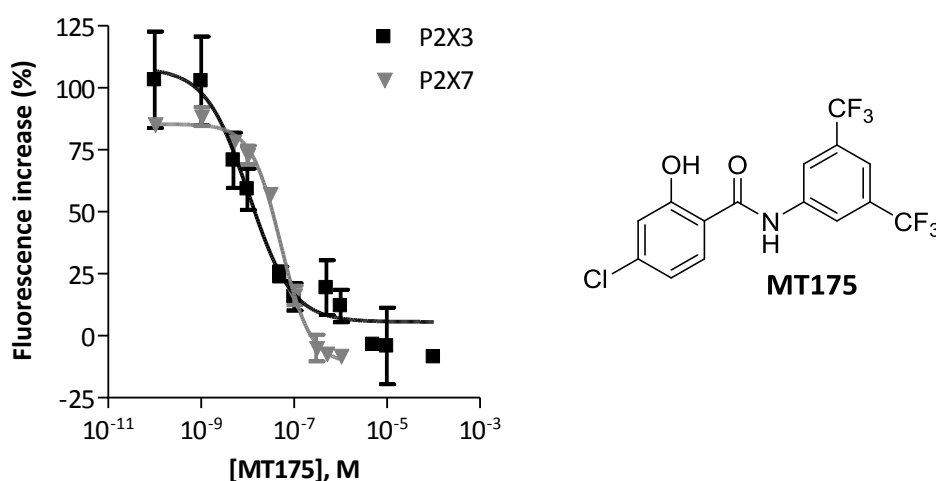
<sup>a</sup>: n. c. calculation of IC<sub>50</sub> not successful in three independent experiments



MT164 was around three times more potent than niclosamide at the P2X7 receptor, whereas the activity at the P2X3 receptor remained unchanged. By eliminating the hydroxyl substituent in the *ortho*-position of ring A (MT165), the inhibitory activity at both receptor subtypes was diminished to lower than 20 % at 0.1  $\mu$ M concentration. A similar effect was observed when the chlorine in position 5 was removed (MT166), when the hydroxyl function was methylated (MT205), and when both substituents were replaced with hydrogen (MT 259).

When chlorine in position 5 of the 2-hydroxybenzamide is exchanged for a methyl (MT169), a nitro (MT264), a second hydroxyl (MT265), a methoxy group (MT305) or to fluorine (MT303), the inhibitory potency at the P2X3 receptor is reduced in comparison to niclosamide. Only the fluorine-substituted compound MT303 has comparable activity to MT164 at the P2X7 receptor, the methoxy- and nitro derivative's potency were significantly lower ( $IC_{50}$   $0.572 \pm 0.170$   $\mu$ M and  $0.739 \pm 0.163$   $\mu$ M, respectively). The compounds with methyl or hydroxyl substituents in the same position already showed inhibitory activity lower than 20 % when screened at a final concentration of 0.1  $\mu$ M.

When chlorine is moved from position 5 to 4 (MT175), the inhibitory potency at both receptor subtypes was markedly increased ( $IC_{50}$   $0.0109 \pm 0.0052$   $\mu$ M and  $0.0513 \pm 0.0025$   $\mu$ M, respectively, see also Figure 5.8). MT175 was the most active compound of this series at both receptors, and therefore selected for further experiments along with MT164 discussed in later chapters. Its activity at the P2X3 receptor was comparable to MT164 and niclosamide. MT175 was about six times more potent at the P2X7 receptor when compared to niclosamide.



**Figure 5.8:** Mean dose-response curves and structure of MT175 at the P2X3 and the P2X7 receptor. Data is presented as mean  $\pm$  SEM from 3-6 independent experiments.

When chlorine is moved from position 4 to 3 (MT173), the inhibitory potency at the P2X7 receptor was reduced. The activity of MT173 at the P2X3 receptor is comparable to MT175, but even at higher concentrations, it was not possible to inhibit the receptor completely. An exchange of chlorine for fluorine (MT240), a methyl (MT244) or a nitro residue (MT246) reduced the activity at both receptor subtypes.

The elimination of chlorine in position 5 followed by the introduction of a second hydroxyl group in position 6 (MT283) shows inhibitory potency at P2X3 and P2X7 receptors comparable to niclosamide. However, the potency at the P2X7 receptor is almost ten times less than MT175, the most potent antagonist of this series.

The substitution pattern was also varied at the second phenyl ring B. When one trifluoromethyl residue is removed (MT167), the inhibitory potency at the P2X7 receptor is reduced to less than 20 % at 0.1  $\mu\text{M}$  final concentration, but not at the P2X3 receptor. However, it was not possible to conduct successful concentration-response experiments. When the one remaining trifluoromethyl residue was moved to position 2, the activity at the P2X3 receptor was comparable to niclosamide, but the calcium influx could not be completely blocked. The transfer to position 4 diminished the inhibitory potency in comparison to both niclosamide and the leading structure MT164. Both substitution patterns lead to less potency at the P2X7 receptor.

When the one trifluoromethyl residue in position 2 was exchanged to a nitrile (MT184),  $\text{SO}_2\text{CF}_3$  (MT221), ethynyl (MT274) or isobutyl group (MT227), the affinity at the P2X3 receptor at a final concentration of 0.1  $\mu\text{M}$  was reduced to less than 40 %, respectively. A nitro substituent in this position (MT182) was potent during the first screening experiments, but almost eight times less active than niclosamide. Less activity was also observed for the exchange against a trifluoromethoxy group (MT309). The substitution against a  $\text{SO}_2\text{CF}_3$  (MT221), trifluoromethoxy or isobutyl residue led to inhibitory potency at the P2X7 receptor, but was demonstrated to be less potent in comparison to the lead structure MT164 and the most active compound MT175.

Moving the one remaining trifluoromethyl residue to position 4 (MT170) led to a potent compound. The activity of MT170 at the P2X3 receptor was comparable to niclosamide. The exchange to nitrile (MT304) was tolerated, but did not improve potency. Fluorine in the *para*-position diminished the inhibitory activity. Neither MT170 nor the fluorine- or nitrile derivative showed higher potency than niclosamide or MT164 at the P2X7 receptor.

The complete exchange of both trifluoromethyl residues for two methyl residues (MT177), two methoxy (MT186), two hydroxyl (MT267) or two nitro substituents (MT275) reduced the inhibition of both targets to less than 20 % at a concentration of 0.1  $\mu\text{M}$ . MT215 at the P2X3

receptor was the only exception; here the receptor activity was reduced to 44 %. When exchanged for two chlorine substituents, the compound MT179 showed inhibitory potency comparable to MT164 at the P2X3, but was slightly less potent at the P2X7 receptor.

In conclusion, it can be stated that the hydroxyl function in position 2 of ring A plays an important role for high inhibitory potency with nanomolar IC<sub>50</sub> values at both receptors. A small elongation or replacement by other polar residues reduced the activity. Chlorine in position 4 or 5 did not have the same importance for high affinity of the compound. In ring B, various substituents were tolerated; the most common substitution pattern with high inhibitory activity was two substituents in the *meta*-positions 3 and 5, both polar and nonpolar. All hits were comparable or at least three to four times more potent at the P2X3 receptor than at P2X7, except MT227, the only compound with a bulky isobutyl residue in position 5 of ring B. Since no further elongations of side chains on both phenyl rings were available, no clear estimation can be made about the tolerance of bulky residues at the pharmacophore. This could be a possibility for the future development of a selective P2X7 ligand.

### 5.3.2.3 Selectivity of niclosamide derivatives

Nearly all niclosamide derivatives were proven to be very potent antagonists of both P2X3 and P2X7 receptors. Screening experiments at human P2X1, P2X2 and P2X4 receptor were conducted for the two most interesting compounds MT164 and MT175 in order to determine whether the compounds are selective towards other P2X receptor subtypes. The results are presented in Table 5.12.

**Table 5.12:** Inhibitory potency of niclosamide derivatives MT164 and MT175 at human P2X receptors (mean ± SEM, n = 3-4).

	IC <sub>50</sub> ± SEM [μM] or inhibition (%) at 10 μM				
	P2X1	P2X2	P2X3	P2X4	P2X7
<b>MT164</b>	<b>0.0192 ± 0.0041<sup>a</sup></b>	> 10 (34 %)	<b>0.0147 ± 0.0103</b>	<b>6.14 ± 2.44</b>	<b>0.128 ± 0.019</b>
<b>MT175</b>	<b>0.0231 ± 0.0036<sup>a</sup></b>	> 10 (48 %)	<b>0.0109 ± 0.0052</b>	<b>6.34 ± 1.56</b>	<b>0.0513 ± 0.0025</b>

<sup>a</sup>: Data determined by Dr. Aliaa Abdelrahman by measurement of calcium influx in 1321N1 astrocytoma cells stably transfected with human P2X1 receptor. Data not yet published.

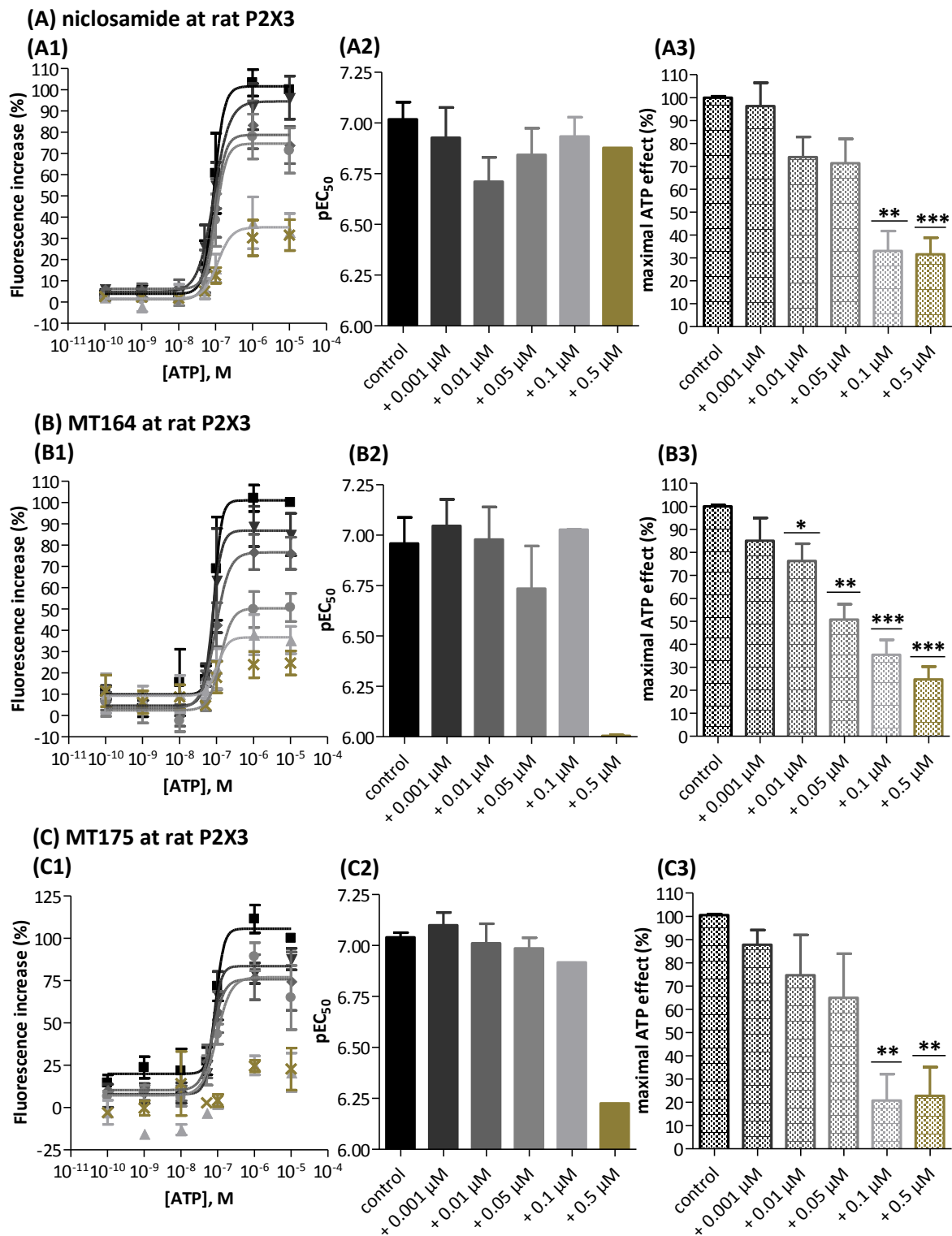
Both compounds were proven to be selective towards the human P2X2 and P2X4 receptor. However, Dr. Aliaa Abdelrahman previously identified the compounds to be potent antagonists of the human P2X1 receptor (data not yet published). The activity at this subtype was comparable to the affinity determined for the P2X3 receptor. Due to the high structural

similarity and generally high potency, it is likely that niclosamide derivatives are selective towards P2X2 and P2X4 receptors, but not among the remaining subtypes.

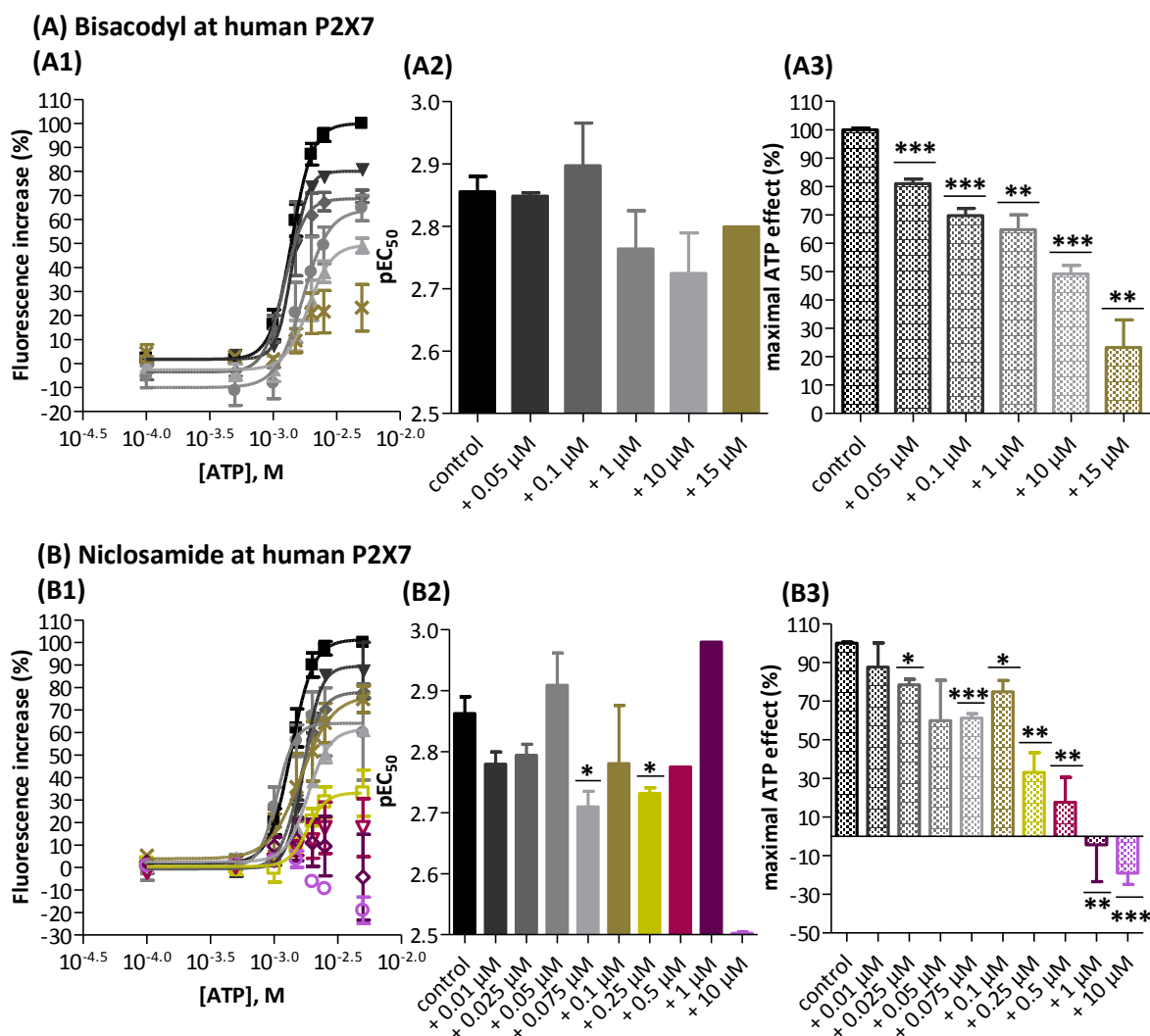
### 5.3.3 Determination of inhibition mechanism at P2X3 and P2X7 receptors

Several drugs of the compound library were proven to be potent ligands at P2X receptors. In order to better characterize their mode of action, the most interesting hits were selected for ATP curve shift experiments determining their effect on the ATP potency at the respective receptor. Bisacodyl and niclosamide were already discussed as interesting agents at the P2X3 and the P2X7 receptor, respectively. Additionally, the niclosamide-like derivatives MT164 and MT175 were tested. The resulting ATP curves in the presence and absence of antagonist are presented in Figure 5.9 A1-C1 for the P2X3 and in Figure 5.11 A1-D1 for the human P2X7 receptor.

For several of the higher concentrations tested, the calculation of  $EC_{50}$  concentrations was either not successful (MT164 0.5  $\mu$ M at P2X3, niclosamide 10  $\mu$ M, MT164 0.25  $\mu$ M and 0.5  $\mu$ M, and MT175 1  $\mu$ M and 10  $\mu$ M at the P2X7 receptor), or only one of three to four experiments gave a interpretable result (niclosamide 0.5  $\mu$ M, MT164 0.1  $\mu$ M, and MT175 1  $\mu$ M and 10  $\mu$ M at the P2X3, bisacodyl 15  $\mu$ M, niclosamide 0.5  $\mu$ M and 1  $\mu$ M, and MT175 0.5  $\mu$ M at the P2X7 receptor). MT175 10  $\mu$ M was only tested twice at the P2X7 receptor. The decrease of maximal fluorescence signal was visualized by plotting the fluorescence increase caused by the highest ATP concentrations used in the experiments, 10  $\mu$ M for the P2X3 and 5 mM for the rP2X7 receptor against the respective concentration of test compound.



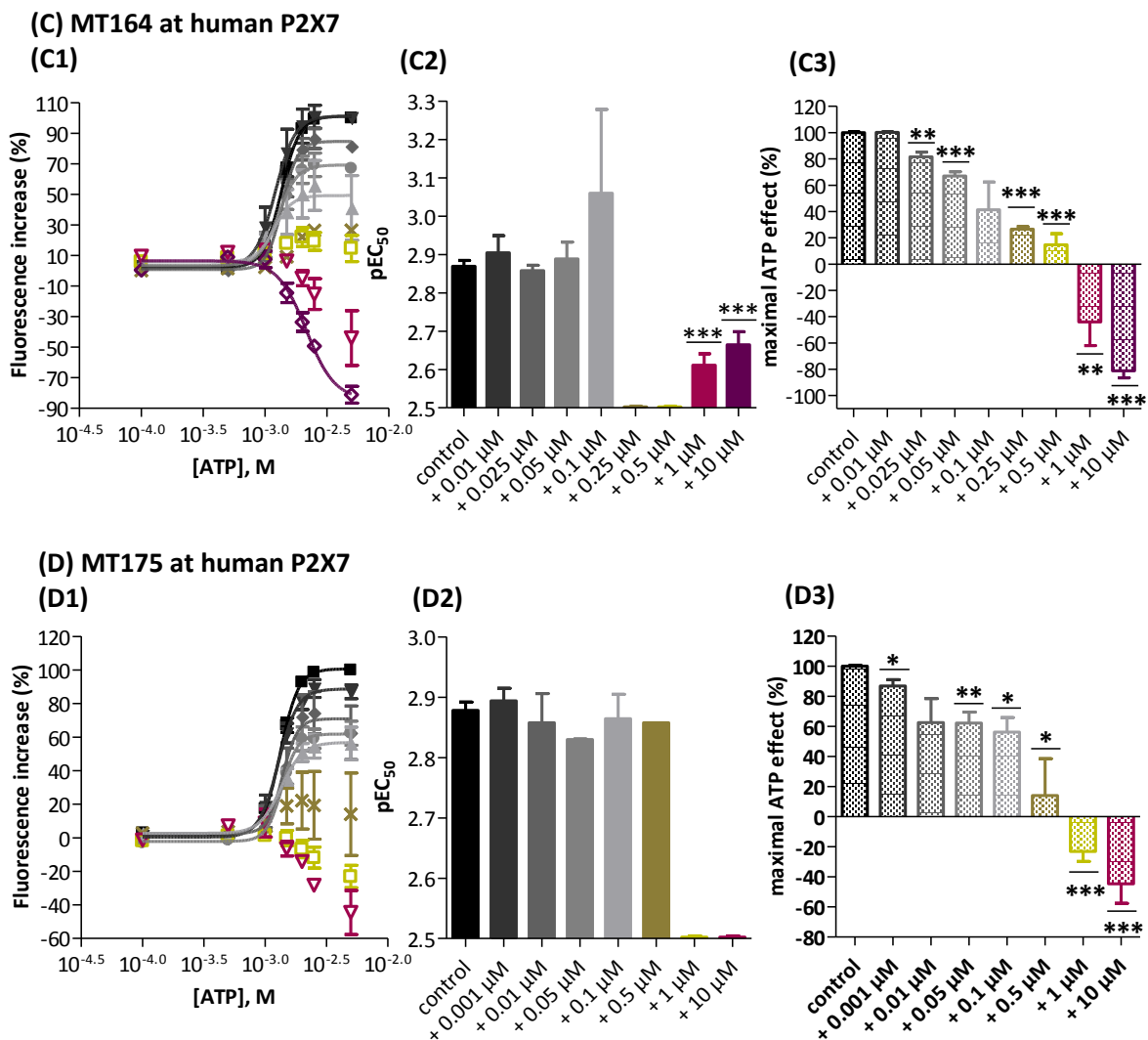
**Figure 5.9:** (A1-C1) Mean ATP dose response curves, (A2-C2) ATP pEC<sub>50</sub> values and (3) maximal ATP effect (A) niclosamide, (B) MT164 and (C) MT175 at the rat P2X3 receptor. Cells were incubated with compounds concentrations 0.001  $\mu$ M (▼), 0.01  $\mu$ M (◆), 0.05  $\mu$ M (●), 0.1  $\mu$ M (▲) and 0.5  $\mu$ M (×) prior to stimulation with ATP 0.0001 to 10  $\mu$ M, respectively. Buffer containing 1% DMSO without compound was used as control (■). The unpaired Student's t-test for significant differences of means was conducted for pEC<sub>50</sub> values and maximal fluorescence increase. Significant differences ( $p < 0.05$ ) are marked with (\*), very significant differences ( $p < 0.01$ ) with (\*\*) and highly significant differences ( $p < 0.001$ ) with (\*\*\*). Data is presented as mean  $\pm$  SEM from 2 to 4 independent experiments.



**Figure 5.10:** (A1-C1) Mean ATP dose response curves, (2) ATP  $pEC_{50}$  values and (3) ATP 5 mM-induced fluorescence signal characterizing the influence of (A) bisacodyl 0.05  $\mu$ M-15  $\mu$ M and (B) niclosamide 0.01  $\mu$ M-10  $\mu$ M at the rat P2X3 receptor. Cells were incubated with respective compound concentration prior to stimulation with ATP 0.0001 to 10  $\mu$ M. Buffer containing 1 % DMSO without compound was used as control (■). The unpaired Student's t-test for significant differences of means was conducted for  $pEC_{50}$  values and maximal fluorescence increase. Significant differences ( $p < 0.05$ ) are marked with (\*), very significant differences ( $p < 0.01$ ) with (\*\*), and highly significant differences ( $p < 0.001$ ) with (\*\*\*). Data is presented as mean  $\pm$  SEM from 2 to 4 independent experiments.

No  $EC_{50}$  concentrations for bisacodyl at the P2X3 receptor could be calculated, so the compound was not tested at the P2X3 receptor in this experimental setting. All compounds diminished the maximal ATP effect at both receptors, while the  $EC_{50}$  concentration was barely affected. Therefore, a Schild plot analysis for determination of orthosteric receptor antagonism, where the receptor can always be activated to the full level upon agonist concentration increase, was not possible. The  $pEC_{50}$  values of ATP in presence and absence of various antagonist concentrations are presented in Figure 5.9 to Figure 5.11 A2-B2. They visualize the minor change

in ATP potency at the respective receptor subtype. MT164 and MT175 both reversed the fluorescence increase to a decrease when used at high concentrations above 0.5  $\mu\text{M}$ . The inversely proportional correlation between the maximal ATP effect and the concentration of antagonist with which cells were incubated prior to ATP injection is shown in Figure 5.9 to Figure 5.11 A3-D3, respectively. The higher the antagonist concentration, the lower was the maximal receptor activation level. Both observations indicate that bisacodyl, niclosamide, MT164 and MT175 are likely to be allosteric antagonists of P2X3 and human P2X7 receptors, respectively.



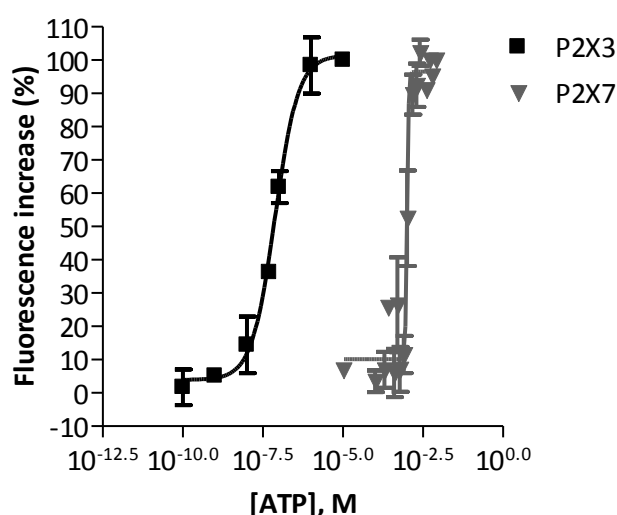
**Figure 5.11:** (A1-C1) Mean ATP dose response curves, (2) ATP  $pEC_{50}$  values and (3) maximal ATP effect characterizing the influence of (A) MT164 0.01  $\mu\text{M}$ -10  $\mu\text{M}$  and (B) MT175 0.001  $\mu\text{M}$ -10  $\mu\text{M}$  at the rat P2X3 receptor. Cells were incubated with respective compound concentration prior to stimulation with ATP 0.0001 to 10  $\mu\text{M}$ , respectively. Buffer containing 1% DMSO without compound was used as control (■). The unpaired Student's t-test for significant differences of means was conducted for  $pEC_{50}$  values and maximal fluorescence increase. Significant differences ( $p < 0.05$ ) are marked with (\*), very significant differences ( $p < 0.01$ ) with (\*\*), and highly significant differences ( $p < 0.001$ ) with (\*\*\*) Data is presented as mean  $\pm$  SEM from 2 to 4 independent experiments.

## 5.4 Enhancement of maximal ATP effect

An apparent increase of the maximal ATP effect was observed during the initial screening experiments of the drug library for some compounds, similar to the observation already discussed for the anthraquinone derivatives at the P2X3 receptor in chapter 3.4.2. The affected P2X receptor subtypes were rat P2X3 (14 enhancing hits) and human P2X7 (11 enhancing hits). Additional experiments were conducted to determine whether this observation could be attributed to a true binding effect or if it was a measuring error. Furthermore, it was tested whether the effect was concentration-dependent, and if the enhancement was due to agonistic effects.

### 5.4.1 ATP concentrations used for receptor stimulation

Prior to this experimental series, new cells carrying the P2X3 and P2X7 receptor had to be defrosted from liquid nitrogen and cultured. In order to characterize receptor expression, ATP curves of both cell lines were conducted at the beginning and for the P2X7 receptor also in between the respective experiments for investigation of enhancement. The  $EC_{50}$  concentrations determined were  $0.0760 \pm 0.0032 \mu\text{M}$  for r P2X3 and  $2.70 \pm 1.8 \text{ mM}$  for P2X7 receptors. Based on these results, the ATP concentration used in the enhancement experiments was adjusted to 2.5 mM for P2X7, in order to ensure 50% receptor stimulation. The concentration used for the P2X3 receptor remained unchanged at 0.05  $\mu\text{M}$  ATP.



**Figure 5.12:** Mean dose-response curves of ATP at P2X3 and P2X7 receptors. Data is presented as mean  $\pm$  SEM from 2-6 independent experiments.

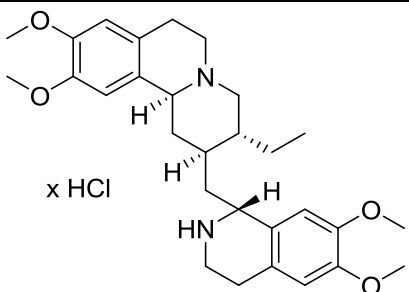
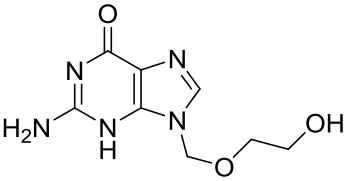
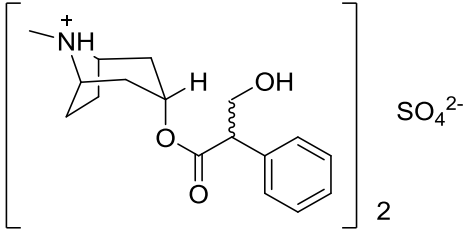
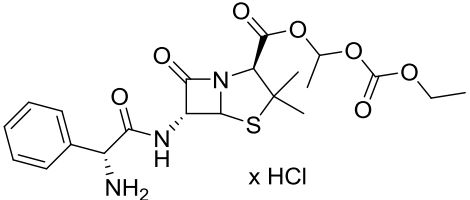


### 5.4.2 Enhancing hits at the rat P2X3 receptor

All enhancing hits detected during the initial screening experiments using 20  $\mu\text{M}$  final concentration were first tested in dose-response experiments using the 0.05  $\mu\text{M}$  ATP for receptor stimulation. The results are presented in Table 5.13.

Most drugs which enhanced the ATP-induced fluorescence signal during the initial screening did not show any concentration-dependent potentiation of ATP effect upon further characterization. Only one compound, emetine, a natural drug from ipecac root and clinically used as an anti-amoebic and antiemetic, did further increase the maximal ATP effect in a concentration-dependent manner by  $132 \pm 36\%$  in cells stimulated with  $\text{EC}_{50}$  concentration of ATP (0.05  $\mu\text{M}$ ).

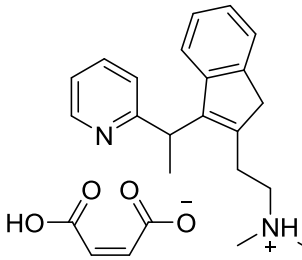
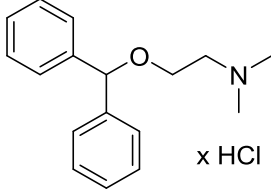
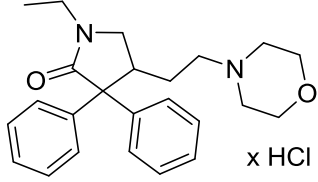
**Table 5.13:** Potency of enhancing hits of enhancing hits at the rat P2X3 receptor identified during initial screening experiments at 20  $\mu\text{M}$  final concentration. Data is presented as mean  $\pm$  SEM from 2-3 independent experiments

Name	Structure	$\text{EC}_{50\text{Enhancement}} \pm \text{SEM} [\mu\text{M}]$ or inhibition (%) at 20 $\mu\text{M}$
Emetine-HCl		$9.75 \pm 3.82$ (stimulation with ATP 0.05 $\mu\text{M}$ )  <b>n. c.<sup>a</sup></b> (stimulation with ATP 10 $\mu\text{M}$ )
Aciclovir		<b>n. c.<sup>b</sup></b> (-192 %)
Atropine sulfate		<b>n. c.<sup>b</sup></b> (-163 %)
Bacampicillin HCl		<b>n. c.<sup>b</sup></b> (-112 %)

Continuation of Table 5.13

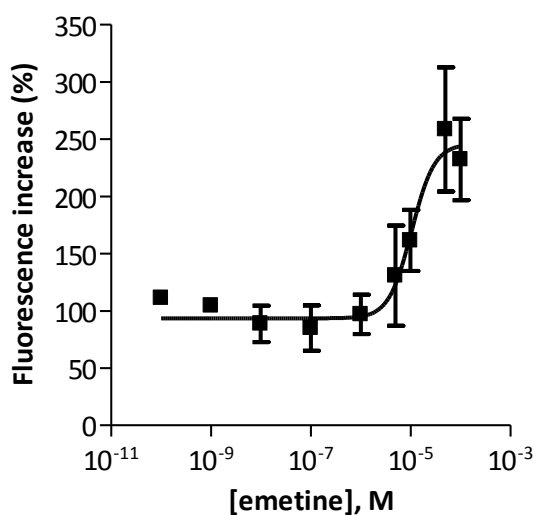
<b>Benzathine-Benzylpenicillin</b>		<b>n. c.<sup>b</sup> (-107 %)</b>
<b>Barbaloin</b>		<b>n. c.<sup>b</sup> (-168 %)</b>
<b>Benserazide HCl</b>		<b>n. c.<sup>b</sup> (-143 %)</b>
<b>Betamethasone dipropionate</b>		<b>n. c.<sup>b</sup> (-109 %)</b>
<b>Bezafibrate</b>		<b>n. c.<sup>b</sup> (-188 %)</b>
<b>Bromperidol</b>		<b>n. c.<sup>b</sup> (-102 %)</b>
<b>Brompheniramine maleate</b>		<b>n. c.<sup>b</sup> (-287 %)</b>

Continuation of Table 5.13

<b>Dimetindene maleate</b>		<b>n. c.<sup>b</sup></b> (-104 %)
<b>Diphenhydramine HCl</b>		<b>n. c.<sup>b</sup></b> (-108 %)
<b>Doxapram HCl</b>		<b>n. c.<sup>b</sup></b> (-124 %)

<sup>a</sup>: n. c. no convergence in 4 independent experiments<sup>b</sup>: n. c. no convergence in 2 independent experiments

When tested in cells stimulated with 10  $\mu\text{M}$  ATP, an increase of maximal receptor activation could be observed, but the concentration-response relation was inconclusive. This indicates that the magnitude of receptor enhancement is dependent on the agonist concentration. The concentration-response curve for the experiments with ATP 0.05  $\mu\text{M}$  is presented in Figure 5.13.



**Figure 5.13:** Mean dose-response curves of emetine at the P2X3 receptor, stimulated with ATP 0.05  $\mu\text{M}$ . Data is presented as mean  $\pm$  SEM from 3 to 4 independent experiments.

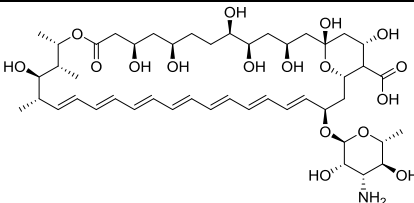
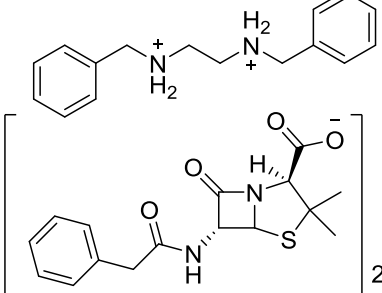
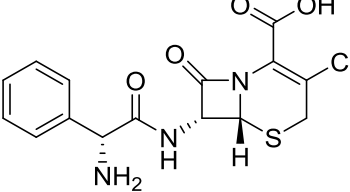
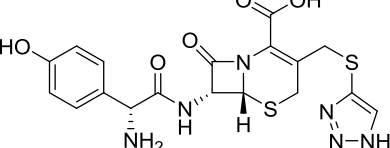
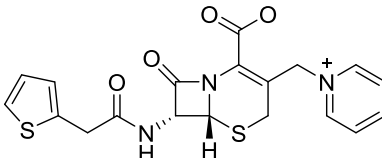
The enhancing effect may also be attributed to agonistic properties of the compound. An experiment was conducted in order to determine any agonism of emetine at the P2X3 receptor by injection of various compound concentrations between 0.0001 and 100  $\mu\text{M}$  instead of ATP. No fluorescence signal increase was detected. This excludes any agonistic activity of the compound.

The influence of a single concentration of enhancer on the  $\text{EC}_{50}$  concentration of ATP was determined for further characterization. The experiment is related to the determination of inhibition mechanism, which was discussed for various antagonists in chapters 3.4.1.3, 4.3.6, and 5.3.3. Cells were incubated with one single concentration of emetine (1  $\mu\text{M}$ , 10  $\mu\text{M}$  and 100  $\mu\text{M}$ , respectively), and then stimulated with various concentrations of ATP ranging from 10 to 5000  $\mu\text{M}$ . Although the ATP control experiment worked, the generation of dose-response curves under influence of any emetine concentration was not successful. The final mechanism how emetine is capable of enhancing the maximal ATP effect could not be further cleared through these experiments.

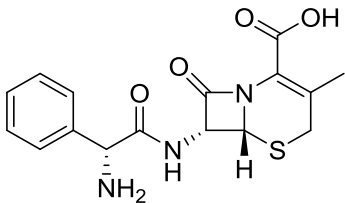
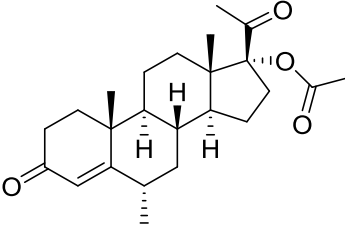
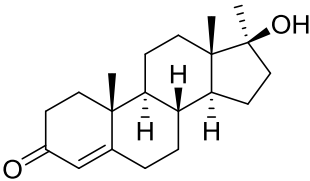
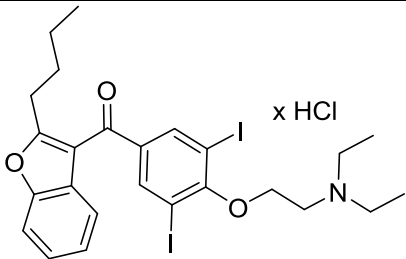
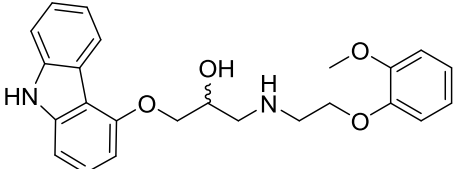
### 5.4.3 Enhancing hits at the human P2X7 receptor

Not all of the initially identified potential enhancers of P2X7 receptor could be confirmed. Table 5.14 gives an overview over all initially identified enhancing compounds and their enhancing potency at the P2X7 receptor.

**Table 5.14:** Potency of enhancing hits at the human P2X7 receptor identified during initial screening experiments at 20  $\mu\text{M}$  final concentration. Data is presented as mean  $\pm$  SEM from 2-4 independent experiments.

Name	Structure	$\text{EC}_{50\text{Enhancement}} \pm \text{SEM}$ [ $\mu\text{M}$ ] and inhibition $\pm$ SEM (%) at 20 $\mu\text{M}$ final concentration	Enhancement of maximal ATP effect $\pm$ SEM [%]
<b>P2X7</b>			
<b>Amphotericin B</b>		<b>3.90 <math>\pm</math> 3.39</b>	<b>56 <math>\pm</math> 24</b>
<b>Benzathine-benzylpenicillin</b>		<b>12.5 <math>\pm</math> 5.4</b>	<b>82 <math>\pm</math> 57</b>
<b>Cefaclor</b>		<b>&gt; 100</b>	<b>19 <math>\pm</math> 6</b> (at 100 $\mu\text{M}$ carvedilol)
<b>Cefatrizine</b>		<b>&gt; 100</b>	<b>54 <math>\pm</math> 10</b> (at 100 $\mu\text{M}$ cefatrizine)
<b>Cephaloridine</b>		<b>15.2 <math>\pm</math> 7.9</b>	<b>105 <math>\pm</math> 56</b>

Continuation of Table 5.14.

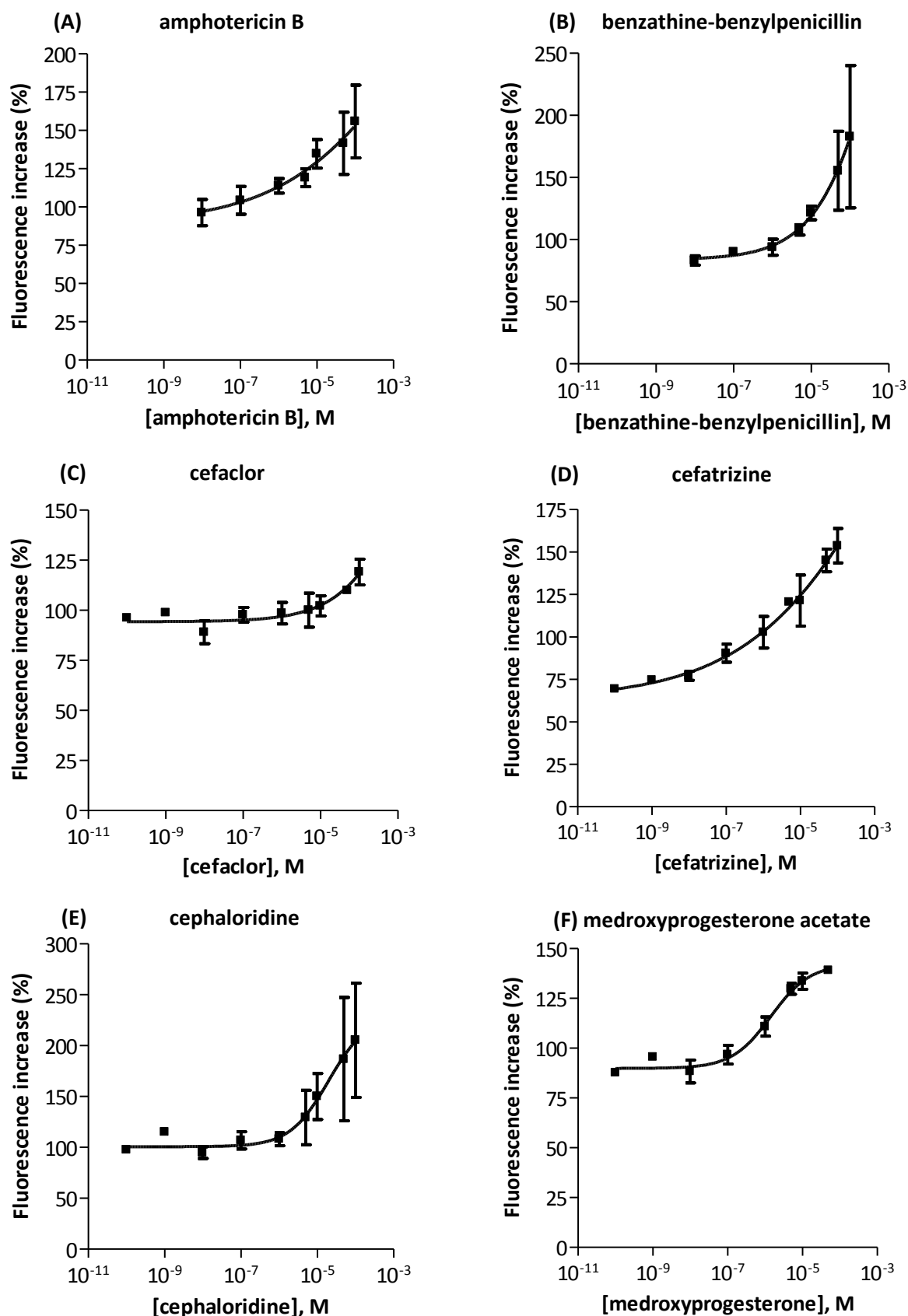
<b>Cephadrine</b>		<b>n. c.<sup>a</sup> (-142 %)</b>	-
<b>Medroxy-progesterone acetate</b>		<b>1.06 ± 0.56</b>	<b>39 ± 1</b>
<b>Methyl-testosterone</b>		<b>n. c.<sup>a</sup> (-92 %)</b>	-
<b>Amiodarone-HCl</b>		<b>n. c.<sup>a</sup> (-183 %)</b>	-
<b>Carvedilol</b>		<b>n. c.<sup>a</sup> (-102 %)</b>	-

<sup>a</sup>: no convergence in 2 independent experiments

Cefaclor and cefatrizin showed a concentration-dependent enhancement of maximal ATP effect, but the  $EC_{50\text{Enhancement}}$  concentration was calculated to be higher than 100  $\mu\text{M}$ , which was the highest concentration used. The experiment was successful for amphotericin B, benzathine-benzylpenicillin, cephaloridine and medroxyprogesterone acetate. The respective concentration-response curves are presented in Figure 5.14. When compared to the enhancing hits at the other receptor subtypes, a common structural feature could be detected. Cefaclor, cephaloridine, cephradine and cefatrizine are broad-spectrum antibiotics of the cephalosporin class. Benzylpenicillin, also known as penicillin G, the first known antibiotic, bears close structural relation to cephalosporins. Both classes belong to the so-called  $\beta$ -lactam antibiotics. Cephradine, cefatrizine and cephaloridine are part of the first generation cephalosporines. Cephradine is

orally available, same as the second generation drug cefaclor. Cephaloridine is unique among the cephalosporin antibiotics due to its zwitterionic nature. Like the penicillin drugs, cephalosporins act bactericidal by inhibition of penicillin-binding transpeptidases. This disrupts the bacterial cell wall synthesis, which leads to cell lysis. The diverging antibacterial activity of cephalosporins is attributed to side chain substitutions at position C7 in the lactam-ring. The bioavailability of oral cephalosporins is higher than 95 %. The drugs are eliminated rapidly from the blood in the space of two hours by renal excretion in their unchanged form.<sup>335</sup> Penicillin G was available in combination with benzathine, building a water soluble depot complex that is administered intramuscularly. A single dose of 1.2 million units leads to a maximal plasma concentration of 0.154  $\mu\text{M}$  in adults (0.14 mg/l).<sup>336</sup> Since the available stock solution contained the water-soluble depot complex, any effect could not be clearly attributed to benzathine or benzylpenicillin, respectively. The common structural feature indicated that the cephalosporin core could be a possible scaffold for positive modulators for purinergic P2X7 receptors. Since cephalosporins and penicillin are present in the blood, interaction with P2X7 receptors expressed in macrophages is possible, but the low plasma concentrations reached by intramuscular depot injection would not be high enough to cause any effect.

The  $\text{EC}_{50\text{Enhancement}}$  concentrations of cephalosporins were comparable, but the magnitude of enhancement showed considerable standard error for depot penicillin combination benzathine-benzylpenicillin and cephaloridine, and also varied between compounds. The highest enhancement of maximal ATP effect was determined for cephaloridine ( $105 \pm 56\%$ ), while the concentration-dependent enhancement measured for cefaclor was barely above the normal ATP-induced fluorescence signal ( $19 \pm 6\%$ ). Medroxyprogesterone acetate showed the best reproducibility, the lowest  $\text{EC}_{50\text{Enhancement}}$  concentration and the least standard error of all hits. None of the other steroidal drugs showed enhancement of maximal ATP effect to this extent. They are prone to show inhibition of calcium influx in stably transfected cells (see chapter 5.3.1.1).



**Figure 5.14:** Mean dose-response curves for determination of enhancement of maximal ATP effect of (A) amphotericin B, (B) benzathine-benzylpenicillin, (C) cefaclor, (D) cefatrizine, (E) cephaloridine and (F) medroxyprogesterone acetate at the P2X7 receptor. Data is presented as mean  $\pm$  SEM from 3 to 4 independent experiments.



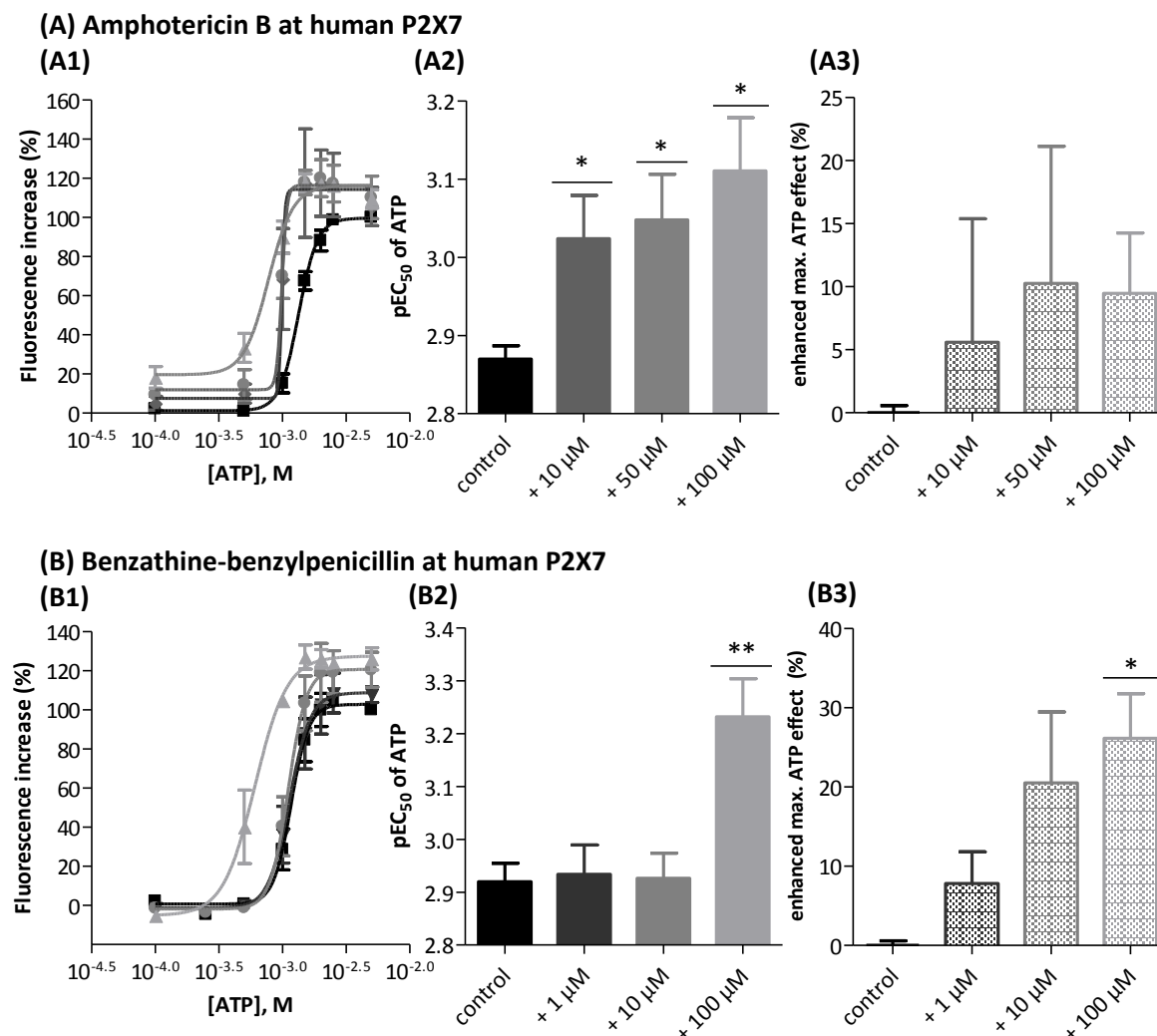
Medroxyprogesterone acetate is a synthetic derivative of the female sexual hormone progesterone. It structurally differs from progesterone by introduction of a methyl residue at carbon 6 and an acetate group at carbon 17, which enhances oral bioavailability and progestational potency. It is approved as a contraceptive and for postmenopausal hormone replacement therapy. In the Women's Health Initiative trial, the use of postmenopausal medroxyprogesterone acetate was associated with increased risk for the development of breast cancer and cardiovascular diseases. This led to a downturn of its use in postmenopausal osteoporosis prevention therapy. Medroxyprogesterone acetate is potent at both the androgen and the glucocorticoid receptor. The application of a 10 mg oral dose leads to peak serum concentrations between 0.0088  $\mu\text{M}$  and 0.011  $\mu\text{M}$  (3.4-4.4 ng/ml).<sup>337, 338</sup> These serum concentrations would be insufficient for any enhancing effect on the P2X7 receptor *in vivo*.

Despite the high structural similarity to medroxyprogesterone acetate, the enhancing effect of methyltestosterone was not quantifiable. This indicates that the acetyl residue in position 17 plays an important role for the positive modulating effect.

An experiment for testing whether the observed enhancement is due to agonistic activity of the drug itself was conducted for amphotericin B, benzathine-benzylpenicillin, cephaloridine and medroxyprogesterone acetate by injecting various concentrations of the respective drugs instead of ATP. No fluorescence signal increase for any compound was observed. The enhancing effect therefore cannot be attributed to any agonistic activity at the P2X7 receptor.

The influence of several single concentrations of the most active enhancers amphotericin B, benzathine-benzylpenicillin, cephaloridine and medroxyprogesterone acetate (1  $\mu\text{M}$ , 10  $\mu\text{M}$  and 100  $\mu\text{M}$  of all compounds, respectively, medroxyprogesterone acetate was additionally tested in a final concentration of 50  $\mu\text{M}$ ), on the  $\text{EC}_{50}$  concentration of ATP at the P2X7 receptor were tested. The respective ATP dose-response curves are presented in Figure 5.15 and Figure 5.16.

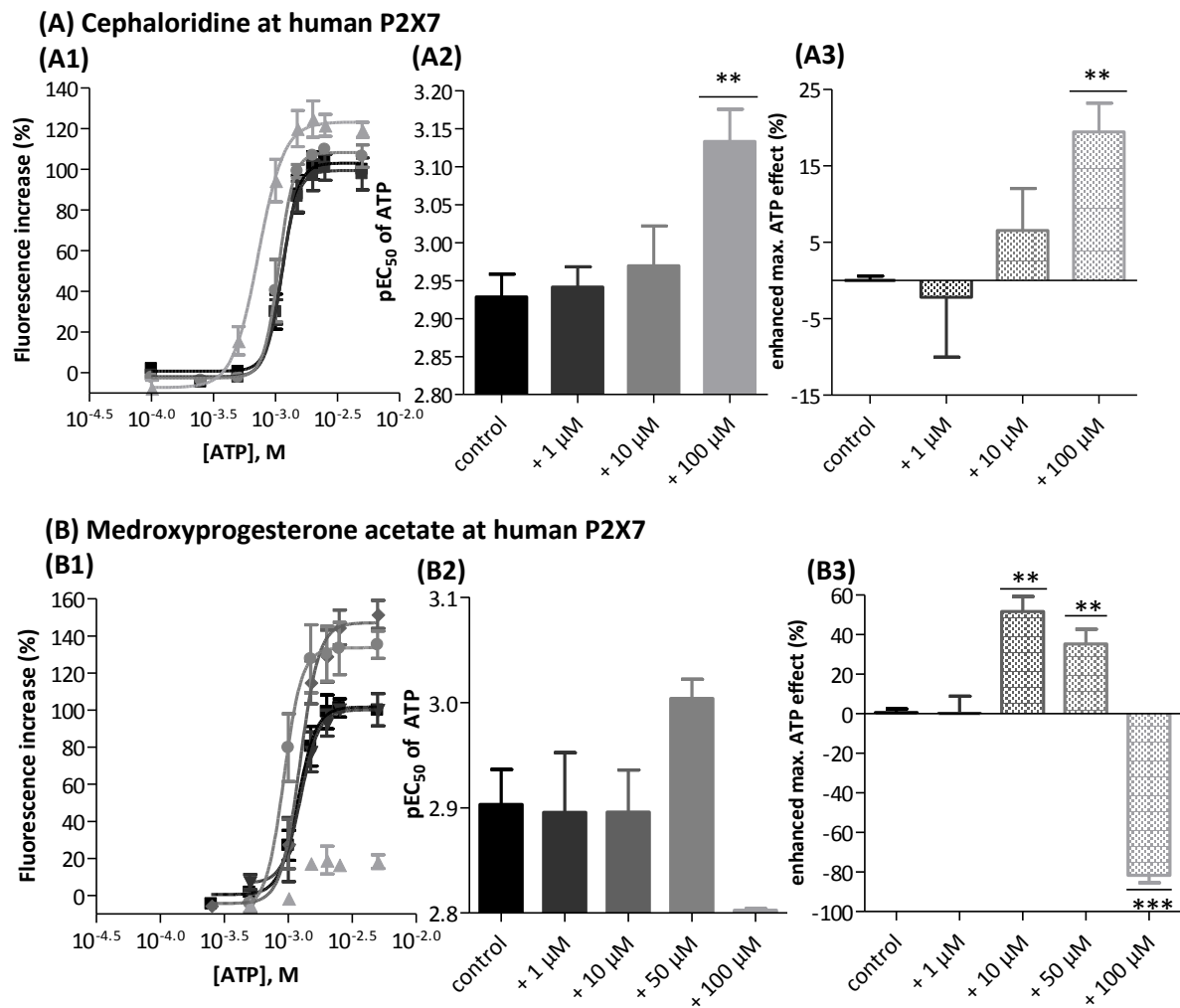
Amphotericin B, benzathine-benzylpenicillin and cephaloridine caused a shift of the ATP  $\text{EC}_{50}$  values to the left. The shift was prominent upon incubation with the highest concentration (100  $\mu\text{M}$ ). This indicates an increase of ATP affinity as a possible cause for the observed enhancement of receptor activity. The conclusion was supported by the marginal and non-significant effect of the different compound concentration on the maximal ATP effect, determined from the highest ATP concentration used in the experiment (5 mM).



**Figure 5.15:** (1) Mean ATP dose response curves, (2) ATP  $pEC_{50}$  values and (3) enhancement of maximal ATP effect characterizing the influence of (A) amphotericin B and (B) benzathine-benzylpenicillin at the human P2X7 receptor. Cells were stimulated with ATP 10  $\mu$ M-5000  $\mu$ M after preincubation with 1  $\mu$ M ( $\blacktriangledown$ ), 10  $\mu$ M ( $\blacklozenge$ ), 50  $\mu$ M ( $\bullet$ ) or 100  $\mu$ M ( $\blacktriangle$ ), respectively. Enhancement of fluorescence increase was calculated of cells stimulated with the highest ATP concentration (5 mM), with ATP control ( $\blacksquare$ ) based as 0%. The unpaired Student's t-test for determination of significant differences of means was conducted for  $pEC_{50}$  and enhanced fluorescence increase. Significant differences ( $p < 0.05$ ) are marked with (\*) and very significant differences ( $p < 0.01$ ) are marked with (\*\*). Data is presented as mean  $\pm$  SEM from 3-4 independent experiments.

A slight shift of the  $EC_{50}$  value to the left could be observed upon incubation with increasing concentrations of medroxyprogesterone acetate. The maximal ATP effect also increased. No ATP  $EC_{50}$  value and no fluorescence signal increase could be determined upon incubation with 100  $\mu$ M medroxyprogesterone acetate. The mismatch to the other three compounds tested indicates a different mechanism of enhancement that increases both the affinity of the

physiological ligand ATP and its effect. A different binding site or a variable conformational change upon the binding of the ligand could be the reason for this effect.



**Figure 5.16:** (1) Mean ATP dose response curves, (2) ATP pEC<sub>50</sub> values and (3) enhancement of maximal ATP effect characterizing the influence of (A) cephaloridine and (B) medroxyprogesterone acetate at the human P2X7 receptor. Cells were stimulated with ATP 10 μM-5000 μM after preincubation with 1 μM (▼), 10 μM (◆), 50 μM (●) or 100 μM (▲), respectively. Enhancement of fluorescence increase was calculated of cells stimulated with the highest ATP concentration (5 mM), with ATP control (■) based as 0 %. The unpaired Student's t-test for determination of significant differences of means was conducted for pEC<sub>50</sub> and enhanced fluorescence increase. Significant differences ( $p < 0.05$ ) are marked with (\*), very significant differences ( $p < 0.01$ ) are marked with (\*\*), and highly significant differences ( $p < 0.001$ ) are marked with (\*\*\*). Data is presented as mean  $\pm$  SEM from 3-4 independent experiments.

### 5.5 Discussion

A library containing 440 approved drugs was tested at human P2X receptor subtypes P2X1, P2X2, P2X4, P2X7 and rat receptor mutant P2X3. Several hits were detected. Three compounds, bromperidol, ambroxol and flavoxate were identified as selective antagonists at the P2X1 receptor with micromolar potency. No inhibitory or enhancing potency at the other P2X receptor subtypes was detected for both drugs when tested at 20  $\mu$ M final concentration. Furthermore, bisacodyl and niclosamide were determined as potent antagonists at the P2X3 and the P2X7 receptor, respectively. A library of derivatives closely related to niclosamide was already available. A small sublibrary with structurally similar compounds was newly synthesized based on bisacodyl, and SARs were analyzed.

Niclosamide is approved as an antihelmintic agent against infections with *Taenia saginata*, *Taenia solium*, *diphyllobothrium latum* and *hymenolepis nana* (beef, pork, fish and dwarf tapeworm) under the tradename Yomesan<sup>®</sup>. The treatment lasts for one day, consisting of four single doses of 500 mg. In case of an infection with *Hymenolepis nana*, another two chewable tablets have to be taken until day 7.<sup>339</sup> The antihelmintic effect is attributed to inhibition of oxidative phosphorylation and a stimulation of adenosine triphosphatase activity in mitochondria of the cestodes, leading to cell damage and its promoting digestion by the infected host. It is well tolerated in humans.<sup>340, 341</sup> The absorption of the drug from the gastrointestinal system is relatively low, which is attributed to the poor water solubility of the drug.<sup>342</sup> Pharmacokinetic studies in mice reveal maximal plasma concentrations of 893.7 ng/ml (2.73  $\mu$ M), that decreases to 40-50 ng/ml (0.122-0.153  $\mu$ M) within 30-45 minutes and rebounds to 78 ng/ml (0.238  $\mu$ M) at 1.5 hours after oral application of 200 mg/kg niclosamide.<sup>343</sup> Another pharmacokinetic study in rats describes a maximal plasma concentration of  $354 \pm 152$  ng/ml ( $1.08 \pm 0.46$   $\mu$ M) at 30 minutes that decrease to  $83.6 \pm 31.7$  ng/ml ( $0.256 \pm 0.097$   $\mu$ M) after 1 hour and to  $37.5 \pm 10.6$  ng/ml ( $0.115 \pm 0.032$   $\mu$ M) at 2 hours after an oral dose of 5 mg/kg. After 24 hours, the plasma concentration was lower than 0.5 ng/ml, the limit of quantitation. The bioavailability was 10 % of the oral dose.<sup>344</sup> These plasma concentrations are high enough to inhibit P2X3 and P2X7 receptors *in vivo* when compared to our results. Niclosamide is physiologically metabolized in the liver via CYP1A2 by hydroxylation to 3-hydroxy-niclosamide and glucuronidated by UGT1A1 in position 2.<sup>345</sup> Besides its long known antihelmintic properties, niclosamide was recently discovered as a potent agent in a broad variety of diseases and targets. It is reported to inhibit the Wnt/ $\beta$ -catenin pathway in ovarian cancer stem cells, downregulating cell proliferation and increasing cell death.<sup>346</sup> The Wnt/ $\beta$ -catenin pathway is an important part in organ and tissue development and homeostasis. More than 80 % of hereditary cancers of the

gastrointestinal system have been associated with hyperactivity of the Wnt/ $\beta$ -catenin pathway due to mutations mainly in the APC, but also in  $\beta$ -catenin or axin 2 genes.<sup>347</sup> There are several hints that the mechanism of niclosamide-induced inhibition of Wnt/ $\beta$ -catenin pathway depends on the cancer cell line used in the respective experiments.<sup>348, 349</sup> Other targets affected by niclosamide are the mammalian target of rapamycin complex 1 (mTORC1), which plays an important role in the expression of mRNAs essential for cell growth and metabolism, the STAT3 pathway and NF $\kappa$ B signaling.<sup>341, 350-352</sup> The inhibition of cell growth and promotion of cell death make niclosamide a suitable candidate for clinical development as a new and potent anticancer agent for the treatment of aggressive tumors like glioblastoma, prostate cancer to diminish resistance to antiandrogen enzalutamide or lung cancer to reduce radioresistance.<sup>351, 353, 354</sup> Haygood et al. describe the *in vitro* anticancer activity of two niclosamide derivatives. One of the two was identical to MT170, which was part of the hydroxybenzamide library. The compounds were tested on cells harvested from ascites and tumor samples of patients suffering from ovarian cancer. Cells were incubated with the test compound for 48 hours. Cell viability was determined by the ATPlite luminescence-based assay, yielding IC<sub>50</sub> values of 0.1-5  $\mu$ M for niclosamide and 0.15-5  $\mu$ M for MT170.<sup>355</sup> These values are comparable to the inhibitory potency determined at the P2X7 receptor in this experimental setting, and lower than its potency at the P2X3 receptor. The P2X7 subtype was associated to play an important role in solid tumor progression, although it cannot be determined clearly whether the inhibition or enhancement of receptor activity reduces cancer progression.<sup>178</sup> It is possible that the inhibition of the P2X7 receptor by niclosamide and its derivatives contributes to the anticancer effect of the drugs.

Furthermore, the P2X7 receptor is involved in inflammatory processes due to its widespread expression in immune cells.<sup>178</sup> It is also associated with chronic pain, which often occurs in tandem with cancer in late stages, as is the P2X3 receptor.<sup>356</sup> No evidence could be found that niclosamide was ever tested in a pain model, but one study demonstrates its ability to modulate the function of dendritic cells and reduce the production of inflammatory cytokines and the antigen specific T-cell responses. Niclosamide dose-dependently reduced the release of pro-inflammatory cytokines and chemokines in lipopolysaccharide-stimulated mature mouse bone marrow-derived dendritic cells. The concentrations used were between 0.3125  $\mu$ M and 1.25  $\mu$ M.<sup>357</sup> Since P2X7 receptors are also expressed in these cells and have previously been associated to have a proinflammatory effect by influencing the activity of IL-1 $\beta$ , it is possible that they could be the mediating factor of niclosamide effect. Currently, the theory cannot be proven, since the exact mechanism of niclosamide action in dendritic cells is not yet determined.

The role of niclosamide in inhibition of Wnt/ $\beta$ -catenin pathway and internalization of Frizzled receptor was recently further investigated. The Frizzled receptor consists of seven transmembrane regions. It is activated by secreted Wnt glycoproteins together with the single transmembrane receptor LRP5/6. The binding of Wnt leads to activation of the cytosolic protein Dishevelled, which forces internalization of the Frizzled receptor. Niclosamide has previously been associated with downregulation of Dishevelled,  $\beta$ -catenin and Wnt-signaling in general. In order to improve its pharmacokinetic properties without loss of inhibitory potency on the Wnt/ $\beta$ -catenin pathway, several derivatives of niclosamide were synthesized and evaluated. Some of these derivatives are identical to members of the library tested in our experiments. The concerned compounds are MT170, MT301, MT304 and MT310 the derivatives with a single residue ( $\text{NO}_2$ ,  $\text{CF}_3$  or Cl) introduced in position 4, MT167 and MT188 with a single residue ( $\text{CF}_3$  or Cl) introduced in position 3 and MT179 with two chlorine residues introduced in position 3 and 5 of ring B of the niclosamide scaffold respectively. Internalization of Frizzled 1 receptor was determined via confocal microscopy in cells stably transfected with the receptor linked to YFP. Furthermore, the inhibition of Wnt/ $\beta$ -catenin was measured via TOPflash reporter assay. The observed  $\text{IC}_{50}$  values of the respective compounds were in the high nanomolar to low micromolar range. High nanomolar inhibitory potency was always connected to high internalization of the Frizzled 1 receptor. The highest potency was detected for the compound MT170 with an  $\text{IC}_{50}$  value of  $0.29 \pm 0.06 \mu\text{M}$ .<sup>358</sup> The potency determined in our experiments at the P2X3 receptor was either comparable or at least tenfold higher than described for the inhibition of the Wnt/ $\beta$ -catenin pathway, including the lead compound niclosamide. The inhibitory potency at the P2X7 receptor was comparable to the values described in the Wnt/ $\beta$ -catenin study.

Guo et al. describe a direct connection between the P2X7 receptor and the Wnt/ $\beta$ -catenin pathway. In E10 cells stably transfected with P2X7, a downregulation of Wnt/ $\beta$ -catenin signaling was observed upon P2X7 receptor stimulation with BzATP. The activation of the P2X7 receptor is associated with an increase in apoptosis and cell death in HEK293, A549, H441 RLE-6TN and RFL-6 cancer cell lines.<sup>359</sup> However, the activation of the P2X7 receptor in several melanoma cell lines was associated with reduced apoptosis and cell death.<sup>360, 361</sup> Inhibition of both Wnt/ $\beta$ -catenin and P2X7 receptor signaling could mean a beneficial effect in both enhancing apoptosis and reduction of inflammation.

P2X3 receptors are mainly found in the central nervous system. So far, the receptor was not associated with immune response or management. Niclosamide therefore could be a potential candidate for chronic pain treatment, since P2X3 receptors were identified to be a particular

part of this. An experiment to determine antinociceptive effects of niclosamide in a chronic pain or cancer pain model could help determining its benefit on this matter further.

The high inhibitory potency of the niclosamide derivatives at P2X3 and P2X7 receptors suggests that various patterns of small hydrophilic and lipophilic substituents introduced at rings A and B are well tolerated by both receptor subtypes. Although the sublibrary contained compounds with various substitution patterns, P2X receptor selectivity could not be obtained. Furthermore, the compounds were first developed as potent antagonists of the human P2X1 receptor, and the preliminary data indicates that nearly all compounds have comparable or less potency at both P2X3 and P2X7 receptors than this intended target (data not yet published). For compounds MT303, MT283, MT304, MT282 and MT309, a considerable selectivity at the P2X3 receptor could be observed, with almost 100-fold selectivity towards the human P2X1 receptor ( $IC_{50}$   $1.66 \pm 0.49 \mu\text{M}$ ,  $8.00 \pm 2.01 \mu\text{M}$ ,  $> 10 \mu\text{M}$ ,  $13.5 \pm 1.3 \mu\text{M}$  and  $7.62 \pm 2.98 \mu\text{M}$  at P2X1, respectively). MT282 also displayed over 20-fold selectivity towards the P2X7 in comparison to the P2X1 receptor. Since the human stable P2X3-2 receptor mutant could not be expressed successfully in 1321N1 astrocytoma cells after retroviral transfection, a test for species selectivity of niclosamide derivatives was not possible. No assumption can be made if niclosamide derivatives are also candidates for selective P2X3 receptor ligand development in humans. If the selective potency can be confirmed in humans, these five structures could be the basis for further drug development.

Bisacodyl was identified as a very potent and interesting hit at human P2X7 and rat P2X3 receptors. The initially detected high inhibitory potency at the P2X3 receptor could not be confirmed during concentration-response experiments. Bisacodyl was proven to be the most potent antagonist at the P2X7 receptor of this drug library. Bisacodyl is a laxative approved for the short-term treatment of obstipation and bowel evacuation prior to gastrointestinal surgery and diagnostic investigation.<sup>362</sup> It is rapidly cleaved to the active metabolite bis(*p*-hydroxyphenyl)-pyridyl-2-methane (BHPM) by deacetylases found on the intestinal mucosa and then glucuronidated extrahepatically in the gut wall. BHPM is identical to THV-B01, one member of the nine bisacodyl derivatives tested in our experiments. It is also the active metabolite of sodium picosulfate, a structurally closely related laxative, by cleavage of the sulfate residues by desulfatase enzymes of the colonic microflora. Bisacodyl and sodium picosulfate themselves are not absorbed into the body after oral application. A single oral dose of 10 mg bisacodyl leads to maximal plasma concentrations of 64.6 ng/ml of total BHPM (free and in its glucuronidated form). Free BHPM could not be measured in plasma.<sup>363</sup> The urinary excretion is reported to be  $3.4 \pm 0.5 \%$  up to  $9.2 \pm 3.3 \%$  when administered as tablet or suppository, and around 50 % of

one dose is eliminated as the active metabolite in the faeces. The urinary excretion increases up to  $43.4 \pm 15.0\%$ , when the drug is administered in solution.<sup>364, 365</sup> BHPM is subjected to an intensive cycle of metabolism. It is secreted again to the lumen after glucuronidation, where the glucuronide is cleaved and resorption in intestinal epithelial cells begins again. The laxative effect of bisacodyl is attributed to an increase of prostaglandin E<sub>2</sub> (PGE<sub>2</sub>). This leads to inhibition of Na<sup>+</sup>/K<sup>+</sup>-ATPase, resulting in raising the osmotic pressure in the intestinal tract. This again is associated with an enhanced secretion of sodium and potassium ions and water into the intestinal lumen.<sup>366, 367</sup> Ikarashi et al. found evidence that bisacodyl indirectly decreases the expression of aquaporine water channels, which play a very important role in intestinal water transport, by enhancing the secretion of PGE<sub>2</sub>. The laxative effect was therefore rather associated with the inhibition of water resorption due to a deprivation of aquaporine water channels in the epithelial mucosa of the intestine than to an increase of osmotic pressure in the lumen, as was assumed previously.<sup>368</sup> P2X7 receptors have mainly been associated with inflammatory processes in the gastrointestinal tract, but not in normal healthy GI tissue in rats.<sup>369</sup> No information can be found which supports the idea that P2X7 as a channel capable of performing pores is also involved in the water resorption process in the colon. It is therefore unlikely that the inhibitory effect of bisacodyl detected in this experimental series can contribute to the laxative mode of action of the drug. The test of the cleaved and etherified bisacodyl derivatives indicates that the ester moieties are essential for successful P2X7 receptor inhibition. The derivatization shifts the affinity of the compounds towards the rat receptor mutant P2X3, which is another indication that P2X7 receptors are most likely not involved in the mode of action of bisacodyl. Furthermore, bisacodyl itself is not the laxative compound, but its hydrolyzed metabolite BHPM. THV-B01, which is equivalent to BHPM, did not show inhibitory potency at P2X7 higher than 50 %. Concentration-response experiments were not successful. Sodium picosulfate, a closely related laxative drug like bisacodyl, did also not show any inhibitory potency at the P2X7 receptor at 100  $\mu$ M. The results show that the P2X7 receptor is not a part of the mechanism of action of bisacodyl.

The active metabolite BHPM (THV-B01) was a potent antagonist at the P2X3 receptor with low nanomolar potency, as were the etherified derivatives. Since P2X3 receptors are widely expressed in the gastrointestinal nervous system and mainly associated with perception and forwarding of pain signals, these findings could be the start for the development of new ligands with primarily gastrointestinal located action.<sup>370</sup> It is possible that the P2X3 receptor is a previously unknown part of the molecular mechanism of bisacodyl efficacy in the colon.



Furthermore, most of the compounds seem to be selective for the P2X3 receptor. The determination of affinity at the human P2X3 receptor will complete the picture.

A lot of the drugs were initially identified as potential enhancers at human P2X1, P2X7 and rat P2X3 receptor. Most of them were identified as false hits. Only one compound at the P2X3 (emetine) and four compounds at the P2X7 receptor demonstrated a dose-dependent and reproducible ATP-induced enhancement of receptor function. Among those four compounds were two antibiotics, one penicillin and one cephalosporin. Furthermore, two additional cephalosporin antibiotics, cefaclor and cefatrizine, were demonstrated to enhance ATP-induced receptor activity. They were not the first PAMs identified for the P2X7 receptor. Nörenberg et al. identified clemastine as a potent and potentially selective positive enhancer at the P2X7 receptor. The enhancing effect was found to be concentration-dependent, did not occur in the absence of agonist, and was caused by an increase of ATP potency and not by an increase of maximal receptor activity.<sup>197</sup> Clemastine was also part of the drug library tested here. In the initial screening, the results of Nörenberg et al. could be confirmed, but concentration-response experiments showed inhibition of P2X7 receptor at concentrations above 10  $\mu$ M and no enhancement of ATP activity at all. It is possible that the enhancing effect of clemastine is dependent on the ATP concentration used for receptor stimulation. Nörenberg et al describe an increased sensitization of P2X7 to its physiological agonist ATP resulting in full receptor activation at non-saturating ATP concentrations.<sup>197</sup>

Ivermectin was also identified as a PAM at human P2X7, which was not observed in this experimental setting.<sup>156</sup> Instead, ivermectin was identified as an antagonist at the human P2X1 and rat P2X3 receptor with inhibitory potency in the low micromolar range, and showed neither inhibitory nor enhancing activity at the P2X7 and the P2X2 receptor. The lack of enhancement at the P2X7 receptor correlates with previous findings indicating ivermectin to be relatively selective towards the P2X4 receptor.<sup>101</sup> Other previously identified PAMs of the P2X7 receptor are phenothiazine antipsychotics prochlorperazine and trifluoperazine, which were not part of the drug library tested in these experiments here.<sup>193</sup> The structurally related compounds fluphenazine and perphenazine did not show enhancing but weak inhibitory potency at human P2X7 receptor. Therefore, the enhancing effect at P2X7 most likely cannot be attributed to all phenothiazine compounds per se. Literature demonstrates that positive allosteric modulation of P2X receptors is no rarity and can be observed for a variety of drugs and compounds. For further confirmation of their enhancing effect, penicillin and cephalosporin antibiotics should be tested in an independent experiment to confirm their allosteric enhancing capabilities and further characterize their affinity and efficacy.

### 6 Summary

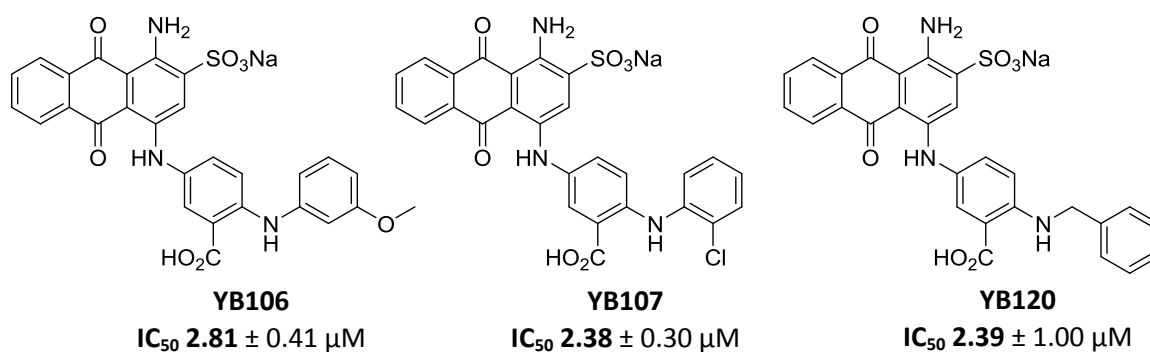
P2X receptors are widely expressed in the body. They are associated with numerous physiological and pathophysiological processes such as cancer, inflammation and pain, which make them important targets for drug development. Several selective antagonists have already been described for the P2X3 and the P2X7 receptor. The published antagonists for P2X1, P2X2 and P2X4 receptors either show only moderate potency or are not selective towards one P2X subtype.

#### **Characterization of the S15V mutant of the rat P2X3 receptor and use for library screening**

The pharmacological testing of P2X1 and P2X3 receptors is complicated by their fast desensitization upon agonist stimulation. In order to enable pharmacological evaluation at the rat P2X3 receptor, a stable non-desensitizing receptor mutant was created by exchange of the amino acid serine in position 15 to valine (S15V). The mutant (P2X3) was then used for the testing of a library of anthraquinone derivatives synthesized by Dr. Younis Baqi by measurement of calcium influx. The aim was:

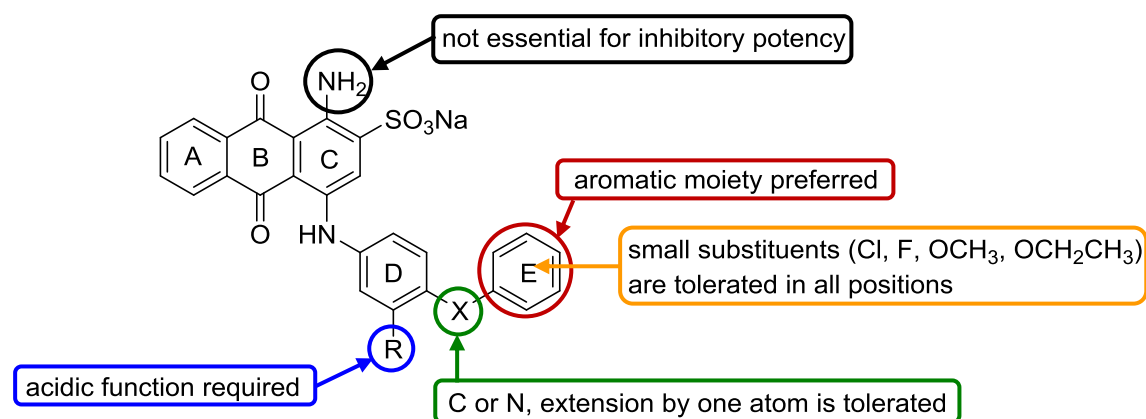
- (i) to determine whether the new mutant is suitable for high throughput screening via calcium measurement and
- (ii) the identification of new P2X3 receptor ligands.

The Z'-factor was calculated for assessing the quality and reliability of the assays. An average value of  $0.64 \pm 0.02$  was determined which demonstrates the suitability of the assay using the receptor mutant for high-throughput screening experiments. The testing of an anthraquinone compound library led to the identification of several antagonists for the P2X3 receptor. The most potent compounds shared common structural features. Selected antagonists and their respective  $IC_{50}$  values are presented in Figure 6.1.



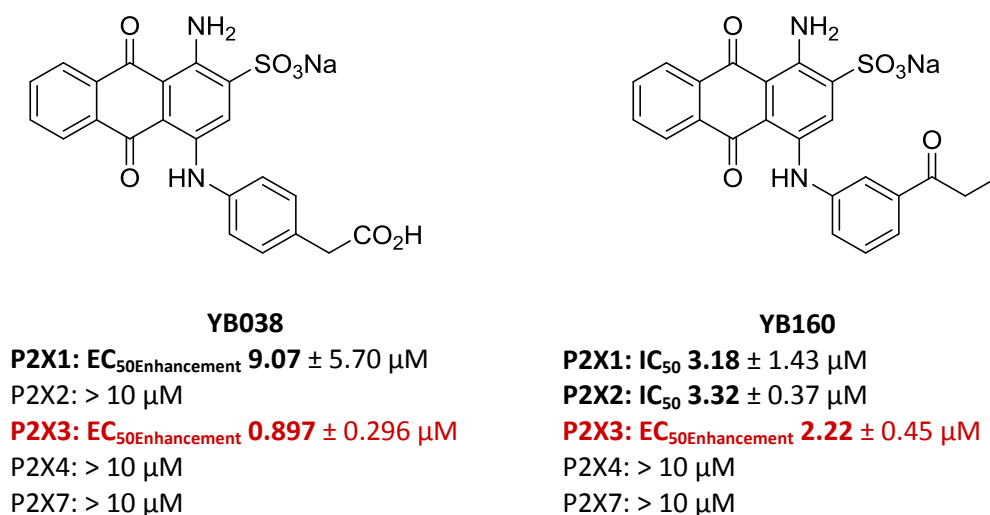
**Figure 6.1:** Structures and inhibitory potencies of three of most potent newly identified P2X3 receptor antagonists, the anthraquinone derivatives YB106, YB107 and YB120.

The structure-activity relationships of anthraquinone derivatives are summarized in Figure 6.2. ATP curve shift experiments with the antagonist YB120 indicated a competitive mode of inhibition.



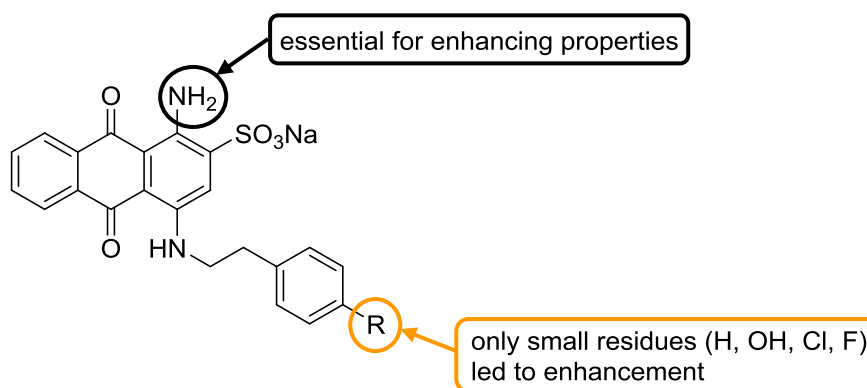
**Figure 6.2:** Summary of structure-activity relationships of anthraquinone derivatives with inhibitory potency at the P2X3 receptor.

Several of the investigated anthraquinone derivatives showed positive allosteric modulation of the P2X3 receptor. Structures of positive allosteric modulators (PAMs) differed from those of antagonists. Selected potent PAMs are displayed in Figure 6.3.



**Figure 6.3:** Selected anthraquinone derivatives that showed positive allosteric modulation of the P2X3 receptor.

The enhancing properties were dependent on the compound concentration and on the ATP level. The compounds were not active in the absence of ATP. Some of the identified PAMs showed a common structural feature. The scaffold and the structure-activity relationships are presented in Figure 6.4.



**Figure 6.4:** Structure-activity relationships of anthraquinone derivatives with positive modulating properties at the P2X3 receptor.

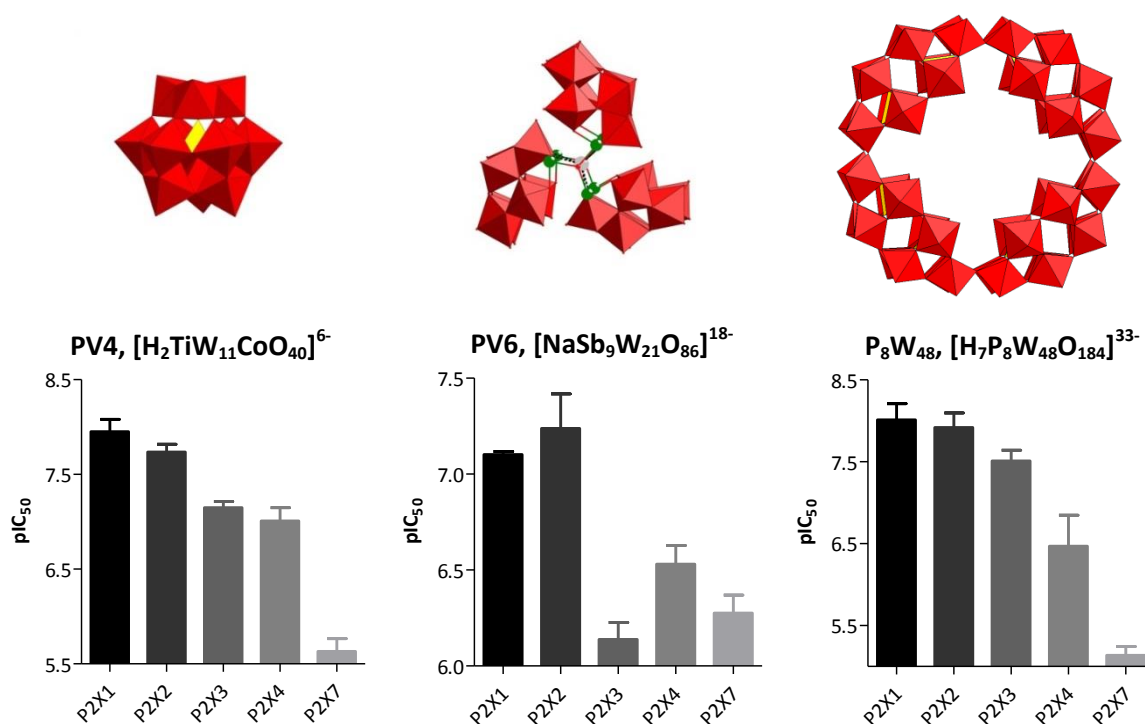
Our study demonstrated that the S15V mutant of the rat P2X3 receptor is suitable for fluorescent measurements of agonist-dependent calcium influx, and that anthraquinone derivatives are potent modulators of P2X3 receptors.

### Inhibitory potency of polyoxometalates at P2X receptors

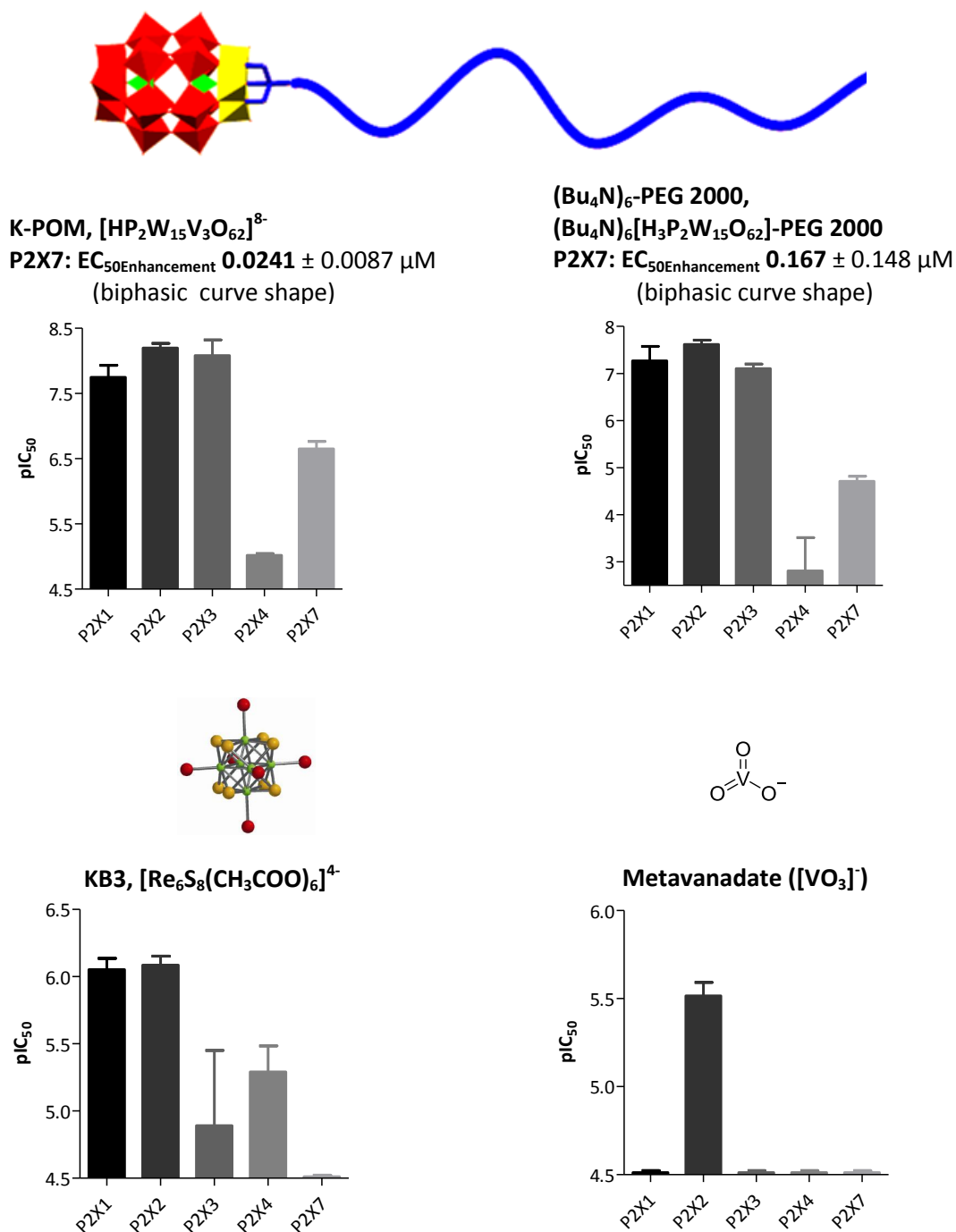
POMs are inorganic transition metal clusters with high negative charges and diverse three-dimensional shapes. They have previously been demonstrated to be potent inhibitors of nucleotide-degrading enzymes, namely NPPs, NTPDases and ecto-5'-nucleotidases.<sup>221, 271</sup> The investigated POM library contained seventeen polyoxotungstates, four rhenium-based compounds and two vanadium cluster compounds. The aim of our study was:

- the determination of inhibitory potency of POMs at P2X receptors
- to characterize the influence of PEGylation on the potency of POMs
- to determine the compounds' selectivity
- gain further insight into the mechanism of inhibition of P2X receptors by POMs.

Almost all of the metal cluster compounds were found to be potent antagonists of P2X receptors. The most potent compounds are presented in Figure 6.5 and Figure 6.6.



**Figure 6.5:** Structures and potencies of selected polyoxotungstates at P2X receptors.



**Figure 6.6:** Structures and potencies of selected POMs and related cluster compounds at P2X receptors.

Compound selectivity could be demonstrated for some polyoxotungstates versus the P2X4 and P2X7 receptors, at which they were less potent. The inhibitory potency at P2X1, P2X2 and P2X3 receptors was comparable in most cases. The rhenium clusters showed weaker potency at P2X receptors than the polyoxotungstates. KB1 and KB2 were the only POMs that preferably inhibited the P2X2 over the P2X1 receptor. Of the vanadium-based compounds, the

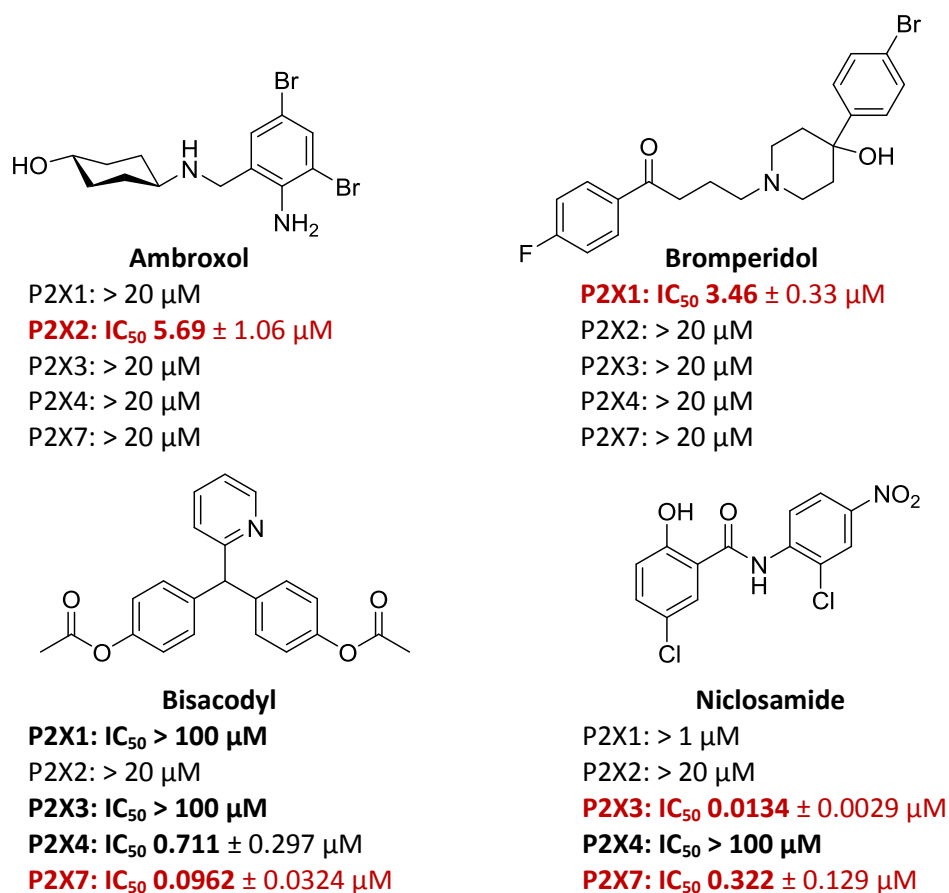
metavanadate was able to inhibit the P2X2 but none of the other P2X subtypes. Orthovanadate did not show inhibitory potency at any of the P2X receptor subtypes. The non-PEGylated compound K-POM was the most potent antagonist of the library with low nanomolar potency at P2X1 and P2X2 receptors. Its PEGylation resulted in only a minor decrease in potency. All PEGylated compounds as well as their two non-PEGylated precursors showed biphasic curves at the P2X7 receptor with concentration-dependent enhancement of receptor activity followed by inhibition. ATP shift curves and subsequent Schild plot analyses indicated that several POMs are orthosteric antagonists of P2X receptors. Cell viability assays (MTT) revealed a large separation between P2X receptor blocking and cytotoxic concentrations. It could be demonstrated that POMs are potent but non-selective antagonists of P2X receptors.

### **Interaction of approved drugs with P2X receptors**

A library of 440 approved drugs of widespread indications and diverse structures were screened at 20  $\mu$ M final concentration. Compounds inhibiting the receptors by more than 50 % at 1  $\mu$ M were further investigated by recording of concentration-response curves. Selected potent hit compounds are presented in Figure 6.7.

Ambroxol was identified as a selective antagonist of the P2X2 receptor. The drug is approved as an expectorant for children and adults. It increases mucin secretion, mucus hydration and the production of surfactant in the lung. The drug may be suitable as a lead structure for the development of new potent and selective P2X2 receptor antagonists.

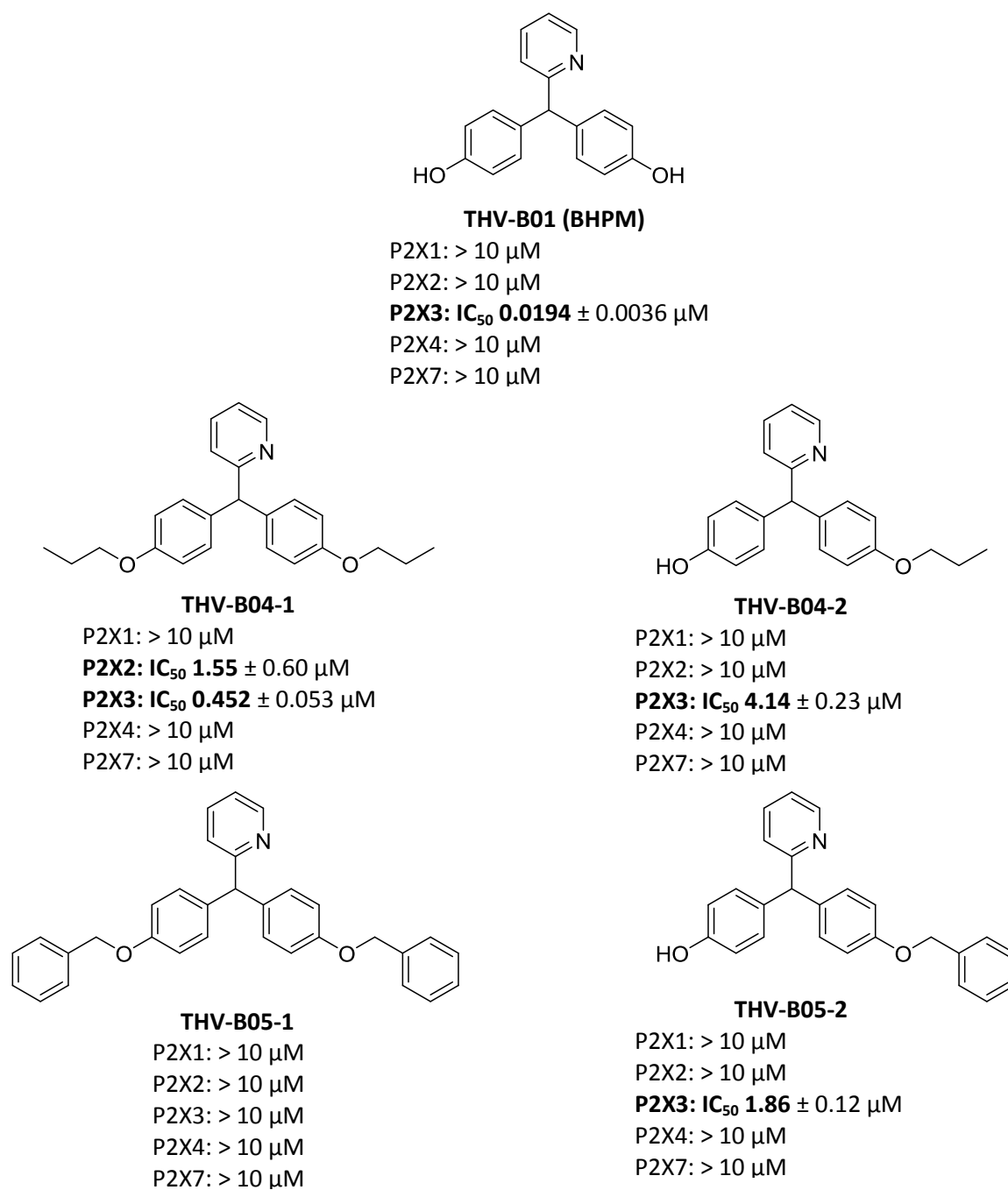
The antipsychotic drug bromperidol, a dopamine D<sub>2</sub> antagonist, was identified as a selective antagonist at the P2X1 receptor. Due to the high potency and selectivity, the compound might be a good candidate for the development of new, selective P2X1 receptor antagonists.



**Figure 6.7:** Structure and inhibitory potency of selected hit compounds of the drug library at P2X receptors.

Bisacodyl is approved as a laxative for the treatment of chronic obstipation. We discovered that it acts as a potent antagonist of the P2X4 and the P2X7 receptor with eight-fold selectivity for the P2X7 versus the P2X4 receptor. Due its high potency, a small library of derivatives based on the structure of bisacodyl was synthesized by The-Hung Vu. One of the compounds represents the hydrolysis product of bisacodyl, termed BHPM, which is believed to be the biologically active laxative agent that is formed from the prodrug bisacodyl in the gut wall. It is an even more potent P2X receptor antagonist with high selectivity for the P2X3 receptor subtype (IC<sub>50</sub> 19.4 nM). P2X3 receptor blockade may contribute to the pharmacological effects of bisacodyl. The etherification of the phenolic groups led to a reduction of inhibitory potency at the P2X3 receptor when compared to BHPM.

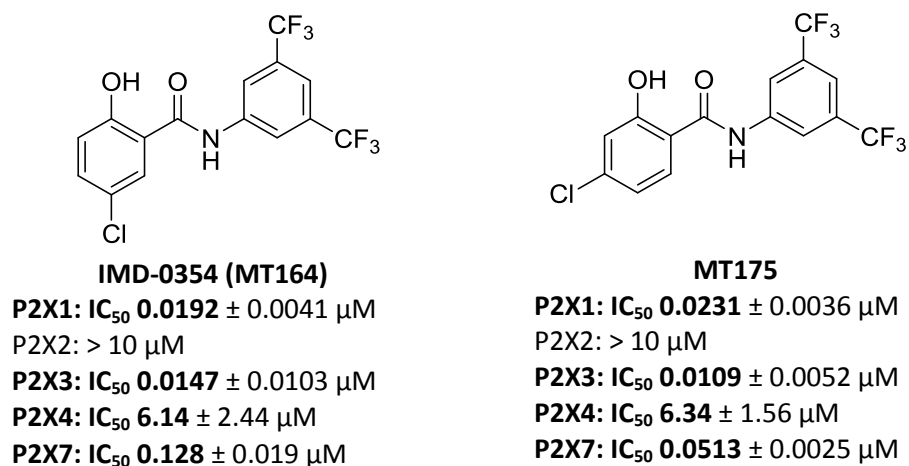




**Figure 6.8:** Structures and potencies of bisacodyl derivatives at P2X receptors. Data is presented as mean  $\pm$  SEM from 3-4 independent experiments.

Nicosamide was identified as a potent antagonist at both the P2X3 and the P2X7 receptor. It is approved as an antihelmintic drug and has recently been reported to also show anti-cancer activity.<sup>346, 351</sup>

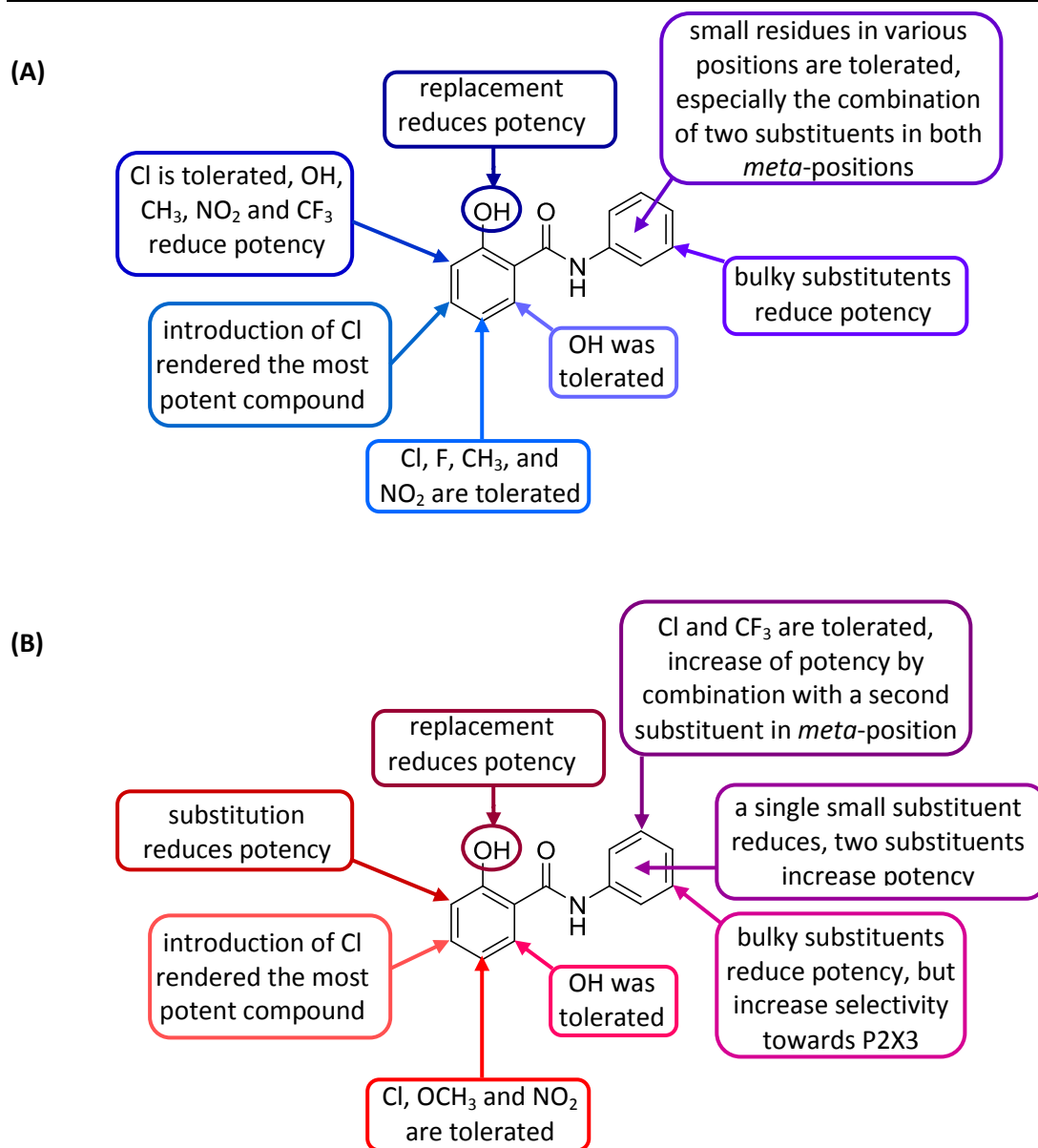
The structurally closely related benzanilide derivative IMD-0354, part of a commercial TOCRIS library, has previously been identified in our group as a potent antagonist of the P2X1 receptor by Sabrina Densborn and Dr. Aliaa Abdelrahman (data not yet published). Based on this scaffold, a library of hydroxybenzamide derivatives was synthesized by Dr. Maoqun Tian. The results for the lead structure IMD-0354 and the most potent compound at both P2X3 and P2X7 receptors are presented in Figure 6.9.



**Figure 6.9:** Structure and potency of selected benzanilide derivatives at P2X receptors.

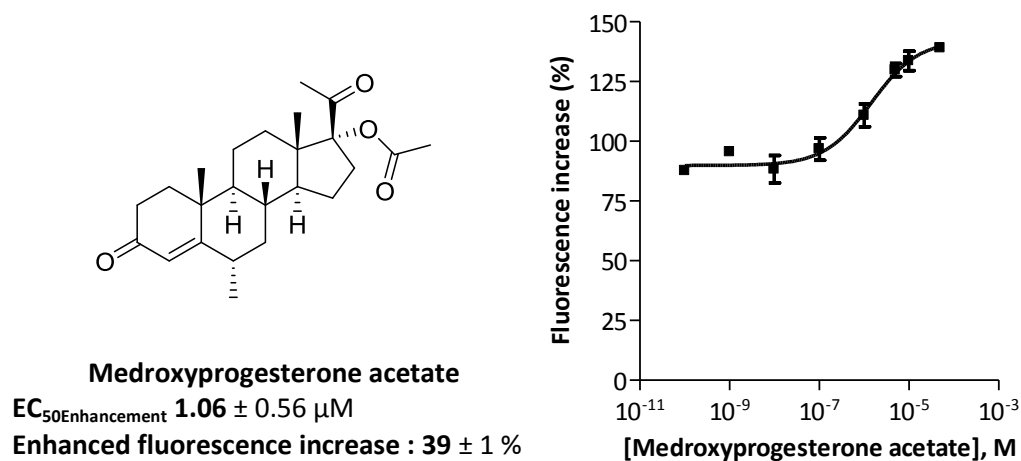
Figure 6.10 summarizes the most important structure-activity relationships of benzanilide derivatives for both the P2X3 and P2X7 receptor.

Bisacodyl, niclosamide and the related compounds MT164 and MT175 were shown by ATP curve shift experiments to act as allosteric antagonists of P2X3 and P2X7 receptors.



**Figure 6.10:** Summary of structure-activity relationships of niclosamide derivatives with inhibitory potency (A) at the P2X3 (blue) and (B) the P2X7 receptor (red).

Some approved drugs were found to enhance the maximal activation level of P2X7 receptors in the initial screening experiment. The most potent hit compound is presented in Figure 6.11.



**Figure 6.11:** Structure and enhancing potency of medroxyprogesterone acetate at the P2X7 receptor. The receptor was stimulated with ATP 2.5 mM (half-maximal activation).

The enhancing properties of medroxyprogesterone acetate were concentration-dependent. Enhancement was only seen at the stimulated receptor, no agonistic properties of the compound itself could be detected. None of the other investigated steroid-based drug was identified as a PAM at P2X7 receptor besides medroxyprogesterone acetate. ATP shift curve experiments indicate an increase of ATP affinity as cause for the allosteric P2X7 receptor modulation.

## 7 Conclusion and Outlook

Screening assays suitable for high-throughput screening and for the characterization of hit compounds and optimized derivatives in 1321N1 astrocytoma cell lines stably transfected with one of the P2X receptor subtypes were established. These allow the use of ATP, the natural agonist of P2X receptors, since 1321N1 astrocytoma cells do not show any signal upon ATP stimulation – in contrast to other commonly used cell lines. Such an assay system is essential, since the effects of allosteric modulators can be highly probe-dependent, leading to different results when using a synthetic agonist for activation as compared to applying the physiological ligand.

The first screening campaigns have provided a considerable number of hit compounds, including competitive antagonists, allosteric antagonists (negative allosteric modulators, NAMs), and even positive allosteric modulators (PAMs). Future studies should be directed towards improving their properties, such as potency, selectivity and pharmacokinetic properties by medicinal chemistry approaches.

## 8 Reference List

1. Katz, B.; Miledi, R. Membrane noise produced by acetylcholine. *Nature* **1970**, *226*, 962-963.
2. Delmas, P.; Coste, B. Mechano-gated ion channels in sensory systems. *Cell* **2013**, *155*, 278-284.
3. Lu, B.; Su, Y.; Das, S.; Liu, J.; Xia, J.; Ren, D. The neuronal channel NALCN contributes resting sodium permeability and is required for normal respiratory rhythm. *Cell* **2007**, *129*, 371-383.
4. Miller, P. S.; Smart, T. G. Binding, activation and modulation of Cys-loop receptors. *Trends Pharmacol. Sci.* **2010**, *31*, 161-174.
5. Sobolevsky, A. I. Structure and gating of tetrameric glutamate receptors. *J. Physiol* **2015**, *593*, 29-38.
6. Ion channels. Accessed on 14/12/2015. IUPHAR/BPS Guide to PHARMACOLOGY, <http://www.guidetopharmacology.org/GRAC/FamilyDisplayForward?familyId=689>.
7. Coste, B.; Mathur, J.; Schmidt, M.; Earley, T. J.; Ranade, S.; Petrus, M. J.; Dubin, A. E.; Patapoutian, A. Piezo1 and Piezo2 are essential components of distinct mechanically activated cation channels. *Science* **2010**, *330*, 55-60.
8. Lee, J. H.; Cribbs, L. L.; Perez-Reyes, E. Cloning of a novel four repeat protein related to voltage-gated sodium and calcium channels. *FEBS Lett.* **1999**, *445*, 231-236.
9. Cochet-Bissuel, M.; Lory, P.; Monteil, A. The sodium leak channel, NALCN, in health and disease. *Front Cell Neurosci.* **2014**, *8*, 132.
10. Noda, M.; Shimizu, S.; Tanabe, T.; Takai, T.; Kayano, T.; Ikeda, T.; Takahashi, H.; Nakayama, H.; Kanaoka, Y.; Minamino, N.; . Primary structure of Electrophorus electricus sodium channel deduced from cDNA sequence. *Nature* **1984**, *312*, 121-127.
11. Tanabe, T.; Takeshima, H.; Mikami, A.; Flockerzi, V.; Takahashi, H.; Kangawa, K.; Kojima, M.; Matsuo, H.; Hirose, T.; Numa, S. Primary structure of the receptor for calcium channel blockers from skeletal muscle. *Nature* **1987**, *328*, 313-318.
12. Papazian, D. M.; Schwarz, T. L.; Tempel, B. L.; Jan, Y. N.; Jan, L. Y. Cloning of genomic and complementary DNA from Shaker, a putative potassium channel gene from *Drosophila*. *Science* **1987**, *237*, 749-753.
13. de Lera, R. M.; Kraus, R. L. Voltage-Gated Sodium Channels: Structure, Function, Pharmacology, and Clinical Indications. *J. Med. Chem.* **2015**, *58*, 7093-7118.
14. Payandeh, J.; Scheuer, T.; Zheng, N.; Catterall, W. A. The crystal structure of a voltage-gated sodium channel. *Nature* **2011**, *475*, 353-358.

15. Miceli, F.; Soldovieri, M. V.; Ambrosino, P.; De, M. M.; Manocchio, L.; Medoro, A.; Tagliatela, M. Molecular pathophysiology and pharmacology of the voltage-sensing module of neuronal ion channels. *Front Cell Neurosci.* **2015**, *9*, 259.
16. Miller, P. S.; Aricescu, A. R. Crystal structure of a human GABAA receptor. *Nature* **2014**, *512*, 270-275.
17. Sobolevsky, A. I.; Rosconi, M. P.; Gouaux, E. X-ray structure, symmetry and mechanism of an AMPA-subtype glutamate receptor. *Nature* **2009**, *462*, 745-756.
18. RCSB PDB database, URL [www.rcsb.org](http://www.rcsb.org), accessed on 14/12/2015
19. Bouzat, C. New insights into the structural bases of activation of Cys-loop receptors. *J. Physiol Paris* **2012**, *106*, 23-33.
20. Flores-Soto, M. E.; Chaparro-Huerta, V.; Escoto-Delgadillo, M.; Vazquez-Valls, E.; Gonzalez-Castaneda, R. E.; Beas-Zarate, C. Structure and function of NMDA-type glutamate receptor subunits. *Neurologia* **2012**, *27*, 301-310.
21. Langen, P.; Hucho, F. Karl Lohmann and the discovery of ATP. *Angew. Chem. Int. Ed Engl.* **2008**, *47*, 1824-1827.
22. Drury, A. N.; Szent-Gyorgyi, A. The physiological activity of adenine compounds with especial reference to their action upon the mammalian heart. *J. Physiol* **1929**, *68*, 213-237.
23. Burnstock, G. Purinergic nerves. *Pharmacol. Rev.* **1972**, *24*, 509-581.
24. Burnstock, G.; Cocks, T.; Kasakov, L.; Wong, H. K. Direct evidence for ATP release from non-adrenergic, non-cholinergic ("purinergic") nerves in the guinea-pig taenia coli and bladder. *Eur. J. Pharmacol.* **1978**, *49*, 145-149.
25. Burnstock, G.; Kennedy, C. Is there a basis for distinguishing two types of P2-purinoceptor? *Gen. Pharmacol.* **1985**, *16*, 433-440.
26. Fredholm, B. B.; IJzerman, A. P.; Jacobson, K. A.; Linden, J.; Muller, C. E. International Union of Basic and Clinical Pharmacology. LXXXI. Nomenclature and classification of adenosine receptors--an update. *Pharmacol. Rev.* **2011**, *63*, 1-34.
27. Khakh, B. S. Molecular physiology of P2X receptors and ATP signalling at synapses. *Nat. Rev. Neurosci.* **2001**, *2*, 165-174.
28. Coddou, C.; Yan, Z.; Obsil, T.; Huidobro-Toro, J. P.; Stojilkovic, S. S. Activation and regulation of purinergic P2X receptor channels. *Pharmacol. Rev.* **2011**, *63*, 641-683.
29. Abbracchio, M. P.; Burnstock, G.; Boeynaems, J. M.; Barnard, E. A.; Boyer, J. L.; Kennedy, C.; Knight, G. E.; Fumagalli, M.; Gachet, C.; Jacobson, K. A.; Weisman, G. A. International Union of Pharmacology LVIII: update on the P2Y G protein-coupled nucleotide receptors: from molecular mechanisms and pathophysiology to therapy. *Pharmacol. Rev.* **2006**, *58*, 281-341.

30. Abbracchio, M. P.; Burnstock, G. Purinoceptors: are there families of P2X and P2Y purinoceptors? *Pharmacol. Ther.* **1994**, *64*, 445-475.
31. Surprenant, A.; North, R. A. Signaling at purinergic P2X receptors. *Annu. Rev. Physiol.* **2009**, *71*, 333-359.
32. North, R. A.; Verkhratsky, A. Purinergic transmission in the central nervous system. *Pflugers Arch.* **2006**, *452*, 479-485.
33. Illes, P.; Verkhratsky, A.; Burnstock, G.; Franke, H. P2X receptors and their roles in astroglia in the central and peripheral nervous system. *Neuroscientist.* **2012**, *18*, 422-438.
34. Burnstock, G. Purinergic signalling and disorders of the central nervous system. *Nat. Rev. Drug Discov.* **2008**, *7*, 575-590.
35. Jarvis, M. F.; Khakh, B. S. ATP-gated P2X cation-channels. *Neuropharmacology* **2009**, *56*, 208-215.
36. Ralevic, V.; Dunn, W. R. Purinergic transmission in blood vessels. *Auton. Neurosci.* **2015**, *191*, 48-66.
37. Morandini, A. C.; Savio, L. E.; Coutinho-Silva, R. The role of P2X7 receptor in infectious inflammatory diseases and the influence of ectonucleotidases. *Biomed. J.* **2014**, *37*, 169-177.
38. North, R. A. Molecular physiology of P2X receptors. *Physiol Rev.* **2002**, *82*, 1013-1067.
39. Egan, T. M.; Samways, D. S.; Li, Z. Biophysics of P2X receptors. *Pflugers Arch.* **2006**, *452*, 501-512.
40. North, R. A.; Surprenant, A. Pharmacology of cloned P2X receptors. *Annu. Rev. Pharmacol. Toxicol.* **2000**, *40*, 563-580.
41. Egan, T. M.; Cox, J. A.; Voigt, M. M. Molecular structure of P2X receptors. *Curr. Top. Med. Chem.* **2004**, *4*, 821-829.
42. Hattori, M.; Gouaux, E. Molecular mechanism of ATP binding and ion channel activation in P2X receptors. *Nature* **2012**, *485*, 207-212.
43. Kawate, T.; Michel, J. C.; Birdsong, W. T.; Gouaux, E. Crystal structure of the ATP-gated P2X(4) ion channel in the closed state. *Nature* **2009**, *460*, 592-598.
44. Nicke, A.; Baumert, H. G.; Rettinger, J.; Eichele, A.; Lambrecht, G.; Mutschler, E.; Schmalzing, G. P2X1 and P2X3 receptors form stable trimers: a novel structural motif of ligand-gated ion channels. *EMBO J.* **1998**, *17*, 3016-3028.
45. Barrera, N. P.; Ormond, S. J.; Henderson, R. M.; Murrell-Lagnado, R. D.; Edwardson, J. M. Atomic force microscopy imaging demonstrates that P2X2 receptors are trimers but that P2X6 receptor subunits do not oligomerize. *J. Biol. Chem.* **2005**, *280*, 10759-10765.



46. Saul, A.; Hausmann, R.; Kless, A.; Nicke, A. Heteromeric assembly of P2X subunits. *Front Cell Neurosci.* **2013**, *7*, 250.
47. Ennion, S.; Hagan, S.; Evans, R. J. The role of positively charged amino acids in ATP recognition by human P2X(1) receptors. *J. Biol. Chem.* **2000**, *275*, 29361-29367.
48. Wilkinson, W. J.; Jiang, L. H.; Surprenant, A.; North, R. A. Role of ectodomain lysines in the subunits of the heteromeric P2X2/3 receptor. *Mol. Pharmacol.* **2006**, *70*, 1159-1163.
49. Bodnar, M.; Wang, H.; Riedel, T.; Hintze, S.; Kato, E.; Fallah, G.; Groger-Arndt, H.; Giniatullin, R.; Grohmann, M.; Hausmann, R.; Schmalzing, G.; Illes, P.; Rubini, P. Amino acid residues constituting the agonist binding site of the human P2X3 receptor. *J. Biol. Chem.* **2011**, *286*, 2739-2749.
50. Jiang, L. H.; Rassendren, F.; Surprenant, A.; North, R. A. Identification of amino acid residues contributing to the ATP-binding site of a purinergic P2X receptor. *J. Biol. Chem.* **2000**, *275*, 34190-34196.
51. Roberts, J. A.; Evans, R. J. Cysteine substitution mutants give structural insight and identify ATP binding and activation sites at P2X receptors. *J. Neurosci.* **2007**, *27*, 4072-4082.
52. Roberts, J. A.; Valente, M.; Allsopp, R. C.; Watt, D.; Evans, R. J. Contribution of the region Glu181 to Val200 of the extracellular loop of the human P2X1 receptor to agonist binding and gating revealed using cysteine scanning mutagenesis. *J. Neurochem.* **2009**, *109*, 1042-1052.
53. Li, M.; Silberberg, S. D.; Swartz, K. J. Subtype-specific control of P2X receptor channel signaling by ATP and Mg<sup>2+</sup>. *Proc. Natl. Acad. Sci. U. S. A* **2013**, *110*, E3455-E3463.
54. Ennion, S. J.; Ritson, J.; Evans, R. J. Conserved negatively charged residues are not required for ATP action at P2X(1) receptors. *Biochem. Biophys. Res. Commun.* **2001**, *289*, 700-704.
55. Chataigneau, T.; Lemoine, D.; Grutter, T. Exploring the ATP-binding site of P2X receptors. *Front Cell Neurosci.* **2013**, *7*, 273.
56. Roberts, J. A.; Digby, H. R.; Kara, M.; El, A. S.; Sutcliffe, M. J.; Evans, R. J. Cysteine substitution mutagenesis and the effects of methanethiosulfonate reagents at P2X2 and P2X4 receptors support a core common mode of ATP action at P2X receptors. *J. Biol. Chem.* **2008**, *283*, 20126-20136.
57. Marquez-Klaka, B.; Rettinger, J.; Bhargava, Y.; Eisele, T.; Nicke, A. Identification of an intersubunit cross-link between substituted cysteine residues located in the putative ATP binding site of the P2X1 receptor. *J. Neurosci.* **2007**, *27*, 1456-1466.
58. Walker, J. E.; Saraste, M.; Runswick, M. J.; Gay, N. J. Distantly related sequences in the alpha- and beta-subunits of ATP synthase, myosin, kinases and other ATP-requiring enzymes and a common nucleotide binding fold. *EMBO J.* **1982**, *1*, 945-951.

59. Fischer, W.; Zadori, Z.; Kullnick, Y.; Groger-Arndt, H.; Franke, H.; Wirkner, K.; Illes, P.; Mager, P. P. Conserved lysin and arginin residues in the extracellular loop of P2X(3) receptors are involved in agonist binding. *Eur. J. Pharmacol.* **2007**, *576*, 7-17.
60. Allsopp, R. C.; El, A. S.; Schmid, R.; Evans, R. J. Cysteine scanning mutagenesis (residues Glu52-Gly96) of the human P2X1 receptor for ATP: mapping agonist binding and channel gating. *J. Biol. Chem.* **2011**, *286*, 29207-29217.
61. Zemkova, H.; Yan, Z.; Liang, Z.; Jelinkova, I.; Tomic, M.; Stojilkovic, S. S. Role of aromatic and charged ectodomain residues in the P2X(4) receptor functions. *J. Neurochem.* **2007**, *102*, 1139-1150.
62. Neelands, T. R.; Burgard, E. C.; Uchic, M. E.; McDonald, H. A.; Niforatos, W.; Faltynek, C. R.; Lynch, K. J.; Jarvis, M. F. 2', 3'-O-(2,4,6-trinitrophenyl)-ATP and A-317491 are competitive antagonists at a slowly desensitizing chimeric human P2X3 receptor. *Br. J. Pharmacol.* **2003**, *140*, 202-210.
63. Bianchi, B. R.; Lynch, K. J.; Touma, E.; Niforatos, W.; Burgard, E. C.; Alexander, K. M.; Park, H. S.; Yu, H.; Metzger, R.; Kowaluk, E.; Jarvis, M. F.; van, B. T. Pharmacological characterization of recombinant human and rat P2X receptor subtypes. *Eur. J. Pharmacol.* **1999**, *376*, 127-138.
64. Hernandez-Olmos, V.; Abdelrahman, A.; El-Tayeb, A.; Freudendahl, D.; Weinhausen, S.; Muller, C. E. N-substituted phenoxazine and acridone derivatives: structure-activity relationships of potent P2X4 receptor antagonists. *J. Med. Chem.* **2012**, *55*, 9576-9588.
65. Watano, T.; Matsuoka, I.; Kimura, J. Characteristics of ATP-induced current through P2X7 receptor in NG108-15 cells: unique antagonist sensitivity and lack of pore formation. *Jpn. J. Pharmacol.* **2002**, *88*, 428-435.
66. Glanzel, M.; Bultmann, R.; Starke, K.; Frahm, A. W. Constitutional isomers of Reactive Blue 2 - selective P2Y-receptor antagonists? *Eur. J. Med. Chem.* **2003**, *38*, 303-312.
67. Wildman, S. S.; Brown, S. G.; Rahman, M.; Noel, C. A.; Churchill, L.; Burnstock, G.; Unwin, R. J.; King, B. F. Sensitization by extracellular Ca(2+) of rat P2X(5) receptor and its pharmacological properties compared with rat P2X(1). *Mol. Pharmacol.* **2002**, *62*, 957-966.
68. Chen, C. C.; Akopian, A. N.; Sivilotti, L.; Colquhoun, D.; Burnstock, G.; Wood, J. N. A P2X purinoceptor expressed by a subset of sensory neurons. *Nature* **1995**, *377*, 428-431.
69. Pratt, E. B.; Brink, T. S.; Bergson, P.; Voigt, M. M.; Cook, S. P. Use-dependent inhibition of P2X3 receptors by nanomolar agonist. *J. Neurosci.* **2005**, *25*, 7359-7365.
70. Asatryan, L.; Popova, M.; Woodward, J. J.; King, B. F.; Alkana, R. L.; Davies, D. L. Roles of ectodomain and transmembrane regions in ethanol and agonist action in purinergic P2X2 and P2X3 receptors. *Neuropharmacology* **2008**, *55*, 835-843.

71. Freissmuth, M.; Boehm, S.; Beindl, W.; Nickel, P.; Uzman, A. P.; Hohenegger, M.; Nanoff, C. Suramin analogues as subtype-selective G protein inhibitors. *Mol. Pharmacol.* **1996**, *49*, 602-611.
72. Jentsch, K. D.; Hunsmann, G.; Hartmann, H.; Nickel, P. Inhibition of human immunodeficiency virus type I reverse transcriptase by suramin-related compounds. *J. Gen. Virol.* **1987**, *68 (Pt 8)*, 2183-2192.
73. Syed, N. I.; Tengah, A.; Paul, A.; Kennedy, C. Characterisation of P2X receptors expressed in rat pulmonary arteries. *Eur. J. Pharmacol.* **2010**, *649*, 342-348.
74. Meng, E.; Chang, H. Y.; Chang, S. Y.; Sun, G. H.; Yu, D. S.; Cha, T. L. Involvement of purinergic neurotransmission in ketamine induced bladder dysfunction. *J. Urol.* **2011**, *186*, 1134-1141.
75. Burnstock, G. Purinergic signalling in the urinary tract in health and disease. *Purinergic. Signal.* **2014**, *10*, 103-155.
76. Franco, M.; Bautista, R.; Tapia, E.; Soto, V.; Santamaria, J.; Osorio, H.; Pacheco, U.; Sanchez-Lozada, L. G.; Kobori, H.; Navar, L. G. Contribution of renal purinergic receptors to renal vasoconstriction in angiotensin II-induced hypertensive rats. *Am. J. Physiol Renal Physiol* **2011**, *300*, F1301-F1309.
77. Mahaut-Smith, M. P.; Jones, S.; Evans, R. J. The P2X1 receptor and platelet function. *Purinergic. Signal.* **2011**, *7*, 341-356.
78. Banks, F. C.; Knight, G. E.; Calvert, R. C.; Thompson, C. S.; Morgan, R. J.; Burnstock, G. The purinergic component of human vas deferens contraction. *Fertil. Steril.* **2006**, *85*, 932-939.
79. Valera, S.; Hussy, N.; Evans, R. J.; Adami, N.; North, R. A.; Surprenant, A.; Buell, G. A new class of ligand-gated ion channel defined by P2x receptor for extracellular ATP. *Nature* **1994**, *371*, 516-519.
80. Ennion, S. J.; Evans, R. J. Agonist-stimulated internalisation of the ligand-gated ion channel P2X(1) in rat vas deferens. *FEBS Lett.* **2001**, *489*, 154-158.
81. Buell, G.; Michel, A. D.; Lewis, C.; Collo, G.; Humphrey, P. P.; Surprenant, A. P2X1 receptor activation in HL60 cells. *Blood* **1996**, *87*, 2659-2664.
82. Allsopp, R. C.; Evans, R. J. The intracellular amino terminus plays a dominant role in desensitization of ATP-gated P2X receptor ion channels. *J. Biol. Chem.* **2011**, *286*, 44691-44701.
83. Werner, P.; Seward, E. P.; Buell, G. N.; North, R. A. Domains of P2X receptors involved in desensitization. *Proc. Natl. Acad. Sci. U. S. A* **1996**, *93*, 15485-15490.
84. Roberts, J. A.; Bottrill, A. R.; Mistry, S.; Evans, R. J. Mass spectrometry analysis of human P2X1 receptors; insight into phosphorylation, modelling and conformational changes. *J. Neurochem.* **2012**, *123*, 725-735.
85. North, R. A.; Jarvis, M. F. P2X receptors as drug targets. *Mol. Pharmacol.* **2013**, *83*, 759-769.

86. Jacobson, K. A.; Kim, Y. C.; Wildman, S. S.; Mohanram, A.; Harden, T. K.; Boyer, J. L.; King, B. F.; Burnstock, G. A pyridoxine cyclic phosphate and its 6-azoaryl derivative selectively potentiate and antagonize activation of P2X1 receptors. *J. Med. Chem.* **1998**, *41*, 2201-2206.
87. Jaime-Figueroa, S.; Greenhouse, R.; Padilla, F.; Dillon, M. P.; Gever, J. R.; Ford, A. P. Discovery and synthesis of a novel and selective drug-like P2X(1) antagonist. *Bioorg. Med. Chem. Lett.* **2005**, *15*, 3292-3295.
88. Braun, K.; Rettinger, J.; Ganso, M.; Kassack, M.; Hildebrandt, C.; Ullmann, H.; Nickel, P.; Schmalzing, G.; Lambrecht, G. NF449: a subnanomolar potency antagonist at recombinant rat P2X1 receptors. *Naunyn Schmiedeberg's Arch. Pharmacol.* **2001**, *364*, 285-290.
89. Hulsmann, M.; Nickel, P.; Kassack, M.; Schmalzing, G.; Lambrecht, G.; Markwardt, F. NF449, a novel picomolar potency antagonist at human P2X1 receptors. *Eur. J. Pharmacol.* **2003**, *470*, 1-7.
90. Rettinger, J.; Schmalzing, G.; Damer, S.; Muller, G.; Nickel, P.; Lambrecht, G. The suramin analogue NF279 is a novel and potent antagonist selective for the P2X(1) receptor. *Neuropharmacology* **2000**, *39*, 2044-2053.
91. Soto, F.; Lambrecht, G.; Nickel, P.; Stuhmer, W.; Busch, A. E. Antagonistic properties of the suramin analogue NF023 at heterologously expressed P2X receptors. *Neuropharmacology* **1999**, *38*, 141-149.
92. Lynch, K. J.; Touma, E.; Niforatos, W.; Kage, K. L.; Burgard, E. C.; van, B. T.; Kowaluk, E. A.; Jarvis, M. F. Molecular and functional characterization of human P2X(2) receptors. *Mol. Pharmacol.* **1999**, *56*, 1171-1181.
93. Kanjhan, R.; Housley, G. D.; Burton, L. D.; Christie, D. L.; Kippenberger, A.; Thorne, P. R.; Luo, L.; Ryan, A. F. Distribution of the P2X2 receptor subunit of the ATP-gated ion channels in the rat central nervous system. *J. Comp Neurol.* **1999**, *407*, 11-32.
94. Khakh, B. S.; Gittermann, D.; Cockayne, D. A.; Jones, A. ATP modulation of excitatory synapses onto interneurons. *J. Neurosci.* **2003**, *23*, 7426-7437.
95. Yang, R.; Montoya, A.; Bond, A.; Walton, J.; Kinnamon, J. C. Immunocytochemical analysis of P2X2 in rat circumvallate taste buds. *BMC. Neurosci.* **2012**, *13*, 51.
96. Hausmann, R.; Bodnar, M.; Woltersdorf, R.; Wang, H.; Fuchs, M.; Messemer, N.; Qin, Y.; Gunther, J.; Riedel, T.; Grohmann, M.; Nieber, K.; Schmalzing, G.; Rubini, P.; Illes, P. ATP binding site mutagenesis reveals different subunit stoichiometry of functional P2X2/3 and P2X2/6 receptors. *J. Biol. Chem.* **2012**, *287*, 13930-13943.
97. Jiang, R.; Martz, A.; Gonin, S.; Taly, A.; de Carvalho, L. P.; Grutter, T. A putative extracellular salt bridge at the subunit interface contributes to the ion channel function of the ATP-gated P2X2 receptor. *J. Biol. Chem.* **2010**, *285*, 15805-15815.
98. Kracun, S.; Chaptal, V.; Abramson, J.; Khakh, B. S. Gated access to the pore of a P2X receptor: structural implications for closed-open transitions. *J. Biol. Chem.* **2010**, *285*, 10110-10121.

99. Lorca, R. A.; Coddou, C.; Gazitua, M. C.; Bull, P.; Arredondo, C.; Huidobro-Toro, J. P. Extracellular histidine residues identify common structural determinants in the copper/zinc P2X2 receptor modulation. *J. Neurochem.* **2005**, *95*, 499-512.
100. Wildman, S. S.; King, B. F.; Burnstock, G. Modulatory activity of extracellular H<sup>+</sup> and Zn<sup>2+</sup> on ATP-responses at rP2X1 and P2X3 receptors. *Br. J. Pharmacol.* **1999**, *128*, 486-492.
101. Coddou, C.; Stojilkovic, S. S.; Huidobro-Toro, J. P. Allosteric modulation of ATP-gated P2X receptor channels. *Rev. Neurosci.* **2011**, *22*, 335-354.
102. Wolf, C.; Rosefort, C.; Fallah, G.; Kassack, M. U.; Hamacher, A.; Bodnar, M.; Wang, H.; Illes, P.; Kless, A.; Bahrenberg, G.; Schmalzing, G.; Hausmann, R. Molecular determinants of potent P2X2 antagonism identified by functional analysis, mutagenesis, and homology docking. *Mol. Pharmacol.* **2011**, *79*, 649-661.
103. Baqi, Y.; Hausmann, R.; Rosefort, C.; Rettinger, J.; Schmalzing, G.; Muller, C. E. Discovery of potent competitive antagonists and positive modulators of the P2X2 receptor. *J. Med. Chem.* **2011**, *54*, 817-830.
104. Jacobson, K. A.; Kim, Y. C.; King, B. F. In search of selective P2 receptor ligands: interaction of dihydropyridine derivatives at recombinant rat P2X(2) receptors. *J. Auton. Nerv. Syst.* **2000**, *81*, 152-157.
105. Bongartz, E. V.; Rettinger, J.; Hausmann, R. Aminoglycoside block of P2X2 receptors heterologously expressed in *Xenopus laevis* oocytes. *Purinergic. Signal.* **2010**, *6*, 393-403.
106. Fabbretti, E. ATP P2X3 receptors and neuronal sensitization. *Front Cell Neurosci.* **2013**, *7*, 236.
107. Cockayne, D. A.; Hamilton, S. G.; Zhu, Q. M.; Dunn, P. M.; Zhong, Y.; Novakovic, S.; Malmberg, A. B.; Cain, G.; Berson, A.; Kassotakis, L.; Hedley, L.; Lachnit, W. G.; Burnstock, G.; McMahon, S. B.; Ford, A. P. Urinary bladder hyporeflexia and reduced pain-related behaviour in P2X3-deficient mice. *Nature* **2000**, *407*, 1011-1015.
108. Lewis, C.; Neidhart, S.; Holy, C.; North, R. A.; Buell, G.; Surprenant, A. Coexpression of P2X2 and P2X3 receptor subunits can account for ATP-gated currents in sensory neurons. *Nature* **1995**, *377*, 432-435.
109. Sokolova, E.; Skorinkin, A.; Moiseev, I.; Agrachev, A.; Nistri, A.; Giniatullin, R. Experimental and modeling studies of desensitization of P2X3 receptors. *Mol. Pharmacol.* **2006**, *70*, 373-382.
110. Giniatullin, R.; Nistri, A. Desensitization properties of P2X3 receptors shaping pain signaling. *Front Cell Neurosci.* **2013**, *7*, 245.
111. Hautaniemi, T.; Petrenko, N.; Skorinkin, A.; Giniatullin, R. The inhibitory action of the antimigraine nonsteroidal anti-inflammatory drug naproxen on P2X3 receptor-mediated responses in rat trigeminal neurons. *Neuroscience* **2012**, *209*, 32-38.

112. Jiang, L. H.; Kim, M.; Spelta, V.; Bo, X.; Surprenant, A.; North, R. A. Subunit arrangement in P2X receptors. *J. Neurosci.* **2003**, *23*, 8903-8910.
113. Kowalski, M.; Hausmann, R.; Schmid, J.; Dopychai, A.; Stephan, G.; Tang, Y.; Schmalzing, G.; Illes, P.; Rubini, P. Flexible subunit stoichiometry of functional human P2X<sub>2/3</sub> heteromeric receptors. *Neuropharmacology* **2015**, *99*, 115-130.
114. Torres, G. E.; Egan, T. M.; Voigt, M. M. Hetero-oligomeric assembly of P2X receptor subunits. Specificities exist with regard to possible partners. *J. Biol. Chem.* **1999**, *274*, 6653-6659.
115. Koshimizu, T. A.; Ueno, S.; Tanoue, A.; Yanagihara, N.; Stojilkovic, S. S.; Tsujimoto, G. Heteromultimerization modulates P2X receptor functions through participating extracellular and C-terminal subdomains. *J. Biol. Chem.* **2002**, *277*, 46891-46899.
116. Dunn, P. M.; Liu, M.; Zhong, Y.; King, B. F.; Burnstock, G. Diinosine pentaphosphate: an antagonist which discriminates between recombinant P2X<sub>(3)</sub> and P2X<sub>(2/3)</sub> receptors and between two P2X receptors in rat sensory neurones. *Br. J. Pharmacol.* **2000**, *130*, 1378-1384.
117. Brotherton-Pleiss, C. E.; Dillon, M. P.; Ford, A. P.; Gever, J. R.; Carter, D. S.; Gleason, S. K.; Lin, C. J.; Moore, A. G.; Thompson, A. W.; Villa, M.; Zhai, Y. Discovery and optimization of RO-85, a novel drug-like, potent, and selective P2X<sub>3</sub> receptor antagonist. *Bioorg. Med. Chem. Lett.* **2010**, *20*, 1031-1036.
118. Hausmann, R.; Bahrenberg, G.; Kuhlmann, D.; Schumacher, M.; Braam, U.; Bieler, D.; Schlusche, I.; Schmalzing, G. A hydrophobic residue in position 15 of the P2X<sub>3</sub> receptor slows desensitization and reveals properties beneficial for pharmacological analysis and high-throughput screening. *Neuropharmacology* **2014**, *79*, 603-615.
119. Jarvis, M. F.; Burgard, E. C.; McGaraughty, S.; Honore, P.; Lynch, K.; Brennan, T. J.; Subieta, A.; van, B. T.; Cartmell, J.; Bianchi, B.; Niforatos, W.; Kage, K.; Yu, H.; Mikusa, J.; Wismer, C. T.; Zhu, C. Z.; Chu, K.; Lee, C. H.; Stewart, A. O.; Polakowski, J.; Cox, B. F.; Kowaluk, E.; Williams, M.; Sullivan, J.; Faltynek, C. A-317491, a novel potent and selective non-nucleotide antagonist of P2X<sub>3</sub> and P2X<sub>2/3</sub> receptors, reduces chronic inflammatory and neuropathic pain in the rat. *Proc. Natl. Acad. Sci. U. S. A* **2002**, *99*, 17179-17184.
120. Carter, D. S.; Alam, M.; Cai, H.; Dillon, M. P.; Ford, A. P.; Gever, J. R.; Jahangir, A.; Lin, C.; Moore, A. G.; Wagner, P. J.; Zhai, Y. Identification and SAR of novel diaminopyrimidines. Part 1: The discovery of RO-4, a dual P2X<sub>(3)</sub>/P2X<sub>(2/3)</sub> antagonist for the treatment of pain. *Bioorg. Med. Chem. Lett.* **2009**, *19*, 1628-1631.
121. Gever, J. R.; Soto, R.; Henningsen, R. A.; Martin, R. S.; Hackos, D. H.; Panicker, S.; Rubas, W.; Oglesby, I. B.; Dillon, M. P.; Milla, M. E.; Burnstock, G.; Ford, A. P. AF-353, a novel, potent and orally bioavailable P2X<sub>3</sub>/P2X<sub>2/3</sub> receptor antagonist. *Br. J. Pharmacol.* **2010**, *160*, 1387-1398.

122. Jahangir, A.; Alam, M.; Carter, D. S.; Dillon, M. P.; Bois, D. J.; Ford, A. P.; Gever, J. R.; Lin, C.; Wagner, P. J.; Zhai, Y.; Zira, J. Identification and SAR of novel diaminopyrimidines. Part 2: The discovery of RO-51, a potent and selective, dual P2X(3)/P2X(2/3) antagonist for the treatment of pain. *Bioorg. Med. Chem. Lett.* **2009**, *19*, 1632-1635.
123. Ford, A. P.; Udem, B. J. The therapeutic promise of ATP antagonism at P2X3 receptors in respiratory and urological disorders. *Front Cell Neurosci.* **2013**, *7*, 267.
124. Gum, R. J.; Wakefield, B.; Jarvis, M. F. P2X receptor antagonists for pain management: examination of binding and physicochemical properties. *Purinergic. Signal.* **2012**, *8*, 41-56.
125. Hausmann, R.; Rettinger, J.; Gerevich, Z.; Meis, S.; Kassack, M. U.; Illes, P.; Lambrecht, G.; Schmalzing, G. The suramin analog 4,4',4'',4'''-(carbonylbis(imino-5,1,3-benzenetriylbis (carbonylimino)))tetra-kis-benzenesulfonic acid (NF110) potentially blocks P2X3 receptors: subtype selectivity is determined by location of sulfonic acid groups. *Mol. Pharmacol.* **2006**, *69*, 2058-2067.
126. Jung, K. Y.; Moon, H. D.; Lee, G. E.; Lim, H. H.; Park, C. S.; Kim, Y. C. Structure-activity relationship studies of spinorphin as a potent and selective human P2X(3) receptor antagonist. *J. Med. Chem.* **2007**, *50*, 4543-4547.
127. Alexander, K.; Niforatos, W.; Bianchi, B.; Burgard, E. C.; Lynch, K. J.; Kowaluk, E. A.; Jarvis, M. F.; van, B. T. Allosteric modulation and accelerated resensitization of human P2X(3) receptors by cibacron blue. *J. Pharmacol. Exp. Ther.* **1999**, *291*, 1135-1142.
128. Bo, X.; Zhang, Y.; Nassar, M.; Burnstock, G.; Schoepfer, R. A P2X purinoceptor cDNA conferring a novel pharmacological profile. *FEBS Lett.* **1995**, *375*, 129-133.
129. Bo, X.; Kim, M.; Nori, S. L.; Schoepfer, R.; Burnstock, G.; North, R. A. Tissue distribution of P2X4 receptors studied with an ectodomain antibody. *Cell Tissue Res.* **2003**, *313*, 159-165.
130. Gever, J. R.; Cockayne, D. A.; Dillon, M. P.; Burnstock, G.; Ford, A. P. Pharmacology of P2X channels. *Pflugers Arch.* **2006**, *452*, 513-537.
131. Tsuda, M.; Kuboyama, K.; Inoue, T.; Nagata, K.; Tozaki-Saitoh, H.; Inoue, K. Behavioral phenotypes of mice lacking purinergic P2X4 receptors in acute and chronic pain assays. *Mol. Pain* **2009**, *5*, 28.
132. Tsuda, M.; Masuda, T.; Tozaki-Saitoh, H.; Inoue, K. P2X4 receptors and neuropathic pain. *Front Cell Neurosci.* **2013**, *7*, 191.
133. Toyomitsu, E.; Tsuda, M.; Yamashita, T.; Tozaki-Saitoh, H.; Tanaka, Y.; Inoue, K. CCL2 promotes P2X4 receptor trafficking to the cell surface of microglia. *Purinergic. Signal.* **2012**, *8*, 301-310.
134. Yang, R.; Beqiri, D.; Shen, J. B.; Redden, J. M.; Dodge-Kafka, K.; Jacobson, K. A.; Liang, B. T. P2X4 receptor-eNOS signaling pathway in cardiac myocytes as a novel protective mechanism in heart failure. *Comput. Struct. Biotechnol. J.* **2015**, *13*, 1-7.

135. Nagata, K.; Imai, T.; Yamashita, T.; Tsuda, M.; Tozaki-Saitoh, H.; Inoue, K. Antidepressants inhibit P2X4 receptor function: a possible involvement in neuropathic pain relief. *Mol. Pain* **2009**, *5*, 20.
136. Sim, J. A.; North, R. A. Amitriptyline does not block the action of ATP at human P2X4 receptor. *Br. J. Pharmacol.* **2010**, *160*, 88-92.
137. Balazs, B.; Danko, T.; Kovacs, G.; Koles, L.; Hediger, M. A.; Zsembery, A. Investigation of the inhibitory effects of the benzodiazepine derivative, 5-BDBD on P2X4 purinergic receptors by two complementary methods. *Cell Physiol Biochem.* **2013**, *32*, 11-24.
138. Tian, M.; Abdelrahman, A.; Weinhausen, S.; Hinz, S.; Weyer, S.; Dosa, S.; El-Tayeb, A.; Muller, C. E. Carbamazepine derivatives with P2X4 receptor-blocking activity. *Bioorg. Med. Chem.* **2014**, *22*, 1077-1088.
139. Ase, A. R.; Honson, N. S.; Zaghdane, H.; Pfeifer, T. A.; Seguela, P. Identification and characterization of a selective allosteric antagonist of human P2X4 receptor channels. *Mol. Pharmacol.* **2015**, *87*, 606-616.
140. Jiang, L. H.; Mackenzie, A. B.; North, R. A.; Surprenant, A. Brilliant blue G selectively blocks ATP-gated rat P2X(7) receptors. *Mol. Pharmacol.* **2000**, *58*, 82-88.
141. Muller, C. E. Medicinal chemistry of P2X receptors: allosteric modulators. *Curr. Med. Chem.* **2015**, *22*, 929-941.
142. Tabakoff, B.; Saba, L.; Printz, M.; Flodman, P.; Hodgkinson, C.; Goldman, D.; Koob, G.; Richardson, H. N.; Kechris, K.; Bell, R. L.; Hubner, N.; Heinig, M.; Pravenec, M.; Mangion, J.; Legault, L.; Dongier, M.; Conigrave, K. M.; Whitfield, J. B.; Saunders, J.; Grant, B.; Hoffman, P. L. Genetical genomic determinants of alcohol consumption in rats and humans. *BMC. Biol.* **2009**, *7*, 70.
143. Khakh, B. S.; Proctor, W. R.; Dunwiddie, T. V.; Labarca, C.; Lester, H. A. Allosteric control of gating and kinetics at P2X(4) receptor channels. *J. Neurosci.* **1999**, *19*, 7289-7299.
144. Asatryan, L.; Popova, M.; Perkins, D.; Trudell, J. R.; Alkana, R. L.; Davies, D. L. Ivermectin antagonizes ethanol inhibition in purinergic P2X4 receptors. *J. Pharmacol. Exp. Ther.* **2010**, *334*, 720-728.
145. Yardley, M. M.; Wyatt, L.; Khoja, S.; Asatryan, L.; Ramaker, M. J.; Finn, D. A.; Alkana, R. L.; Huynh, N.; Louie, S. G.; Petasis, N. A.; Bortolato, M.; Davies, D. L. Ivermectin reduces alcohol intake and preference in mice. *Neuropharmacology* **2012**, *63*, 190-201.
146. Franklin, K. M.; Asatryan, L.; Jakowec, M. W.; Trudell, J. R.; Bell, R. L.; Davies, D. L. P2X4 receptors (P2X4Rs) represent a novel target for the development of drugs to prevent and/or treat alcohol use disorders. *Front Neurosci.* **2014**, *8*, 176.
147. Zemkova, H.; Tvrdonova, V.; Bhattacharya, A.; Jindrichova, M. Allosteric modulation of ligand gated ion channels by ivermectin. *Physiol Res.* **2014**, *63 Suppl 1*, S215-S224.



148. Gonzalez, C. A.; Sahagun Prieto, A. M.; Jose Diez, L. M.; Martinez, N. F.; Vega, M. S.; Vieitez, J. J. The pharmacokinetics and metabolism of ivermectin in domestic animal species. *Vet. J.* **2009**, *179*, 25-37.
149. Zemkova, H.; Khadra, A.; Rokic, M. B.; Tvrdonova, V.; Sherman, A.; Stojilkovic, S. S. Allosteric regulation of the P2X4 receptor channel pore dilation. *Pflugers Arch.* **2015**, *467*, 713-726.
150. Priel, A.; Silberberg, S. D. Mechanism of ivermectin facilitation of human P2X4 receptor channels. *J. Gen. Physiol* **2004**, *123*, 281-293.
151. Jelinkova, I.; Yan, Z.; Liang, Z.; Moonat, S.; Teisinger, J.; Stojilkovic, S. S.; Zemkova, H. Identification of P2X4 receptor-specific residues contributing to the ivermectin effects on channel deactivation. *Biochem. Biophys. Res. Commun.* **2006**, *349*, 619-625.
152. Michel, A. D.; Miller, K. J.; Lundstrom, K.; Buell, G. N.; Humphrey, P. P. Radiolabeling of the rat P2X4 purinoceptor: evidence for allosteric interactions of purinoceptor antagonists and monovalent cations with P2X purinoceptors. *Mol. Pharmacol.* **1997**, *51*, 524-532.
153. Miller, K. J.; Michel, A. D.; Chessell, I. P.; Humphrey, P. P. Cibacron blue allosterically modulates the rat P2X4 receptor. *Neuropharmacology* **1998**, *37*, 1579-1586.
154. Tomioka, A.; Ueno, S.; Kohama, K.; Goto, F.; Inoue, K. Propofol potentiates ATP-activated currents of recombinant P2X(4) receptor channels expressed in human embryonic kidney 293 cells. *Neurosci. Lett.* **2000**, *284*, 167-170.
155. Hasaka, M.; Mori, T.; Matsuura, T.; Narahashi, T.; Kuno, M.; Asada, A.; Nishikawa, K. Effects of general anesthetics on P2X4 receptors in a mouse microglial cell line. *Neuroreport* **2012**, *23*, 601-605.
156. Norenberg, W.; Sobottka, H.; Hempel, C.; Plotz, T.; Fischer, W.; Schmalzing, G.; Schaefer, M. Positive allosteric modulation by ivermectin of human but not murine P2X7 receptors. *Br. J. Pharmacol.* **2012**, *167*, 48-66.
157. Collo, G.; North, R. A.; Kawashima, E.; Merlo-Pich, E.; Neidhart, S.; Surprenant, A.; Buell, G. Cloning OF P2X5 and P2X6 receptors and the distribution and properties of an extended family of ATP-gated ion channels. *J. Neurosci.* **1996**, *16*, 2495-2507.
158. Le, K. T.; Paquet, M.; Nouel, D.; Babinski, K.; Seguela, P. Primary structure and expression of a naturally truncated human P2X ATP receptor subunit from brain and immune system. *FEBS Lett.* **1997**, *418*, 195-199.
159. Bo, X.; Jiang, L. H.; Wilson, H. L.; Kim, M.; Burnstock, G.; Surprenant, A.; North, R. A. Pharmacological and biophysical properties of the human P2X5 receptor. *Mol. Pharmacol.* **2003**, *63*, 1407-1416.
160. Garcia-Guzman, M.; Soto, F.; Laube, B.; Stuhmer, W. Molecular cloning and functional expression of a novel rat heart P2X purinoceptor. *FEBS Lett.* **1996**, *388*, 123-127.
161. Brandle, U.; Guenther, E.; Irrle, C.; Wheeler-Schilling, T. H. Gene expression of the P2X receptors in the rat retina. *Brain Res. Mol. Brain Res.* **1998**, *59*, 269-272.

162. Coutinho-Silva, R.; Stahl, L.; Cheung, K. K.; de Campos, N. E.; de Oliveira, S. C.; Ojcius, D. M.; Burnstock, G. P2X and P2Y purinergic receptors on human intestinal epithelial carcinoma cells: effects of extracellular nucleotides on apoptosis and cell proliferation. *Am. J. Physiol Gastrointest. Liver Physiol* **2005**, *288*, G1024-G1035.
163. Le, K. T.; Boue-Grabot, E.; Archambault, V.; Seguela, P. Functional and biochemical evidence for heteromeric ATP-gated channels composed of P2X1 and P2X5 subunits. *J. Biol. Chem.* **1999**, *274*, 15415-15419.
164. Haines, W. R.; Torres, G. E.; Voigt, M. M.; Egan, T. M. Properties of the novel ATP-gated ionotropic receptor composed of the P2X(1) and P2X(5) isoforms. *Mol. Pharmacol.* **1999**, *56*, 720-727.
165. Compan, V.; Ulmann, L.; Stelmashenko, O.; Chemin, J.; Chaumont, S.; Rassendren, F. P2X2 and P2X5 subunits define a new heteromeric receptor with P2X7-like properties. *J. Neurosci.* **2012**, *32*, 4284-4296.
166. Rubio, M. E.; Soto, F. Distinct Localization of P2X receptors at excitatory postsynaptic specializations. *J. Neurosci.* **2001**, *21*, 641-653.
167. Jones, C. A.; Vial, C.; Sellers, L. A.; Humphrey, P. P.; Evans, R. J.; Chessell, I. P. Functional regulation of P2X6 receptors by N-linked glycosylation: identification of a novel alpha beta-methylene ATP-sensitive phenotype. *Mol. Pharmacol.* **2004**, *65*, 979-985.
168. Aschrafi, A.; Sadtler, S.; Niculescu, C.; Rettinger, J.; Schmalzing, G. Trimeric architecture of homomeric P2X2 and heteromeric P2X1+2 receptor subtypes. *J. Mol. Biol.* **2004**, *342*, 333-343.
169. Ormond, S. J.; Barrera, N. P.; Qureshi, O. S.; Henderson, R. M.; Edwardson, J. M.; Murrell-Lagnado, R. D. An uncharged region within the N terminus of the P2X6 receptor inhibits its assembly and exit from the endoplasmic reticulum. *Mol. Pharmacol.* **2006**, *69*, 1692-1700.
170. King, B. F.; Townsend-Nicholson, A.; Wildman, S. S.; Thomas, T.; Spyer, K. M.; Burnstock, G. Coexpression of rat P2X2 and P2X6 subunits in Xenopus oocytes. *J. Neurosci.* **2000**, *20*, 4871-4877.
171. Le, K. T.; Babinski, K.; Seguela, P. Central P2X4 and P2X6 channel subunits coassemble into a novel heteromeric ATP receptor. *J. Neurosci.* **1998**, *18*, 7152-7159.
172. Surprenant, A.; Rassendren, F.; Kawashima, E.; North, R. A.; Buell, G. The cytolytic P2Z receptor for extracellular ATP identified as a P2X receptor (P2X7). *Science* **1996**, *272*, 735-738.
173. Rassendren, F.; Buell, G. N.; Virginio, C.; Collo, G.; North, R. A.; Surprenant, A. The permeabilizing ATP receptor, P2X7. Cloning and expression of a human cDNA. *J. Biol. Chem.* **1997**, *272*, 5482-5486.

174. Wickert, L. E.; Blanchette, J. B.; Waldschmidt, N. V.; Bertics, P. J.; Denu, J. M.; Denlinger, L. C.; Lenertz, L. Y. The C-terminus of human nucleotide receptor P2X7 is critical for receptor oligomerization and N-linked glycosylation. *PLoS. One.* **2013**, *8*, e63789.
175. Collo, G.; Neidhart, S.; Kawashima, E.; Kosco-Vilbois, M.; North, R. A.; Buell, G. Tissue distribution of the P2X7 receptor. *Neuropharmacology* **1997**, *36*, 1277-1283.
176. Jiang, L. H.; Rassendren, F.; Mackenzie, A.; Zhang, Y. H.; Surprenant, A.; North, R. A. N-methyl-D-glucamine and propidium dyes utilize different permeation pathways at rat P2X(7) receptors. *Am. J. Physiol Cell Physiol* **2005**, *289*, C1295-C1302.
177. Iyer, S. S.; Pulskens, W. P.; Sadler, J. J.; Butter, L. M.; Teske, G. J.; Ulland, T. K.; Eisenbarth, S. C.; Florquin, S.; Flavell, R. A.; Leemans, J. C.; Sutterwala, F. S. Necrotic cells trigger a sterile inflammatory response through the Nlrp3 inflammasome. *Proc. Natl. Acad. Sci. U. S. A* **2009**, *106*, 20388-20393.
178. Roger, S.; Jelassi, B.; Couillin, I.; Pelegrin, P.; Besson, P.; Jiang, L. H. Understanding the roles of the P2X7 receptor in solid tumour progression and therapeutic perspectives. *Biochim. Biophys. Acta* **2015**, *1848*, 2584-2602.
179. Neves, A. R.; Castelo-Branco, M. T.; Figliuolo, V. R.; Bernardazzi, C.; Buongusto, F.; Yoshimoto, A.; Nanini, H. F.; Coutinho, C. M.; Carneiro, A. J.; Coutinho-Silva, R.; de Souza, H. S. Overexpression of ATP-activated P2X7 receptors in the intestinal mucosa is implicated in the pathogenesis of Crohn's disease. *Inflamm. Bowel. Dis.* **2014**, *20*, 444-457.
180. Marques, C. C.; Castelo-Branco, M. T.; Pacheco, R. G.; Buongusto, F.; do, R. A., Jr.; Schanaider, A.; Coutinho-Silva, R.; de Souza, H. S. Prophylactic systemic P2X7 receptor blockade prevents experimental colitis. *Biochim. Biophys. Acta* **2014**, *1842*, 65-78.
181. Monif, M.; Burnstock, G.; Williams, D. A. Microglia: proliferation and activation driven by the P2X7 receptor. *Int. J. Biochem. Cell Biol.* **2010**, *42*, 1753-1756.
182. Eser, A.; Colombel, J. F.; Rutgeerts, P.; Vermeire, S.; Vogelsang, H.; Braddock, M.; Persson, T.; Reinisch, W. Safety and Efficacy of an Oral Inhibitor of the Purinergic Receptor P2X7 in Adult Patients with Moderately to Severely Active Crohn's Disease: A Randomized Placebo-controlled, Double-blind, Phase IIa Study. *Inflamm. Bowel. Dis.* **2015**, *21*, 2247-2253.
183. Bartlett, R.; Stokes, L.; Sluyter, R. The P2X7 receptor channel: recent developments and the use of P2X7 antagonists in models of disease. *Pharmacol. Rev.* **2014**, *66*, 638-675.
184. Humphreys, B. D.; Virginio, C.; Surprenant, A.; Rice, J.; Dubyak, G. R. Isoquinolines as antagonists of the P2X7 nucleotide receptor: high selectivity for the human versus rat receptor homologues. *Mol. Pharmacol.* **1998**, *54*, 22-32.
185. Donnelly-Roberts, D. L.; Namovic, M. T.; Han, P.; Jarvis, M. F. Mammalian P2X7 receptor pharmacology: comparison of recombinant mouse, rat and human P2X7 receptors. *Br. J. Pharmacol.* **2009**, *157*, 1203-1214.

186. Nelson, D. W.; Gregg, R. J.; Kort, M. E.; Perez-Medrano, A.; Voight, E. A.; Wang, Y.; Grayson, G.; Namovic, M. T.; Donnelly-Roberts, D. L.; Niforatos, W.; Honore, P.; Jarvis, M. F.; Faltynek, C. R.; Carroll, W. A. Structure-activity relationship studies on a series of novel, substituted 1-benzyl-5-phenyltetrazole P2X7 antagonists. *J. Med. Chem.* **2006**, *49*, 3659-3666.
187. Honore, P.; Donnelly-Roberts, D.; Namovic, M.; Zhong, C.; Wade, C.; Chandran, P.; Zhu, C.; Carroll, W.; Perez-Medrano, A.; Iwakura, Y.; Jarvis, M. F. The antihyperalgesic activity of a selective P2X7 receptor antagonist, A-839977, is lost in IL-1 $\alpha$  knockout mice. *Behav. Brain Res.* **2009**, *204*, 77-81.
188. Michel, A. D.; Chambers, L. J.; Clay, W. C.; Condreay, J. P.; Walter, D. S.; Chessell, I. P. Direct labelling of the human P2X7 receptor and identification of positive and negative cooperativity of binding. *Br. J. Pharmacol.* **2007**, *151*, 103-114.
189. Broom, D. C.; Matson, D. J.; Bradshaw, E.; Buck, M. E.; Meade, R.; Coombs, S.; Matchett, M.; Ford, K. K.; Yu, W.; Yuan, J.; Sun, S. H.; Ochoa, R.; Krause, J. E.; Wustrow, D. J.; Cortright, D. N. Characterization of N-(adamantan-1-ylmethyl)-5-[(3R-aminopyrrolidin-1-yl)methyl]-2-chloro-benzamide, a P2X7 antagonist in animal models of pain and inflammation. *J. Pharmacol. Exp. Ther.* **2008**, *327*, 620-633.
190. Honore, P.; Donnelly-Roberts, D.; Namovic, M. T.; Hsieh, G.; Zhu, C. Z.; Mikusa, J. P.; Hernandez, G.; Zhong, C.; Gauvin, D. M.; Chandran, P.; Harris, R.; Medrano, A. P.; Carroll, W.; Marsh, K.; Sullivan, J. P.; Faltynek, C. R.; Jarvis, M. F. A-740003 [N-(1-[[[(cyanoimino)(5-quinolinylamino) methyl]amino]-2,2-dimethylpropyl]-2-(3,4-dimethoxyphenyl)acetamide], a novel and selective P2X7 receptor antagonist, dose-dependently reduces neuropathic pain in the rat. *J. Pharmacol. Exp. Ther.* **2006**, *319*, 1376-1385.
191. Stokes, L.; Jiang, L. H.; Alcaraz, L.; Bent, J.; Bowers, K.; Fagura, M.; Furber, M.; Mortimore, M.; Lawson, M.; Theaker, J.; Laurent, C.; Braddock, M.; Surprenant, A. Characterization of a selective and potent antagonist of human P2X(7) receptors, AZ11645373. *Br. J. Pharmacol.* **2006**, *149*, 880-887.
192. Letavic, M. A.; Lord, B.; Bischoff, F.; Hawryluk, N. A.; Pieters, S.; Rech, J. C.; Sales, Z.; Velter, A. I.; Ao, H.; Bonaventure, P.; Contreras, V.; Jiang, X.; Morton, K. L.; Scott, B.; Wang, Q.; Wickenden, A. D.; Carruthers, N. I.; Bhattacharya, A. Synthesis and Pharmacological Characterization of Two Novel, Brain Penetrating P2X7 Antagonists. *ACS Med. Chem. Lett.* **2013**, *4*, 419-422.
193. Hempel, C.; Norenberg, W.; Sobottka, H.; Urban, N.; Nicke, A.; Fischer, W.; Schaefer, M. The phenothiazine-class antipsychotic drugs prochlorperazine and trifluoperazine are potent allosteric modulators of the human P2X7 receptor. *Neuropharmacology* **2013**, *75*, 365-379.
194. Bhattacharya, A.; Wang, Q.; Ao, H.; Shoblock, J. R.; Lord, B.; Aluisio, L.; Fraser, I.; Nepomuceno, D.; Neff, R. A.; Welty, N.; Lovenberg, T. W.; Bonaventure, P.; Wickenden, A. D.; Letavic, M. A. Pharmacological characterization of a novel centrally permeable P2X7 receptor antagonist: JNJ-47965567. *Br. J. Pharmacol.* **2013**, *170*, 624-640.

195. Ferrari, D.; Pizzirani, C.; Adinolfi, E.; Forchap, S.; Sitta, B.; Turchet, L.; Falzoni, S.; Minelli, M.; Baricordi, R.; Di, V. F. The antibiotic polymyxin B modulates P2X7 receptor function. *J. Immunol.* **2004**, *173*, 4652-4660.
196. Nakanishi, M.; Mori, T.; Nishikawa, K.; Sawada, M.; Kuno, M.; Asada, A. The effects of general anesthetics on P2X7 and P2Y receptors in a rat microglial cell line. *Anesth. Analg.* **2007**, *104*, 1136-44, tables.
197. Norenberg, W.; Hempel, C.; Urban, N.; Sobottka, H.; Illes, P.; Schaefer, M. Clemastine potentiates the human P2X7 receptor by sensitizing it to lower ATP concentrations. *J. Biol. Chem.* **2011**, *286*, 11067-11081.
198. Zhang, J. H.; Chung, T. D.; Oldenburg, K. R. A Simple Statistical Parameter for Use in Evaluation and Validation of High Throughput Screening Assays. *J. Biomol. Screen.* **1999**, *4*, 67-73.
199. Cirillo, C.; Capasso, R. Constipation and Botanical Medicines: An Overview. *Phytother. Res.* **2015**, *29*, 1488-1493.
200. Evison, B. J.; Sleebs, B. E.; Watson, K. G.; Phillips, D. R.; Cutts, S. M. Mitoxantrone, More than Just Another Topoisomerase II Poison. *Med. Res. Rev.* **2015**.
201. Martinelli, B. F.; Vacchi, L.; Rovaris, M.; Capra, R.; Comi, G. Mitoxantrone for multiple sclerosis. *Cochrane. Database. Syst. Rev.* **2013**, *5*, CD002127.
202. Kingwell, E.; Koch, M.; Leung, B.; Isserow, S.; Geddes, J.; Rieckmann, P.; Tremlett, H. Cardiotoxicity and other adverse events associated with mitoxantrone treatment for MS. *Neurology* **2010**, *74*, 1822-1826.
203. Glanzel, M.; Bultmann, R.; Starke, K.; Frahm, A. W. Structure-activity relationships of novel P2-receptor antagonists structurally related to Reactive Blue 2. *Eur. J. Med. Chem.* **2005**, *40*, 1262-1276.
204. Clonis, Y. D.; Labrou, N. E.; Kotsira, V. P.; Mazitsos, C.; Melissis, S.; Gogolas, G. Biomimetic dyes as affinity chromatography tools in enzyme purification. *J. Chromatogr. A* **2000**, *891*, 33-44.
205. Weyler, S.; Baqi, Y.; Hillmann, P.; Kaulich, M.; Hunder, A. M.; Muller, I. A.; Muller, C. E. Combinatorial synthesis of anilinoanthraquinone derivatives and evaluation as non-nucleotide-derived P2Y2 receptor antagonists. *Bioorg. Med. Chem. Lett.* **2008**, *18*, 223-227.
206. Baqi, Y.; Atzler, K.; Kose, M.; Glanzel, M.; Muller, C. E. High-affinity, non-nucleotide-derived competitive antagonists of platelet P2Y12 receptors. *J. Med. Chem.* **2009**, *52*, 3784-3793.
207. Goto, S.; Tamura, N.; Eto, K.; Ikeda, Y.; Handa, S. Functional significance of adenosine 5'-diphosphate receptor (P2Y(12)) in platelet activation initiated by binding of von Willebrand factor to platelet GP Ialpha induced by conditions of high shear rate. *Circulation* **2002**, *105*, 2531-2536.

208. Baqi, Y.; Muller, C. E. Rapid and efficient microwave-assisted copper(0)-catalyzed ullmann coupling reaction: general access to anilinoanthraquinone derivatives. *Org. Lett.* **2007**, *9*, 1271-1274.
209. Baqi, Y.; Muller, C. E. Catalyst-free microwave-assisted amination of 2-chloro-5-nitrobenzoic acid. *J. Org. Chem.* **2007**, *72*, 5908-5911.
210. Baqi, Y.; Muller, C. E. Synthesis of alkyl- and aryl-amino-substituted anthraquinone derivatives by microwave-assisted copper(0)-catalyzed Ullmann coupling reactions. *Nat. Protoc.* **2010**, *5*, 945-953.
211. Hoffmann, K.; Baqi, Y.; Morena, M. S.; Glanzel, M.; Muller, C. E.; von, K., I Interaction of new, very potent non-nucleotide antagonists with Arg256 of the human platelet P2Y12 receptor. *J. Pharmacol. Exp. Ther.* **2009**, *331*, 648-655.
212. Baqi, Y.; Lee, S. Y.; Iqbal, J.; Ripphausen, P.; Lehr, A.; Scheiff, A. B.; Zimmermann, H.; Bajorath, J.; Muller, C. E. Development of potent and selective inhibitors of ecto-5'-nucleotidase based on an anthraquinone scaffold. *J. Med. Chem.* **2010**, *53*, 2076-2086.
213. Baqi, Y.; Weyler, S.; Iqbal, J.; Zimmermann, H.; Muller, C. E. Structure-activity relationships of anthraquinone derivatives derived from bromaminic acid as inhibitors of ectonucleoside triphosphate diphosphohydrolases (E-NTPDases). *Purinergic. Signal.* **2009**, *5*, 91-106.
214. Zebisch, M.; Baqi, Y.; Schafer, P.; Muller, C. E.; Strater, N. Crystal structure of NTPDase2 in complex with the sulfoanthraquinone inhibitor PSB-071. *J. Struct. Biol.* **2014**, *185*, 336-341.
215. Lachnit, W. G.; Oglesby, I. B.; Gever, J. R.; Gever, M.; Huang, C.; Li, X. C.; Jin, H.; McGivern, J. G.; Ford, A. P. Regulated expression of the rat recombinant P2X(3) receptor in stably transfected CHO-K1 tTA cells. *J. Auton. Nerv. Syst.* **2000**, *81*, 75-81.
216. Khmyz, V.; Maximyuk, O.; Teslenko, V.; Verkhatsky, A.; Krishtal, O. P2X3 receptor gating near normal body temperature. *Pflugers Arch.* **2008**, *456*, 339-347.
217. Hasenknopf, B. Polyoxometalates: introduction to a class of inorganic compounds and their biomedical applications. *Front Biosci.* **2005**, *10*, 275-287.
218. Muller, A.; Peters, F.; Pope, M. T.; Gatteschi, D. Polyoxometalates: Very Large Clusters-Nanoscale Magnets. *Chem. Rev.* **1998**, *98*, 239-272.
219. Izarova, N. V.; Pope, M. T.; Kortz, U. Noble metals in polyoxometalates. *Angew. Chem. Int. Ed Engl.* **2012**, *51*, 9492-9510.
220. Pope, M. T.; Kortz, U. Polyoxometalates. In *Encyclopedia of Inorganic and Bioinorganic Chemistry*; John Wiley & Sons, Ltd: 2011.
221. Muller, C. E.; Iqbal, J.; Baqi, Y.; Zimmermann, H.; Rollich, A.; Stephan, H. Polyoxometalates--a new class of potent ecto-nucleoside triphosphate diphosphohydrolase (NTPDase) inhibitors. *Bioorg. Med. Chem. Lett.* **2006**, *16*, 5943-5947.

222. Plewinsky, B.; Stock, H. P.; Pänke, R. Ramanspektroskopische und Ultrazentrifugen-Messungen zur Untersuchung der Hydrolyse der Dodekawolframatophosphorsäure. *Z. anorg. allg. Chem.* **1977**, *434*, 192-200.
223. Meißner, T.; Bergmann, R.; Oswald, J.; Rode, K.; Stephan, H.; Richter, W.; Zänker, H.; Kraus, W.; Emmerling, F.; Reck, G. Ä. Chitosan-encapsulated Keggin Anion  $[\text{Ti}_2\text{W}_{10}\text{PO}_{40}]^{7-}$ . Synthesis, Characterization and Cellular Uptake Studies. *Transition Met Chem* **2006**, *31*, 603-610.
224. Pope, M. T.; Varga, G. M. Proton magnetic resonance of aqueous metatungstate ion: evidence for two central hydrogen atoms. *Chem. Commun. (London)* **1966**, 653-654.
225. Brown, G. M.; Noe-Spirlet, M. R.; Busing, W. R.; Levy, H. A. Dodecatungstophosphoric acid hexahydrate,  $(\text{H}_5\text{O}_2^+)_3(\text{PW}_{12}\text{O}_{40}^{3-})$ . The true structure of Keggin's 'pentahydrate' from single-crystal X-ray and neutron diffraction data. *Acta Cryst. B* **1977**, *33*, 1038-1046.
226. Evans, H. T.; Tourne, C. M.; Tourne, G. F.; Weakley, T. J. R. X-Ray crystallographic and tungsten-183 nuclear magnetic resonance structural studies of the  $[\text{M}_4(\text{H}_2\text{O})_2(\text{XW}_9\text{O}_{34})_2]^{10-}$  heteropolyanions (M = Co<sup>II</sup> or Zn, X = P or As). *J. Chem. Soc., Dalton Trans.* **1986**, 2699-2705.
227. Fischer, J.; Ricard, L.; Weiss, R. The structure of the heteropolytungstate  $(\text{NH}_4)_{17}\text{Na}[\text{NaW}_{21}\text{Sb}_9\text{O}_{86}]-14\text{H}_2\text{O}$ . An inorganic cryptate. *J. Am. Chem. Soc.* **1976**, *98*, 3050-3052.
228. Weakley, T. J. R.; Evans, H. T.; Showell, J. S.; Tourne, G. F.; Tourne, C. M. 18-Tungstotetracobalto(II)diphosphate and related anions: a novel structural class of heteropolyanions. *J. Chem. Soc., Chem. Commun.* **1973**, 139-140.
229. Hill, C. L.; Weeks, M. S.; Schinazi, R. F. Anti-HIV-1 activity, toxicity, and stability studies of representative structural families of polyoxometalates. *J. Med. Chem.* **1990**, *33*, 2767-2772.
230. Alizadeh, M. H.; Harmaker, S. P.; Jeannin, Y.; Martin-Frere, J.; Pope, M. T. A heteropolyanion with fivefold molecular symmetry that contains a nonlabile encapsulated sodium ion. The structure and chemistry of  $[\text{NaP}_5\text{W}_{30}\text{O}_{110}]^{14-}$ . *J. Am. Chem. Soc.* **1985**, *107*, 2662-2669.
231. Acerete, R.; Server-Carrio, J.; Vegas, A.; Martinez-Ripoll, M. Synthesis and x-ray crystal structure determination of a novel chiral heteropolyanion: the "3:1" octadecatungstohexaphosphate. *J. Am. Chem. Soc.* **1990**, *112*, 9386-9387.
232. Boyd, T.; Mitchell, S. G.; Gabb, D.; Long, D. L.; Cronin, L. Investigating cation binding in the polyoxometalate-super-crown  $[\text{P}_8\text{W}_{48}\text{O}_{184}]^{40-}$ . *Chemistry*. **2011**, *17*, 12010-12014.
233. Contant, R.; Teze, A. A new crown heteropolyanion  $\text{K}_{28}\text{Li}_5\text{H}_7\text{P}_8\text{W}_{48}\text{O}_{184}\cdot 92\text{H}_2\text{O}$ : synthesis, structure, and properties. *Inorg. Chem.* **1985**, *24*, 4610-4614.

234. Kortz, U.; Jameson, G. B.; Pope, M. T. Polyoxometalate Diphosphate Complexes. Folded Macrocyclic Dodecatungstates,  $[(O_3PXPO_3)_4W_{12}O_{36}]^{16-}$  (X = O, CH<sub>2</sub>). *J. Am. Chem. Soc.* **1994**, *116*, 2659-2660.
235. Tang, J.; Yu, W.; Hu, M. B.; Xiao, Y.; Wang, X. G.; Ren, L. J.; Zheng, P.; Zhu, W.; Chen, Y.; Wang, W. Bottom-Up Hybridization: A Strategy for the Preparation of a Thermostable Polyoxometalate-Polymer Hybrid with Hierarchical Hybrid Structures. *ChemPlusChem* **2014**, *79*, 1455-1462.
236. Tang, J.; Ma, C.; Li, X. Y.; Ren, L. J.; Wu, H.; Zheng, P.; Wang, W. Self-Assembling a Polyoxometalate-PEG Hybrid into a Nanoenhancer To Tailor PEG Properties. *Macromolecules* **2015**, *48*, 2723-2730.
237. Yarovoi, S. S.; Mironov, Y. V.; Solodovnikov, S. F.; Naumov, D. Y.; Moroz, N. K.; Kozlova, S. G.; Simon, A.; Fedorov, V. E. Unexpected ligand substitutions in the cluster core {Re<sub>6</sub>Se<sub>8</sub>}: synthesis and structure of the novel cluster compound Cs<sub>11</sub>(H<sub>3</sub>O)[Re<sub>6</sub>Se<sub>4</sub>(O)<sub>4</sub>Cl<sub>6</sub>]<sub>3</sub>·4H<sub>2</sub>O. *Chem. Commun. (Camb.)* **2005**, 719-721.
238. Brylev, K. A.; Mironov, Y. V.; Yarovoi, S. S.; Naumov, N. G.; Fedorov, V. E.; Kim, S. J.; Kitamura, N.; Kuwahara, Y.; Yamada, K.; Ishizaka, S.; Sasaki, Y. A family of octahedral rhenium cluster complexes [Re<sub>6</sub>Q<sub>8</sub>(H<sub>2</sub>O)<sub>n</sub>(OH)<sub>6-n</sub>]<sup>n-4</sup> (Q=S, Se; n=0-6): structural and pH-dependent spectroscopic studies. *Inorg. Chem.* **2007**, *46*, 7414-7422.
239. Brylev, K. A.; Mironov, Y. V.; Kozlova, S. G.; Fedorov, V. E.; Kim, S. J.; Pietzsch, H. J.; Stephan, H.; Ito, A.; Ishizaka, S.; Kitamura, N. The first octahedral cluster complexes with terminal formate ligands: synthesis, structure, and properties of K<sub>4</sub>[Re<sub>6</sub>S<sub>8</sub>(HCOO)<sub>6</sub>] and Cs<sub>4</sub>[Re<sub>6</sub>S<sub>8</sub>(HCOO)<sub>6</sub>]. *Inorg. Chem.* **2009**, *48*, 2309-2315.
240. Brylev, K. A.; Mironov, Y. V.; Fedorov, V. E.; Kim, S. J.; Pietzsch, H. J. r.; Stephan, H.; Ito, A.; Kitamura, N. A new hexanuclear rhenium cluster complex with six terminal acetate ligands: Synthesis, structure, and properties of K<sub>4</sub>[Re<sub>6</sub>S<sub>8</sub>(CH<sub>3</sub>COO)<sub>6</sub>]<sub>3</sub>·8H<sub>2</sub>O. *Inorganica Chimica Acta* **2010**, *363*, 2686-2691.
241. Sodium orthovanadate; Product Information S6508. Sigma Aldrich Chemie GmbH, Taufkirchen. Available at [http://www.sigmaaldrich.com/content/dam/sigmaaldrich/docs/Sigma/Product\\_Information\\_Sheet/1/s6508pis.pdf](http://www.sigmaaldrich.com/content/dam/sigmaaldrich/docs/Sigma/Product_Information_Sheet/1/s6508pis.pdf). Accessed on 06/01/2016.
242. Sodium metavanadate; MSDS No. 72060. Sigma Aldrich Chemie GmbH, Taufkirchen. Available at <http://sigmaaldrich.com/>. Accessed on 06/01/2016.
243. Dong, Z.; Tan, R.; Cao, J.; Yang, Y.; Kong, C.; Du, J.; Zhu, S.; Zhang, Y.; Lu, J.; Huang, B.; Liu, S. Discovery of polyoxometalate-based HDAC inhibitors with profound anticancer activity in vitro and in vivo. *Eur. J. Med. Chem.* **2011**, *46*, 2477-2484.
244. Wang, X.; Li, F.; Liu, S.; Pope, M. T. New liposome-encapsulated-polyoxometalates: synthesis and antitumoral activity. *J. Inorg. Biochem.* **2005**, *99*, 452-457.
245. Wang, X.; Liu, J.; Li, J.; Yang, Y.; Liu, J.; Li, B.; Pope, M. T. Synthesis and antitumor activity of cyclopentadienyltitanium substituted polyoxotungstate [CoW<sub>11</sub>O<sub>39</sub>(CpTi)]<sup>7-</sup> (Cp=η<sup>5</sup>-C<sub>5</sub>H<sub>5</sub>). *J. Inorg. Biochem.* **2003**, *94*, 279-284.



246. Yanagie, H.; Ogata, A.; Mitsui, S.; Hisa, T.; Yamase, T.; Eriguchi, M. Anticancer activity of polyoxomolybdate. *Biomed. Pharmacother.* **2006**, *60*, 349-352.
247. Mitsui, S.; Ogata, A.; Yanagie, H.; Kasano, H.; Hisa, T.; Yamase, T.; Eriguchi, M. Antitumor activity of polyoxomolybdate,  $[\text{NH}_3\text{Pr}^I]_6[\text{Mo}_7\text{O}_{24}]x3\text{H}_2\text{O}$ , against, human gastric cancer model. *Biomed. Pharmacother.* **2006**, *60*, 353-358.
248. Yamase, T.; Fukuda, N.; Tajima, Y. Synergistic effect of polyoxotungstates in combination with beta-lactam antibiotics on antibacterial activity against methicillin-resistant *Staphylococcus aureus*. *Biol. Pharm. Bull.* **1996**, *19*, 459-465.
249. Inoue, M.; Segawa, K.; Matsunaga, S.; Matsumoto, N.; Oda, M.; Yamase, T. Antibacterial activity of highly negative charged polyoxotungstates,  $\text{K}_{27}[\text{KAs}_4\text{W}_{40}\text{O}_{140}]$  and  $\text{K}_{18}[\text{KSb}_9\text{W}_{21}\text{O}_{86}]$ , and Keggin-structural polyoxotungstates against *Helicobacter pylori*. *J. Inorg. Biochem.* **2005**, *99*, 1023-1031.
250. Inoue, M.; Suzuki, T.; Fujita, Y.; Oda, M.; Matsumoto, N.; Yamase, T. Enhancement of antibacterial activity of beta-lactam antibiotics by  $[\text{P}_2\text{W}_{18}\text{O}_{62}]^{6-}$ ,  $[\text{SiMo}_{12}\text{O}_{40}]^{4-}$ , and  $[\text{PTi}_2\text{W}_{10}\text{O}_{40}]^{7-}$  against methicillin-resistant and vancomycin-resistant *Staphylococcus aureus*. *J. Inorg. Biochem.* **2006**, *100*, 1225-1233.
251. Shigeta, S.; Mori, S.; Yamase, T.; Yamamoto, N.; Yamamoto, N. Anti-RNA virus activity of polyoxometalates. *Biomed. Pharmacother.* **2006**, *60*, 211-219.
252. Sarafianos, S. G.; Kortz, U.; Pope, M. T.; Modak, M. J. Mechanism of polyoxometalate-mediated inactivation of DNA polymerases: an analysis with HIV-1 reverse transcriptase indicates specificity for the DNA-binding cleft. *Biochem. J.* **1996**, *319* ( Pt 2), 619-626.
253. Flutsch, A.; Schroeder, T.; Grutter, M. G.; Patzke, G. R. HIV-1 protease inhibition potential of functionalized polyoxometalates. *Bioorg. Med. Chem. Lett.* **2011**, *21*, 1162-1166.
254. Qi, Y. F.; Zhang, H.; Wang, J.; Jiang, Y.; Li, J.; Yuan, Y.; Zhang, S.; Xu, K.; Li, Y.; Li, J.; Niu, J.; Wang, E. In vitro anti-hepatitis B and SARS virus activities of a titanium-substituted-heteropolytungstate. *Antiviral Res.* **2012**, *93*, 118-125.
255. Rhule, J. T.; Hill, C. L.; Judd, D. A.; Schinazi, R. F. Polyoxometalates in Medicine. *Chem. Rev.* **1998**, *98*, 327-358.
256. Nomiya, K.; Torii, H.; Hasegawa, T.; Nemoto, Y.; Nomura, K.; Hashino, K.; Uchida, M.; Kato, Y.; Shimizu, K.; Oda, M. Insulin mimetic effect of a tungstate cluster. Effect of oral administration of homo-polyoxotungstates and vanadium-substituted polyoxotungstates on blood glucose level of STZ mice. *J. Inorg. Biochem.* **2001**, *86*, 657-667.
257. Crans, D. C. Chemistry and insulin-like properties of vanadium(IV) and vanadium(V) compounds. *J. Inorg. Biochem.* **2000**, *80*, 123-131.
258. Srivastava, A. K.; Mehdi, M. Z. Insulino-mimetic and anti-diabetic effects of vanadium compounds. *Diabet. Med.* **2005**, *22*, 2-13.

259. Ilyas, Z.; Shah, H. S.; Al-Oweini, R.; Kortz, U.; Iqbal, J. Antidiabetic potential of polyoxotungstates: in vitro and in vivo studies. *Metallomics*. **2014**, *6*, 1521-1526.
260. Cibert, C.; Jasmin, C. Determination of the intracellular localization of a polyoxotungstate (HPA-23) by Raman Laser and X fluorescence spectroscopies. *Biochem. Biophys. Res. Commun.* **1982**, *108*, 1424-1433.
261. Ni, L.; Greenspan, P.; Gutman, R.; Kelloes, C.; Farmer, M. A.; Boudinot, F. D. Cellular localization of antiviral polyoxometalates in J774 macrophages. *Antiviral Res.* **1996**, *32*, 141-148.
262. Kohler, D.; Eckle, T.; Faigle, M.; Grenz, A.; Mittelbronn, M.; Laucher, S.; Hart, M. L.; Robson, S. C.; Muller, C. E.; Eltzhig, H. K. CD39/ectonucleoside triphosphate diphosphohydrolase 1 provides myocardial protection during cardiac ischemia/reperfusion injury. *Circulation* **2007**, *116*, 1784-1794.
263. Wall, M. J.; Wigmore, G.; Lopatar, J.; Frenguelli, B. G.; Dale, N. The novel NTPDase inhibitor sodium polyoxotungstate (POM-1) inhibits ATP breakdown but also blocks central synaptic transmission, an action independent of NTPDase inhibition. *Neuropharmacology* **2008**, *55*, 1251-1258.
264. Sun, W.; Vanhooke, J. L.; Sondek, J.; Zhang, Q. High-throughput fluorescence polarization assay for the enzymatic activity of GTPase-activating protein of ADP-ribosylation factor (ARFGAP). *J. Biomol. Screen.* **2011**, *16*, 717-723.
265. Melani, A.; Corti, F.; Stephan, H.; Muller, C. E.; Donati, C.; Bruni, P.; Vannucchi, M. G.; Pedata, F. Ecto-ATPase inhibition: ATP and adenosine release under physiological and ischemic in vivo conditions in the rat striatum. *Exp. Neurol.* **2012**, *233*, 193-204.
266. Malek, R. A. Interaktion von Polyoxometalaten und anderen Metallclusterverbindungen mit P2Y Rezeptoren. *Masterarbeit*, Universität Bonn, **2011**.
267. Kang, J. S.; Deluca, P. P.; Lee, K. C. Emerging PEGylated drugs. *Expert. Opin. Emerg. Drugs* **2009**, *14*, 363-380.
268. Veronese, F. M.; Mero, A. The impact of PEGylation on biological therapies. *BioDrugs*. **2008**, *22*, 315-329.
269. Leon, I. E.; Porro, V.; Astrada, S.; Egusquiza, M. G.; Cabello, C. I.; Bollati-Fogolin, M.; Etcheverry, S. B. Polyoxometalates as antitumor agents: Bioactivity of a new polyoxometalate with copper on a human osteosarcoma model. *Chem. Biol. Interact.* **2014**, *222C*, 87-96.
270. Dianat, S.; Bordbar, A. K.; Tangestaninejad, S.; Yadollahi, B.; Zarkesh-Esfahani, S. H.; Habibi, P. ctDNA binding affinity and in vitro antitumor activity of three Keggin type polyoxotungstates. *J. Photochem. Photobiol. B* **2013**, *124*, 27-33.
271. Lee, S. Y.; Fiene, A.; Li, W.; Hanck, T.; Brylev, K. A.; Fedorov, V. E.; Lecka, J.; Haider, A.; Pietzsch, H. J.; Zimmermann, H.; Sevigny, J.; Kortz, U.; Stephan, H.; Muller, C. E. Polyoxometalates--potent and selective ecto-nucleotidase inhibitors. *Biochem. Pharmacol.* **2015**, *93*, 171-181.

272. Zimmermann, H.; Zebisch, M.; Strater, N. Cellular function and molecular structure of ecto-nucleotidases. *Purinergic. Signal.* **2012**, *8*, 437-502.
273. Langedijk, J.; Mantel-Teeuwisse, A. K.; Slijkerman, D. S.; Schutjens, M. H. Drug repositioning and repurposing: terminology and definitions in literature. *Drug Discov. Today* **2015**, *20*, 1027-1034.
274. Ashburn, T. T.; Thor, K. B. Drug repositioning: identifying and developing new uses for existing drugs. *Nat. Rev. Drug Discov.* **2004**, *3*, 673-683.
275. Kale, V. P.; Amin, S. G.; Pandey, M. K. Targeting ion channels for cancer therapy by repurposing the approved drugs. *Biochim. Biophys. Acta* **2015**, *1848*, 2747-2755.
276. Jin, G.; Wong, S. T. Toward better drug repositioning: prioritizing and integrating existing methods into efficient pipelines. *Drug Discov. Today* **2014**, *19*, 637-644.
277. Zheng, C.; Guo, Z.; Huang, C.; Wu, Z.; Li, Y.; Chen, X.; Fu, Y.; Ru, J.; Ali, S. P.; Wang, Y.; Wang, Y. Large-scale Direct Targeting for Drug Repositioning and Discovery. *Sci. Rep.* **2015**, *5*, 11970.
278. McCabe, B.; Liberante, F.; Mills, K. I. Repurposing medicinal compounds for blood cancer treatment. *Ann. Hematol.* **2015**, *94*, 1267-1276.
279. Swinney, D. C.; Anthony, J. How were new medicines discovered? *Nat. Rev. Drug Discov.* **2011**, *10*, 507-519.
280. Swamidass, S. J.; Agarwal, P. Drug repositioning from the combined evaluation of phenotypic and target-based screening. *AMIA. Jt. Summits. Transl. Sci. Proc.* **2013**, *2013*, 161.
281. Swinney, D. C. Phenotypic vs. target-based drug discovery for first-in-class medicines. *Clin. Pharmacol. Ther.* **2013**, *93*, 299-301.
282. Swinney, D. C.; Xia, S. The discovery of medicines for rare diseases. *Future. Med. Chem* **2014**, *6*, 987-1002.
283. Lee, J. A.; Shinn, P.; Jaken, S.; Oliver, S.; Willard, F. S.; Heidler, S.; Peery, R. B.; Oler, J.; Chu, S.; Southall, N.; Dexheimer, T. S.; Smallwood, J.; Huang, R.; Guha, R.; Jadhav, A.; Cox, K.; Austin, C. P.; Simeonov, A.; Sittampalam, G. S.; Husain, S.; Franklin, N.; Wild, D. J.; Yang, J. J.; Sutherland, J. J.; Thomas, C. J. Novel Phenotypic Outcomes Identified for a Public Collection of Approved Drugs from a Publicly Accessible Panel of Assays. *PLoS. One.* **2015**, *10*, e0130796.
284. National Center for Advancing Translational Sciences Repurposing Drugs. Available at <http://www.ncats.nih.gov/research/reengineering/rescue-repurpose/rescue-repurpose.html>. Accessed on 06/01/2016.
285. Medical Research Council Biomedical Catalyst: Developmental Pathway Funding Scheme. Available at <http://www.mrc.ac.uk/funding/browse/developmental-pathway-funding-scheme/>. Accessed on 06./01/2016.

286. Netherlands Organisation for Health Research and Development (ZonMw) Drug Rediscovery/Off-label. Available at <http://zonmw.nl/nl/themas/thema-detail/geneesmiddelen/drug-rediscoveryoff-label/>. Accessed on 06/01/2016.
287. Kouznetsova, J.; Sun, W.; Martinez-Romero, C.; Tawa, G.; Shinn, P.; Chen, C. Z.; Schimmer, A.; Sanderson, P.; McKew, J. C.; Zheng, W.; Garcia-Sastre, A. Identification of 53 compounds that block Ebola virus-like particle entry via a repurposing screen of approved drugs. *Emerg. Microbes. Infect.* **2014**, *3*, e84.
288. Johansen, L. M.; DeWald, L. E.; Shoemaker, C. J.; Hoffstrom, B. G.; Lear-Rooney, C. M.; Stossel, A.; Nelson, E.; Delos, S. E.; Simmons, J. A.; Grenier, J. M.; Pierce, L. T.; Pajouhesh, H.; Lehar, J.; Hensley, L. E.; Glass, P. J.; White, J. M.; Olinger, G. G. A screen of approved drugs and molecular probes identifies therapeutics with anti-Ebola virus activity. *Sci. Transl. Med.* **2015**, *7*, 290ra89.
289. Jahchan, N. S.; Dudley, J. T.; Mazur, P. K.; Flores, N.; Yang, D.; Palmerton, A.; Zmoos, A. F.; Vaka, D.; Tran, K. Q.; Zhou, M.; Krasinska, K.; Riess, J. W.; Neal, J. W.; Khatri, P.; Park, K. S.; Butte, A. J.; Sage, J. A drug repositioning approach identifies tricyclic antidepressants as inhibitors of small cell lung cancer and other neuroendocrine tumors. *Cancer Discov.* **2013**, *3*, 1364-1377.
290. Ghofrani, H. A.; Olschewski, H.; Seeger, W.; Grimminger, F. [Sildenafil for treatment of severe pulmonary hypertension and commencing right-heart failure]. *Pneumologie* **2002**, *56*, 665-672.
291. FDA Drug Safety Communication: FDA recommends against use of Revatio (sildenafil) in children with pulmonary hypertension. Issued August **2012**. Available at <http://www.fda.gov/Drugs/DrugSafety/ucm317123.htm>. Accessed on 06/01/2016.
292. Vargesson, N. Thalidomide-induced teratogenesis: history and mechanisms. *Birth Defects Res. C. Embryo. Today* **2015**, *105*, 140-156.
293. Rajkumar, S. V. Thalidomide: tragic past and promising future. *Mayo Clin. Proc.* **2004**, *79*, 899-903.
294. McBride, W. G. Thalidomide and Congenital Abnormalities. *The Lancet* **1961**, *278*, 1358.
295. Lenz, W.; Pfeiffer, R. A.; Kosenow, W.; Hayman, D. J. Thalidomide and Congenital Abnormalities. *The Lancet* **1962**, *279*, 45-46.
296. Cavo, M.; Zamagni, E.; Tosi, P.; Tacchetti, P.; Cellini, C.; Cangini, D.; de, V. A.; Testoni, N.; Nicci, C.; Terragna, C.; Grafone, T.; Perrone, G.; Ceccolini, M.; Tura, S.; Baccarani, M. Superiority of thalidomide and dexamethasone over vincristine-doxorubicin-dexamethasone (VAD) as primary therapy in preparation for autologous transplantation for multiple myeloma. *Blood* **2005**, *106*, 35-39.
297. Sheskin, J. Thalidomide in the Treatment of Lepra Reactions. *Clin. Pharmacol. Ther.* **1965**, *6*, 303-306.
298. Kim, Y.; Schmidt-Wolf, I. G. Lenalidomide in multiple myeloma. *Expert. Rev. Anticancer Ther.* **2015**, *15*, 491-497.

299. Fouquet, G.; Bories, C.; Guidez, S.; Renaud, L.; Herbaux, C.; Javed, S.; Facon, T.; Leleu, X. Pomalidomide for multiple myeloma. *Expert. Rev. Hematol.* **2014**, *7*, 719-731.
300. Johansson, S.; Lindholm, P.; Gullbo, J.; Larsson, R.; Bohlin, L.; Claeson, P. Cytotoxicity of digitoxin and related cardiac glycosides in human tumor cells. *Anticancer Drugs* **2001**, *12*, 475-483.
301. Knipping, K.; Garssen, J.; van't Land, B. An evaluation of the inhibitory effects against rotavirus infection of edible plant extracts. *Virol. J.* **2012**, *9*, 137.
302. Zhou, X.; Zhao, L.; Liu, X.; Li, X.; Jia, F.; Zhang, Y.; Wang, Y. Antimycobacterial and synergistic effects of 18beta-glycyrrhetic acid or glycyrrhetic acid-30-piperazine in combination with isoniazid, rifampicin or streptomycin against *Mycobacterium bovis*. *Phytother. Res.* **2012**, *26*, 253-258.
303. Puchner, A.; Hayer, S.; Niederreiter, B.; Hladik, A.; Blueml, S.; Bonelli, M.; Scheinecker, C.; Smolen, J.; Redlich, K. Effects of 18beta-Glycyrrhetic acid in hTNFtg mice - a model of rheumatoid arthritis. *Wien. Klin. Wochenschr.* **2012**, *124*, 170-176.
304. Jaszczyszyn, A.; Gasiorowski, K.; Swiatek, P.; Malinka, W.; Cieslik-Boczula, K.; Petrus, J.; Czarnik-Matusiewicz, B. Chemical structure of phenothiazines and their biological activity. *Pharmacol. Rep.* **2012**, *64*, 16-23.
305. Ohlow, M. J.; Moosmann, B. Phenothiazine: the seven lives of pharmacology's first lead structure. *Drug Discov. Today* **2011**, *16*, 119-131.
306. Seeman, P.; Tallerico, T. Antipsychotic drugs which elicit little or no parkinsonism bind more loosely than dopamine to brain D2 receptors, yet occupy high levels of these receptors. *Mol. Psychiatry* **1998**, *3*, 123-134.
307. Mullur, R.; Liu, Y. Y.; Brent, G. A. Thyroid hormone regulation of metabolism. *Physiol Rev.* **2014**, *94*, 355-382.
308. Ursella, S.; Testa, A.; Mazzone, M.; Gentiloni, S. N. Amiodarone-induced thyroid dysfunction in clinical practice. *Eur. Rev. Med. Pharmacol. Sci.* **2006**, *10*, 269-278.
309. Science Information Cordarex® (Amiodarone). Status of information: September **2014**. Available at <http://www.fachinfo.de/>. Accessed on 06/01/2016.
310. Malerba, M.; Ragnoli, B. Ambroxol in the 21st century: pharmacological and clinical update. *Expert. Opin. Drug Metab Toxicol.* **2008**, *4*, 1119-1129.
311. Weiser, T.; Wilson, N. Inhibition of tetrodotoxin (TTX)-resistant and TTX-sensitive neuronal Na(+) channels by the secretolytic ambroxol. *Mol. Pharmacol.* **2002**, *62*, 433-438.
312. Weiser, T. Ambroxol: a CNS drug? *CNS. Neurosci. Ther.* **2008**, *14*, 17-24.
313. Vergin, H.; Bishop-Freudling, G. B.; Miczka, M.; Nitsche, V.; Strobel, K.; Matzkies, F. [The pharmacokinetics and bioequivalence of various dosage forms of ambroxol]. *Arzneimittelforschung.* **1985**, *35*, 1591-1595.

314. Lee, H. J.; Joung, S. K.; Kim, Y. G.; Yoo, J. Y.; Han, S. B. Bioequivalence assessment of ambroxol tablet after a single oral dose administration to healthy male volunteers. *Pharmacol. Res.* **2004**, *49*, 93-98.
315. Qian, J. Q. Cardiovascular pharmacological effects of bisbenzylisoquinoline alkaloid derivatives. *Acta Pharmacol. Sin.* **2002**, *23*, 1086-1092.
316. Wang, G.; Lemos, J. R. Tetrandrine: A new ligand to block voltage-dependent Ca<sup>2+</sup> and Ca<sup>2+</sup>-activated K<sup>+</sup> channels. *Life Sciences* **1994**, *56*, 295-306.
317. Kwan, C. Y.; Achike, F. I. Tetrandrine and related bis-benzylisoquinoline alkaloids from medicinal herbs: cardiovascular effects and mechanisms of action. *Acta Pharmacol. Sin.* **2002**, *23*, 1057-1068.
318. Cheung, K. K.; Marques-da-Silva, C.; Vairo, L.; dos Santos, D. S.; Goldenberg, R.; Coutinho-Silva, R.; Burnstock, G. Pharmacological and molecular characterization of functional P2 receptors in rat embryonic cardiomyocytes. *Purinergic. Signal.* **2015**, *11*, 127-138.
319. Zhang, Y. H.; Hancox, J. C. Mode-dependent inhibition by quinidine of Na<sup>+</sup>-Ca<sup>2+</sup> exchanger current from guinea-pig isolated ventricular myocytes. *Clin. Exp. Pharmacol. Physiol.* **2002**, *29*, 777-781.
320. Odds, F. C.; Brown, A. J.; Gow, N. A. Antifungal agents: mechanisms of action. *Trends Microbiol.* **2003**, *11*, 272-279.
321. Dietz, M.; Mohr, P.; Kuhn, B.; Maerki, H. P.; Hartman, P.; Ruf, A.; Benz, J.; Grether, U.; Wright, M. B. Comparative molecular profiling of the PPARalpha/gamma activator aleglitazar: PPAR selectivity, activity and interaction with cofactors. *ChemMedChem.* **2012**, *7*, 1101-1111.
322. Kubo, N.; Shirakawa, O.; Kuno, T.; Tanaka, C. Antimuscarinic effects of antihistamines: quantitative evaluation by receptor-binding assay. *Jpn. J. Pharmacol.* **1987**, *43*, 277-282.
323. Huang, W.; Zhang, J.; Wei, P.; Schrader, W. T.; Moore, D. D. Meclizine is an agonist ligand for mouse constitutive androstane receptor (CAR) and an inverse agonist for human CAR. *Mol. Endocrinol.* **2004**, *18*, 2402-2408.
324. Lau, A. J.; Yang, G.; Rajaraman, G.; Baucom, C. C.; Chang, T. K. Differential effect of meclizine on the activity of human pregnane X receptor and constitutive androstane receptor. *J. Pharmacol. Exp. Ther.* **2011**, *336*, 816-826.
325. Arcaniolo, D.; Conquy, S.; Tarcan, T. Flavoxate: present and future. *Eur. Rev. Med. Pharmacol. Sci.* **2015**, *19*, 719-731.
326. Bertoli, M.; Conti, F.; Conti, M.; Cova, A.; Setnikar, I. Pharmacokinetics of Flavoxate in man. *Pharmacol. Res. Commun.* **1976**, *8*, 417-428.
327. Douchamps, J.; Derenne, F.; Stockis, A.; Gangji, D.; Juvent, M.; Herchuelz, A. The pharmacokinetics of oxybutynin in man. *Eur. J. Clin. Pharmacol.* **1988**, *35*, 515-520.

328. Hughes, K. M.; Lang, J. C.; Lazare, R.; Gordon, D.; Stanton, S. L.; Malone-Lee, J.; Geraint, M. Measurement of oxybutynin and its N-desethyl metabolite in plasma, and its application to pharmacokinetic studies in young, elderly and frail elderly volunteers. *Xenobiotica* **1992**, *22*, 859-869.
329. Stoll, R. E.; Blanchard, K. T.; Stoltz, J. H.; Majeska, J. B.; Furst, S.; Lilly, P. D.; Mennear, J. H. Phenolphthalein and bisacodyl: assessment of genotoxic and carcinogenic responses in heterozygous p53 (+/-) mice and syrian hamster embryo (SHE) assay. *Toxicol. Sci.* **2006**, *90*, 440-450.
330. Ye, T.; Xiong, Y.; Yan, Y.; Xia, Y.; Song, X.; Liu, L.; Li, D.; Wang, N.; Zhang, L.; Zhu, Y.; Zeng, J.; Wei, Y.; Yu, L. The anthelmintic drug niclosamide induces apoptosis, impairs metastasis and reduces immunosuppressive cells in breast cancer model. *PLoS. One.* **2014**, *9*, e85887.
331. Tanaka, A.; Konno, M.; Muto, S.; Kambe, N.; Morii, E.; Nakahata, T.; Itai, A.; Matsuda, H. A novel NF-kappaB inhibitor, IMD-0354, suppresses neoplastic proliferation of human mast cells with constitutively activated c-kit receptors. *Blood* **2005**, *105*, 2324-2331.
332. Tanaka, A.; Muto, S.; Konno, M.; Itai, A.; Matsuda, H. A new IkappaB kinase beta inhibitor prevents human breast cancer progression through negative regulation of cell cycle transition. *Cancer Res.* **2006**, *66*, 419-426.
333. Zheng, J. P.; Zhang, Y.; Edvinsson, L.; Hjalt, T.; Xu, C. B. NF-kappaB signaling mediates vascular smooth muscle endothelin type B receptor expression in resistance arteries. *Eur. J. Pharmacol.* **2010**, *637*, 148-154.
334. Lennikov, A.; Kitaichi, N.; Noda, K.; Ando, R.; Dong, Z.; Fukuhara, J.; Kinoshita, S.; Namba, K.; Mizutani, M.; Fujikawa, T.; Itai, A.; Ohno, S.; Ishida, S. Amelioration of endotoxin-induced uveitis treated with an IkappaB kinase beta inhibitor in rats. *Mol. Vis.* **2012**, *18*, 2586-2597.
335. Kalman, D.; Barriere, S. L. Review of the pharmacology, pharmacokinetics, and clinical use of cephalosporins. *Tex. Heart Inst. J.* **1990**, *17*, 203-215.
336. Neely, M.; Kaplan, E. L.; Blumer, J. L.; Faix, D. J.; Broderick, M. P. A population pharmacokinetic modeling approach shows that serum penicillin G concentrations are below inhibitory concentrations by two weeks after benzathine penicillin G injection in the majority of young adults. *Antimicrob. Agents Chemother.* **2014**, *58*, 6735-6741.
337. Hiroi, M.; Stanczyk, F. Z.; Goebelsmann, U.; Brenner, P. F.; Lumkin, M. E.; Mishell, D. R., Jr. Radioimmunoassay of serum medroxyprogesterone acetate (Provera) in women following oral and intravaginal administration. *Steroids* **1975**, *26*, 373-386.
338. Stanczyk, F. Z.; Bhavnani, B. R. Use of medroxyprogesterone acetate for hormone therapy in postmenopausal women: is it safe? *J. Steroid Biochem. Mol. Biol.* **2014**, *142*, 30-38.
339. Science Information Yomesan® (Niclosamide). Status of information: June **2014**. Available at <http://www.fachinfo.de/>. Accessed on 06/01/2016.

340. Weinbach, E. C.; Garbus, J. Mechanism of action of reagents that uncouple oxidative phosphorylation. *Nature* **1969**, *221*, 1016-1018.
341. Li, Y.; Li, P. K.; Roberts, M. J.; Arend, R. C.; Samant, R. S.; Buchsbaum, D. J. Multi-targeted therapy of cancer by niclosamide: A new application for an old drug. *Cancer Lett.* **2014**, *349*, 8-14.
342. Pan, J. X.; Ding, K.; Wang, C. Y. Niclosamide, an old antihelminthic agent, demonstrates antitumor activity by blocking multiple signaling pathways of cancer stem cells. *Chin J. Cancer* **2012**, *31*, 178-184.
343. Osada, T.; Chen, M.; Yang, X. Y.; Spasojevic, I.; Vandeusen, J. B.; Hsu, D.; Clary, B. M.; Clay, T. M.; Chen, W.; Morse, M. A.; Lyerly, H. K. Antihelminth compound niclosamide downregulates Wnt signaling and elicits antitumor responses in tumors with activating APC mutations. *Cancer Res.* **2011**, *71*, 4172-4182.
344. Chang, Y. W.; Yeh, T. K.; Lin, K. T.; Chen, W. C.; Yao, H. T.; Lan, S. J.; Wu, Y. S.; Hsieh, H. P.; Chen, C. M.; Chen, C. T. Pharmacokinetics of Anti-SARS-CoV Agent Niclosamide and Its Analogs in Rats. *Journal of Food and Drug Analysis* **2006**, *14*, 329-333.
345. Lu, D.; Ma, Z.; Zhang, T.; Zhang, X.; Wu, B. Metabolism of the anthelmintic drug niclosamide by cytochrome P450 enzymes and UDP-glucuronosyltransferases: metabolite elucidation and main contributions from CYP1A2 and UGT1A1. *Xenobiotica* **2015**, 1-13.
346. Arend, R. C.; Londono-Joshi, A. I.; Samant, R. S.; Li, Y.; Conner, M.; Hidalgo, B.; Alvarez, R. D.; Landen, C. N.; Straughn, J. M.; Buchsbaum, D. J. Inhibition of Wnt/beta-catenin pathway by niclosamide: a therapeutic target for ovarian cancer. *Gynecol. Oncol.* **2014**, *134*, 112-120.
347. Barker, N.; Clevers, H. Mining the Wnt pathway for cancer therapeutics. *Nat. Rev. Drug Discov.* **2006**, *5*, 997-1014.
348. Lu, W.; Lin, C.; Roberts, M. J.; Waud, W. R.; Piazza, G. A.; Li, Y. Niclosamide suppresses cancer cell growth by inducing Wnt co-receptor LRP6 degradation and inhibiting the Wnt/beta-catenin pathway. *PLoS. One.* **2011**, *6*, e29290.
349. Londono-Joshi, A. I.; Arend, R. C.; Aristizabal, L.; Lu, W.; Samant, R. S.; Metge, B. J.; Hidalgo, B.; Grizzle, W. E.; Conner, M.; Forero-Torres, A.; Lobuglio, A. F.; Li, Y.; Buchsbaum, D. J. Effect of niclosamide on basal-like breast cancers. *Mol. Cancer Ther.* **2014**, *13*, 800-811.
350. Li, M.; Khambu, B.; Zhang, H.; Kang, J. H.; Chen, X.; Chen, D.; Vollmer, L.; Liu, P. Q.; Vogt, A.; Yin, X. M. Suppression of lysosome function induces autophagy via a feedback down-regulation of MTOR complex 1 (MTORC1) activity. *J. Biol. Chem.* **2013**, *288*, 35769-35780.
351. Liu, C.; Lou, W.; Armstrong, C.; Zhu, Y.; Evans, C. P.; Gao, A. C. Niclosamide suppresses cell migration and invasion in enzalutamide resistant prostate cancer cells via Stat3-AR axis inhibition. *Prostate* **2015**, *75*, 1341-1353.



352. Jin, Y.; Lu, Z.; Ding, K.; Li, J.; Du, X.; Chen, C.; Sun, X.; Wu, Y.; Zhou, J.; Pan, J. Antineoplastic mechanisms of niclosamide in acute myelogenous leukemia stem cells: inactivation of the NF-kappaB pathway and generation of reactive oxygen species. *Cancer Res.* **2010**, *70*, 2516-2527.
353. Wieland, A.; Trageser, D.; Gogolok, S.; Reinartz, R.; Hofer, H.; Keller, M.; Leinhaas, A.; Schelle, R.; Normann, S.; Klaas, L.; Waha, A.; Koch, P.; Fimmers, R.; Pietsch, T.; Yachnis, A. T.; Pincus, D. W.; Steindler, D. A.; Brustle, O.; Simon, M.; Glas, M.; Scheffler, B. Anticancer effects of niclosamide in human glioblastoma. *Clin. Cancer Res.* **2013**, *19*, 4124-4136.
354. You, S.; Li, R.; Park, D.; Xie, M.; Sica, G. L.; Cao, Y.; Xiao, Z. Q.; Deng, X. Disruption of STAT3 by niclosamide reverses radioresistance of human lung cancer. *Mol. Cancer Ther.* **2014**, *13*, 606-616.
355. Walters Haygood, C. L.; Arend, R. C.; Gangrade, A.; Chettiar, S.; Regan, N.; Hassmann, C. J.; Li, P. K.; Hidalgo, B.; Straughn, J. M., Jr.; Buchsbaum, D. J. Niclosamide Analogs for Treatment of Ovarian Cancer. *Int. J. Gynecol. Cancer* **2015**, *25*, 1377-1385.
356. Franceschini, A.; Adinolfi, E. P2X receptors: New players in cancer pain. *World J. Biol. Chem.* **2014**, *5*, 429-436.
357. Wu, C. S.; Li, Y. R.; Chen, J. J.; Chen, Y. C.; Chu, C. L.; Pan, I. H.; Wu, Y. S.; Lin, C. C. Antihelminthic niclosamide modulates dendritic cells activation and function. *Cell Immunol.* **2014**, *288*, 15-23.
358. Mook, R. A., Jr.; Wang, J.; Ren, X. R.; Chen, M.; Spasojevic, I.; Barak, L. S.; Lyerly, H. K.; Chen, W. Structure-activity studies of Wnt/beta-catenin inhibition in the Niclosamide chemotype: Identification of derivatives with improved drug exposure. *Bioorg. Med. Chem.* **2015**, *23*, 5829-5838.
359. Guo, Y.; Mishra, A.; Weng, T.; Chintagari, N. R.; Wang, Y.; Zhao, C.; Huang, C.; Liu, L. Wnt3a mitigates acute lung injury by reducing P2X7 receptor-mediated alveolar epithelial type I cell death. *Cell Death. Dis.* **2014**, *5*, e1286.
360. Deli, T.; Varga, N.; Adam, A.; Kenessey, I.; Raso, E.; Puskas, L. G.; Tovari, J.; Fodor, J.; Feher, M.; Szigeti, G. P.; Csernoch, L.; Timar, J. Functional genomics of calcium channels in human melanoma cells. *Int. J. Cancer* **2007**, *121*, 55-65.
361. Di, V. F.; Chiozzi, P.; Falzoni, S.; Ferrari, D.; Sanz, J. M.; Venketaraman, V.; Baricordi, O. R. Cytolytic P2X purinoceptors. *Cell Death. Differ.* **1998**, *5*, 191-199.
362. Science Information Dulcolax® (Bisacodyl). Status of information: January **2014**. Available at <http://www.fachinfo.de/>. Accessed on 06/01/2016.
363. Friedrich, C.; Richter, E.; Trommeshauser, D.; de, K. S.; van, I. T.; Mandel, K.; Gessner, U. Absence of excretion of the active moiety of bisacodyl and sodium picosulfate into human breast milk: an open-label, parallel-group, multiple-dose study in healthy lactating women. *Drug Metab Pharmacokinet.* **2011**, *26*, 458-464.
364. Flig, E.; Hermann, T. W.; Zabel, M. Is bisacodyl absorbed at all from suppositories in man? *Int. J. Pharm.* **2000**, *196*, 11-20.

365. Roth, W.; Beschke, K. [Pharmacokinetics and laxative effect of bisacodyl following administration of various dosage forms]. *Arzneimittelforschung*. **1988**, *38*, 570-574.
366. Schreiner, J.; Nell, G.; Loeschke, K. Effect of diphenolic laxatives on Na<sup>+</sup>-K<sup>+</sup>-activated ATPase and cyclic nucleotide content of rat colon mucosa in vivo. *Naunyn Schmiedebergs Arch. Pharmacol.* **1980**, *313*, 249-255.
367. Rachmilewitz, D.; Karmeli, F.; Okon, E. Effects of bisacodyl on cAMP and prostaglandin E2 contents, (Na + K) ATPase, adenylyl cyclase, and phosphodiesterase activities of rat intestine. *Dig. Dis. Sci.* **1980**, *25*, 602-608.
368. Ikarashi, N.; Baba, K.; Ushiki, T.; Kon, R.; Mimura, A.; Toda, T.; Ishii, M.; Ochiai, W.; Sugiyama, K. The laxative effect of bisacodyl is attributable to decreased aquaporin-3 expression in the colon induced by increased PGE2 secretion from macrophages. *Am. J. Physiol Gastrointest. Liver Physiol* **2011**, *301*, G887-G895.
369. Antonioli, L.; Giron, M. C.; Colucci, R.; Pellegrini, C.; Sacco, D.; Caputi, V.; Orso, G.; Tuccori, M.; Scarpignato, C.; Blandizzi, C.; Fornai, M. Involvement of the P2X7 purinergic receptor in colonic motor dysfunction associated with bowel inflammation in rats. *PLoS. One.* **2014**, *9*, e116253.
370. Burnstock, G. Purinergic signalling in the gastrointestinal tract and related organs in health and disease. *Purinergic. Signal.* **2014**, *10*, 3-50.

## Abbreviations

(Bu <sub>4</sub> N) <sup>+</sup>	Tetrabutylammonium
2-meSATP	2-Methylthioadenosine-5'-O-triphosphate
5-BDBD	5-(3-Bromophenyl)-1,3-dihydro-2H-benzofuro[3,2-e]-1,4-diazepin-2-one
5-HT	5-Hydroxytryptamine
ADP	Adenosine 5'-diphosphate
AMP	Adenosine 5'-monophosphate
AMPA	α-Amino-3-hydroxy-5-methyl-4-isoxazolepropionic acid
APC	Adenomatous polyposis coli
Arg (R)	Arginine
Asn (N)	Asparagine
Asp (D)	Aspartic acid
ATD	Amino terminal domain
ATP	Adenosine-5'-triphosphate
BBG	Brilliant Blue G
BHPM	Bis(p-hydroxyphenyl)-pyridyl-2-methane
BzATP	2'(3')-O-(4-Benzoylbenzoyl)adenosine-t'-triphosphate
CCL21	Chemokine C-C motif ligand 21
CCR2	C-C chemokine receptor type 2
cDNA	complementary deoxyribonucleic acid
CFA	complete Freund's adjuvant-induced arthritic rat model
CK 2	Protein kinase 2 (Casein kinase II)
CNS	Central nervous system
COX	Cyclooxygenase
ctDNA	Calf thymus DNA
Cys (C)	Cysteine
DMEM	Dulbecco's modified Eagle medium
DMSO	Dimethyl sulfoxide
DR	Dose ratio
EC <sub>50</sub>	Concentration of half-maximal receptor activation
EDTA	Ethylenediaminetetraacetic acid
eNOS	Endothelial nitric oxide synthase

## Abbreviations

---

FCS	Fetal calf serum
Fluo-4 AM	Fluo-4 acetoxymethyl ester
G418	Geneticin
GABA <sub>A/C</sub>	$\gamma$ -Aminobutyric acid receptor subtype A/C
GI	Gastrointestinal
Glu (E)	Glutamic acid
GP+envAM12	Amphotropic mouse fibroblast packaging cell line
GPCR	G protein-coupled receptor
GSH/GSSG	Glutathione/glutathione disulfide
HAD	High affinity desensitization
HBSS	Hank's balanced salt solution
HDAC	Histone deacetylase
HEPES	4-(2-Hydroxyethyl)-1-piperazineethanesulfonic acid
His (H)	Histidine
HIV	Human immune deficiency virus
HTS	High-throughput screening
IC <sub>50</sub>	Concentration of half-maximal receptor inhibition
Ile (I)	Isoleucine
IRF8	Interferon regulatory factor 8
KA	Kainic acid
KB	Estimated antagonist affinity constant
K <sub>D</sub>	Dissociation constant
K <sub>i</sub>	Inhibition constant
LBD	Ligand binding domain
Leu (L)	Leucine
LGIC	Ligand-gated ion channel
Lys (K)	Lysine
max.	maximal
Met (M)	Methionine
MFCA	3-Methyl-flavone-8-carboxylic acid
mRNA	Messenger RNA
MRSA	Methicillin-resistant <i>Staphylococcus aureus</i>
msec	Milliseconds
mTORC1	Mammalian target of rapamycin complex 1

MTT	3-(4,5-Dimethylthiazol-2-yl)-2,5-diphenyltetrazolium bromide
n. c.	no convergence
n. d.	not determined
nACh	nicotinic acetylcholine receptor
NALCN	Sodium leak channel
NAM	negative allosteric modulator
NavAb	Voltage-gated sodium channel
NF023	8,8'-[Carbonyl-bis(imino-3,1-phen-ylene-carbonylimino)]bis-1,3,5-naphthalene-trisulfonic acid
NF110	4,4',4'',4'''-(carbonylbis(imino-5,1,3-benzenetriylbis(carbonylimino)))tetra-kis-benzenesulfonic acid
NF279	8,8'-[Carbonyl-bis(imino-4,1-phenylenecarbonylimino-4,1-phenylene-carbonyl-imino)]bis-1,3,5-naphthalene trisulfonic acid
NF449	4,4',4'',4'''-[Carbonylbis-(imino-5,1,3-benzenetriyl-bis(carbonylimino))]tetrakis-1,3-benzenedisulfonic acid
NF770	7,7'-(Carbonylbis(imino-3,1-phenylene-carbonylimino-3,1-(4-methyl-phenylene)carbonyl-imino))bis-(1-methoxy-naphthalene-3,6-disulfonic acid
NMDA	N-methyl-D-aspartate
NSAID	Non-steroidal anti-inflammatory drug
PAM	Positive allosteric modulator
pEC <sub>50</sub>	negative decadic logarithm of EC <sub>50</sub> value
PEG	Polyethylene glycol
Phe (F)	Phenylalanine
pIC <sub>50</sub>	negative decadic logarithm of IC <sub>50</sub> value
POM	Polyoxometalate
PPADS	Pyridoxalphosphate-6-azophenyl-2'-4'-disulfonic acid
PPAR $\alpha$	Peroxisome proliferator-activated receptor $\alpha$
PSB-1011	Disodium 1-amino-4-[3-(4,6-dichloro[1,3,5]triazine-2-ylamino)-4-sulfophenylamino]-9,10-dioxo-9,10-dihydroanthracene-2-sulfonate
PSB-10211	Sodium 1-amino-4-[3-(4,6-dichloro[1,3,5]triazine-1-ylamino)-phenylamino]-9,10-dioxo-9,10-dihydroanthracene-2-sulfonate
PSB-12054	N-(benzyloxycarbonyl)phenoxazine
PSB-12062	N-( <i>p</i> -methylphenylsulfonyl)phenoxazine

## Abbreviations

---

pVSV-G	Vesicular stomatitis virus-expressing vector
RB-2	Reactive Blue-2
RNA	Ribonucleic acid
RSV	Anti-respiratory syncytial virus
RT	Room temperature
S15VrP2X3	Mutant of rat P2X3 receptor with a point mutation in position 15 (serine was exchanged to valine)
SARS	Severe acute respiratory syndrome
SEM	Standard error of the mean
Ser (S)	Serine
STAT3	Signal transducer and activator of transcription 3
TCA	Tricyclic antidepressant
Thr (T)	Threonine
TM	Transmembrane $\alpha$ -helix
TMD	Transmembrane domain
TNP-ATP	2'-3'-O-(2, 4,6-Trinitrophenyl)adenosine-5'-triphosphate
TRIS	Tris(hydroxymethyl)aminomethane
UDP	Uridine 5'-diphosphate
UTP	Uridine 5'-triphosphate
VGCC	Voltage-gated calcium channel
VGIC	Voltage-gated ion channel
VGKC	Voltage-gated potassium channel
VGNC	Voltage-gated sodium channel
VSD	Voltage-sensing domain
YFP	Yellow-fluorescent protein
zfP2X4	Zebrafish P2X4 receptor
$\alpha,\beta$ -MeATP	$\alpha,\beta$ -Methylene-adenosine 5'-triphosphate
$\beta,\gamma$ -MeATP	$\beta,\gamma$ -Methylene-adenosine 5'-triphosphate

## Danksagung

Mein besonderer Dank gilt zunächst Frau Prof. Dr. Christa E. Müller für die Möglichkeit, diese Arbeit in den letzten Jahren in ihrem Arbeitskreis anfertigen zu können. Sie hat es mir ermöglicht, viele verschiedene Aspekte und Methoden der pharmazeutischen Forschung kennen zu lernen und eigenständig zu arbeiten. Ihre hilfreichen Anregungen waren mir stets eine große Stütze.

PD Dr. Anke C. Schiedel möchte ich für die Übernahme des Koreferats und für ihre stetige Unterstützung danken. Sie stand mir jederzeit mit Rat und Tat bei Problemen im Isolabor oder molekularbiologischen Fragen zur Seite.

Zusätzlich möchte ich mich bei Prof. Dr. Klaus Mohr und Prof. Dr. Rainer Manthey herzlich für ihr Mitwirken in der Promotionskommission danken.

Des Weiteren danke ich unseren Kooperationspartnern, insbesondere Dr. Ralf Hausmann, Dr. Holger Stephan, Prof. Dr. Ulrich Körtz, Dr. Jin Tang und Prof. Dr. Wei Wang für die Bereitstellung der Testverbindungen und die gute Zusammenarbeit.

Bei Prof. Dr. Katarzyna Kieć-Kononowicz und Tadeusz Karcz möchte ich mich für die freundliche Aufnahme und die tolle Zusammenarbeit während meines einmonatigen Aufenthaltes an der Jagiellonen Universität in Krakau, Polen bedanken.

Vielen Dank auch an Dr. Aliaa Abdelrahman und Stefanie Weyer für die Bereitstellung der transfizierten P2X Rezeptor Zelllinien und die gute Zusammenarbeit.

Dem gesamten Arbeitskreis, allen aktuellen und ehemaligen Kollegen danke ich für die gute Zusammenarbeit und die kollegiale Atmosphäre. Ganz besonders möchte ich meinen Kollegen Marianne, Clara, Katharina und Steffi danken für die wunderbare Zeit. Ich werde unsere Gesprächsrunden und die vielen Rewe-Trips schmerzlich vermissen! Trinkt ein Bier (und für mich ein Korn 😊)!

Danke auch an Michael, Dominik, Christin, Anika, Angelika, Markus und Muhammad für die tatkräftige Hilfe im Labor bzw. am PC, für Übernahme von Zellpflege, Beratung bei Experimenten usw. Danke für die wunderbare und unkomplizierte Zusammenarbeit, eure stete Hilfsbereitschaft und tatkräftige Unterstützung!

Ein riesengroßes Dankeschön auch an Dr. Ralf Mayer und an alle meine aktuellen und ehemaligen Mitassistenten des 7. Semesters, insbesondere Marianne, Clara, Daniel, Dominik,

## Danksagung

---

Wessam, Hung, Samer, Christian und Wenjin. Danke für die vielen tollen Stunden in der Aufsicht, bei Besprechungen und Klausurkorrekturen! Schwefelsäure hat uns nicht umgebracht!

Darüber hinaus möchte ich mich bei meinen Freunden aus Schule und Studium bedanken, insbesondere Susanne, Steffi, Lisa, Sebastian W., David, Melanie, Alex und Anne. Ein ganz besonderer Dank gilt Astrid, Sebastian B. und Sonja. Danke, dass ihr immer für mich da ward! Danke, dass ihr immer ein offenes Ohr hattet, mich immer wieder aufgebaut habt, wenn der Frust zu hoch war, und mir mit Rat und Tat zur Seite standet!

Der größte Dank gilt allerdings meiner Familie, insbesondere meinen Eltern. Ohne eure stetige und uneingeschränkte Unterstützung wäre nichts von alledem, weder Studium noch Master noch Promotion möglich gewesen! Danke für alles!!!



## Publication List

### Congress contributions

Spanier, C.; Abdelrahman, A.; Tang, J.; Hausmann, R.; Haider, A.; Kortz, U.; Schmalzing, G.; Stephan, H.; Wang, W.; Müller, C.E. Polyoxometalates with potent inhibitory activity at P2X receptors. *Purinergic Signaling 2016*, Vancouver, January **2016** (Poster)

Weinhausen, S.; Namasivayam, V.; Spanier, C.; Hanck, T.; Abdelrahman, A.; Müller, C.E. Binding site of the allosteric P2X4 receptor modulator ivermectin. *Purinergic Signaling 2016*, Vancouver, January **2016** (Poster)

Köse, M.; Karcz, T.; Gollos, S.; Fiene, A.; Heisig, F.; Spanier, C.; Kieć-Kononowicz, K.; Müller, C.E. A homogenous A2B adenosine receptor fluorescence binding assay based on flow cytometry. *Purines 2015*, Hamburg, July **2015** (Poster)

Spanier, C.; Baqi, Y.; Malik, E.M.; Hausmann, R.; Müller, C.E. Structure-activity relationships of anthraquinone derivatives as modulators of P2X3 receptors. *Purines 2014*, Bonn, July **2014** (Poster). Abstract was published in *Purinergic Signalling* **2014**, 10, 779

Spanier, C.; Stephan, H.; Kortz, U.; Haider, A.; Hausmann, R.; Abdelrahman, A.; Müller, C.E. Polyoxometalates as potent inhibitors of P2X receptors. *Purines 2014*, Bonn, July **2014** (Poster). Abstract was published in *Purinergic Signalling* **2014**, 10, 778